Lars Olof Nord

Pre-combustion CO_2 capture: Analysis of integrated reforming combined cycle

Doctoral thesis
for the degree of philosophiae doctor

Trondheim, June 2010

Norwegian University of Science and Technology
Faculty of Engineering Science and Technology
Department of Energy and Process Engineering

NTNU
Norwegian University of
Science and Technology

NTNU

Norwegian University of Science and Technology

Doctoral thesis
for the degree of philosophiae doctor

Faculty of Engineering Science and Technology
Department of Energy and Process Engineering

ISBN 978-82-471-2125-2 (printed version)
ISBN 978-82-471-2126-9 (electronic version)
ISSN 1503-8181

Doctoral theses at NTNU, 2010:82

Printed by Tapir Uttrykk

Preface

The thesis is submitted in partial fulfillment of the requirements for the degree of philosophiæ doctor (PhD) at the Norwegian University of Science and Technology (NTNU). The work was carried out at the Department of Energy and Process Engineering at the Faculty of Engineering Science and Technology, with Prof. Olav Bolland as supervisor. The research was founded by the Norwegian Research Council and Statoil.

Abstract

This thesis presents processes for reducing CO_2 emissions from natural gas (NG) power plants, which could help attenuate the rise in atmospheric temperature. Objectives for the thesis work were process design and integration of NG pre-combustion CO_2 capture plants, and evalution, through process simulation, of the concepts. An important aspect of the evaluation was investigation of plant flexibility, specifically off-design analysis. Contributions comprised detailed heat recovery steam generator (HRSG) design for NG pre-combustion cycles and off-design behavior of the integrated reforming combined cycle (IRCC). Additional contributions were quantification of the efficiency potential of a process, subsystem efficiency losses, and model uncertainties.

The IRCC with pre-combustion CO_2 capture is a process for generating power with very low CO_2 emissions, typically below 100 g CO_2/net kWh electricity. This should be compared to a state-of-the-art natural gas combined cycle (NGCC) with CO_2 emissions around 365 g CO_2/net kWh electricity. The IRCC process reforms natural gas to a syngas, converts the CO to CO_2 in the shift reactors, separates the CO_2 in the capture subsystem, and the resulting hydrogen-rich fuel is used for the gas turbine (GT) in a combined cycle setup. For the reforming of natural gas, an air-blown autothermal reformer was selected for the processes studied. Included in the study of the IRCC were process design and integration, reliability analysis, thermodynamic analyses through process simulation, analysis of efficiency losses and efficiency potential, and uncertainty analysis.

As part of the design process, HRSG design proved important. The design of an HRSG for an IRCC plant requires the ability to operate on both a hydrogen-rich fuel and on NG. Also, since a significant amount of steam is produced from the heat generated in the autoreforming process, the HRSG design differs from a design in an NGCC plant. For an IRCC with a lot of high-pressure saturated steam generated in the process, a single-pressure steam cycle can actually perform in parity with a dual- or triple-pressure system (with or without reheat). Preheating of process streams further add to the complexity. The complexity of selecting an HRSG design increased when also considering that steam could be superheated and low-pressure and intermediate-pressure steam could be generated in the reforming process heat exchangers. For the concept studied it was also of importance to maintain a high net plant efficiency when operating on NG. Therefore the selection of HRSG design had to be a compromise between NGCC and IRCC operating modes. Duct burning proved positive for plant flexibility and the option to switch between a hydrogen-rich fuel and NG for the GT.

Functional analysis and FMECA are important steps in a system reliability analysis, as they can serve as a platform and basis for further analysis. Also, the results from the FMECA can be interesting for determining how the failures propagate through the system and their failure effects on the operation of the process. From the FMECA performed in

this work, it is clear that the gas turbine is the most critical equipment in an IRCC plant. One of the reasons for this is the process integration between the power island and the pre-combustion process. For example, the gas turbine feeds air to the ATR and receives fuel from the pre-combustion process. This integration has an effect on the overall reliability of the system. In addition to the integration issues, the gas turbine technology is less mature for hydrogen fuels than for natural gas fuels. It should also be mentioned that even in an NG-fired combined cycle plant the gas turbine is the most critical equipment. The need for part load analysis and consideration to dual fuel capability were important conclusions from the reliability analysis since many of the failures resulted in IRCC plant shutdown (if no backup fuel) or operation at reduced load.

Thermodynamic analyses through process simulation were conducted as part of the thesis work. By combining simulation tools for chemical engineering and power plant engineering analyses respectively, a representation of the overall system could be accomplished for an IRCC process. The reforming and CO_2 capture processes were simulated in Aspen Plus; the power island was simulated in GT PRO/GT MASTER. The IRCC process involved process integration between the power cycle and the reforming process meaning an efficient way of linking the softwares were important. The Aspen Simulation Workbook and Thermoflow's E-link proved capable of performing this task for an IRCC process. Design simulations showed net plant efficiencies between 41.9% and 45.3% with net plant power output in the range of 350–420 MW. The CO_2 capture rate ranged between 85.1% and 93.4% for the IRCC processes studied. The off-design simulations, as part of the plant flexibility analysis, showed the possibility to operate an IRCC plant at part load conditions down to approximately 60% gas turbine load with capture efficiency penalties at part load similar to full load operation. Also, it can be concluded that considering off-design conditions, such as part load steam turbine extraction pressures and air booster compressor pressure ratio, are important during the design stage of a plant.

Analysis of the contribution to efficiency losses in the IRCC process showed that the reforming losses were almost twice as high as the CO_2 capture losses. From the analysis, it was evident that to decrease the efficiency losses in an IRCC process, efforts should be concentrated towards improving (1) the reforming process to decrease fuel conversion losses and needed steam mass flow, (2) the CO_2 capture process to decrease the reboiler duty, (3) the gas turbine technology to allow for a higher firing temperature, and (4) the CO_2 compression process.

When investigating the efficiency potential of the type of IRCC concepts studied in the thesis work, net plant efficiencies of 49% was achieved and based on these results it is conceivable that efficiencies up towards 50% could be realistic in a 5–10 years time horizon. Challenges to overcome to reach these high efficiencies include attenuating or eliminating process limitations due to metal dusting and reduced GT turbine inlet temperature.

For the IRCC setup studied in the uncertainty analysis, results showed that there was considerable uncertainty in the predicted net power output whereas net plant efficiency, CO_2 capture rate, and CO_2 emitted were less affected by input uncertainties. Parameters with the largest impact on uncertainties of power output and efficiency predictions proved to be gas turbine inlet temperature, and compressor and turbine efficiencies. For the CO_2 emissions, the equipment pressure drop and the steam-to-carbon ratio proved important. Therefore, the focus of future work should be to reduce uncertainties in these parameters in order to improve the confidence in the IRCC model.

Sammendrag

Denne avhandlingen presenterer prosesser for å redusere CO_2-utslipp fra gasskraftverk. Disse prosessene kan være en del i en strategi for å motvirke økningen av temperaturen i atmosfæren. Målet for avhandlingen er prosessdesign og integrasjon samt evaluering, ved bruk av prosessimulering, av naturgassbaserte "pre-combustion" innfangingsanlegg for CO_2. En viktig del av evalueringen har vært anleggsfleksibilitet og da spesielt off-design analyse. Bidrag omfatter detaljert design av avgaskjel for naturgassbasert "pre-combustion" CO_2-innfangingsanlegg og driftsevne ved dellast for den integrerte reformerings- og gass-dampturbinprosessen (IRCC). Ytterligere bidrag er kvantifisering av virkningsgradspotential, virkningsgradstap for delprosesser og usikkerheter i modellen.

IRCC med "pre-combustion" innfanging av CO_2 er en kraftgenererings-prosess med veldig lave karbondioksidutslipp, typisk under 100 g CO_2/netto kWh elektrisitet. Dette kan sammenlignes med et toppmoderne kombinert gass-dampturbinanlegg (NGCC) med CO_2-utslipp på cirka 365 g CO_2/netto kWh elektrisitet. IRCC reformerer naturgass til en syntesgass, konverterer CO till CO_2 i shiftreaktorene, separerer CO_2 i utskillingsystemet, og den resulterende hydrogenrike gassen brukes som brensel i gassturbinen i en kombinert gass-dampturbinprosess. For reformering av naturgass var det valgt en luftblåst autotermisk reformer (ATR). Studien av IRCC inkluderte prosessdesign og integrasjon, pålitelighetsanalyse, termodynamiske analyser ved bruk av prosessimulering, analyse av virkningsgradstap og virkningsgradspotensial samt usikkerhetsanalyse.

Som en del av designprosedyren var avgaskjelen viktig. Avgaskjelen for et IRCC-anlegg krever drift både med en hydrogenrik gass og naturgass. I tillegg er avgaskjelens design annerledes enn i en NGCC, fordi en stor del av dampen produseres fra generert varme i den autotermiske reformeringsprosessen. For et IRCC-anlegg, hvor store mengde av damp produseres fra varmen i reformeringsprosessen, kan en entrykks dampprosess faktisk ha ytelse likeverdig med et to- eller tretrykksystem (med eller uten mellomoverheting). Forvarming av prosessstrømmer gir økt kompleksitet for prosessen. Kompleksiteten ved valg av avgaskjeldesign økte når hensyn ble tatt for muligheten til å overhete damp, og lav- og mellomtrykkdamp kunne genereres i prosessvarmevekslene. For konseptene i studien var det også viktig å oppholde en høy virkningsgrad ved bruk av naturgass som brensel. Derfor var valget av avgaskjeldesign et kompromiss mellom NGCC- og IRCC-driftsmåter. Tilleggsfyring viste seg å være positivt for anleggsfleksibilitet og ga muligheten for å veksle mellom et hydrogenrikt brensel og naturgass for gassturbinen.

Funksjonsanalyse og FMECA er viktige trinn i en pålitelighetsanalyse av et system, fordi de kan være et grunnlag for videre analyse. I tillegg kan resultatene fra en FMECA være interessante når det bestemmes hvordan feil fortplanter seg i systemet og feilens effekt på driften av anlegget. Fra FMECA som gjennomførtes er det tydelig at gassturbinen

er den mest kritiske delen i et IRCC-anlegg. En grunn til dette var prosessintegrasjon. For eksempel tilfører gassturbinen luft til reformeren og får brensel fra "pre-combustion" prosessen. Denne integrasjonen har en effekt på den totale påliteligheten for systemet. I tillegg til integrasjonsutfordringene er teknologien for gassturbiner mindre utviklet for hydrogenbrensler enn for naturgass. Det bør også nevnes at i NGCC er gassturbinen den mest kritiske komponenten. Behov for dellastanalyse og hensyn til drift med forskjellige brensler var viktige konklusjoner fra pålitelighetsanalysen, fordi mange av feilene resulterte i driftsstopp av anlegget (uten reservebrensel) eller drift ved redusert last.

Termodynamiske analyser ved bruk av prosessimulering har vært en del av avhandlingsarbeidet. Simuleringsverktøy fra både kjemi- og energiteknikk ble benyttet for å evaluere IRCC. Reformerings- og separasjonsprosessen ble simulert i Aspen Plus; kraftprosessen ble simulert i GT PRO/GT MASTER. IRCC prosessen omfattet prosessintegrasjon mellom kraftprosessen og reformeringprosessen. Derfor var det viktig å koble sammen simuleringsverktøyene på en effektiv måte. Aspen Simulation Workbook og Thermoflows E-link viste seg å være i stand til å gjennomføre dette. Simuleringer resulterte i nettovirkningsgrader for anlegget mellom 41.9% og 45.3% med nettokraftproduksjon på 350–420 MW. Utskillingsgraden for CO_2 varierte mellom 85.1% og 93.4% for prosessene i analysene. Off-designsimuleringene, som var en del av analysen av anleggsfleksibilitet, viste at det er mulig å kjøre et IRCC anlegg ned til cirka 60% gassturbindellast. Likeså kan det konkluderes med at vurdering av off-design betingelser, som avtappningstrykk for dampturbinen og trykkforhold for luftkompressoren, er viktig ved design av anlegget.

Analyse av bidrag til virkningsgradstap i en IRCC viste at reformeringstapt var nesten dobbelt så stor som tapet i separasjonsprosessen for CO_2. Fra denne analysen er det klart at, for å minske virkningsgradstapen i en IRCC, insatsen bør rettes mot (1) reformeringsprosessen, (2) separasjonsprosessen for CO_2, (3) gassturbinteknologien og (4) prosessen med kompresjon av CO_2.

Undersøkelse av virkningsgradspotensial for denne type av IRCC resulterte i virkningsgrader på 49%. Basert på disse resultatene er det tenkbart at virkningsgrader opp mot 50% kan være realistisk i en 5–10 års tidshorisont. Utfordringer som gjenstår, for å oppnå høye virkningsgrader, inkluderer reduksjon eller eliminering av prosessbegrensninger på grunn av "metal dusting" og redusert inløpstemperatur til gassturbinen.

For IRCC-anlegget, som var studert i usikkerhetsanalysen, viste resultatene at det var vesentlig usikkerhet i estimert netto kraftproduksjon. Beregnet virkningsgrad, utskillingsgrad og utslipp av CO_2 var mindre påvirket av usikkerheter i inndata. Parametrene som mest påvirket usikkerheter i netto kraftproduksjon og virkningsgrad viste seg å være inløpstemperatur til gassturbinen samt kompressor- og turbinvirkningsgrader. Trykktap og damp-karbon-forholdet var viktige for hvor mye CO_2 som slippes ut. Derfor bør fokus på videre arbeid være rettet mot å redusere usikkerheter i disse parametrene for å forbedre tilliten til IRCC-modellen.

Sammanfattning

Denna avhandling presenterar processer för att reducera koldioxidutsläpp från naturgaskraftverk. Dessa processer kan vara en del av en strategi för att dämpa ökningen av temperaturen i atmosfären. Syftet med avhandlingen var processdesign och integration samt evaluering, med hjälp av processimulering, av naturgasbaserade "pre-combustion" koldioxidavskiljninganläggningar. En viktig del av evalueringen var anläggningflexibilitet och då specifikt off-design analys. Avhandlingens bidrag omfattade detaljerad design av avgaspannan för naturgasbaserade "pre-combustion" koldioxidavskiljninganläggningar och driftsegenskaper vid dellast för den integrerade reformerings- och gas-ångturbinprocessen (IRCC). Ytterligare bidrag var kvantificering av verkningsgradspotential, verkningsgradsförluster för delprocesser och osäkerheter i modellen.

IRCC med "pre-combustion" koldioxidavskiljning är en kraftgenereringsprocess med väldigt låga koldioxidutsläpp, med värden under 100 g CO_2/netto kWh elektricitet. Detta ska jämföras med en toppmodern kombinerad gas-ångturbinanläggning (NGCC) med koldioxidutsläpp på cirka 365 g CO_2/netto kWh elektricitet. IRCC reformerar naturgas till en syntesgas, konverterar CO till CO_2 i shiftreaktorerna, separerar CO_2 i avskiljningssystemet, och den resulterande väterika gasen används till gasturbinen i en kombinerad gas-ångturbinprocess. För reformering av naturgas valdes en luftblåst autotermisk reformator (ATR). Inkluderat i studien av IRCC var processdesign och integration, pålitlighetsanalys, termodynamiska analyser genom processimulering, analys av verkningsgradsförluster och verkningsgradspotential samt osäkerhetsanalys.

Som en del av designproceduren var avgaspannan viktig. För en IRCC-anläggning krävs drift både med en väterik gas och naturgas. I tillägg, eftersom en stor del av ångan produceras från genererad värme i den autotermiska reformeringsprocessen, är avgaspannans design annorlunda än i en NGCC. För en IRCC-anläggning, där stora mängder ånga produceras från värmen i reformeringsprocessen, kan en entrycks ångprocess faktiskt ha prestanda likvärdig med ett två- eller tretryckssystem (med eller utan mellanöverhettning). Förvärmning av processströmmar ger ökad komplexitet av processen. Komplexiteten vid val av avgaspannedesign ökade också när hänsyn togs till möjligheten att överhetta ånga samt att låg- och mellantrycksånga kunde genereras i processvärmeväxlarna. För koncepterna i studien var det också viktigt att upprätthålla en hög verkningsgrad vid naturgasdrift. Således var valet av avgaspannedesign en kompromiss mellan NGCC- och IRCC-driftssätt. Tillsatseldning visade sig vara positivt för anläggningsflexibilitet och gav möjligheten till att växla mellan ett väterikt bränsle och naturgas för gasturbinen.

Funktionsanalys och FMECA är viktiga steg i en pålitlighetsanalys av ett system då de kan vara en utgångspunkt för vidare analys. I tillägg kan resultaten från en FMECA vara intressanta för att visa hur fel fortplantar sig i systemet och vilken effekt de har

på driften av anläggningen. Från FMECAn som genomfördes är det tydligt att gasturbinen är den mest kritiska delen i en IRCC-anläggning. En av anledningarna till detta var processintegration. Till exempel förser gasturbinen luft till reformatorn och får bränsle från "pre-combustion" processen. Denna integration har en effekt på den totala pålitligheten for systemet. I tillägg till integrationsföljderna är teknologin för gasturbiner mindre utvecklad för vätebränslen än för naturgasbränslen. Det bör också nämnas att även i en NGCC är gasturbinen den mest kritiska utrustningen. Behov för dellastanalys och hänsynstagande till drift med olika bränslen var viktiga slutsatser från pålitlighetsanalysen, eftersom många av felen resulterade i avställning av anläggningen (utan reservbränsle) eller dellastsdrift.

Termodynamiska analyser genom processimulering genomfördes som en del av avhandlingsarbetet. Simuleringsverktyg för både kemi- och energiteknik användes för att evaluera IRCC. Reformerings- och koldioxidavskiljningprocesserna simulerades i Aspen Plus; kraftprocessen simulerades i GT PRO/GT MASTER. IRCC innefattade processintegration mellan kraftprocessen och reformeringsprocessen, vilket innebar att ett effektivt sätt att koppla samman simuleringsverktygen var viktigt. Aspen Simulation Workbook och Thermoflows E-link visade sig vara kapabla att genomföra detta. Simuleringar resulterade i nettoverkningsgrader för anläggningen mellan 41.9% och 45.3% med nettoeffekter på 350–420 MW. Koldioxidavskiljningsgraden varierade mellan 85.1% och 93.4% for processerna i analyserna. Off-designsimuleringarna, som var en del av analysen av anläggningsflexibilitet, visade på möjligheten att köra en IRCC anläggning ned till cirka 60% gasturbindellast. Likaså kan det konkluderas att hänsynstagande till off-design betingelser, såsom avtappningstryck för ångturbinen och luftkompressorns tryckförhållande, är viktigt under designen av anläggningen.

Analys av bidrag till verkningsgradförlust i en IRCC visade att reformeringsförlusterna var nästan dubbelt så stora som förlusterna i koldioxidavskiljningsdelen. Från denna analys står det klart att, för att minska verkningsgradsförlusterna i en IRCC, insatserna bör riktas mot (1) reformeringsprocessen, (2) koldioxidavskiljningsprocessen, (3) gasturbinteknologin och (4) koldioxidkompressionsprocessen.

Undersökning av verkningsgradspotentialen för den typ av IRCC resulterade i verkningsgrader på 49%. Baserat på dessa resultat är det tänkbart att verkningsgrader uppemot 50% kan vara realistiskt i en 5–10 års tidshorisont. Utmaningar som kvarstår, för att uppnå dessa höga verkningsgrader, inkluderar minskning eller eliminering av processbegränsningar på grund av "metal dusting" och reducerad inloppstemperatur till gasturbinen.

För IRCC-anläggningen, som studerades i osäkerhetsanalysen, visade resultaten att det var avsevärd osäkerhet i den estimerade nettoeffekten. Beräknad verkningsgrad, koldioxidavkiljningsgrad och koldioxidutsläpp var mindre påverkade av osäkerheter i indata. Parametrarna som mest påverkade osäkerheter i nettoeffekt och verkningsgrad visade sig vara inloppstemperatur till gasturbinen samt kompressor- och turbinverkningsgrader. Tryckförluster och ång-kol-förhållandet var viktiga för hur mycket koldioxid som släpps ut. Därför borde fokus på vidare arbete vara riktad mot att reducera osäkerheter i dessa parametrar för att förbättra tilliten till IRCC-modellen.

Acknowledgments

Many thanks to supervisor Prof. Olav Bolland allowing for independent work while supplying guidance as needed. And for never doubting me (at least not to my knowledge :) Plus for his advice on catching fish in mountain lakes, which even helped convince my father that it's not all about worms.

Join me in applauding the administrative staff at the Department of Energy and Process Engineering. A special hurrah goes to Anita Yttersian. Thanks to all NTNU coworkers for all the discussions and coffee breaks. This includes Rahul Anantharaman for many giving discussions, the occassional bike trip, and the once-in-a-blue-moon chess game. And Audun Aspelund, Knut Arild Maråk, and Torleif Weydahl for helping me, as a Swede, adjust to the Norwegian culture and lifestyle :) This included Tippeligaen (Audun), 17. mai (Knut), and Nidarosdomen (Torleif).

Thanks to Trondheim for all the wonderful skiing opportunities and for providing a super atmosphere for both work and recreation. NTNU-BIL innebandy for all the nice practices and games, and for giving me the opportunity to take penalty shots even though I missed all the important ones. A handshake of gratitude to all golf mates in the SINTEF Energy Research golf group for wonderful times at Byneset and other courses. Many thanks to my friends, not the least Joseph.

Mother and father, Linnéa and Stig, for their moral support and for always showing great interest in my work and life. And for the yearly cabin trip to Storlien and salmon fishing trip to the Namsen river in Nord-Trøndelag. Thanks to my nephew Philip and niece Josephine for their visits, which gave me pleasant breaks from the studies. Deep bow of gratitude to future wife (oops...:) Nataša for her unwavering support, fruitful discussions, all the skiing trips, and of course for the excellent cooking and all the other good times together. Plus for her patience in reviewing the thesis.

Thanks to the MIT team who was part of this project, including Prof. Greg McRae, Howard Herzog, Bo Gong, and Anusha Kothandaraman. My visits to MIT always gave me inspiration for continued research work. Thanks to the Norwegian Research Council and Statoil for funding the project. Thanks to committee members, Prof. Jan M. Øverli, Prof. Umberto Desideri, and Dr. Matthias Finkenrath, for their work with reviewing the thesis.

Contents

Nomenclature

Latin symbols

A	heat transfer area (m^2)
a_c	carbon activity
a_k	coefficient of expansion
C	constant
c_p	heat capacity (J/kg·K)
CP	heat capacity flow rate (W/K)
D	diameter (m)
dp/dx	pressure gradient (Pa/m)
F_T	heat exchanger correction factor (-)
f	Darcy friction factor (-)
H_k	orthogonal polynomial function
h	convective heat transfer coefficient ($W/m^2 \cdot K$)
K	thermodynamic equilibrium constant
k	thermal conductivity (W/m·K)
k_{ij}	binary interaction parameter (-)
LHV	lower heating value (kJ/kg)
$\dot{m}$	mass flow (kg/s)
N	rotational speed (1/s)
Nu	Nusselt number (-)
P	thermal effectiveness (-)
p	pressure (Pa; bar)
p_0	stagnation pressure (Pa)

p_i	partial pressure of component i (bar; atm)
Pr	Prandtl number (-)
Q	heat duty (W)
Q_{re}	reboiler duty (J/kg CO_2 cap.)
q	heat content per unit mass (J/kg)
R	heat capacity rate ratio (-)
$\bar{R}$	universal gas constant (J/mol·K)
Re	Reynolds number (-)
R_f	fouling factor (m^2· K/W)
R_w	wall conduction factor (K/W)
S_L	longitudinal pitch (m)
S_T	transverse pitch (m)
T	temperature (°C; K)
T_0	stagnation temperature (K)
T_s	supply temperature (°C)
T_t	target temperature (°C)
U	overall heat transfer coefficient (W/m^2·K)
u_m	mean fluid velocity (m/s)
$\dot{W}$	power (W)
$\dot{W}_{gt,rel}$	relative gas turbine load (%)
x	axial position (m)
x_m	mean step steam quality (-)
x_u	Gaussian uncertain parameter
$\tilde{y}$	molar fraction (-)

Greek symbols

β	Baumann coefficient (-)
ΔT_{lm}	log mean temperature difference (K)
η	efficiency (-)

μ	dynamic viscosity (kg/s·m)
$\overline{\mu}$	mean value
ξ	Gaussian random variable
Π	pressure ratio (-)
ρ	density (kg/m^3)
σ	standard deviation
$\tilde{v}$	molar volume (m^3/mol)
ω	acentric factor (-)

Subscripts

$1; in$	inlet
$2; out$	outlet
aux	auxiliary
$boost$	air booster compressor
c	cold
$comp$	air and CO_2 compression
cr	critical
cv	control volume
d	design
$drive$	drives for compressors and pumps
gen	generator
gtc	GT compressor
gtt	GT turbine
h	hot
i	component i
is	isentropic
m	mechanical
o	overall surface
p	pump

r	reactor
st	steam turbine
gt	gas turbine
loss	fuel conversion loss
ngcc	natural gas combined cycle reference plant

Abbreviations

ASU	air separation unit
ATR	autothermal reformer
BM	Boston-Mathias
CCI	comparative complexity indicator
CDM	clean development mechanism
CDOF	control degrees of freedom
DB	duct burner
DEMM	deterministic equivalent modeling method
EOS	equation of state
FMECA	failure mode, effects, and criticality analysis
GE	General Electric
GHG	greenhouse gases
GT	gas turbine
GTW	Gas Turbine World Handbook
GWP	global warming potential
HP	high-pressure
HPB	high-pressure boiler
HPE	high-pressure economizer
HPS	high-pressure superheater
HRSG	heat recovery steam generator
HTS	high-temperature shift reactor
HX	heat exchanger

IAPWS	International Association for the Properties of Water and Steam
IEA	International Energy Agency
IGCC	integrated gasification combined cycle
IP	intermediate-pressure
IPB	intermediate-pressure boiler
IPCC	Intergovernmental Panel on Climate Change
IPE	intermediate-pressure economizer
IPS	intermediate-pressure superheater
IRCC	integrated reforming combined cycle
ISO	International Organization for Standardization
ITM	oxygen ion transport membrane
JI	joint implementation
LMTD	log mean temperature difference
LP	low-pressure
LTE	low-temperature economizer
LTS	low-temperature shift reactor
MDEA	methyl diethanolamine
MEA	monoethanolamine
MIT	Massachusetts Institute of Technology
NBS	US National Bureau of Standards
NG	natural gas
NGCC	natural gas combined cycle
NOAA	National Oceanic and Atmospheric Administration
NRC	National Research Council of Canada
NRTL	non-random two liquid model
NTNU	Norwegian University of Science and Technology
OEM	original equipment manufacturer
OTM	oxygen transport membrane

PDF	probability density function
PhD	Doctor of Philosophy
POX	partial oxidation
ppm	parts per million
ppmvd	parts per million volume dry
PR	Peng-Robinson
RH	reheater
RKS	Redlich-Kwong-Soave
RPN	risk priority number
S/C	steam-to-carbon ratio
SCR	selective catalytic reduction
SR	steam reforming
ST	steam turbine
syngas	synthesis gas
TIT	turbine inlet temperature
UNFCCC	United Nations Framework Convention on Climate Change
VGV	variable guide vane

Chapter 1

Introduction

1.1 Project background

This project was one out of three projects in a joint PhD program within natural gas (NG) technology at Norwegian University of Science and Technology (NTNU) and Massachusetts Institute of Technology (MIT). The program was anchored within the strategic area "Energy and Petroleum – Resources and Environment" at NTNU, and the MIT Energy Initiative. Each project within the program was made up by balanced teams from MIT and NTNU consisting of a pair of PhD students supported by senior personnel. The project was sponsored by the Norwegian Research Council under the CLIMIT program, and by Statoil.

1.2 Motivation

For decades, Norway was a net exporter of clean hydro power. However, during the late 1990s Norway became a net importer of electric power, enforced by a growing demand. And, owing to recent preservation acts, further large-scale harnessing of hydro power has come to a standstill. Although the intermittent power deficiency can be covered by import, there is a growing concern for three main reasons: 1) price stability, 2) uncertainty regarding sufficiency of supply, especially in dry years, and 3) environmental issues because the marginal import of electric power is predominantly generated from coal in Poland and Denmark.

In a future perspective, the deficiency that may occur in extremely dry years could exceed the capacity of existing overseas transmission lines. This means, that the Norwegian power sector is facing a critical situation. And, despite that the energy content in the Norwegian export of gas is seven times the domestic electricity demand (2008 numbers), Norway is de facto prevented from making use of its own gas following the Kyoto protocol (1% increase of CO_2 as referred to the 1990 base line of 50 million tons CO_2 equivalents). In contrast to many countries, Norway cannot obtain any mitigating effect from fuel switching in the power sector because of the predominance of hydro power (over 99%, which is the highest fraction in the world). As any additional use of fossil fuels may contradict the Kyoto commitment, Norway is in the stricter sense left to generate electric power in systems that entirely obviate greenhouse gas emissions, or eventually, to make use of subordinate Kyoto mechanisms (JI and CDM) or otherwise make use of the quota

system under establishment within the European Union.

This unique situation calls for immediate actions aimed at resolving the future energy demand in compliance with the Kyoto accord by year 2008–2012. Hence, in order for Norway to make use of its huge gas reserves domestically, new gas power plants featuring capture and safe storage of CO_2 at acceptable cost and reasonable efficiency could be an option. This option could include exporting low-carbon power to Europe rather than exporting natural gas.

1.3 Objectives

The primary overall objective of this joint project was to promote the implementation of CO_2 reducing technologies for power generation by providing a technology and knowledge base unique for Norway. A subset of this was to develop a strategic alliance, in order to enhance excellence, between the leading technical university in Norway, NTNU, with a leading US university, MIT, and Norway's largest company, Statoil. Within this cooperation, it was decided that MIT was to focus on post-combustion capture technologies and NTNU on pre-combustion capture technologies.

Specifically for this thesis work, the objectives were:

- Process design and integration of NG pre-combustion CO_2 capture plants. The design was to include detailed study of heat recovery steam generator (HRSG) design and options.

- With the design in place for a given process, the concepts were to be *evaluated* in a transparent way by:

    1. Performing thermodynamic analyses through process simulation to arrive at, among other outputs, net plant efficiency and CO_2 capture rate. The analyses were to be performed by process simulation tools such as Aspen Plus by AspenTech, and GT PRO and GT MASTER by Thermoflow.
    2. Investigating plant flexibility both qualitatively and quantitatively. That is, trying to answer the question: *how flexible is the plant to changes in operating conditions?* Off-design simulations and evaluations were to be the key components of the plant flexibility analysis. From a qualitative standpoint, items such as dual fuel capability and operability were to be considered.
    3. Examining the potential, in terms of efficiency, of a concept while still keeping realistic process constraints. In 5–10 years, what could be the net plant efficiency of a specific process? Analysis to be performed should remain within realistic bounds but a detailed process design was not sought for.

1.4 Contribution

The main contributions of the thesis are:

1. HRSG design for NG pre-combustion cycles.

2. Plant flexibility for NG pre-combustion cycles. Specifically, off-design behavior of the integrated reforming combined cycle (IRCC). Highlighting the importance of considering off-design during the process design.

3. Process potential in terms of efficiency, i.e., answering what the potential in net plant efficiency of a specific process is within the nearest future.

4. Quantifying the efficiency losses for subsystems within an IRCC process.

5. Quantifying the uncertainty in IRCC process model outputs.

In addition to author's work, the following persons have contributed to the work presented in the thesis:

- Rahul Anantharaman, NTNU: operability analysis of IRCC presented in Paper II in Appendix B.
- Bo Gong, MIT: methodology for uncertainty analysis presented in Paper IV in Appendix B.
- Anusha Kothandaraman, MIT: hot potassium carbonate CO_2 capture subsystem used in several of the IRCC models.

1.5 Thesis organization

The thesis comprises seven chapters and four papers with analyses of four different plant configurations. Chapter 2 gives a technical background including a description of subsystems in an NG pre-combustion capture plant, and process selections for the thesis. The HRSG design selection is discussed in Section 2.4.3 and the analyzed systems are summarized in Section 2.4.8. Chapter 3 describes the methodologies used for the thesis work. In Chapter 4 the main process, an IRCC with a dual-pressure reheat HRSG, for the thesis is described and analyzed. In Chapter 5 an IRCC process with a single-pressure HRSG is presented. This cycle is also analyzed in Papers III and IV. A case with relaxed practical constraints to investigate the potential, in terms of efficiency, of a concept is presented in Chapter 6. Conclusions and suggestions for further work are given in Chapter 7. Stream data are presented in Appendix A. A process with a lower system pressure and with a triple-pressure HRSG, without air-boosting, but with a fuel compressor, is described and analyzed in Papers I and II. The four papers are located in Appendix B.

Specifically, the analyses of the four plant configuration were divided into the thesis chapters and papers as follows:

- IRCC with dual-pressure reheat HRSG (IRCC 2PR) — Chapter 4.
- IRCC with single-pressure HRSG
  - Design and off-design analyses — Paper III.
  - Uncertainty analysis — Paper IV.
  - Process with modified assumptions to compare to IRCC 2PR — Chapter 5.

- IRCC with single-pressure HRSG and relaxed practical constraints — Chapter 6.
- IRCC with triple-pressure HRSG
  - Design and off-design analyses — Paper I.
  - Reliability analysis — Paper II.

1.6 Papers published during thesis work

Paper I

Nord, L.O., Anantharaman, R., Bolland, O., 2009. Design and off-design analyses of a pre-combustion CO_2 capture process in a natural gas combined cycle power plant. International Journal of Greenhouse Gas Control 3 (4), 385–392.

In this study, a cycle designed for capturing the greenhouse gas CO_2 in a natural gas combined cycle power plant has been analyzed. The process is a pre-combustion CO_2 capture cycle utilizing reforming of natural gas and removal of the carbon in the fuel prior to combustion in the gas turbine. The power cycle consists of a H_2–fired gas turbine and a triple pressure steam cycle. Nitrogen is used as fuel diluent and steam is injected into the flame for additional NO_x control. The heat recovery steam generator includes pre-heating for the various process streams. The pre-combustion cycle consists of an air-blown auto thermal reformer, water-gas shift reactors, an amine absorption system to separate out the CO_2, as well as a CO_2 compression block. Included in the thermodynamic analysis are design calculations, as well as steady-state off-design calculations. Even though the aim is to operate a plant, as the one in this study, at full load there is also a need to be able to operate at part load, meaning off-design analysis is important. A reference case which excludes the pre-combustion cycle and only consists of the power cycle without CO_2 capture was analyzed at both design and off-design conditions for comparison. A high degree of process integration is present in the cycle studied. This can be advantageous from an efficiency stand-point but the complexity of the plant increases. The part load calculations is one way of investigating how flexible the plant is to off-design conditions. In the analysis performed, part load behavior is rather good with efficiency reductions from base load operation comparable to the reference combined cycle plant.

Paper II

Nord, L.O., Anantharaman, R., Rausand, M., Bolland, O., 2009. A qualitative reliability and operability analysis of an integrated reforming combined cycle plant with CO_2 capture. International Journal of Greenhouse Gas Control 3 (4), 411–421.

Most of the current CO_2 capture technologies are associated with large energy penalties that reduce their economic viability. Efficiency has therefore become the most important issue when designing and selecting power plants with CO_2 capture. Other aspects, like reliability and operability, have been given less importance, if any at all, in the literature. This article deals with qualitative reliability and operability analyses of an integrated reforming combined cycle (IRCC) concept. The plant reforms natural gas into a syngas,

the carbon is separated out as CO_2 after a water-gas shift section, and the hydrogen-rich fuel is used for a gas turbine. The qualitative reliability analysis in the article consists of a functional analysis followed by a failure mode, effects, and criticality analysis (FMECA). The operability analysis introduces the comparative complexity indicator (CCI) concept. Functional analysis and FMECA are important steps in a system reliability analysis, as they can serve as a platform and basis for further analysis. Also, the results from the FMECA can be interesting for determining how the failures propagate through the system and their failure effects on the operation of the process. The CCI is a helpful tool in choosing the level of integration and to investigate whether or not to include a certain process feature. Incorporating the analytical approach presented in the article during the design stage of a plant can be advantageous for the overall plant performance.

Paper III

Nord, L.O., Kothandaraman, A., Herzog, H., McRae, G., Bolland, O., 2009. A modeling software linking approach for the analysis of an integrated reforming combined cycle with hot potassium carbonate CO_2 capture. Energy Procedia 1 (1), 741–748.

The focus of this study is the analysis of an integrated reforming combined cycle (IRCC) with natural gas as fuel input. This IRCC consisted of a hydrogen-fired gas turbine (GT) with a single-pressure steam bottoming cycle for power production. The reforming process section consisted of a pre-reformer and an air-blown auto thermal reformer (ATR) followed by water-gas shift reactors. The air to the ATR was discharged from the GT compressor and boosted up to system pressure by an air booster compressor. For the CO_2 capture sub-system, a chemical absorption setup was modeled. The design case model was modeled in GT PRO by Thermoflow, and in Aspen Plus. The Aspen Plus simulations consisted of two separate models, one that included the reforming process and the water-gas shift reactors. In this model were also numerous heat exchangers including the whole pre-heating section. Air and CO_2 compression was also incorporated into the model. As a separate flow sheet the chemical absorption process was modeled as a hot potassium carbonate process. The models were linked by Microsoft Excel. For the CO_2 capture system the model was not directly linked to Excel but instead a simple separator model was included in the reforming flow sheet with inputs such as split ratios, temperatures, and pressures from the absorption model. Outputs from the potassium model also included pump work and reboiler duty. A main focal point of the study was off-design simulations. For these steady-state off-design simulations GT MASTER by Thermoflow in conjunction with Aspen Plus were used. Also, inputs such as heat exchanger areas, compressor design point, etc., were linked in from the Aspen Plus reforming design model. Results indicate a net plant efficiency of 43.2% with approximately a 2%-point drop for an 80% part load case. Another off-design simulation, at 60% load, was simulated with a net plant efficiency around 39%. The CO_2 capture rate for all cases was about 86%, except for the reference case which had no CO_2 capture.

Paper IV

Nord, L.O., Gong. B., Bolland, O., McRae, G.J., in press. Incorporation of uncertainty analysis in modeling of integrated reforming combined cycle. Energy Conversion and Management.

A systematic approach to quantify uncertainties in an integrated reforming combined cycle (IRCC) process model employing CO_2 capture is presented. IRCC involves reforming of natural gas into a hydrogen-rich fuel which is then used as gas turbine fuel. Included in an IRCC plant is also a steam bottoming cycle. The analysis treats uncertain parameters as random variables whose probability distributions are estimated from limited existing information using entropy maximization. Uncertainties of model parameters were propagated through the process model using the deterministic equivalent modeling method as a computationally efficient alternative to Monte Carlo simulations. The method also quantifies the effect of each parameter on the total uncertainty of model outputs. The IRCC process model was evaluated in terms of four performance metrics: (1) net plant power output, (2) net plant efficiency, (3) CO_2 capture rate, and (4) CO_2 emitted per kWh of generated electricity. Simulation results showed that there was considerable uncertainty in the predicted net power output whereas the other three variables were less affected by input uncertainties. The IRCC plant was predicted to have a median net plant efficiency of 43.4% with a standard deviation of 0.5%, representing a loss of approximately 13%-points compared to a natural gas combined cycle plant without CO_2 capture. Results also indicated that the probability of meeting the requirement of at least 85% CO_2 capture rate for the plant was approximately 95%. Parameters with the largest impact on uncertainties of power output and efficiency predictions proved to be gas turbine inlet temperature, and compressor and turbine efficiencies. For the CO_2 emissions, the equipment pressure drop and the steam-to-carbon ratio proved important. Therefore, the focus of future work should be to reduce uncertainties in these parameters in order to improve the confidence of the IRCC model.

Chapter 2

Technical background

2.1 Climate change and CO_2 emissions

Carbon dioxide, methane, and other greenhouse gases are on the rise and are contributing to the warming of the atmosphere due to the greenhouse effect. Natural causes can only explain part of this global warming effect. Fossil fueled power generation, transportation, industrial processes, and other man-made greenhouse gas emission sources add to the picture. So does, but to a lesser extent, land use change. One thing is certain; the planet is heating up.

Fig. 2.1 shows plotted data from the combined global land and marine surface temperature record from 1850 to 2008 (Brohan et al., 2006). This time series is being compiled jointly by the Climatic Research Unit and the UK Met. Office Hadley Centre. The year 2008 was tenth warmest on record. The 1990s were the warmest decade in the series. The warmest year of the entire series has been 1998, with a temperature of about 0.5 °C above the 1961–90 mean. Thirteen of the fourteen warmest years in the series have now occurred in the past fourteen years (1995–2008). The only year in the last fourteen not among the warmest fourteen is 1996 (replaced in the warm list by 1990). The period 2001–2008 (about 0.4 °C above 1961–90 mean) is about 0.2 °C warmer than the 1991–2000 decade (about 0.2 °C above 1961–90 mean). These records represent how the climate is changing globally. Locally, the variations can be much larger, notably in the Arctic region (Overpeck et al., 1997; Johannessen et al., 2004; ACIA, 2005).

The CO_2 level in the atmosphere is increasing. The carbon dioxide concentration, measured as the mole fraction in dry air, on Mauna Loa, Hawaii constitute the longest record of direct measurements of CO_2 in the atmosphere. Data from the observatory are displayed in Fig. 2.2. The average Mauna Loa CO_2 level for 2008 was 386 ppmvd (based on the monthly averages). The measurements were started by C. David Keeling of the Scripps Institution of Oceanography in March of 1958 at a facility of the National Oceanic and Atmospheric Administration (Keeling et al., 1976). NOAA started its own CO_2 measurements in May of 1974, and they have run in parallel with those made by Scripps since then (Thoning et al., 1989).

For a much longer time frame, data from the Vostok ice core provide an insight to the variations in CO_2 levels and temperatures for the past four glacial-interglacial cycles. In January 1998, the collaborative ice-drilling project between Russia, the United States, and France at the Russian Vostok station in East Antarctica yielded the deepest ice core ever recovered, reaching a depth of 3,623 m (Petit et al., 1999). Data from this project

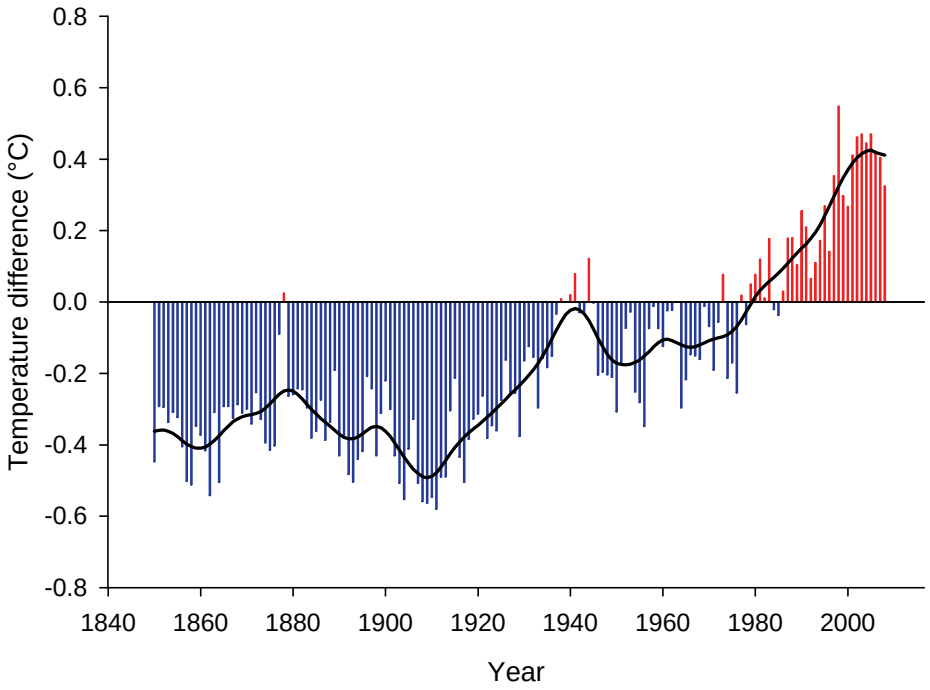

Figure 2.1: Combined global land and marine surface temperature record from 1850 to 2008. The temperature difference is defined as the difference from the 1961–90 mean. Based on Brohan et al. (2006).

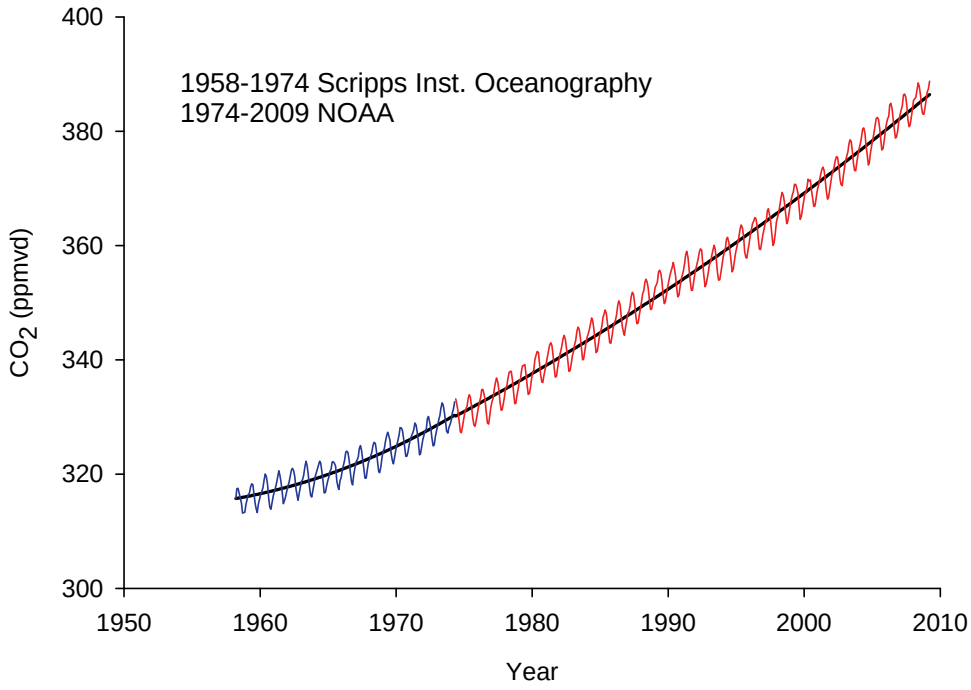

Figure 2.2: Monthly mean atmospheric carbon dioxide at Mauna Loa Observatory, Hawaii.

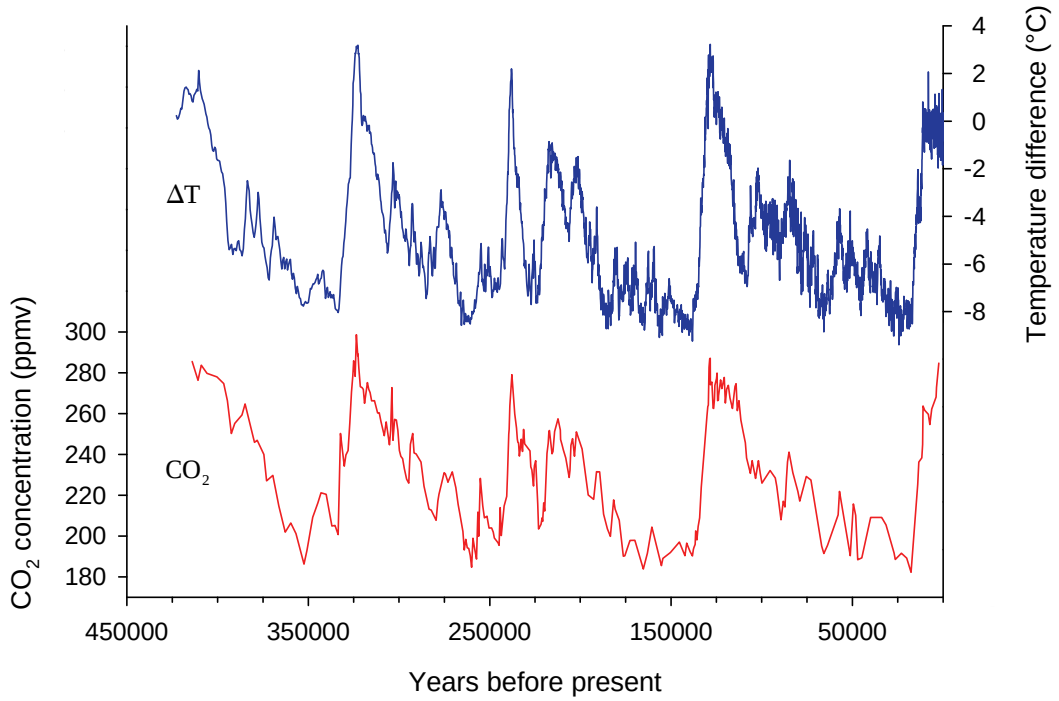

Figure 2.3: Vostok ice core data for 420,000 years. Atmospheric CO_2 concentrations from trapped gas bubbles. Antarctic ambient temperature difference with respect to the mean recent time value. Data from Petit et al. (2001), Vostok Ice Core Data for 420,000 Years, IGBP PAGES/World Data Center for Paleoclimatology Data Contribution Series #2001–076. NOAA/NGDC Paleoclimatology Program, Boulder, CO, USA.

are displayed in Fig. 2.3. The authors conclude, among other things, that atmospheric concentrations of carbon dioxide and methane correlated well with Antarctic air temperature throughout the record. Present day atmospheric burdens of these two important greenhouse gases seem to have been unprecedented during the past 420,000 years.

Table 2.1 shows the global warming potential (GWP) for the three most important greenhouse gases (excluding water vapor). The data are based on IPCC's fourth assessment report (Intergovernmental Panel on Climate Change, 2007). The GWP numbers use CO_2 as baseline, which has been appointed a GWP of 1.

It can be seen that methane and nitrous oxide have a higher GWP than carbon dioxide, however, when comparing the emissions of these gases, as displayed in Table 2.2, it is clear that the overall impact of carbon dioxide as a greenhouse gas is greater. The data

Table 2.1: Global warming potential for carbon dioxide, methane, and nitrous oxide. Data from IPCC's Fourth Assessment Report: Climate Change 2007: The Physical Science Basis.

Gas	Composition	Global Warming Potential 100 years time horizon
Carbon dioxide	CO_2	1
Methane	CH_4	25
Nitrous oxide	N_2O	298

Table 2.2: Greenhouse gas emissions 2006 in CO_2 equivalent. Data based on UNFCCC's 1990 to 2006 compilation of Annex I GHG emission data (FCCC/SBI/2008/12).

Gas	Composition	Greenhouse gas emissions 2006 from UNFCCC Annex I Parties* (million tons CO_2 equivalent)
Carbon dioxide	CO_2	14 860
Methane	CH_4	2 200
Nitrous oxide	N_2O	1 280

* UNFCCC Annex I Parties are in principle the industrialized countries of the world.

Table 2.3: World energy related carbon dioxide emissions by sector for the year 2006. Data from IEA's World Energy Outlook 2008.

Source	CO_2 emissions 2006 (million tons)	CO_2 emissions 2006 (% of total CO_2 emissions)
Power generation	11 400	41
Transport	6 400	23
Industry	4 600	16
Residential and services*	3 300	12
Other	2 200	8
Total	27 900	100

* Includes agriculture.

in Table 2.2 are based on UNFCCC's 1990 to 2006 compilation of Annex I greenhouse gas emission data (United Nations Framework Convention on Climate Change, 2008). The greenhouse gas emission equivalents have been recalculated with the GWPs per Table 2.1. It should be noted that even though the data are from the industrialized countries only, they should be a good indication of the world methane and nitrous oxide emissions in relation to carbon dioxide.

Where does the emissions of CO_2 originate from? The sources of energy related carbon dioxide emissions are shown in Table 2.3 (International Energy Agency, 2008). As can be seen, about 41% originates from the power generation sector. This sector represents the largest CO_2 emitter.

To sum it up:

- the temperature in the atmosphere is rising
- natural causes can only explain part of the warming
- there is a strong coupling between atmospheric temperature and greenhouse gas levels
- CO_2 is the predominant greenhouse gas
- the power sector is the largest CO_2 emitter

Thus, if one tries to control and limit the emission of greenhouse gases and thereby attenuating the rise in atmospheric temperature, CO_2 capture from fossil fuel power plants can be a viable path. In addition to the points above, a power station is a stationary source (in contrast to the transport sector), which would make capture less complicated than for a mobile source.

2.2 CO_2 capture from fossil fuel power plants

The methods for capture of CO_2 from fossil fuel power generation sources can be divided into three main categories:

1) Post-combustion capture, where the CO_2 is captured at the tail end of the plant from the flue gases, i.e., after the combustion. Capture of CO_2 from the flue gases of a power plant may be the best option for capture retrofit of existing power plants. It is also a viable option for new plants. The currently preferred option is capture by absorption processes based on chemical solvents and have been implemented in a number of pilot projects worldwide for CO_2 capture purposes, for example, the Castor pilot project in Denmark (Le Thiez et al., 2004; Knudsen et al., 2006), and the Boundary Dam pilot plant in Canada (Wilson et al., 2004). However, the technology has not reached the large scale needed for a full-scale installation in a fossil fuel fired power plant.

The chemical absorption process is based on the reversible reaction of an aqueous alkaline solvent, typically an amine, with an acidic gas, in this case CO_2. Many different types and mixes of amines have been suggested for CO_2 capture (Chapel and Mariz, 1999). An example of a process flow sheet for chemical absorption by the amine MEA is displayed in Fig. 2.4. In addition to amines, the interest for using ammonia as a solvent has been increasing (Resnik et al., 2004). Alstom, the Electric Power Research Institute, and We Energies have built a pilot plant in Pleasant Prairie, Wisconsin, USA. The pilot system, that utilizes chilled ammonia, captures CO_2 from a portion of the boiler flue gas. Also, potassium and sodium based solutions are alternatives as absorbents. One example is the Benfield^{TM} process which uses an activated, inhibited, hot potassium carbonate solution to remove CO_2, H_2S, and other acid gas components (Bartoo, 1984). This technology is currently applied to synthesis gas (syngas) and natural gas treating. Other post-combustion options include capture by physical absorption, adsorption, membranes, solid sorbents, and the use of cryogenic cooling.

The methods could be used for both natural gas and coal fired plants although the conditions for capture would differ significantly. Firstly, the CO_2 content in the flue gases differ, from as low as 3–4 vol% dry for a gas turbine (GT) and up towards 14–15 vol% dry for a coal fired plant. Secondly, the flue gases from coal combustion contain more pollutants that requires cleanup before entering the post-combustion CO_2 capture process. For both natural gas and coal fired plants one of the main challenges with post-combustion capture is the handling of the massive volume of flue gases at a pressure close to ambient. From a single 260 MW gas turbine, the exhaust volume flow can be around 6 million m^3/h.

2) Pre-combustion capture, where the fossil fuel is used for producing a syngas and the carbon (as CO_2) is separated before the combustion takes place. There exist many possible configurations for a pre-combustion plant (Eide and Bailey, 2005). One such process is the IRCC. The IRCC process reforms natural gas to a syngas, converts the CO to CO_2 in the water-gas shift reactors, separates the CO_2 in the capture subsystem,

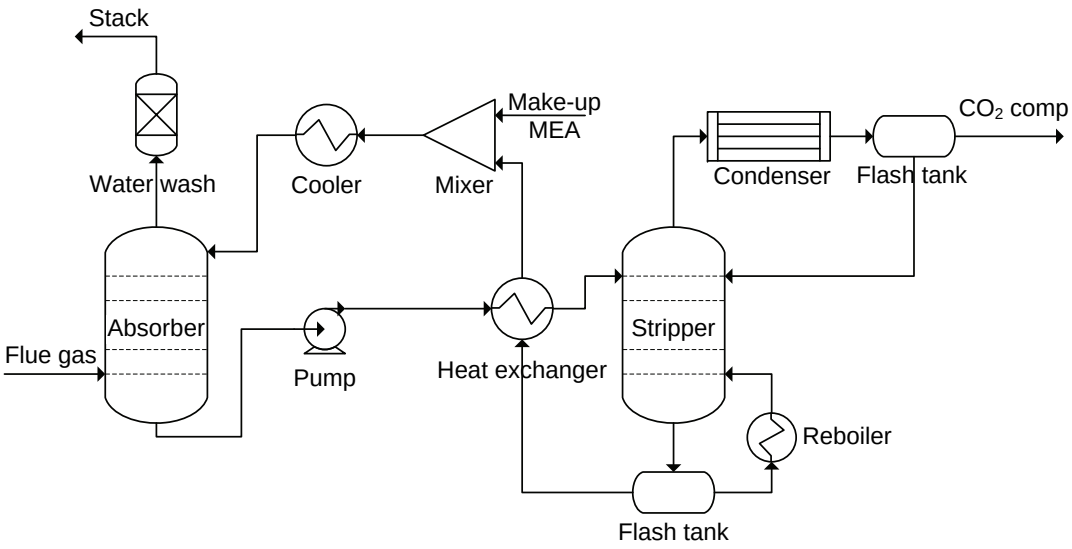

Figure 2.4: Process flow diagram of an example of a post-combustion CO_2 capture cycle.

and the resulting hydrogen-rich fuel is used for the gas turbine in a combined cycle setup. The CO_2 is compressed and stored. Many options exist for the CO_2 separation. One alternative is to use a chemical absorption system utilizing a hot potassium carbonate solution (e.g., see Kohl and Nielsen, 1997). A simplified process schematic of a natural gas pre-combustion setup is shown in Fig. 2.5. In the schematic, the water-gas shift section has been included in the reforming box. Notable in a natural gas pre-combustion setup is the amount of steam produced from heat generated in the reforming process. This is indicated with H_2O streams between the power island and reforming blocks in Fig. 2.5. This steam, which is generated external to the power island, has implications on the design of the HRSG as presented in Section 2.3.4.

An existing technology for power plant applications, the integrated gasification combined cycle (IGCC), could be attractive as part of a coal based pre-combustion CO_2 capture method (e.g., see Bohm et al., 2007).

3) Oxy-fuel combustion, where the oxidizer for the combustion is oxygen instead of air. The advantage of this is the omittance of nitrogen from the air. Without the nitrogen, the combustion products are essentially carbon dioxide and steam, plus some excess oxygen,

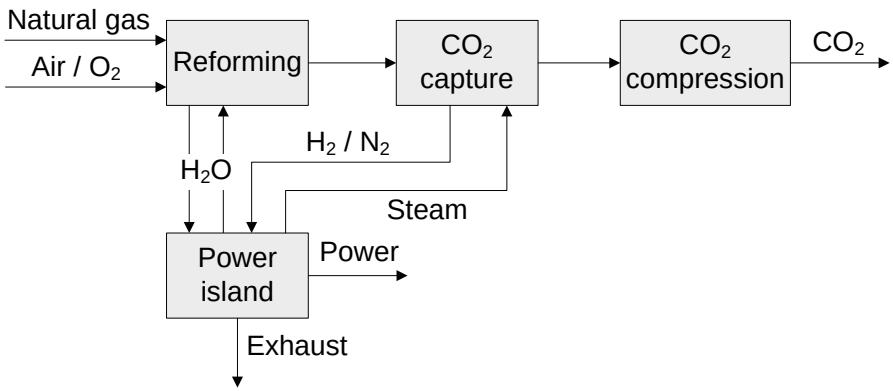

Figure 2.5: Schematic of natural gas pre-combustion capture.

and the CO_2 can be separated by condensing the steam. Many proposals for cycle configurations have been suggested in the oxy-fuel category. Examples include the Graz cycle (Jericha et al., 2004), the Matiant cycle (Mathieu and Nihart, 1999), the advanced zero emissions power plant (Griffin et al., 2005), and chemical looping combustion (Richter and Knoche, 1983; Ishida and Jin, 1994).

The main disadvantage in an oxy-fuel seup is the need for large amounts of pure oxygen. An air separation unit (ASU) would significantly add cost and complexity to the plant. Oxygen could also be supplied by internal air separation as, e.g., with the advanced zero emissions power plant and the chemical looping combustion process. Another obstacle to overcome is the high combustion temperatures when burning a hydrocarbon with oxygen. This can be alleviated by recycling some of the flue gases back into the combustor, or by injecting water or steam.

2.3 Pre-combustion capture: description of subsystems

Since the focus of the thesis is on pre-combustion processes, with natural gas as fuel input, a description of the subsystems in a natural gas pre-combustion process is presented in this section.

2.3.1 Reforming of natural gas

There are three main commercially available alternatives for reforming of natural gas in an IRCC:

1. Steam reforming (SR), where a secondary supply of fuel provides heat for the steam reforming reaction.

2. Non-catalytic partial oxidation reforming (POX), where the hydrocarbon stock is converted by substoichiometric combustion.

3. Autothermal reforming, where some of the hydrocarbon fuel is combusted (substoichiometric) to provide heat for the steam reforming catalytic reaction.

A combination of the above options is also possible (SR+ATR combination is common in methanol plants). In addition to the commercially available technologies, reforming in a membrane reactor could be an alternative for the future.

Steam reforming

In steam reforming (Lozza and Chiesa, 2002b), the hydrocarbon reacts with the steam to form CO and H_2 according to endothermic reaction

$$C_xH_y + xH_2O_{(g)} \rightleftharpoons xCO + (x + \frac{y}{2})H_2 \qquad -\Delta H^0_{298} < 0\,\text{kJ/mol} \tag{2.1}$$

For methane this reaction would be

$$CH_4 + H_2O_{(g)} \rightleftharpoons CO + 3H_2 \qquad -\Delta H^0_{298} = -206\,\text{kJ/mol} \tag{2.2}$$

This steam reforming reaction is often utilizing a nickel-based catalyst. Because of contamination of the catalyst, sulfur compounds from the fuel need to be removed before the reforming reaction. A secondary supply of fuel is needed for the high temperature (700–900 °C) endothermic reforming reaction (2.2). This secondary fuel supply can consist of natural gas, hydrogen, or a combination of exhaust gases (from the gas turbine or the reformer itself) and hydrogen. In addition to the reforming reaction, the water-gas shift reaction will also take place in the reformer

$$CO + H_2O_{(g)} \rightleftharpoons CO_2 + H_2 \qquad -\Delta H^0_{298} = 41\,\text{kJ/mol} \tag{2.3}$$

Partial oxidation

The POX process (Lozza and Chiesa, 2002a) relies on the substoichiometric exothermic reaction between oxygen and the fuel

$$C_xH_y + \frac{x}{2}O_2 \rightarrow xCO + \frac{y}{2}H_2 \qquad -\Delta H^0_{298} > 0\,\text{kJ/mol} \tag{2.4}$$

The temperature for the reaction is typically in the range of 1250–1400 °C. The heat for the reaction is completely supplied by the reacting fuel, meaning no secondary fuel supply is needed. The oxygen can be supplied as pure oxygen, from air, or internally via an oxygen transport membrane (OTM) or an oxygen ion transport membrane (ITM). If the pure oxygen option is selected, an ASU is needed. This would increase the cost of the plant significantly but has the advantage of avoiding the airborne nitrogen. This, in turn, would simplify the separation of the CO_2 after the water-gas shift section.

Autothermal reforming

In autothermal reforming (Christensen and Primdahl, 1994; Dybkjær, 1995; Christensen et al., 1998) the reactor is divided into a combustion zone and a thermal and catalytic zone. The heat generated from burning natural gas in the combustion zone provides heat for the reforming in the thermal and catalytic zone. Simplified, one can consider substoichiometric combustion of a hydrocarbon with the overall reaction

$$C_xH_y + \frac{x + y/2}{2}O_2 \rightarrow xCO + \frac{y}{2}H_2O_{(g)} \qquad -\Delta H^0_{298} > 0\,\text{kJ/mol} \tag{2.5}$$

Specifically, for methane

$$CH_4 + \frac{3}{2}O_2 \rightarrow CO + 2H_2O_{(g)} \qquad -\Delta H^0_{298} = 519\,\text{kJ/mol} \tag{2.6}$$

In the thermal and catalytic zone, below the combustion zone, the main reactions are the water-gas shift reaction (2.3) and the hydrocarbon-steam reforming reaction (2.1). No secondary fuel is supplied. As for the POX process the oxygen can be supplied as pure oxygen, from air, or internally via an OTM or ITM. Operating temperature is typically in the range of 850–1100 °C.

Reforming in membrane reactor

Studies on introducing membranes into the reforming process have been conducted (Abashar, 2004; Jordal et al., 2004). The main purpose of introducing a membrane in the reforming process would be to shift the equilibrium of reaction (2.1) or reaction (2.4) depending on the type of reformer. This would lead to higher conversion rates. One could also combine the process into one stage, meaning the reforming, water-gas shift, and CO_2-H_2 separation would take place in the same reactor. Then the equilibrium of the water-gas shift reaction (2.3) would also shift. Either a CO_2 or an H_2 permeating membrane could be used. Another advantage is that the temperature could be kept lower than with a more conventional reforming process. Disadvantages would be that this is novel technology with all the issues related to that. Also, one is limited to the current performance of membranes, although material research is continuously pushing the limits towards better performing membranes at reduced cost.

Prereforming

An adiabatic prereformer are sometimes utilized for converting higher hydrocarbons than methane (Vannby and Winter Madsen, 1992; Verduijn, 1993; Sperle et al., 2005). This is mainly done to prevent coking in preheaters and in the following reformer(s). For ATR applications, a prereformer is needed when operating at low steam-to-carbon ratio (S/C) or with high preheat temperatures. This is especially true for heavy-hydrocarbon stocks such as naphtha (Christensen and Primdahl, 1994). A nickel-based catalyst is typically used for the catalytic bed in a prereformer.

2.3.2 Water-gas shift

To achieve high CO conversion, the water-gas shift, per reaction (2.3), is divided into a high-temperature shift reactor (HTS) and a low-temperature shift reactor (LTS). Due to the temperature driving force in the HTS, the shift reactor size can be kept smaller. However, the conversion would be too low if only using an HTS. Therefore, an LTS with a lower temperature and a more active catalyst is added. The main alternative would be to have one medium-temperature shift reactor (Eide and Bailey, 2005).

One could also imagine the use of an integrated membrane shift reactor (Yegani et al., 2007). As described in Section 2.3.1, the equilibrium of reaction (2.3) would be shifted towards the products. Both CO_2 and H_2 membranes are possible in such a system.

2.3.3 CO_2 capture

The gas separation techniques for pre-combustion CO_2 capture are essentially the same as the post-combustion techniques described in Section 2.2. The difference lies in the gas composition, flow, and pressure at the inlet of the capture subsystem.

2.3.4 Heat recovery steam generator

The design of the HRSG for the IRCC process was different from an HRSG design in a natural gas combined cycle (NGCC) plant because of the significant amount of steam production from the heat generated in the reforming process. In addition, preheating

(within the HRSG) of some of the process streams could add to the complexity in HRSG design. Also, the plant should be able to operate on natural gas as backup fuel for the GT, that is, in NGCC mode. This is important during startup but also when problems in the reforming or CO_2 capture sections occur. A failure mode, effects, and criticality analysis, presented in Paper II, showed that many failures in an IRCC can lead to plant shutdown (if no backup fuel).

External high-pressure evaporator

For an NGCC plant, a triple-pressure reheat cycle would yield the highest net plant efficiency as is displayed in Fig. 2.6. However, when generating a significant amount of high-pressure (HP) steam external to the HRSG, the picture changes. Fig. 2.7 indicates that a single-pressure system actually performed in parity with a triple-pressure reheat system when more than 60 kg/s of saturated HP steam was generated externally (40% of the total HP steam mass flow). The actual mass flow numbers would vary from case to case, but the key point is that a single-pressure system could yield just as high plant efficiency as a dual- or triple-pressure reheat system when a lot of steam is generated external to the HRSG. Note that the efficiency numbers in Fig. 2.7 only have meaning for 0 kg/s external steam generation since the external steam was considered "free of charge" in the HRSG simulation cases, that is, the externally generated process steam was added to the HRSG without considering the energy required to produce the steam. The purpose of Fig. 2.7 is rather to show the relative relation between different HRSG designs when process steam is available, as it is in a typical IRCC setup. The range of externally evaporated HP steam mass flow, in the various simulations within the thesis, is indicated in Fig. 2.7.

To show the difference between the HRSG options, a T-Q diagram, displaying temperature versus heat transferred for the HRSG flue gas and the water/steam cycle, is illustrative. For the single-pressure system, whose T-Q diagram is displayed in Fig. 2.8, the low-grade heat available in the gas stream was not utilized as well as it could be. As displayed in Fig. 2.8, the flue gas stack temperature (at the 0 MW heat transfer point) was higher than what was required when considering the acid dew point. To keep a sufficient margin to the acid dew point, a stack temperature lower limit of 70 °C was established. For the single pressure system, without any external steam generation, the stack temperature was approximately 140 °C as is shown in Fig. 2.8. This means there was a significant amount of unutilized heat in the flue gas, which was the main reason for the lower net electrical efficiency compared to, for example, a dual-pressure reheat system. A T-Q diagram for a dual-pressure reheat system is displayed in Fig. 2.9. The two pressure levels allowed for better utilization of the low-grade heat in the flue gas. However, as apparent in Fig. 2.10, the situation for the single-pressure system is quite improved when generating 70 kg/s of external HP steam. Now, the low-grade heat in the gas stream can be better utilized and the hot and cold curves are closer together. If studying the total heat transferred from the hot gases in Figs. 2.8 and 2.10, it increased from around 370 MW to 420 MW. In addition, the hot and cold curves are closer together, which is an advantage from an exergy standpoint. By minimizing the distance between the hot and cold curves the irreversibilities in the heat exchange are lower. For the dual-pressure reheat system there was also an improvement in the HRSG T-Q diagram when generating external HP steam, as is displayed in Fig. 2.11. But the improvement was not

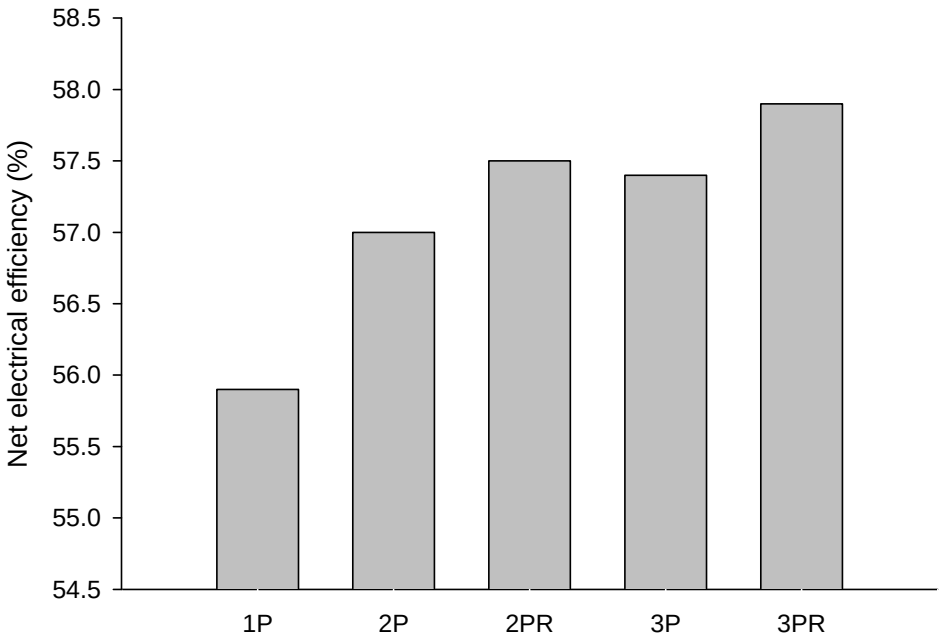

Figure 2.6: Net electrical efficiency (including transformer losses) for combined cycle plants with GE 9FB gas turbine. Steam cycles include: single-pressure (1P), dual-pressure (2P), dual-pressure with reheat (2PR), triple-pressure (3P), and triple-pressure with reheat (3PR).

as pronounced, as can be seen from the slopes in Fig. 2.7. The single-pressure system improvement was steeper than for other HRSG alternatives, up to a certain point. After about 70 kg/s externally generated steam, the slopes are similar between the different HRSG options. This is because at that flow point the lower stack temperature limit had been reached for the single-pressure system and no more heat could be transferred from the flue gas. The only improvement from this point and higher external flows was the added steam flow from the external source and hence, the improvements would be similar for all HRSG options.

External high-pressure economizer and evaporator

If, in addition to the external HP evaporator, an external HP economizer was used, the results were different. Fig. 2.12 shows the effect on net plant efficiency when HP water was transferred to an external economizer *and* evaporator. It was here assumed that the same amount of water was economized as was evaporated. The dual-pressure reheat system showed a higher net plant efficiency for all levels of external economizing and boiling. The low-grade heat of the HRSG flue gas could not be utilized in the single-pressure system if a large part of the economizing took place outside the HRSG even when an external evaporator was present. To illustrate this, a T-Q diagram for a single-pressure system when 70 kg/s of water was economized and evaporated externally is shown in Fig. 2.13. In this case, only about 360 MW of the heat available in the flue gas was transferred to the water/steam cycle and the stack temperature was as high as 160 °C. For a dual-pressure reheat system the low-grade heat could be utilized because of the second (lower) steam pressure level.

The net plant efficiency numbers were higher for the single-pressure system in Fig. 2.12 compared to the system in Fig. 2.7 for high external steam mass flows (above 70 kg/s).

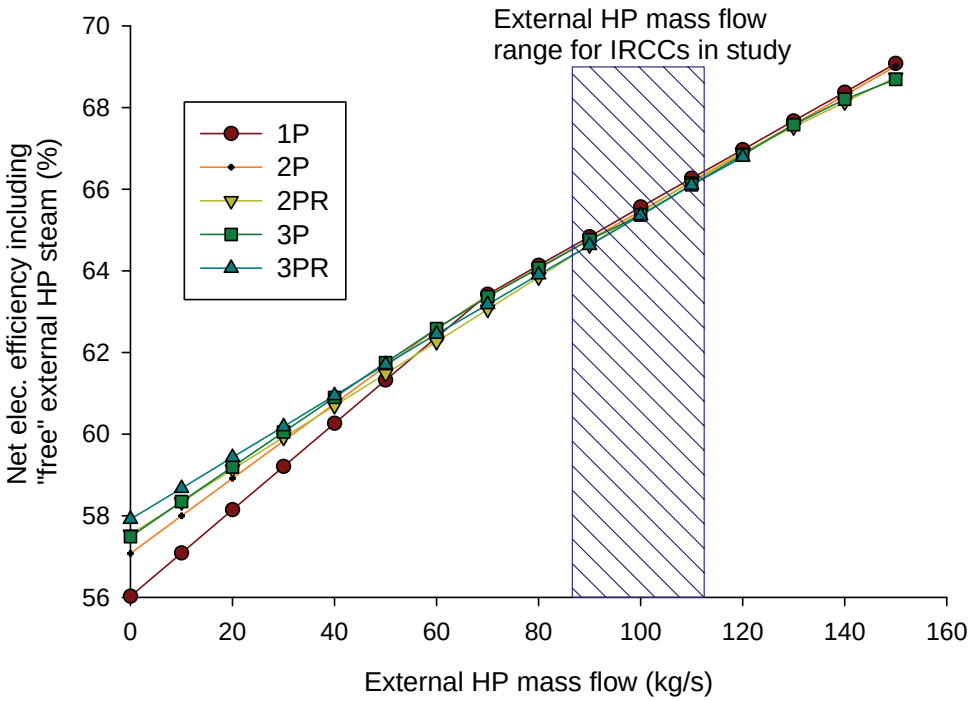

Figure 2.7: Natural gas fired combined cycle plant with external HP steam generation. For reference, 90 kg/s (2PR, 3PR) and 105 kg/s (1P, 2P, 3P) of steam was generated in HRSG evaporator at the 0 kg/s external HP steam mass flow point.

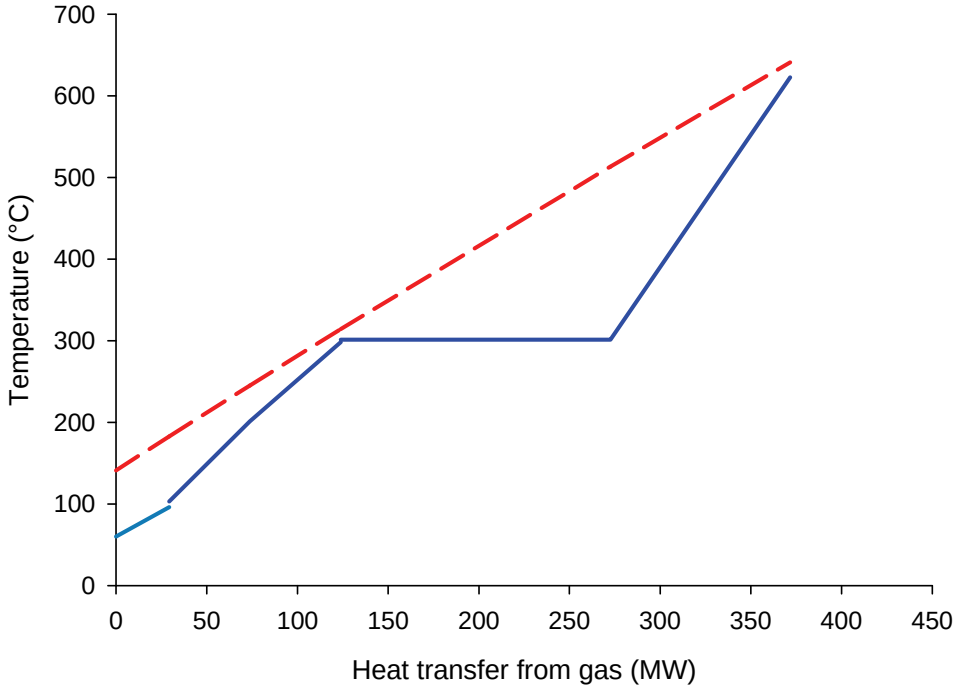

Figure 2.8: T-Q diagram for single-pressure HRSG without external HP steam generation. Dashed lines refer to HRSG flue gas, solid lines to water/steam cycle.

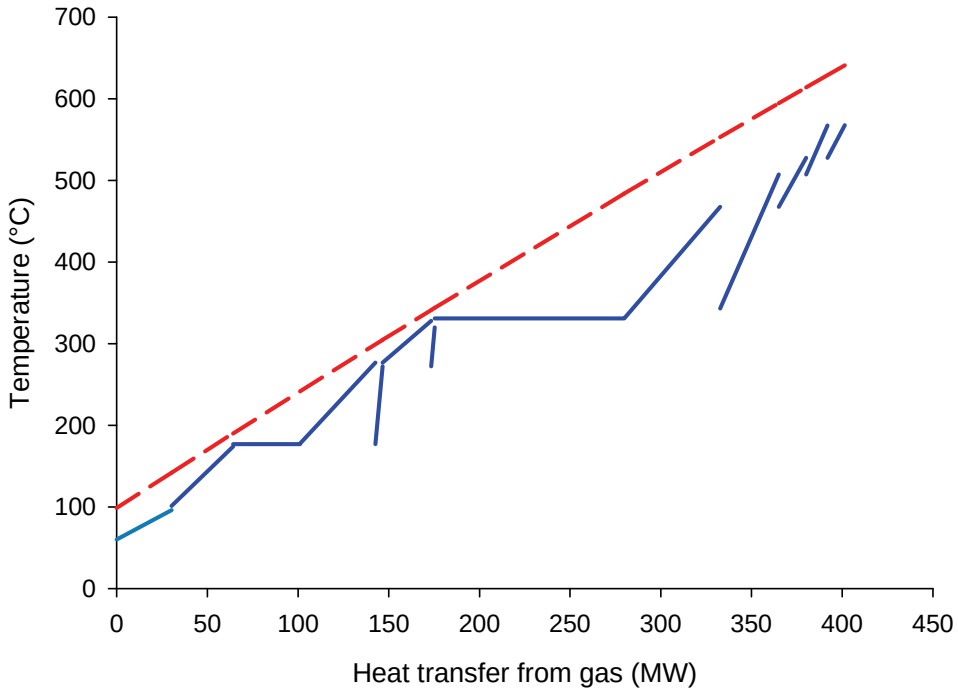

Figure 2.9: T-Q diagram for dual-pressure reheat HRSG without external HP steam generation. Dashed lines refer to HRSG flue gas, solid lines to water/steam cycle.

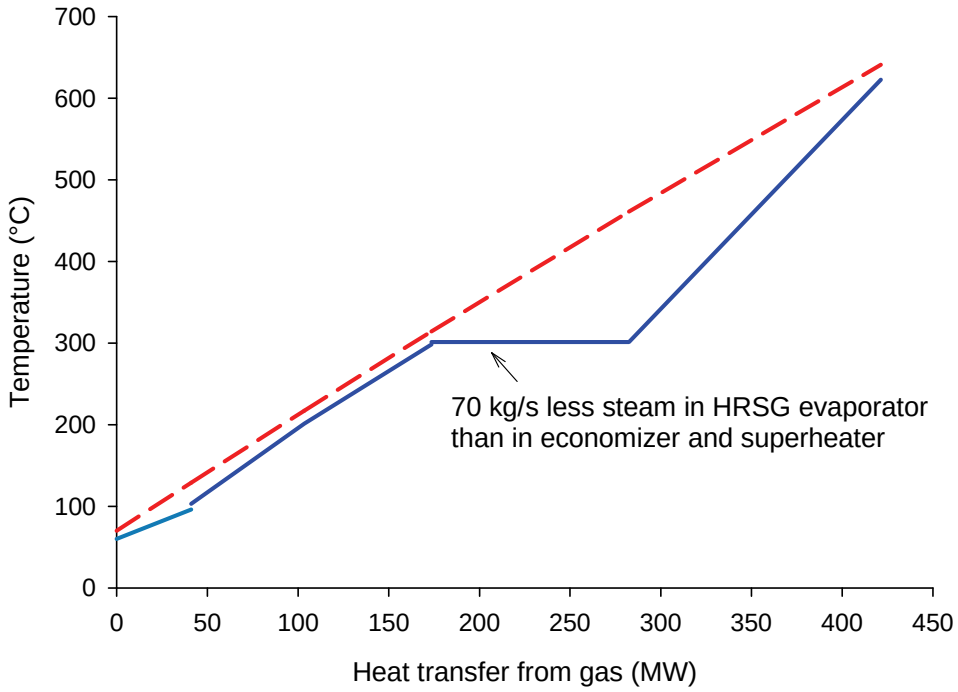

Figure 2.10: T-Q diagram for single-pressure HRSG with 70 kg/s of external HP steam generation. Dashed lines refer to HRSG flue gas, solid lines to water/steam cycle.

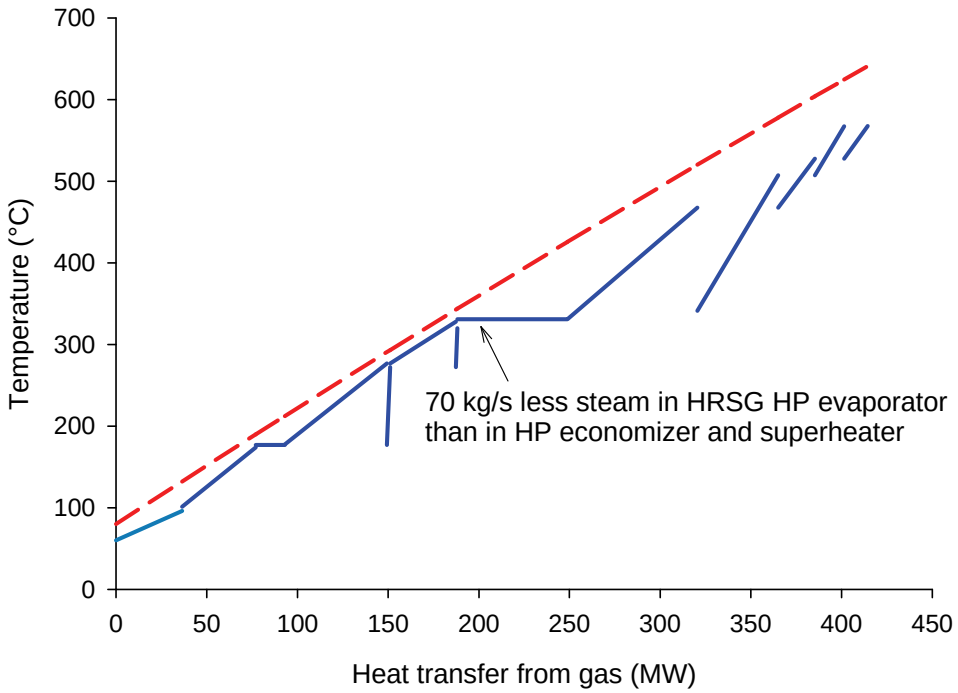

Figure 2.11: T-Q diagram for dual-pressure reheat HRSG with 70 kg/s of external HP steam generation. Dashed lines refer to HRSG flue gas, solid lines to water/steam cycle.

This may be surprising since the energy was added (from external economizer) below the original pinch point (at the evaporator inlet on the water side). If the pinch point location would remain the same no more HRSG steam could be generated if energy (in this case in terms of external economizing) is added below the pinch and hence, the net plant efficiency would not be higher in Fig. 2.12 than in Fig. 2.7. However, due to the minimum allowed stack temperature of 70 °C the pinch point moved to the exhaust end of the HRSG, as is displayed in Fig. 2.10. This meant, more total steam flow could be generated in a single-pressure system if an external economizer was used when the external steam mass flow was sufficiently high compared to a single-pressure system with only an external evaporator. The pinch point is defined as the temperature at which the heat flow is zero.

Steam pressure levels

The steam pressure levels within a certain HRSG setup were to be selected based on several criteria:

- material constraints
- steam quality after steam turbine (ST)
- net plant efficiency
- process needs (process steam pressure levels)
- plant complexity
- flexibility: dual fuel capability

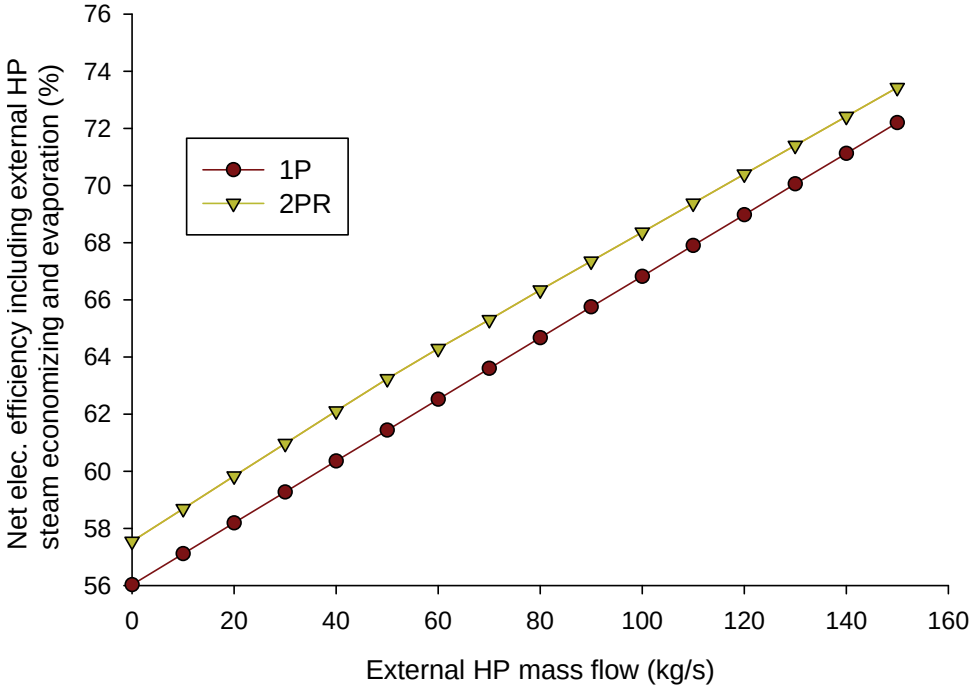

Figure 2.12: Natural gas fired combined cycle plant with external HP economizer and evaporator. For reference, 90 kg/s (2PR, 3PR) and 105 kg/s (1P, 2P, 3P) of steam was generated in HRSG evaporator at the 0 kg/s external HP steam mass flow point.

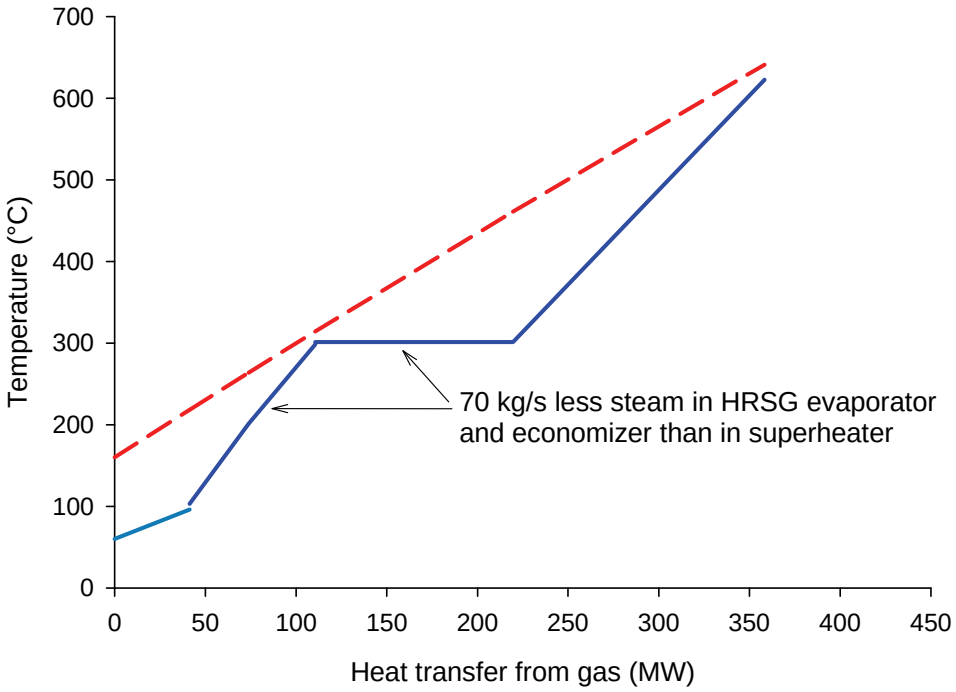

Figure 2.13: T-Q diagram for single-pressure HRSG with 70 kg/s of external HP steam economizing and evaporation. Dashed lines refer to HRSG flue gas, solid lines to water/steam cycle.

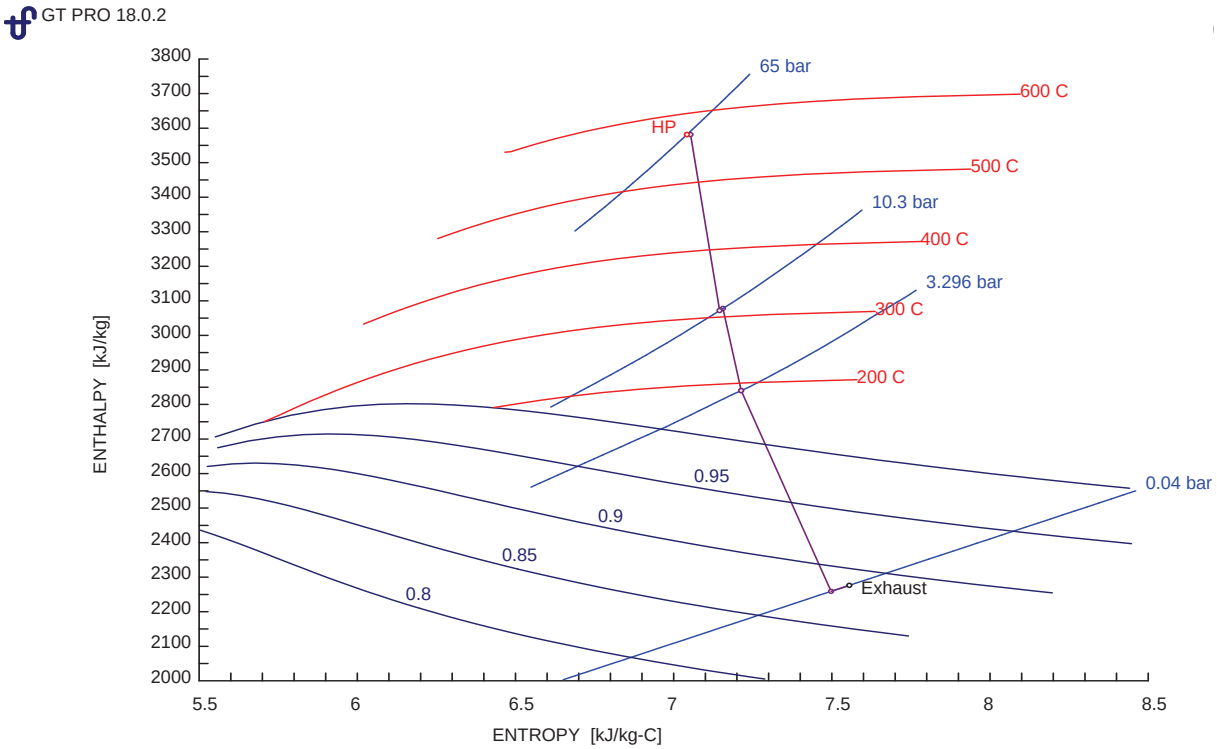

Figure 2.14: Steam expansion path in an h-s diagram for a single-pressure steam cycle with a steam pressure of 65 bar.

There were material limitations in respect to temperature. This limitation determined the maximum superheating temperature for the system. For an HRSG without reheating, the temperature limitation could affect the pressure level selection since lowering the superheating temperature, for the same pressure level, decreases the ST outlet steam quality. To avoid erosion of the last turbine stage the steam quality should preferably not be below 0.88 when it exits the ST (Alvarez, 1990). Kehlhofer et al. (1999) mention a limit of 0.84. This restriction did affect the selection of pressure levels and the steam expansion path needed to be considered. Steam expansion paths for two single-pressure cycles (with the same assumptions except for the HP steam pressure level) are shown in Fig. 2.14 and 2.15. Higher HP steam pressure levels for the same superheating temperature led to a lower steam quality in the ST exhaust as is shown in Fig. 2.15. For the system, whose steam expansion path is displayed in Fig. 2.14, the ST exit steam quality was 0.879. For the system, whose steam expansion path is displayed in Fig. 2.15, the ST exit steam quality was 0.866. For reheat cycles this restriction is not an issue since a high reheat temperature at an intermediate pressure level leads to a higher steam quality in the low-pressure (LP) turbine exhaust. The steam expansion path for a dual-pressure reheat cycle is shown in Fig. 2.16 with an exit steam quality of 0.916.

Net plant efficiency was one of the most important criteria in respect to selection of steam cycle pressure levels. Fig. 2.17 displays the net plant efficiency as a function of the HP steam pressure level for a dual-pressure reheat cycle. In the analysis, all other input parameters were kept constant. It is clear from Fig. 2.17 that as high HP steam pressure level as possible was desirable if only considering the net plant efficiency. However, at some point the solution becomes prohibitively expensive for increasing pressure levels. The cost

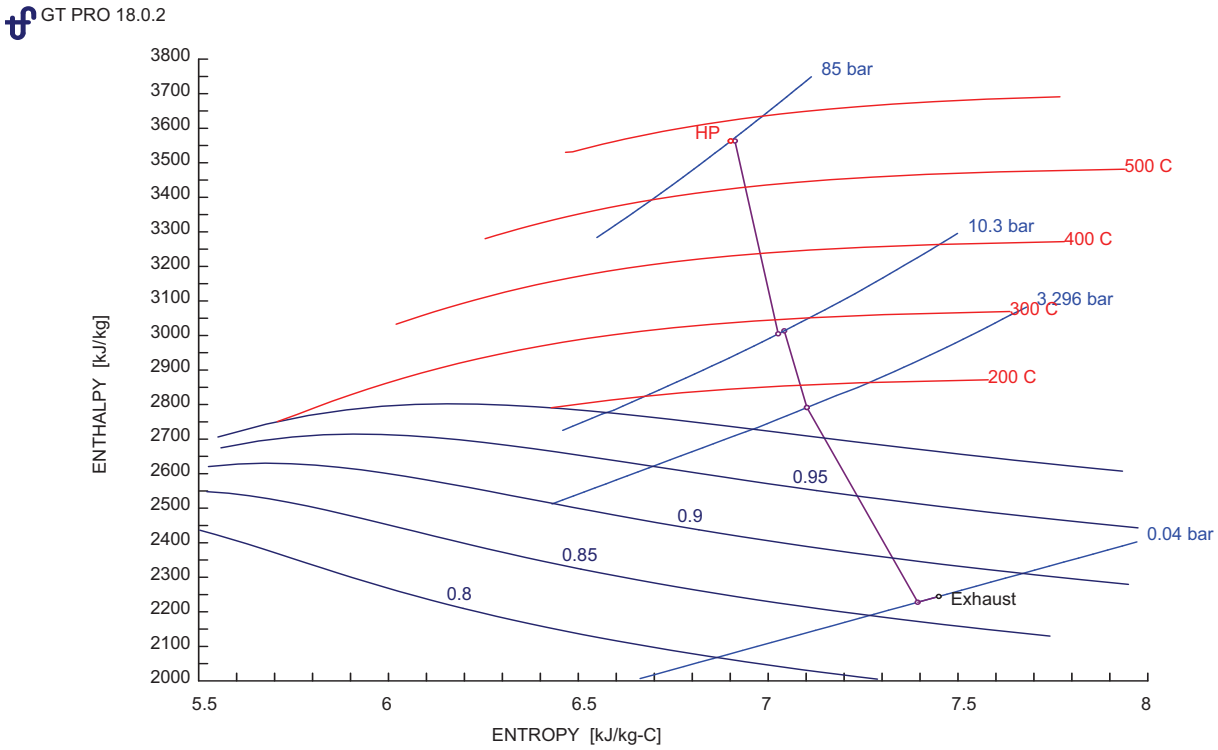

Figure 2.15: Steam expansion path in an h-s diagram for a single-pressure steam cycle with a steam pressure of 85 bar.

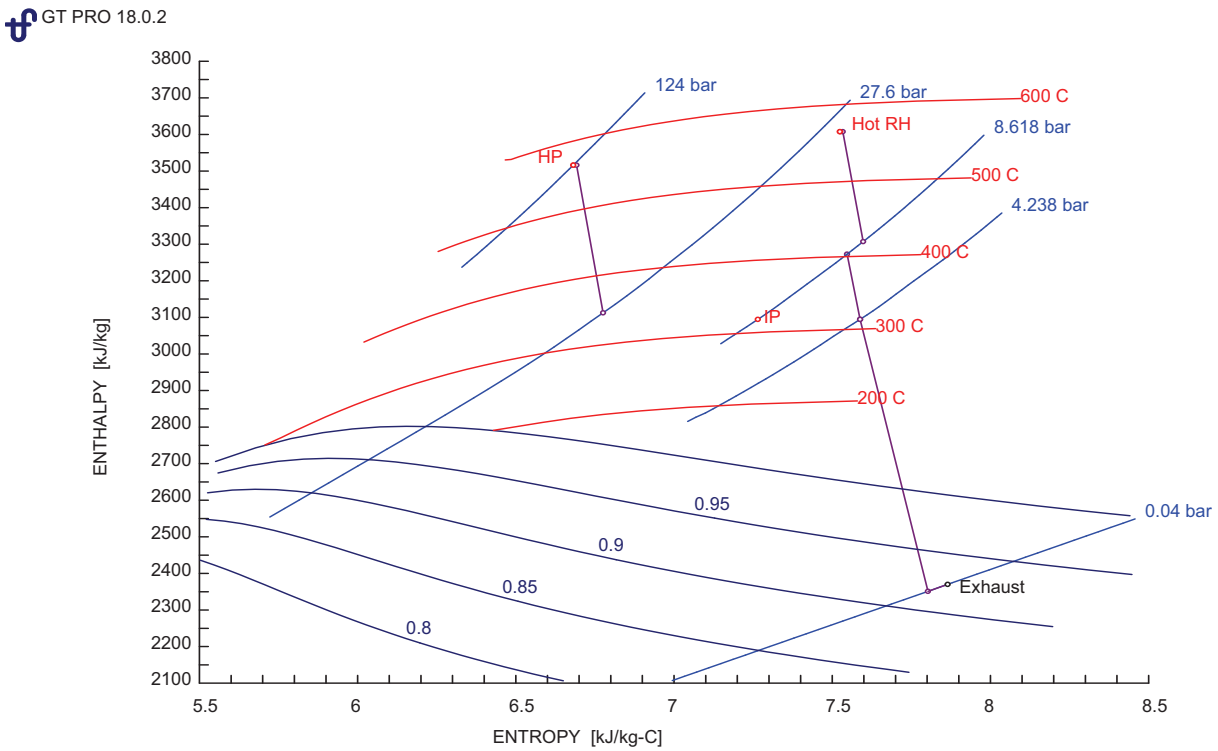

Figure 2.16: Steam expansion path in an h-s diagram for a dual-pressure reheat steam cycle.

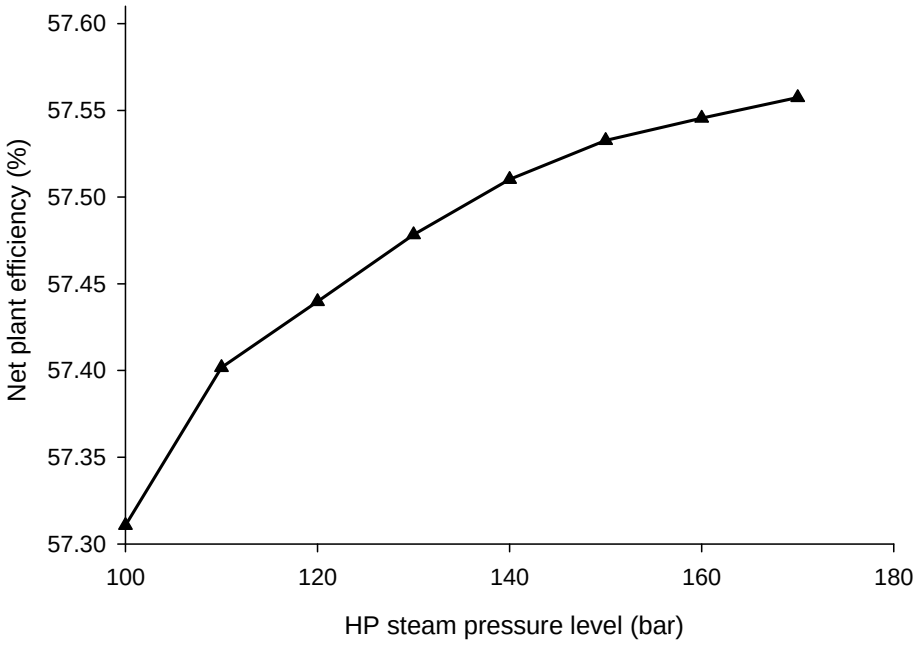

Figure 2.17: Net plant efficiency as a function of HP steam pressure level for a dual-pressure reheat steam cycle in an NGCC plant.

aspect was not directly considered in the thesis, however, economically unrealistic options were not considered and would be excluded.

While considering the net plant efficiency, the process steam pressure levels needed to be regarded as well. Changing the process steam demands (pressure and flow) could affect the selection of steam pressure levels to achieve a higher net plant efficiency. Also, while aiming for a high net plant efficiency, the plant complexity could increase and the end result could be a compromise. In addition, the flexibility of an IRCC plant was important, not the least in respect to the ability to run efficiently on both hydrogen-rich fuel and natural gas. Therefore, dual fuel capability was also considered when selecting an HRSG design.

Duct-firing

Because of features like preheating of reformer process streams and dual fuel capability, duct-firing in the HRSG was considered. Firing the GT with hydrogen fuel leads to an increase in steam content in the turbine compared to when firing natural gas, and the heat transfer rate to the turbine blades increases, which leads to a higher blade metal temperature. To compensate for this, one can decrease the turbine inlet temperature (TIT) of the GT. Doing so decreases the thermal efficiency of the GT and the turbine exhaust temperature, and subsequently the inlet temperature to the HRSG drops. The drop in HRSG flue gas inlet temperature could be compensated with duct-firing. Also, the reformer requires preheating of the inlet streams. If this is done in the HRSG, a significant amount of the flue gas heat content is transferred to the process streams which further warrants duct-firing (50 MW of preheating could be a typical number for a 400 MW IRCC plant). The importance of duct-firing is further highlighted since the GT is to be run on both hydrogen-rich fuel and on natural gas, and the requirements for the HRSG would

be quite different for the different fuel operating modes. In NGCC operating mode, the turbine exhaust temperature would be higher, no preheating would be necessary, and no external steam is generated. Duct-firing would give that required flexibility for the HRSG.

2.3.5 Gas turbine

The gas turbine in an IRCC would be similar to a GT set up for natural gas combustion. The main differences would be related to turbine swallowing capacity, burner design, compressor air extraction, turbine inlet and exhaust temperatures, and control system design. Because of the low molecular weight of hydrogen and due to the need of a fuel diluent, the volume flow to the turbine section could be higher than for an NG GT (depending on amount of air extraction from compressor). This means the turbine section needs to be redesigned compared to an NG GT for a larger swallowing capacity. The burner design is critical for a GT that in addition to the hydrogen-rich fuel needs to be able to operate on NG with steam injection for NO_x abatement (Bonzani and Gobbo, 2007). Because of a higher steam content in the combustor flue gas, the heat transfer to the turbine blades increases. This means, the turbine inlet temperature for an IRCC GT should be lowered compared to an NG GT or the GT should be redesigned (Chiesa et al., 2005). Also, in an IGCC or IRCC setup, the control system needs to be considered (Shilling and Jones, 2003).

2.3.6 Steam turbine

The steam turbine in an IRCC could have significant extractions for reforming and CO_2 capture reboiler steam. This could cause issues when running in NGCC mode since this process steam would not be needed then. Also, the process heat exchangers in the IRCC setup would not generate any steam in NGCC operation mode. This could also have an impact on the steam turbine design.

2.4 Pre-combustion capture: process selection on system level

For natural gas pre-combustion capture, there are many configuration options (Andersen et al., 2000; Lozza and Chiesa, 2002a,b; Ertesvåg et al., 2005; Hoffmann et al., 2009). In addition, there are many possibilities for integration with the power cycle both on the gas and the steam side. Some of the questions to answer during the design phase of such a plant are:

- Which type of reformer should be used?
- Which system pressure level should be adopted?
- How should the HRSG be designed?
- How much process integration should take place?
- Should membranes be employed in the reforming process, the water-gas shift section, or in the CO_2 capture step?

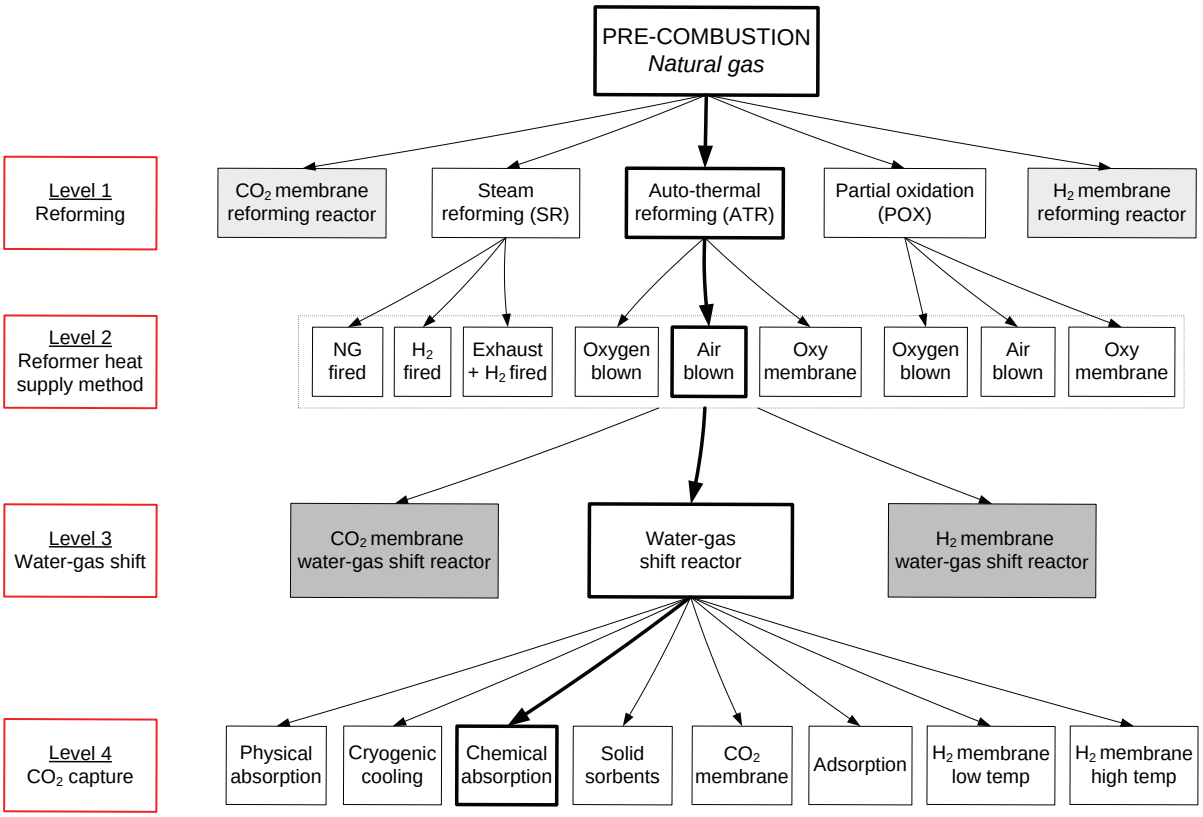

Figure 2.18: Natural gas pre-combustion overview with process selection (bold path).

- Which CO_2 capture method should be employed?

Fig. 2.18 shows an overview of natural gas based pre-combustion CO_2 capture. The bold path in the figure depicts the route selected for the processes analyzed in the thesis.

2.4.1 Reformer

If comparing steam reforming and autothermal reforming technologies, the advantages for the ATR technology, within an IRCC setup, include:

- Flexible operation with short startup times and fast load changes (Christensen and Primdahl, 1994; Lee et al., 2005). An ATR is also easy to restart.
- Soot free operation for a wide range of operating conditions.
- Compact design compared to fired steam reformers.
- Low investment cost (particularly true for air-blown ATR since no ASU is needed).
- Economics of scale; much larger single stream units are possible compared to fired steam reformers (Aasberg-Petersen et al., 2004).
- No secondary fuel supply required. For a steam reformer the heat required for reforming reactions need to be supplied by a secondary fuel supply. The CO_2 emissions from the combustion would either need to be captured in a separate CO_2 capture

subsystem or the overall capture rate of the plant would decrease (if not firing the SR with hydrogen).

The advantages of ATR compared to POX in an IRCC process are not as clear, but one key advantage is the soot free operation for a variety of process conditions. This is not the least important in off-design operation. POX has mainly been used for heavier feedstocks and typically produce syngas with a H_2/CO of 1.7 to 1.8 (Christensen and Primdahl, 1994). A scrubber to remove soot particles would be needed after a POX reactor. A POX would likely be based on gasification technology that has been adapted for a natural gas feed (Aasberg-Petersen et al., 2004). The exit temperature from POX would be higher compared to ATR in order to minimize soot formation and to increase hydrocarbon conversion. Typical exit temperatures is in the range of 1250–1400 °C compared to the ATR exit temperature in the range of 850–1100 °C. Advantages for POX include the possibility to reform at very high pressures (80–100 bar) with low methane slip since the methane-steam reforming reaction is not a dominant reaction (Hoffmann et al., 2009). For an ATR, Le Chatelier's principle favors a lower pressure due to reaction (2.1). A higher pressure in an ATR or SR would lead to a higher methane slip since the equilibrium of reaction (2.1) would be shifted towards the reactants. This can be compensated by using a higher S/C but this has the disadvantage of decreasing the plant efficiency. If operating at these higher pressures, as is possible with POX, the downstream equipment can be kept smaller and the CO_2 separation less energy intensive. However, significant air pressure boosting would be necessary for high-pressure POX applications, which would produce a H_2-rich gas with a higher than necessary pressure for the GT fuel nozzles.

An oxygen-blown reformer has the advantage of a more compact design compared to an air-blown reformer due to the lower volume flow. The downstream equipment, such as heat exchangers, water-gas shift reactors, and the CO_2 capture subsystem can also be kept smaller in size. In addition, the partial pressure of CO_2 would be higher leading to an advantage for the CO_2 separation. However, the large disadvantage with utilizing an oxygen-blown ATR is the energy required for the ASU, which is significant. So is the ASU investment cost. Also, before combusted in the GT combustor, nitrogen diluent from the ASU needs to be introduced to the hydrogen fuel.

Based on these considerations, an air-blown ATR (with and without an adiabatic prereformer) was selected for the processes studied. Certainly, oxygen-blown ATR, POX, and SR are also viable options for an IRCC plant and in the end has to be a project-to-project decision based on metrics such as economics, performance, and flexibility. In the industry today, ATR is mainly used in ammonia and methanol plants and in gas-to-liquid applications.

2.4.2 System pressure level

The system pressure level, in an IRCC with air-blown ATR, is determined by the pressure of the air. Air is extracted from the GT compressor discharge plenum and either directly fed to the ATR or boosted up to a higher pressure before submitted to the ATR. The advantages of utilizing an air booster compressor, and thereby operating at a higher system pressure, are that the downstream equipment can be kept smaller and the lower energy demand for CO_2 separation. Also, there is no need for a syngas compressor to achieve the necessary fuel pressure for the GT combustor. In addition, the pressure of the

NG is utilized, rather than first decreasing the pressure, followed by a syngas compressor in the end. Disadvantages include the need for cooling of the booster compressor inlet air followed by air heating after the compressor. Also, a lower reforming pressure is advantageous for the methane-steam reforming reaction (2.1). Systems both without (Papers I and II) and with (Chapters 4, 5, 6, Papers III and IV) an air booster compressor have been studied.

2.4.3 HRSG

In addition to considering the criteria listed in Section 2.3.4, the complexity of selecting an HRSG design increased when also considering that steam could be superheated and LP and intermediate-pressure (IP) steam could be generated in the process heat exchangers. However, Figs. 2.7 and 2.12 should give an indication of design selection when a lot of HP saturated steam is generated outside the HRSG. For the concepts studied, it was also of importance to maintain a high net plant efficiency when operating on NG. Therefore the selection of HRSG design had to be a compromise between NGCC and IRCC operation modes, while considering the items listed in Section 2.3.4.

When considering the overall design of the IRCC process in this analysis, two HRSG configurations stood out:

1. A single-pressure HRSG with its simplicity while still achieving an IRCC net plant efficiency similar to the more complex HRSG alternatives.

2. A dual-pressure reheat HRSG with its high NGCC net plant efficiency.

The triple-pressure HRSG showed a lower NGCC net plant efficiency than the dual-pressure reheat HRSG, as shown in Fig. 2.6, while having a similar complexity. Also, there was no clear advantage for the triple-pressure system in IRCC operating mode. However, to investigate how the triple-pressure system behaves in the full IRCC setup, a triple-pressure system was utilized in Papers I and II.

When comparing dual-pressure reheat and triple-pressure reheat systems, one setup was not clearly favorable compared to the other setup. However, for a triple-pressure reheat system, the LP and IP boilers within the HRSG became very small (below 1 kg/s steam to the boilers). For this reason, the dual-pressure reheat system was favorable compared to the the triple-pressure reheat system and the resulting decrease in complexity a positive.

To differentiate between the single-pressure system and the dual-pressure reheat system, a full IRCC process design for each setup was necessary, as is presented in Chapters 4 and 5. The main advantage of the single-pressure system was the simplicity of the design and an overall less complex cycle. One disadvantage was the lower steam quality at the ST outlet. A higher steam quality would be achieved if the HP pressure level would be lowered, however, this would lower the net plant efficiency. For the dual-pressure reheat system, the steam quality was not an issue. The higher NGCC net plant efficiency is a clear advantage for a dual-pressure reheat system. In the end, the selection decision would be strongly influenced by economics. Economic analysis was not part of this work.

2.4.4 Gas turbine

The selected gas turbines for the process models were the GE 9FA and GE 9FB models. The reasons for the selection were:

- High thermal efficiency.
- Thermoflow's models of GE (General Electric) machines are well developed. Less information is available for, for example, Alstom GTs.
- GE's involvement in the Hydrokraft project together with Norsk Hydro. A testing program was then developed and executed related to IRCC GTs and information related to this is available in the literature (Todd and Battista, 2000).

2.4.5 Steam turbine

Steam turbine design was selected in accordance with the HRSG pressure level and design. Extraction points were selected based on reforming and capture reboiler needs. Considerations were taken for off-design operation.

2.4.6 CO_2 capture

For the processes presented in Chapters 4, 5, 6, and Papers III and IV, a hot potassium carbonate system was utilized for the CO_2 capture subsystem. For the system presented in Papers I and II, an activated MDEA process was selected. Selection of a hot potassium carbonate system for the majority of the process models was due to several reasons:

1. The environmental impact of potassium carbonate-bicarbonate slippage from the system is minor. If using amines, slippage and other environmental concerns could be an issue (Thitakamol et al., 2007; Veltman et al., 2010). Also, because of environmental considerations, no activator, like piperazine, was implemented in the hot potassium carbonate process.
2. K_2CO_3 models existed within the research group (Kothandaraman et al., 2009).
3. For pressures such as in the IRCC process, a K_2CO_3 system is applicable. The pressure, around 25–30 bar inlet pressure with a CO_2 content around 15 vol%, is on the low end for physical absorption with for example Selexol (Göttlicher, 2004).

MDEA, activated or not, would be the main alternative to the K_2CO_3 system and was selected for one of the processes analyzed. The reboiler duty would be lower for an a-MDEA system compared to a hot potassium carbonate system (Göttlicher, 2004).

2.4.7 Level of process integration

In general, a high level of integration for steam generation, preheating, and GT air was selected. In all process models, steam was generated in the reforming process and reintroduced to the HRSG. Also, air was extracted from GT compressor for the reforming process. Preheating of the process streams was done in the HRSG.

2.4.8 Conclusion of process selection

Based on the previous sections in this chapter, the following four systems were selected for design and analysis in the thesis:

IRCC with dual-pressure reheat HRSG (IRCC 2PR)

The main process of the thesis, as presented in Chapter 4, have the following features:

- air-blown ATR without a prereformer
- elevated system pressure by boosting the GT compressor discharge pressure to 30 bar
- dual-pressure reheat HRSG
- hot potassium carbonate CO_2 capture

IRCC with single-pressure HRSG (IRCC 1P)

The process presented in Chapter 5 and Papers III and IV consisted of:

- air-blown ATR with a prereformer
- elevated system pressure by boosting the GT discharge pressure to approximately 30 bar
- single-pressure HRSG
- hot potassium carbonate CO_2 capture

IRCC with relaxed practical constraints

To investigate the concept's efficiency potential, a process with relaxed practical constraints are presented in Chapter 6. This process did not include a detailed process design but did have the following main features:

- air-blown ATR without a prereformer
- elevated system pressure by boosting up the GT discharge pressure to 22 bar
- single-pressure HRSG
- hot potassium carbonate CO_2 capture

IRCC with triple-pressure HRSG (IRCC 3P)

The process presented in Papers I and II consisted of:

- air-blown ATR with a prereformer
- lower system pressure with an ATR inlet pressure of 16 bar
- fuel compressor
- triple-pressure HRSG
- a-MDEA CO_2 capture

Chapter 3

Methodology

The methodologies used in the thesis will be covered in this chapter. Since several of the methodologies have been described in Papers I–IV, Appendix B, some of the sections were condensed to avoid unnecessary overlap within the thesis.

3.1 Process design and modeling

3.1.1 Design by experience

The starting point and basis for the process designs to be modeled was:

- Literature review, i.e., how IRCC plants have been designed in the available literature.
- Discussions with NTNU and MIT researchers and professors.
- Discussions with GE IGCC group.
- Personal experience from power industry.

From this basis, the designs were developed within the process constraints and practical considerations to arrive at a compromise between high net plant efficiency, CO_2 capture rate, complexity, and technology maturity. The practical considerations included, among other:

- Metal dusting in the syngas cooler downstream of the reformer.
- GT turbine inlet temperature reduction when operating on hydrogen-rich fuel.
- Condensation of flue gas on pipes in cool end of HRSG.
- Off-design considerations at design point to have sufficient air and steam pressures at part load operation.
- Dual fuel capability for the GT and HRSG.

3.1.2 Power island

The power island, including the GT, HRSG, and ST, was modeled with GT PRO (design) and GT MASTER (off-design) version 18 (Thermoflow, 2008).

GT compressor

GT PRO / GT MASTER use built-in compressor maps for each machine to relate corrected inlet air mass flow to compressor pressure ratio and efficiency. The model takes into account turbine cooling air bleed from the compressor as well as process air extractions. Compressor behavior is modified depending on the location and quantity of extracted air. Pressure drops for inlet air filter and ductwork are taken into account.

GT combustor

The combustion model in GT PRO / GT MASTER is based on a mole balance calculation modified by an efficiency. Pressure losses and fuel delivery temperature are accounted for. NO_x, CO, and unburned hydrocarbon emissions have to be entered by user.

GT turbine

In GT PRO / GT MASTER, a turbine map was constructed by Thermoflow for each GT model, relating turbine efficiency to corrected inlet gas mass flow and turbine pressure ratio. Pressure drops in GT exhaust and HRSG are taken into account.

HRSG

The HRSG temperature profile is calculated from its heat balance followed by calculation of the log mean temperature difference (LMTD) and the corresponding UA parameter. The areas for the heat exchangers (HX) is then calculated based on empirical gas-side heat transfer correlations and user input water-side heat transfer coefficients.

Steam turbine

GT PRO divides the ST into an HP and an LP section where the interface between the sections is the juncture where IP steam is added. GT PRO further assumes that the efficiency of each step within a particular group is the same in the absence of steam moisture. This efficiency is defined as the dry step efficiency of the group. To correct for condensing moisture entrained with the steam, GT PRO assumes that the efficiency of a step with wet steam is reduced in proportion to the average moisture present within that step.

The Wilson line represents the steam equilibrium quality at the onset of condensation within the steam turbine. Because of the high velocity and rapid cooling of the steam, it becomes supersaturated before liquid droplets begin to actually form. The default definition of the Wilson line is that it corresponds to an equilibrium quality of 0.97. All steps whose exit quality is below the Wilson line have their efficiency corrected as follows (Thermoflow, 2008):

$$\eta = \eta_{dry} - \beta\,(1 - x_m) \tag{3.1}$$

where η is the corrected step efficiency, η_{dry} the dry step efficiency, x_m the mean step steam quality, and β the Baumann coefficient. If the step is partially above and partially below the Wilson line, the correction is prorated to reflect the proportion below the Wilson line.

Gas and steam properties

For the GT PRO / GT MASTER steam properties, IAPWS-IF97 was used (Wagner et al., 2000). The thermodynamic gas properties are based on fifth order polynomials derived from the JANAF thermochemical tables.

3.1.3 Reforming and CO_2 capture sections

The reforming and CO_2 capture sections were modeled with Aspen Plus version 2006.5 (Aspen Technology, 2008). This section will focus on the property method used and the chemical components considered in the model.

The selection of property method is an important decision for simulation of process models (Carlson, 1996). For the IRCC models presented in Chapters 4, 5, 6, and Papers III–IV, three criteria were used for the selection:

1. AspenTech recommendations (Aspen Technology, 2003).
2. Which equation of state (EOS) has been selected for simulations of similar systems in the literature.
3. Testing of model output sensitivity to choice of EOS.

For mainly real non-polar components, like in hydrocarbon processing, Peng-Robinson (PR), Redlich-Kwong-Soave (RKS), Lee-Kesler Plöcker, or PR and RKS with Boston-Mathias α function (PR-BM and RKS-BM) are recommended by Aspen Technology (2003). More specifically, RKS-BM and PR-BM are advised for syngas applications. For polar components with electrolytes ELECNRTL is recommended.

If studying the literature for analyses of similar systems, RKS appears to be the dominating property method used for the syngas section (e.g., Ertesvåg et al., 2005; Zhang and Lior, 2008; Amann et al., 2009). For comparison of model results, it could be worthwhile using the same EOS method as the majority of the literature has used.

To test how much difference the choice of property method actually would give, the reforming process model was simulated with the following EOSs:

- Redlich-Kwong-Soave
- Redlich-Kwong-Soave with Boston-Mathias α function
- Peng-Robinson

If studying two of the most important model outputs, net plant efficiency and CO_2 capture rate, the differences were very small. For the net plant efficiency, the difference was 0.06%-points between the highest and lowest efficiency results. For the CO_2 capture rate, the maximum difference was 0.13%-points. Based on these results it is evident that the selection between the above property methods is not critical for the system studied. RKS should provide satisfactory results for the model studied and since the majority of

the literature studied used RKS it could make sense to use this, although AspenTech recommends RKS-BM (or PR-BM) for syngas applications.

The RKS EOS form for pure components can be expressed as

$$p = \frac{\bar{R}T}{\tilde{v} - b} - \frac{a(T)}{\tilde{v}(\tilde{v} + b)} \tag{3.2}$$

where

$$a(T) = 0.42747\alpha(T)\frac{(\bar{R}T_{cr})^2}{p_{cr}} \tag{3.3}$$

$$b = 0.08664\frac{\bar{R}T_{cr}}{p_{cr}} \tag{3.4}$$

p is the pressure in Pa, $\tilde{v}$ is the molar volume in m^3/mol, $\bar{R}$ the universal gas constant, and T the temperature in K. $\alpha(T)$ is given by

$$\alpha(T) = \left[1 + m\left(1 - \sqrt{\frac{T}{T_{cr}}}\right)\right]^2 \tag{3.5}$$

where

$$m = 0.480 + 1.574\omega - 0.176\omega^2 \tag{3.6}$$

ω is the acentric factor of the molecule and often tabulated together with critical temperature T_{cr} and critical pressure p_{cr}.

To get the mixture properties from the component properties, mixing rules are needed. The mixing rules for RKS are

$$a = \sum_{i=1}^{n}\sum_{j=1}^{n}\sqrt{\tilde{y}_i\tilde{y}_j a_i a_j}(1 - k_{ij}) \tag{3.7}$$

$$b = \sum_{i=1}^{n}\tilde{y}_i b_i \tag{3.8}$$

where k_{ij} is the binary interaction parameter, n the number of components in the mixture, and $\tilde{y}$ the molar fraction.

For streams with H_2O only and as free-water method, the STMNBS2 was used. The STMNBS2 property method uses:

- 1984 NBS/NRC steam table correlations for thermodynamic properties
- IAPWS correlations for transport properties

For the CO_2 capture subsystem, the property method ELECNRTL, updated with literature data, was used (Kothandaraman et al., 2009). ELECNRTL uses Electrolyte NRTL as liquid phase activity coefficient method and Redlich-Kwong as vapor phase fugacity coefficient method.

Chemical components considered

The chemical components that were considered in the reforming process model are listed in Table 3.1. The chemical components in the capture subsystem model are listed in Table 3.2.

Table 3.1: Chemical components in Aspen Plus reforming model.

Component name	Chemical formula
Argon	Ar
Methane	CH_4
Ethane	C_2H_6
Propane	C_3H_8
iso-Butane	C_4H_{10}
n-Butane	C_4H_{10}
iso-Pentane	C_5H_{12}
n-Pentane	C_5H_{12}
n-Hexane	C_6H_{14}
Water	H_2O
Carbon monoxide	CO
Carbon dioxide	CO_2
Hydrogen	H_2
Nitrogen	N_2
Oxygen	O_2

Table 3.2: Chemical components in Aspen Plus CO_2 capture model.

Component name	Chemical formula
Argon	Ar
Methane	CH_4
Water	H_2O
Carbon monoxide	CO
Carbon dioxide	CO_2
Hydrogen	H_2
Nitrogen	N_2
Oxygen	O_2
Potassium ion	K^+
Carbonate	CO_3^{2-}
Bicarbonate	HCO_3^-
Hydroxide	OH^-
Hydronium	H_3O^+
Potassium carbonate	K_2CO_3
Potassium carbonate (s)	K_2CO_3
Potassium bicarbonate	$KHCO_3$
Potassium bicarbonate (s)	$KHCO_3$

3.1.4 Power and efficiency definitions

The net plant power output was defined as:

$$\dot{W}_{net,plant} = ((\dot{W}_{gtt} - \dot{W}_{gtc}) + \dot{W}_{st})\eta_m\eta_{gen} - (\dot{W}_{comp} + \dot{W}_p)/(\eta_m\eta_{drive}) - \dot{W}_{aux} \quad (3.9)$$

where $\dot{W}_{gtt}$ is the GT turbine power, $\dot{W}_{gtc}$ the GT compressor power, $\dot{W}_{st}$ the ST power, $\dot{W}_{comp}$ the total power consumption by the air and CO_2 compression. $\dot{W}_p$ is the pump power in the absorption subsystem. $\dot{W}_{aux}$ is the auxiliary power requirement. η_m is the mechanical efficiency and η_{gen} is the generator efficiency. η_{drive} is the efficiency of the drives for the different compressors and pumps. Note that all the power terms were defined as their absolute values meaning all power terms were considered positive and the sign handled in the equation itself.

Another key performance metric was the net plant efficiency which was defined as

$$\eta_{net,plant} = \frac{\dot{W}_{net,plant}}{(\dot{m}LHV)_{NG}} \quad (3.10)$$

where $\dot{m}_{NG}$ is the natural gas mass flow entering the system and LHV_{NG} the lower heating value of the natural gas.

3.2 Reliability analysis

Functional analysis and failure modes, effects, and criticality analysis (FMECA) are important steps in a system reliability analysis, as they can serve as a platform and basis for further analysis. Also, the results from the FMECA can be interesting for determining how the failures propagate through the system and their failure effects on the operation of the process.

The first step of the reliability analysis was a detailed functional analysis that was carried out to reveal and define all the required functions of the plant elements. For each function, the associated performance criteria were determined. A thorough understanding of all required functions and their associated performance criteria is a prerequisite for the FMECA.

The FMECA involves analyzing all the potential failure modes of the system elements (components and subsystems) and identify the causes and effects of these failure modes. The FMECA is also used to determine how failures may propagate through the system, and to reveal the failure effects on the operation of the plant. Another purpose of the FMECA was to identify the most important operation modes, critical components, and integration points for further and more detailed analyses at later stages of the project.

3.2.1 Functional analysis

The functional analysis was carried out at the equipment level of the system, as shown in Fig. 3.1. The functional analysis only included the essential functions, meaning that auxiliary functions, protective functions, and so forth, were not covered.

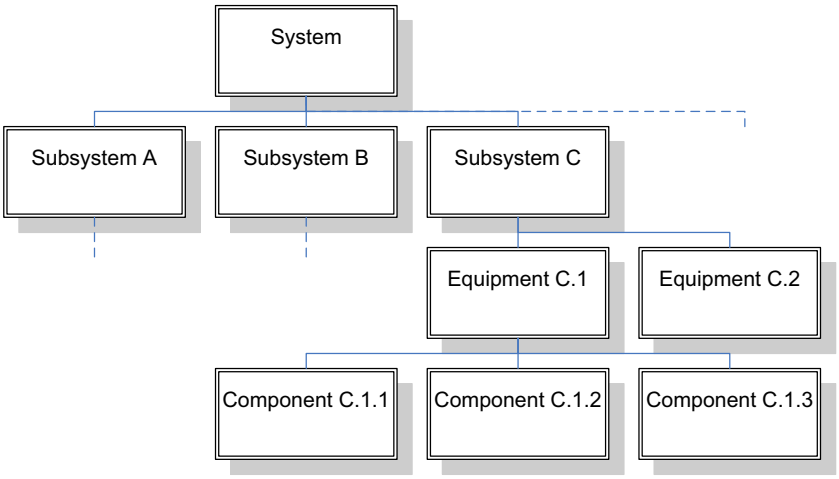

Figure 3.1: Functional levels of a system.

3.2.2 Failure mode, effects, and criticality analysis

FMECA is a widely used qualitative method for reliability analysis (e.g., see Rausand and Høyland, 2004; IEC 60812, 2006). Teng and Ho (1996) discuss the use of FMECA for product design and process control. Teoh and Case (2004) describe, among other topics, the connection between system functional diagrams and FMECA. FMECA can be used to identify critical areas during the design stage of the system. When the criticality of failures is not investigated, the FMECA is sometimes called failure mode and effect analysis (FMEA).

The FMECA approach that was selected for this project is illustrated in Fig. 3.2. In this approach, a risk, or criticality, number is assigned to each and every failure mode as a risk priority number (RPN). The RPN of a failure mode is calculated based on an evaluation of the factors: detection, failure rate, and severity, of a failure mode. Each of these three factors are typically assigned numbers ranging from 1 to 10. There are several approaches for assigning these numbers, one is described by Bevilacqua et al. (2000) where a Monte Carlo simulation approach is used for testing the weights assigned to the RPNs. In this article, the normal 1–10 scale was modified to the more limited 1–3 scale. The reason for this modification was to more readily being able to identify the numbers the RPN are based upon.

The detection scale was defined as: 1 = highly detectable, almost certain detection; 2 = moderately detectable; and 3 = non-detectable. The failure rate scale was defined as: 1 = failure unlikely; 2 = occasional failure; and 3 = frequent failure. The severity scale was defined as: 1 = no, or very small effect; 2 = plant operating at part load or bypassing CO_2 capture; and 3 = plant shutdown.

A failure mode is defined as a failure to meet a functional requirement of a specific equipment. Once a failure mode has been specified, the causes and effects of the failure need to be identified. As a basis for the analysis, it was assumed that the plant was operating at full load when a failure occurs. Furthermore, potential human errors were not considered in the analysis. Regarding failure effects, the effects on the same equipment where the failure occurred were first analyzed. Secondly, the effects on other equipment in the system were investigated, and finally, the overall system effects were identified.

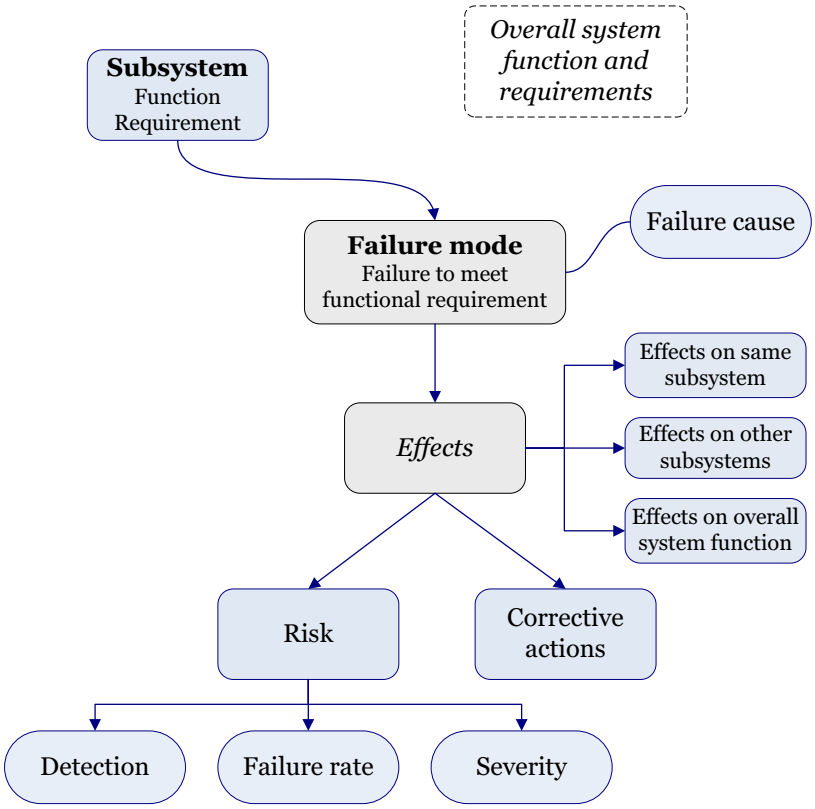

Figure 3.2: Graphical representation of the FMECA approach.

The detection rating was, for the most part, derived based on knowledge in instrumentation and controls. For example, an abnormal temperature or pressure change is easy to detect, whereas a change in a gas composition can be more difficult to sense. With the 1–3 scale, the numbers could readily be assigned. To determine the failure rate numbers, several data sources were consulted (OREDA, 2002; NERC, 2007). The severity ranking was established based on studying the effects of the various failure modes. The RPNs were computed by multiplying the detection, failure rate, and severity numbers, and must therefore range from 1 to 9.

For further details on the reliability methodology, analysis, and results, refer to Paper II, Appendix B.

3.3 Plant flexibility

Plant flexibility was to be investigated both qualitatively and quantitatively. Off-design simulations and evaluations were the key components of the plant flexibility analysis. From a qualitative standpoint, dual fuel capability and operability were analyzed.

3.3.1 Off-design analysis

Off-design analysis investigates how the plant behaves when departure from the design point occurs. For the analysis presented in this thesis, the focus was on plant behavior when the demanded net power output of the plant decreases. For the off-design analyses,

the decreased net power output was defined as relative gas turbine load

$$\dot{W}_{gt,rel} = \frac{\dot{W}_{gt}}{\dot{W}_{gt,d}} \tag{3.11}$$

where $\dot{W}_{gt}$ is the gas turbine gross power output and $\dot{W}_{gt,d}$ is the gas turbine gross power output at design conditions.

Power island

Pressure levels at extraction points need to be considered in design mode to ensure sufficient pressure at part load conditions. As described in Section 3.1.2, GT compressor and turbine maps were used at part load operation.

Reactors

Detailed off-design analysis of the reforming and water-gas shift reactors was not performed. For the ATR, the outlet temperature was controlled by adjusting the inlet air mass flow. Pressure drop changes in the reactors were considered according to Section 3.3.1. For the capture subsystem a constant specific reboiler duty was assumed.

Heat exchangers

In the off-design scenarios the overall heat transfer coefficient U in the heat exchangers will vary. With inclusion of surface fouling and fin effects (extended surface) U can be expressed as

$$\frac{1}{UA} = \frac{1}{(\eta_o h A)_c} + \frac{R''_{f,c}}{(\eta_o A)_c} + R_w + \frac{R''_{f,h}}{(\eta_o A)_h} + \frac{1}{(\eta_o h A)_h} \tag{3.12}$$

In the heat exchanger off-design analysis it is assumed no aging or fouling. The fouling factors $R''_{f,c}$ and $R''_{f,h}$ were therefore set to 0. The wall conduction term R_w was also neglected. η_o is the overall surface efficiency of a finned surface and A is the heat transfer area. Subscripts c and h refer to the cold and hot side of the heat exchanger, respectively. In the preheating heat exchangers in the HRSG, the cold side has a high steam content. In the syngas cooler, as well as in the HXs that act as economizers, boilers, or superheaters, the cold side has water and steam only. Compared to the hot side, which contains gas with a lower steam content, the cold side convective heat transfer coefficient is assumed much larger, that is $h_c >> h_h$. Eq. (3.12) can then be simplified to

$$\frac{1}{UA} = \frac{1}{(\eta_o h A)_h} \tag{3.13}$$

The area A and fin efficiency η_o are constant when comparing design to off-design conditions. Using the Nusselt number and an empirical correlation including the Reynolds and Prandtl numbers (Incropera and DeWitt, 1990)

$$Nu_D \equiv \frac{hD}{k} = CRe_D^m Pr^n \tag{3.14}$$

The constants C, m, and n, are assumed independent of the nature of the fluid. The Prandtl number Pr and thermal conductivity k are assumed constant from design to off-design conditions. The diameter D is constant.

For the simulations, it was of interest relating the off-design UA to the design $(UA)_d$. Eq. (3.13) can then be written as

$$\frac{UA}{(UA)_d} = \frac{Re_D^m}{Re_{D,d}^m} \tag{3.15}$$

By using $Re_D = \frac{\dot{m}D}{A\mu}$, where the dynamic viscosity μ is assumed constant, a simple expression for correction of UA when going from design to off-design simulations can then be derived:

$$\frac{UA}{(UA)_d} = \left(\frac{\dot{m}_h}{\dot{m}_{h,d}}\right)^m \tag{3.16}$$

The m constant is dependent on the geometry of the shell and tube heat exchanger. $\dot{m}$ is the fluid mass flow. Subscript d refers to design conditions. For a staggered tubes configuration with assumed tube pitches of 2.5 (Incropera and DeWitt, 1990):

$$\left.\begin{aligned}\frac{S_T}{D} &= 2.5\\ \frac{S_L}{D} &= 2.5\end{aligned}\right\} \Rightarrow m \simeq 0.57 \tag{3.17}$$

S_T is the transverse pitch, that is, the distance 90° off from the flow direction between the centers of two adjacent tubes. S_L is the longitudinal pitch, that is, the distance in flow direction between the centers of two adjacent tubes. D is the tube diameter in the heat exchanger. Rewriting Eq. (3.16) with the assumed value of m:

$$UA = (UA)_d \left(\frac{\dot{m}_h}{\dot{m}_{h,d}}\right)^{0.57} \tag{3.18}$$

A similar expression, the exception being the m-factor which was set at 0.6, was used by Haag et al. (2007).

For a shell-and-tube heat exchanger with multiple tube passes, the flow arrangement involves part countercurrent and part cocurrent flow. The LMTD, ΔT_{lm}, is then reduced compared to a pure countercurrent HX. In the design, this is accounted for by introducing the factor F_T (Incropera and DeWitt, 1990; Shah and Sekulić, 2003; Smith, 2005):

$$\dot{Q} = UA\Delta T_{lm} F_T \qquad 0 < F_T < 1 \tag{3.19}$$

F_T can be expressed as a function of heat capacity rate ratio R and thermal effectiveness P

$$F_T = f(R, P) \tag{3.20}$$

where

$$R = \frac{(\dot{m}c_p)_c}{(\dot{m}c_p)_h} = \frac{CP_c}{CP_h} = \frac{T_{h,in} - T_{h,out}}{T_{c,out} - T_{c,in}} \tag{3.21}$$

and

$$P = \frac{T_{c,out} - T_{c,in}}{T_{h,in} - T_{c,in}} \tag{3.22}$$

The shape of the function $f(R, P)$ becomes very steep and approaches an asymptote as P increases for a given R. For a large temperature cross, $T_{c,out} - T_{h,out}$, P increases and F_T decreases significantly leading to a very high area requirement for the heat exchanger or an infeasible design. Low values of F_T indicate inefficient use of heat transfer area. Also, for low values of F_T, small changes in inlet and outlet temperatures, and uncertainties and inaccuracies in design data can lead to large changes in F_T and thereby A.

For the analyses in the thesis, an HX with an F_T below 0.75 was considered having an infeasible design.

Compressor maps

For the air booster compressor, a compressor map has been used for calculating the outlet pressure and isentropic efficiency in off-design operating points. The map has been adopted from the original, presented in a map collection by Kurzke (2004), to fit the process in the analysis.

The non-dimensional ratios pressure ratio $\Pi = \frac{p_{02}}{p_{01}}$, corrected mass flow $\frac{\dot{m}\sqrt{T_{01}}}{p_{01}}$, and corrected rotational speed $\frac{N}{\sqrt{T_{01}}}$ were used. p_{01} is the stagnation pressure at compressor inlet and p_{02} at compressor discharge. T_{01} is the stagnation temperature at compressor inlet.

In Fig. 3.3, pressure ratio and isentropic efficiency η_{is} are plotted as a function of corrected mass flow for different corrected speeds. The corrected mass flow and the corrected speed are relative to design value. The surge line is also visible in the figure. For off-design operating conditions it was assumed that the compressor can be speed controlled.

Pressure drop

The Darcy friction factor f is defined as

$$f \equiv \frac{-\left(dp/dx\right) D}{\rho u_m^2/2} \tag{3.23}$$

Assuming fully developed turbulent flow, meaning the pressure gradient dp/dx is a constant, the pressure drop from axial position x_1 to x_2 can be expressed as

$$\Delta p = -\int_{p_1}^{p_2} dp = f\frac{\rho u_m^2}{2D}\int_{x_1}^{x_2} dx = f\frac{\rho u_m^2}{2D}\left(x_2 - x_1\right) \tag{3.24}$$

where u_m is the mean fluid velocity and ρ the density of the fluid. By using $\dot{m} = \rho u_m A$, and comparing to design conditions, the following expression can be derived for off-design conditions

$$\frac{\Delta p}{\Delta p_d} = \left(\frac{\dot{m}}{\dot{m}_d}\right)^2 \frac{\rho_d}{\rho} \tag{3.25}$$

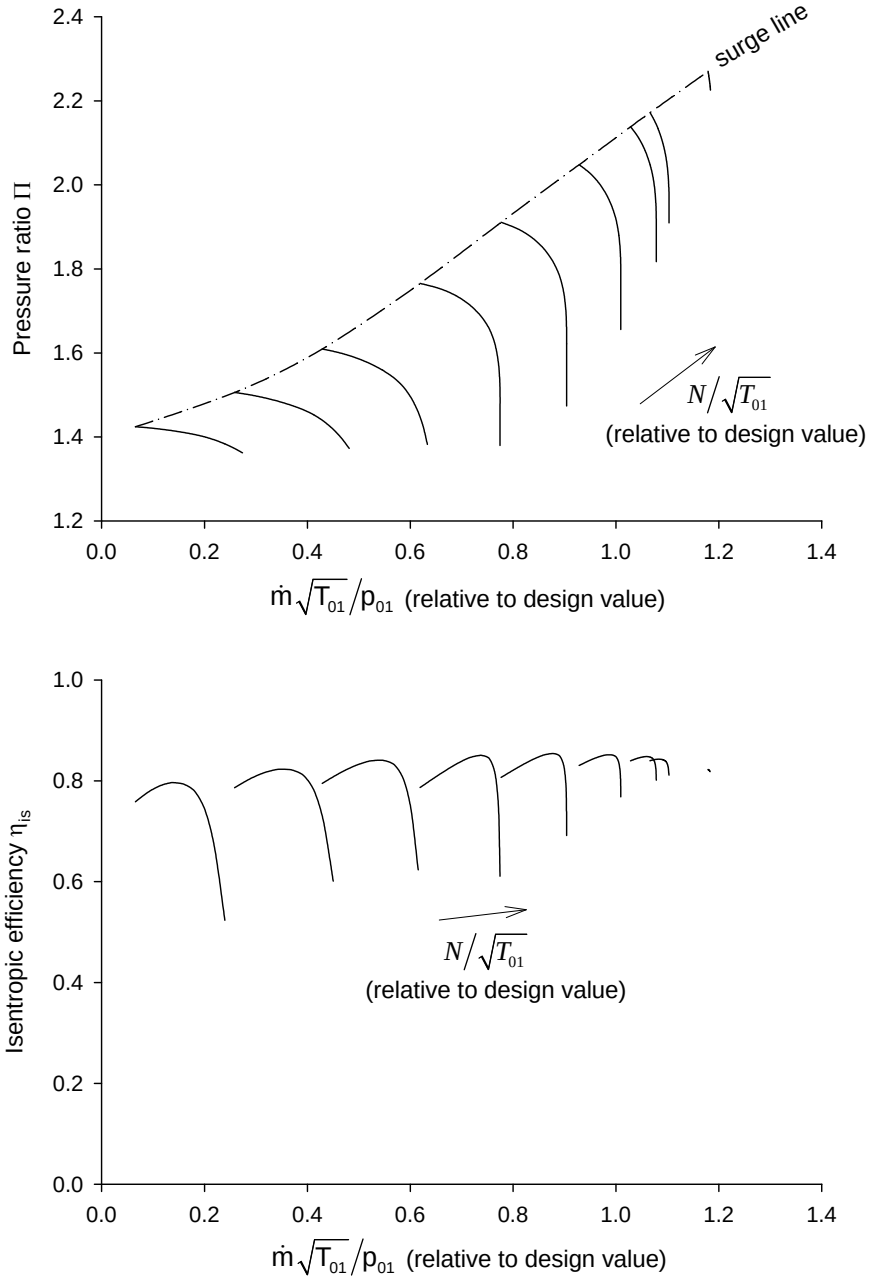

Figure 3.3: Compressor maps for the air booster compressor.

3.3.2 Operability

The complexity and efficiency of a process plant normally increase with the degree of integration. While the increase in efficiency is a desired result, the increased complexity can give rise to operability and risk issues (e.g., see Perrow, 1999), and the operation flexibility of the plant could decrease. The degree of integration in a process plant should therefore be determined based on a trade-off between efficiency and complexity. Operability is dependent on plant design and efforts have been made to incorporate process operability and control at an early stage of the design process (Barton et al., 1991; Blanco and Bandoni, 2003). The procedures presented in literature are computationally intensive and provide a level of rigor not required for the purposes of this work. A new index called the comparative complexity indicator (CCI) is a parameter for comparing complexity of processes that provides a simple guide to the engineer on the extent of integration. As the name suggests, this indicator is useful only when comparing two processes and the absolute value of the indicator for a single process has no significance by itself.

Main contributors to operability problems are (i) component and subsystem failures and (ii) system complexity and coupling between subsystems. The first aspect was discussed in Section 3.2.2. The complexity of a plant and its control system is directly related to the number of manipulated variables. A manipulated variable is the variable that is changed, in a control strategy, to achieve a certain process condition. It is desirable that the complexity of a control system is as low as possible (Skogestad, 2004). The main aim is thus to have a system with a small number of manipulated variables for better operability. As a qualitative measure of the complexity of a process the CCI is introduced as the number of variables that can be manipulated in a process while accounting for integration between different process areas. The CCI is based on a well established concept in control system design — the control degrees of freedom (CDOF), defined to be the number of manipulated variables that can be used in control loops.

For further details on the operability methodology, analysis, and results, refer to Paper II, Appendix B.

3.3.3 Dual fuel capability

Dual fuel capability was only qualitatively evaluated. None of the IRCC models were simulated with natural gas as fuel input for the GT. In the simulations, NG was only used as fuel input for the NGCC reference plants and the duct burners. However, during the process design of the HRSG, dual fuel capability was considered. For example, it was of importance to locate sections that would be dry during NG operation sufficiently far down in the gas path where the gas temperature would be at a level that the metal in the pipes could withstand.

3.4 System losses

In terms of fuel LHV input, losses for the various subsystems were evaluated. Some of the losses were readily quantifiable in terms of loss in plant power output and then as follows from the power loss, a net plant efficiency drop. The readily quantifiable losses included, for example, air and CO_2 compression, losses due to CO_2 capture pumps, and the need for extra auxiliaries due to higher gross power output in the IRCC compared

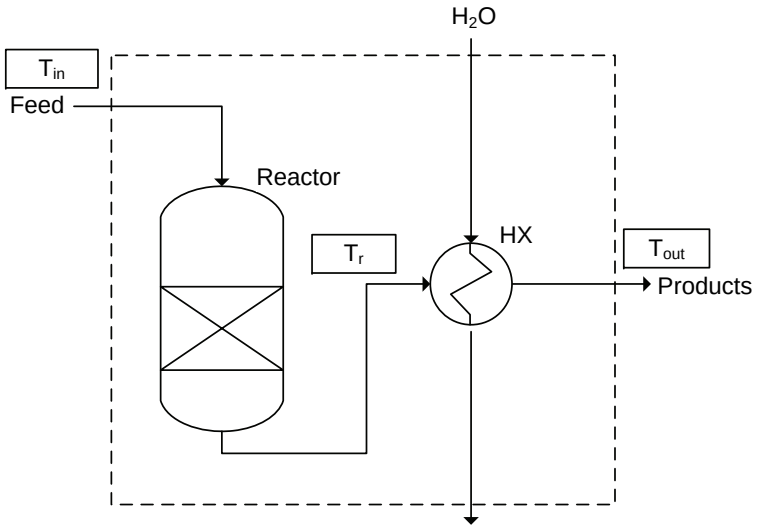

Figure 3.4: Schematic of reactor with system boundary for analysis of system losses.

to the NGCC reference plant. Other losses were more laborious to quantify, like the fuel conversion losses in the reactors and the effect of preheating.

Reactors

Losses due to fuel conversion from natural gas to syngas and then further on to a hydrogen-rich fuel were quantified. Fig. 3.4 displays a schematic of a reactor including the system boundary used for the loss analysis. Included in the figure are the reactor, heat exchanger, and the temperatures T_{in} (feed temperature), T_r (reactor outlet temperature), and T_{out} (temperature of products exiting the system boundary). The control volume for the analysis is indicated by the dashed lines in the figure.

The loss in power due to fuel conversion losses in the reactors, $\dot{W}_{loss}$, was defined as:

$$\dot{W}_{loss} = \eta_{ngcc}[(LHV \cdot \dot{m})_{in} - (LHV \cdot \dot{m})_{out}] - \dot{W}_{st,cv} \tag{3.26}$$

Where η_{ngcc} is the net electrical efficiency (excluding transformer losses) for the reference NGCC plant, $(LHV \cdot \dot{m})_{in}$ is the input in kW from the feed gas to the reactor, $(LHV \cdot \dot{m})_{out}$ is the output in kW from the product gas, and $\dot{W}_{st,cv}$ is the ST power from the steam generated in the control volume in Fig. 3.4. For the analysis, only steam that was generated from the heat of reaction, within each reactor, was considered. That is, T_{out}, as displayed in Fig. 3.4, was set equal to T_{in}.

Preheating

The loss due to duct-firing in the HRSG, for preheating process streams, was defined. The effect of preheating was calculated by taking the difference of the natural gas heat content supplied to the duct burner (with the reference NGCC net plant efficiency) and the additional steam that could have been generated if preheating was not done in the HRSG (and subsequently utilized in an ST).

3.5 Parametric uncertainty

Parametric uncertainties are typically represented by probability distributions. It is therefore important to process available information about model parameters and estimate the probability distributions of model outputs based on input uncertainties. Uncertainties in input parameters can be propagated through the process models to yield estimates of uncertainties in output values. An equally important outcome is sensitivities of output uncertainties to input parameters through which controlling sources of uncertainties can be identified. The methodology for the uncertainty analysis basically consists of the following steps:

1. Selection of input parameters
2. Probability density functions (PDF) of inputs
3. Polynomial representation of process model with *unknown* coefficients
4. Run limited number of full process model simulations
5. Polynomial representation of process model with *known* coefficients
6. Monte Carlo simulations $\Rightarrow$ PDFs of outputs
7. Sensitivity analysis

Input uncertainty quantification

The quantification of input uncertainties comprises steps 1 and 2 in list above. There are several types of uncertain parameters, including material properties, equipment design factors, operating condition parameters, and performance variables. A parameter's value can be uncertain if:

- the parameter is single-valued, deterministic, and constant, but its value is not perfectly known at the time.
- the parameter's value is constantly fluctuating with a random pattern.

Uncertainties of different types can be quantified using different approaches. When data are lacking, estimation of uncertainty has to rely on experience or technical experts. The information prescribed by technical experts generally contain information about the uncertain variables such as range, average value, most likely value, etc. This information is typically insufficient to define a unique probability distribution. There usually exists more than one probability distribution satisfying a single set of conditions. To select an appropriate distribution, the maximum entropy principle was used, as described by, e.g., Robert (1994); Golan et al. (1996).

Uncertainty propagation through process model

The propagation of uncertainties through the process model comprises steps 3–6 in the above list. Uncertainties were simultaneously propagated through the IRCC process model using the deterministic equivalent modeling method (DEMM), a computationally efficient method developed by Tatang (1995). In DEMM, parametric uncertainties are represented by a polynomial chaos expansion of uncertain basis. For instance, a Gaussian uncertain parameter x_u with mean $\overline{\mu}$ and standard deviation σ can be expressed by

$$x_u = \overline{\mu} + \sigma\xi \tag{3.27}$$

where ξ represents the uncertain basis. DEMM approximates the output uncertainties as probabilistically weighted polynomials of uncertain model parameters

$$y = \sum_{k=0}^{\infty} a_k H_k(\xi_1, ..., \xi_M) \tag{3.28}$$

where H_k are orthogonal polynomial functions of ξ_1, ..., ξ_M, which are the basis used to represent uncertain model parameters. Various types of orthogonal polynomial functions can be used for H_k in Eq. (3.28) depending on the nature of the uncertain parameters being considered. In practice, Eq. (3.28) is truncated at a finite order. For the uncertain parameters considered in this work, second-order polynomials were sufficient to approximate their probability distributions with reasonable accuracy. The coefficients a_k of the expansion were computed by evaluating the process model at points specific to the probability distributions of model parameters. With the unknown coefficients computed, Monte Carlo simulations could be performed on the polynomial representation of the process model. Examples of work performed using DEMM include studies by Tatang et al. (1997); Phenix et al. (1997).

Sensitivity analysis

DEMM also provides direct means of evaluating the sensitivity of model output to parametric uncertainties and identifying the parameters contributing the most to output uncertainty. Parametric sensitivities, defined as the portion of variance of model output that is attributable to individual parameters, are possible to compute upon obtaining the coefficients of polynomial expansion from Eq. (3.28). This analysis highlights the parameters where reduction in uncertainty would most effectively improve the predictive performance of the model. Those with negligible contribution to overall uncertainty can be phased out from further analysis.

The methodology is further described in Paper IV, Appendix B.

3.6 Concept potential

To examine the efficiency potential of the IRCC process and investigate the impact of the numerous practical constraints employed in the process, the constraints were relaxed although still kept within realistic bounds. The processes presented in the thesis are employing many constraints due to practical considerations. For the IRCC with relaxed practical constraints, the following simplifications were made:

1. Full gas turbine TIT was assumed (same TIT as for NG-fired GT). No TIT consideration was taken to the difference in the flue gas composition when operating with a hydrogen-rich fuel.

2. Metal dusting in heat exchangers was not considered. This means that, for example, superheating or gas-to-gas heat exchanging could take place right after the ATR.

3. Low reboiler duty for CO_2 capture subsystem was selected. The reboiler duty was dropped from a value of approximately 2 MJ/kg CO_2 captured to 1 MJ/kg CO_2 captured.

4. Low equipment, subsystem, and GT fuel nozzle pressure drops were assumed. The total pressure drop from inlet of ATR to outlet of GT burner fuel nozzles was decreased from approximately 9.7 bar to 5.2 bar. This means the reforming could take place at a lower pressure. Also, the needed air booster power would decrease and the reforming steam could be extracted at a lower pressure.

5. No consideration to off-design was taken. This means that a lower extracted steam pressure and a lower booster pressure ratio were needed.

Analysis and results of the IRCC process with relaxed practical constraints are presented in Chapter 6.

3.6.1 Pinch analysis

In order to evaluate the heat exchanger network, when examining the potential of a concept, energy targets were set. In this way, the performance of the HX network could be evaluated without actually having to carry out the complete network design. The goal of the analysis was to avoid any hot utility and minimizing the need for cooling water as cold utility. As part of this analysis, composite and grand composite curves were constructed by using the ProPi software (CIT Industriell Energianalys, 1999).

For further details on pinch analysis, refer to Smith (2005).

3.7 Process evaluation

When evaluating a process model that has been designed, a number of analysis steps are important, some of which have been described in the previous sections:

1. Thermodynamic analyses through process simulation

2. Investigating plant flexibility, specifically off-design operation

3. Examining the efficiency potential of the concept

4. Performing uncertainty analysis on the model outputs

5. Comparing the model to a reference plant

6. Validating the model by comparing the results to similar studies, pilot plants, or industrial plants

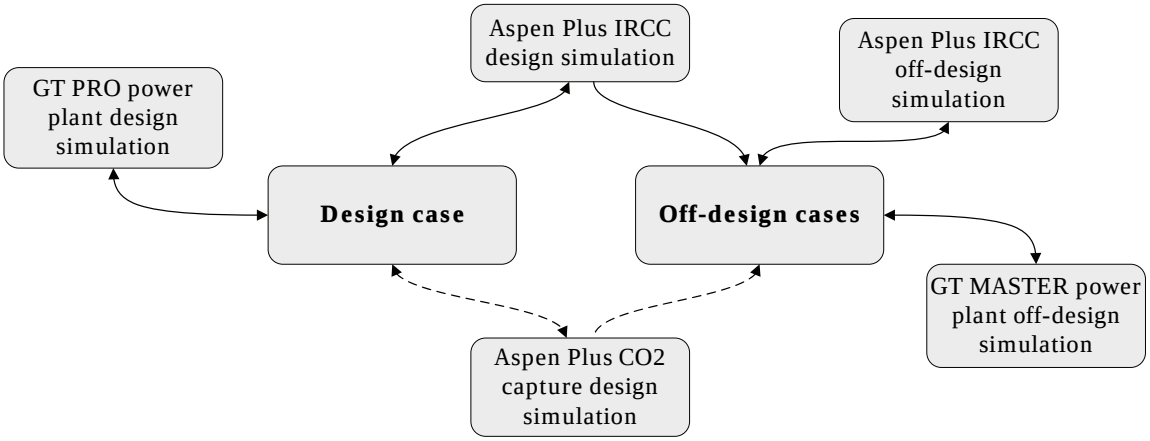

Figure 3.5: Simulation overview with software linking.

Also, for transparency, the inputs and assumptions necessary for near model duplication should be given.

3.8 Process modeling software linking

The design case model was modeled in GT PRO by Thermoflow, and in Aspen Plus by AspenTech as mentioned in previous sections. The Aspen Plus simulations consisted of two separate models. One that included the reforming process and the water-gas shift reactors. In this model, numerous heat exchangers were included, among those the whole preheating section. Air and CO_2 compression was also incorporated into the model. In the other model, the chemical absorption process was designed as a hot potassium carbonate model in a separate flow sheet. The models were linked by Microsoft Excel utilizing Aspen Simulation Workbook and the Thermoflow E-LINK. For the CO_2 capture system the model was not directly linked to Excel, instead a simple separator model was included in the reforming flow sheet with inputs such as split ratios, temperatures, and pressures from the absorption model. Outputs from the capture model also included pump work and reboiler duty.

For the steady-state off-design simulations, GT MASTER by Thermoflow in conjunction with Aspen Plus were used. Also, inputs such as heat exchanger areas, compressor design point, etc., were linked in from the Aspen Plus reforming design model. The overall simulation overview with the linking is displayed in Fig. 3.5.

Chapter 4

IRCC with dual-pressure reheat HRSG

In this chapter, an IRCC process with an air-blown ATR and a dual-pressure reheat HRSG is presented. This process has *not* been analyzed in any of the papers in Appendix B.

4.1 Process description

The process flowsheet for the process is displayed in Fig. 4.1. In the power plant part of the process flowsheet, the GT, ST, and HRSG are displayed. Within the HRSG, the heat exchangers for the different pressure levels are indicated. Included are the low-temperature economizer (LTE), the intermediate-pressure economizer (IPE), boiler (IPB), and superheater (IPS), the reheat section (RH), and the high-pressure economizer (HPE), boiler (HPB), and superheater (HPS). The two duct burners (DB) are also displayed in Fig. 4.1. Note that the IPB is drawn with dotted lines since in the IRCC setup the IPB in the HRSG was not utilized (only used when operating on NG). The schematic of the HRSG is simplified. In fact, some of the heat exchangers in Fig. 4.1 were split into several sections and the detailed layout is shown in Fig. 4.2. In Fig. 4.1 are also temperature indications at various locations in the process.

Reforming of natural gas was modeled as a one-step process in an ATR. The ATR is divided into a combustion zone and a thermal and catalytic zone. The heat generated from burning natural gas in the combustion zone provides heat for the reforming in the thermal and catalytic zone. Simplified, one can consider substoichiometric combustion of a hydrocarbon with the overall reaction

$$C_xH_y + \frac{x + y/2}{2} O_2 \rightarrow xCO + \frac{y}{2} H_2O_{(g)} \qquad -\Delta H^0_{298} > 0\,\text{kJ/mol} \tag{4.1}$$

Specifically, for methane (Christensen and Primdahl, 1994; Aasberg-Petersen et al., 2004)

$$CH_4 + \frac{3}{2} O_2 \rightarrow CO + 2H_2O_{(g)} \qquad -\Delta H^0_{298} = 519\,\text{kJ/mol} \tag{4.2}$$

In the thermal and catalytic zone, below the combustion zone, the main reactions are the water-gas shift reaction (4.4) and the hydrocarbon-steam reforming reaction

$$C_xH_y + xH_2O_{(g)} \rightleftharpoons xCO + (x + \frac{y}{2})H_2 \qquad -\Delta H^0_{298} < 0\,\text{kJ/mol} \tag{4.3}$$

$$CO + H_2O_{(g)} \rightleftharpoons CO_2 + H_2 \qquad -\Delta H^0_{298} = 41\,\text{kJ/mol} \tag{4.4}$$

Specifically, for methane-steam reforming

$$CH_4 + H_2O_{(g)} \rightleftharpoons CO + 3H_2 \qquad -\Delta H^0_{298} = -206\,\text{kJ/mol} \tag{4.5}$$

Desulfurization of the natural gas upstream of the reformer is indicated in the process flowsheet. Sulfur removal is necessary to protect the catalysts in the reforming and water-gas shift reactors. As a first step, sulfur removal requires catalytic hydrogenation to convert sulfur compounds, like COS and mercaptans, in the natural gas to gaseous hydrogen sulfide (Kohl and Nielsen, 1997; Aasberg-Petersen et al., 2004; Moulijn et al., 2007). The sulfur is then removed by flowing of the natural gas through a bed of zinc oxide granules to form solid zinc sulfide according to reaction

$$H_2S + ZnO_{(s)} \rightarrow H_2O_{(g)} + ZnS_{(s)} \tag{4.6}$$

However, in the Aspen Plus model the desulfurization system was not included and the low sulfur content (5 ppmvd) in the NG was neglected in the simulations.

In the HTS and LTS most of the the remaining CO was converted to CO_2 according to reaction (4.4). Downstream of the shift reactors, about 98% of the CO_2 was separated in the CO_2 capture subsystem, and the hydrogen-rich fuel vented from the absorber was used for the GT. The CO_2 capture subsystem consisted of a hot potassium carbonate process. The CO_2 was compressed to 150 bar in the CO_2 compression (four intercooled stages) and pump train.

As the ATR was air-blown there was a significant portion of nitrogen in the syngas. This nitrogen was used as fuel diluent for NO_x abatement in the GT combustor. The air needed for the ATR was bled from the GT compressor discharge plenum (flow-controlled with valve) and boosted up to system pressure with an air compressor. The selected gas turbine was a GE 9FB. The bottoming steam cycle, including the HRSG and an ST, was a dual-pressure reheat system with pressure levels of 130/27.5 bar. The HRSG was duct-fired at two locations in the gas path. One was located in the hottest zone of the HRSG to get the gas temperature up to a level close to what it would be for an NGCC. The IRCC GT exhaust temperature was lower because of the lower TIT. The second supplementary burner was located upstream of the preheating section. The heat added with the second duct burner was very close to the heat removed by the preheating streams. This was a feature enabling dry operation of the preheating section when the plant is operating on natural gas (the duct burners are not in operation during NG operation and thereby the temperature to the preheating section is lower). All duct firing was fueled with natural gas and increased the CO_2 released from the plant. However, this was compensated with a high capture rate (98%) of the CO_2 capture subsystem to result in an overall capture rate around 85%.

A significant amount of steam was produced from heat generated in the autoreforming process. Saturated water from the HPE was supplied to the syngas cooler and saturated steam was generated. From the syngas cooler, the saturated steam was supplied to the HP steam drum (not shown in process flowsheet). The same mass flow of steam as generated in the syngas cooler was supplied to superheaters HPS1A and HPS1B before submitted to the HRSG HPSs. IPE1A is acting as an IP economizer and IPB as an IP evaporator (same mass flow). GTPRE was preheating the fuel gas for the GT to 200 °C and PRE1 was preheating the supplied NG before it was further preheated in the HRSG.

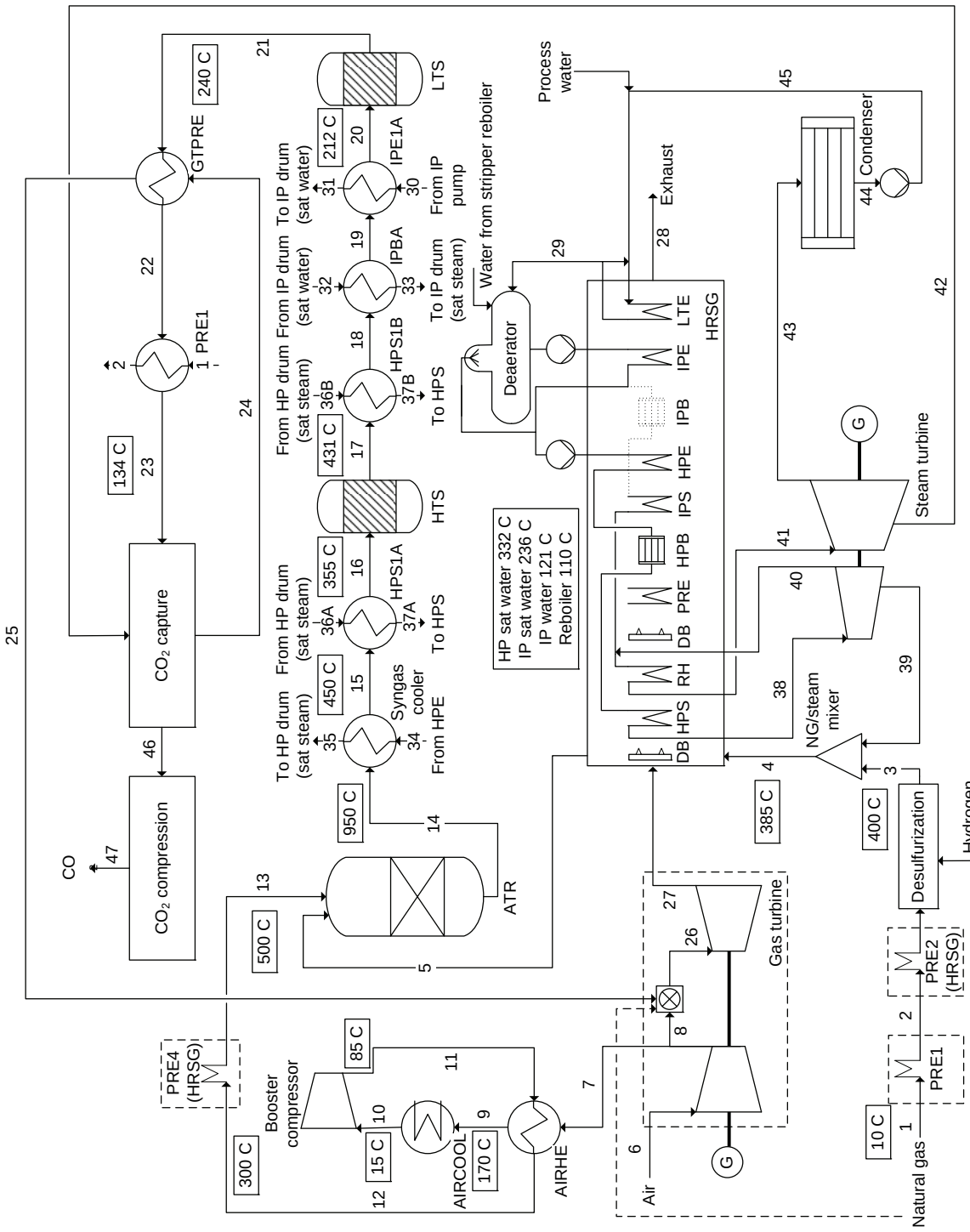

Figure 4.1: IRCC process flowsheet. Stream numbering and temperatures (in °C) are indicated for certain streams.

4.2 Power island model description

A cycle schematic of the power cycle, including the HRSG layout, is displayed in Fig. 4.2. As mentioned in Section 4.1, and shown in Fig. 4.2, the combined cycle power plant setup consisted of one GT, a dual-pressure reheat steam cycle, and an ST (HP and LP sections). The selected gas turbine was a GE 9FB from the GT PRO version 18 library. The turbomachinery was set up in a single-shaft arrangement.

To take into account the change in fuel from NG to a hydrogen-rich fuel, a TIT reduction of 100 K and an increase in turbine swallowing capacity of 6% were implemented in the model. The TIT reduction is further discussed in Section 4.6. Included in the GT model were also inlet filter pressure drop and exhaust losses. The HP pressure level before the stop valve to the ST was set at 130 bar. The IP pressure at the ST LP section inlet was assumed at 27.5 bar. GT PRO divides the ST into an HP and an LP section where the interface between the sections is the juncture where IP steam is added. The steam extractions, visible in Fig. 4.2, were done at 36 bar for the reforming steam to the ATR and at 3 bar for the reboiler in the CO_2 capture subsystem. The reboiler steam was further reduced in pressure to the required 2 bar. The higher than required extraction pressure was needed for the off-design cases when the extraction pressure decreased.

The design of the HRSG for the IRCC process was different from an HRSG design in an NGCC plant due to the significant amount of steam production from the heat generated in the reforming process and the large preheating requirement (close to 50 MW of preheating), as described in Section 2.3.4. The HRSG IPB was only operating when running the gas turbine on natural gas and is therefore not present in Fig. 4.2. When operating the full plant and supplying hydrogen-rich fuel to the GT, the IP boiler in the HRSG would be dry. The flue gas temperature at that location of the HRSG was sufficiently low to allow for dry operation. For the HP system, a majority of the steam was generated outside the HRSG. Of the 152.7 kg/s of steam admitted to the HP ST, 112.4 kg/s (74%) were generated in the process heat exchangers external to the HRSG. Included in the steam cycle were also a deaerator, condenser, and feedwater pumps.

A low-temperature economizer was included to utilize the low grade heat in the HRSG. The LTE water was recirculated to keep the LTE inlet water temperature at 60 °C to avoid corrosion of the tubes (too low temperature leads to condensation of HRSG gas).

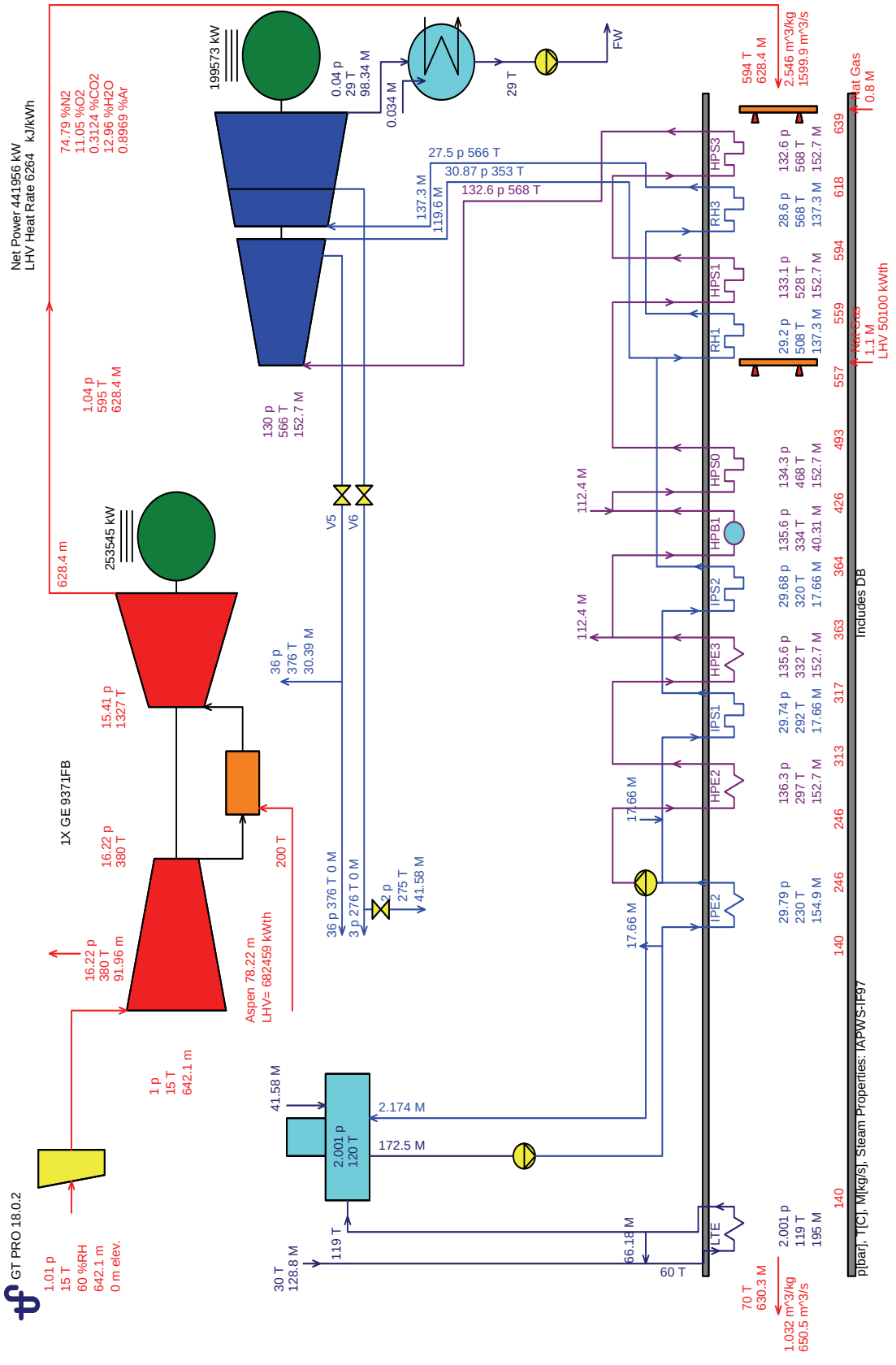

Figure 4.2: Power cycle schematic in GT PRO. Annotations: pressure p (bar); mass flow m/M (kg/s); temperature T (°C). For example, air extracted from the GT compressor with annotation 16.22 p, 380 T, 91.96 m, refer to a pressure of 16.22 bar, a temperature of 380 °C, and a mass flow of 91.96 kg/s.

4.3 Reforming model description

The unit operation blocks used, their inputs, and the design specifications for the Aspen Plus reforming process flowsheet will be described in this section. Refer to program manual (Aspen Technology, 2003) and help files (Aspen Technology, 2008) for further details about the unit operation blocks. The flowsheet, although too large to be represented in graphical form in the thesis, consisted of:

- Process stream preheating HXs which were modeled in Aspen Plus although present in the HRSG.
- Air booster compressor including inlet air cooling and heating of air after compressor.
- ATR and water-gas shift reactors.
- HXs for economizing, boiling, and superheating in the water/steam cycle.
- CO_2 compression and pumping.

4.3.1 Unit operation blocks

Air booster compressor

The air booster compressor was modeled with the Aspen Plus Compr block. Inputs to the model are listed in Table 4.1. For the off-design cases the pressure ratio and isentropic efficiencies were implemented as tabular compressor maps within the performance curve setup of the unit operation block. The compressor maps are shown in Fig. 4.5.

ATR

The ATR was modeled as an adiabatic Gibbs reactor (RGibbs).

CO_2 capture

The capture subsystem absorber and desorber were modeled with Aspen Plus RadFrac columns. However, in the reforming flowsheet the capture subsystem was modeled as a simple separator model (SEP) with inputs such as split ratios, temperatures, and pressures, which were results from the full absorption model.

CO_2 compressor

The CO_2 compression was modeled as a four-stage compressor train with cooling after each stage to decrease power consumption and condense H_2O. For this purpose, the MCompr model was utilized.

CO_2 pump

The pump unit operation block (Pump) was modeled with a fixed discharge pressure.

Air cooler

The cooling of air fed to the air booster compressor was modeled with the Heater unit block with a set outlet temperature.

Flash

Flash tanks before the air booster compressor and after the CO_2 capture subsystem was modeled with the Flash2 block.

Heat exchangers

The heat exchangers in the system were modeled with the HeatX block using the short-cut method (simplified method that does not require exchanger configuration or geometry data). Selected options included 'multiple passes', number of shells in series, minimum correction factor F_T (0.75), pressure drops on cold and hot sides, and heat transfer coefficient U. In addition, to get better convergence in the system, some of the HXs was modeled as heaters/coolers within the Aspen Plus flowsheet. Then, to verify that the HX design was realistic, a separate flowsheet with only HXs was developed and simulated.

Water-gas shift reactors

The HTS and LTS were modeled as adiabatic equilibrium reactors (REquil) with specified reaction (4.4).

NG/steam mixer

The NG/steam mixer was modeled with the Mixer block.

4.3.2 Design specifications

Four design specifications were implemented in the reforming flowsheet:

1. ATR outlet temperature was controlled at 950.0 +/− 0.1 °C by varying the mass flow of air from the GT compressor (via the booster compressor).

2. Fuel gas mass flow output from the model was controlled by varying the NG mass flow into the model. The specification was an input from the GT PRO model. GT PRO determined the necessary fuel mass flow for the GT to reach a certain turbine inlet temperature. The tolerance was set at 0.01 kg/s.

3. HTS inlet temperature was controlled at 355.0 +/− 0.1 °C by varying the steam mass flow in the HPS1A heat exchanger (first HP superheater).

4. Gas temperature out of the IPBA heat exchanger (IP evaporator) was controlled by varying the water mass flow rate from the HRSG IP economizer. The temperature specification was 245 +/− 1 °C.

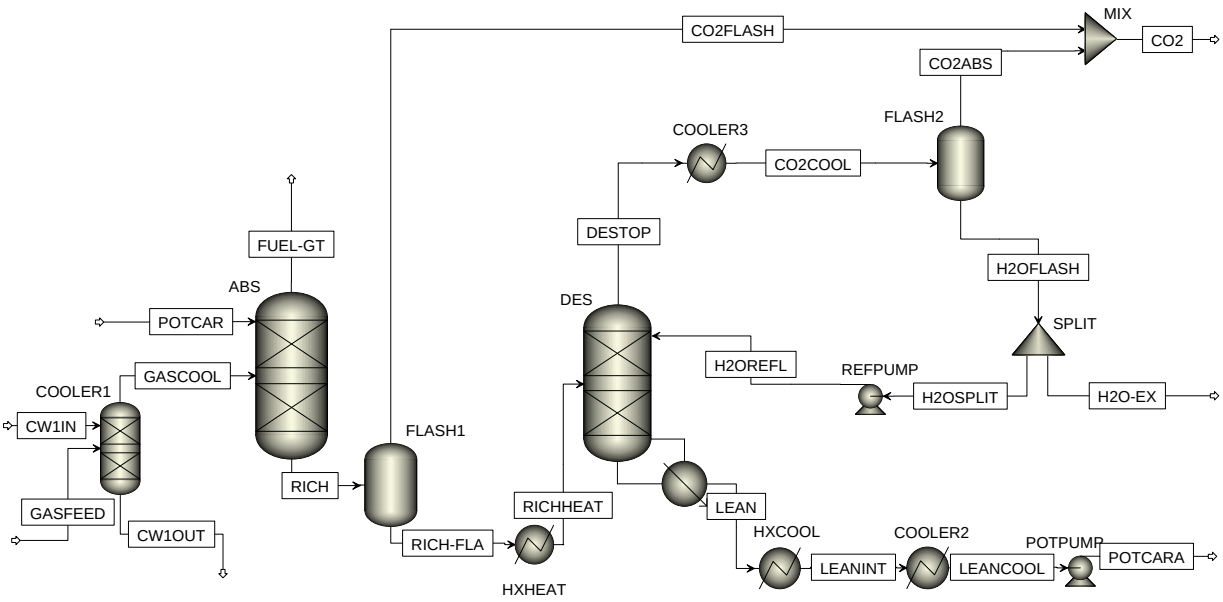

Figure 4.3: Hot potassium carbonate flowsheet modeled in Aspen Plus.

4.4 CO_2 capture model description

The capture model was based on modeling work by Anusha Kothandaraman, as part of the cooperation between NTNU and MIT, and is shown in Fig. 4.3 (Kothandaraman et al., 2009). A 40 wt% K_2CO_3 solvent composition was assumed.

4.4.1 Unit operation blocks

Gas cooler

The cooling of the gas feed (COOLER1 in Fig. 4.3) was modeled as an equilibrium RadFrac column with 5 stages.

Absorber

The absorber (ABS) was modeled as a rate-based RadFrac column with 30 stages. The following reactions were specified:

$$CO_2 + OH^- \rightarrow HCO_3^- \text{ (kinetic)} \tag{4.7}$$

$$HCO_3^- \rightarrow CO_2 + OH^- \text{ (kinetic)} \tag{4.8}$$

$$HCO_3^- + H_2O \rightleftharpoons CO_3^{2-} + H_3O^+ \text{ (equilibrium)} \tag{4.9}$$

$$H_2O \rightleftharpoons H_3O^+ + OH^- \text{ (equilibrium)} \tag{4.10}$$

Desorber

The desorber (DES) was modeled as a rate-based RadFrac column with 20 stages. The same reactions as for the absorber were specified.

Pumps

The pumps (Pump block) were modeled with a fixed discharge pressure.

Water split

The SPLIT (FSplit block) was specified to achieve the wanted reflux ratio.

CO_2 mixer

The Mixer unit operation block was used for the mixing of the CO_2 streams from the CO_2 flash and desorber.

Flash

Flash tanks (FLASH 1 and FLASH2 in Fig. 4.3) were modeled with the Flash2 block with pressure and zero heat duty as inputs.

Heat exchangers

The heat exchangers HXHEAT, HXCOOL, COOLER2, and COOLER3 were modeled with the Heater unit operation block with specified outlet temperatures.

4.4.2 Design specifications

Two design specifications were implemented in the Aspen Plus capture subsystem flowsheet:

1. The CO_2 portion of the GT fuel mass flow was controlled to arrive at a specific capture rate by varying the mole flow of the potassium carbonate stream (POTCAR stream in Fig. 4.3) into the absorber.

2. The CO_3^{2-} portion of the mass flow in the LEANCOOL stream was matched to the POTCAR stream by varying the reboiler heat duty in the desorber.

4.5 Process model assumptions

A list of model assumptions is displayed in Table 4.1. The supplied natural gas had an assumed pressure of 37 bar and a temperature of 10 °C with composition as listed in Table 4.2. The ambient air composition is given in Table 4.3.

Table 4.1: Assumptions made for the process models.

Site	
Ambient T (°C)	15
Ambient pressure (bar)	1.013
Ambient relative humidity (%)	60
Line frequency (Hz)	50
Cooling water system	direct water cooling
Cooling water	sea water
Cooling water T (°C)	8
Cooling water ΔT (K)	10
Gas turbine	
Model type	GE 9FB
TIT (°C)	1327
Turbine nozzle area increase (%)	6
Fuel gas preheating T (°C)	200
Water/steam cycle	
Cycle type	dual-pressure reheat
Pressure levels HP / IP (bar)	130 / 27.5
HP / Reheat T (°C)	566 / 566
Deaerator pressure (bar)	2
Condenser pressure (bar)	0.04
HRSG	
Minimum pinch point IP (K)	13
Approach subcooling IP (K)	3
Minimum pinch point HP (K)	13
Approach subcooling HP (K)	3
Minimum ΔT (K)	5
Minimum stack T (°C)	70
Air booster	
Pressure ratio	1.918
Isentropic efficiency	0.85
Mechanical efficiency	0.995
Syngas processing	
S/C	1.5
Prereformer inlet T (°C)	500
ATR air inlet T (°C)	500
ATR gas inlet T (°C)	500
ATR outlet T (°C)	950
HTS inlet T (°C)	355
LTS inlet T (°C)	212

Table continued on next page

Table 4.1 continued

CO_2 capture	
Capture rate (%)	98
CO_2 compression	
Number of compression stages	4
Stage 1 isentropic efficiency	0.85
Stage 2 isentropic efficiency	0.8
Stage 3 isentropic efficiency	0.8
Stage 4 isentropic efficiency	0.75
Mechanical efficiency	0.995
Intercooling T (°C)	30
Compression outlet pressure (bar)	75
Pump efficiency	0.7
Pump outlet pressure (bar)	150
Pressure drops	
GT inlet (bar)	0.010
GT exhaust & HRSG (bar)	0.023
Process heat exchangers – syngas side (bar)	0.2
ATR (bar)	0.7
Water-gas shift reactors (bar)	0.4

Table 4.2: Natural gas composition in model.

Component name	**Chemical formula**	**Unit**	**Value**
Methane	CH_4	vol%	79.84
Ethane	C_2H_6	vol%	9.69
Propane	C_3H_8	vol%	4.45
iso-Butane	C_4H_{10}	vol%	0.73
n-Butane	C_4H_{10}	vol%	1.23
iso-Pentane	C_5H_{12}	vol%	0.21
n-Pentane	C_5H_{12}	vol%	0.20
Hexane	C_6H_{14}	vol%	0.21
Carbon dioxide	CO_2	vol%	2.92
Nitrogen	N_2	vol%	0.51
Hydrogen sulfide	H_2S	ppmvd	5

Table 4.3: Ambient air composition in model.

Component name	**Chemical formula**	**Unit**	**Value**
Oxygen	O_2	vol%	20.74
Nitrogen	N_2	vol%	77.30
Argon	Ar	vol%	0.92
Carbon dioxide	CO_2	vol%	0.03
Water	H_2O	vol%	1.01

4.6 Practical considerations

A number of practical aspects were considered for the model and are described in this section.

Metal dusting

The syngas cooler is a waste heat boiler generating saturated HP steam. Due to the risk of metal dusting, the temperature of the heat exchanger walls needs to be below the temperature range where metal dusting is most likely. In a carbonized environment with a carbon activity above 1, the temperature range at which metal dusting is most likely to occur have been reported to be 400 °C (or 450 °C) to 800 °C (Grabke et al., 1993a,b; Di Gabriele et al., 2003), although these are not absolute limits. According to Grabke et al. (1993a) the carbon activity in a CO-H_2-H_2O environment results from the reaction

$$CO + H_2 \rightleftharpoons C + H_2O_{(g)} \tag{4.11}$$

The carbon activity a_c can be represented by

$$a_c = \frac{p_{CO} \cdot p_{H_2}}{K \cdot p_{H_2O}} \tag{4.12}$$

here p_i is the partial pressure in atm of component i. The thermodynamic equilibrium constant K can be approximated by

$$log_{10}K = -\frac{7100}{T} + 7.496 \tag{4.13}$$

where T is the temperature in Kelvin.

At the outlet of the ATR, in the process studied, a_c is above 1 at temperatures below approximately 750 °C. Thanks to the circulating water in the boiler tubes the metal temperature can be kept sufficiently low in the syngas cooler. The risk for metal dusting would increase if, for example, superheating steam. However, once the syngas has reached a sufficiently low temperature, superheating could take place. In the model presented, a superheater was installed between the syngas cooler and the HTS. The inlet temperature of the syngas to the superheater was chosen to be 450 °C.

GT

The selected gas turbine was a GE 9FB with a 6% increase in swallowing capacity compared to the NG version. For GE's IGCC application, the FB class turbines are fitted with FA parts. The 9FA has a turbine inlet temperature of 1327 °C and this was the selected TIT for the model, instead of the NG-fired 1427 °C FB TIT. It could be argued that the TIT should be decreased even further due to the increased heat released to the turbine hardware. The steam content from the GT combustion is higher with hydrogen-rich fuel compared to natural gas. This leads to a higher steam content, leading to an increased heat transfer coefficient, and as a result the metal temperatures of the turbine blades and vanes increase for a constant cooling flow. Chiesa et al. (2005) report TIT decreases of 10–34 K for hydrogen combustion with nitrogen or steam diluent (VGV operation cases). But there is uncertainty on how much the decrease should be and for this reason the 1327 °C was selected.

Dual fuel capability

The idea was to be able to operate the plant on hydrogen fuel *and* on natural gas. During startup, natural gas would be used and a fuel switchover would take place above 30% relative GT load. In other situations than startup and shutdown, the plant should also be able to operate on NG with an efficiency comparable (although lower) to an NGCC plant. The duct burners in the HRSG would not be operated when running on NG and the HRSG IPB would be utilized. The preheating section would be dry but has been located sufficiently far down in the HRSG gas path to allow for this. When operating the full IRCC plant, the fuel consisted of approximately 50 vol% hydrogen. This enables use of available IGCC-type diffusion combustors (Todd and Battista, 2000; Shilling and Jones, 2003). Fuel flexibility requires special attention to the burner design (Bonzani and Gobbo, 2007) and the control system (Shilling and Jones, 2003) and it should be possible to run with a mixture of natural gas and the hydrogen-rich fuel.

SCR

Selective catalytic reduction (SCR) has *not* been included in the model. The assumed NO_x emissions are 15 ppmvd at 15% O_2 on hydrogen fuel (with nitrogen diluent) and 25 ppmvd at 15% O_2 on natural gas (with steam injection). The main impact, if incorporating an SCR in the model, would have been additional pressure losses in the HRSG. A medium-temperature catalyst in the SCR has a typical operating temperature range of 260–425 °C although low- and high-temperature catalysts also exist (Heck, 1999). Kohl and Nielsen (1997) mention typical operating temperatures in the range of 315–370 °C. Due to the operating temperature requirement, the SCR would be intermixed with the HRSG heat exchangers. For a plant built in Norway, with a NO_x limit of 5 ppmv at 15% O_2 (Climate and Pollution Agency, 2007), an SCR, or similar technology, would be needed. A typical SCR NO_x removal rate is above 80%, which would be sufficient, both for hydrogen and natural gas operation, to reach the required 5 ppm.

LTE

At the back-end of the HRSG, a low-temperature economizer was located. To keep the lowest metal temperature of the LTE above the dew point of the exhaust gases (with some margin) the water inlet temperature was controlled at 60 °C by recirculation of the LTE exit water as is shown in Figs. 4.1 and 4.2. Also, the minimum stack temperature allowed was set at 70 °C. This low temperature was possible because of the very low sulfur content in the fuel. Fuel sulfur would generate sulfur oxides in the combustion process. Of the sulfur oxides, SO_3 would react with H_2O to form sulfuric acid, H_2SO_4, according to reaction (4.14). If condensing, the H_2O-H_2SO_4 mixture is highly corrosive.

$$SO_3 + H_2O_{(g)} \rightleftharpoons H_2SO_4 \tag{4.14}$$

Increased sulfur content means an increase in the acid dew point. To avoid condensation and corrosion, the stack temperature would then need to be kept higher. One disadvantage with low stack temperature is the risk of a condensation plume out of the stack. This is not popular in residential areas and are often mistaken as air pollution.

CO_2 capture

For reasons specified in Section 2.4.6, a hot potassium carbonate capture subsystem was selected even though the reboiler duty would be lower for an a-MDEA system (Göttlicher, 2004).

Off-design considerations

In order to have sufficient steam pressure for the reboiler and reformer at reduced plant load, the steam extractions were done at higher than necessary pressure levels for the design case. This lowers the design net plant efficiency. The air booster compressor pressure ratio was also higher than necessary at design conditions to allow for sufficient pressure to the GT fuel nozzles at off-design conditions. The compressor maps, as displayed in Fig. 4.5, led to a lower pressure ratio at reduced mass flows for the variable speed air booster compressor. In addition, the delivered pressure from the GT compressor extraction was lower during off-design operation. The combination of these two effects meant a higher design pressure ratio, than required when only considering the design point, was needed.

4.7 Steady-state part load operation

To investigate the plant's ability to operate and its performance at off-design conditions, two steady-state part load cases were simulated. An 80% and a 60% relative GT load case were included in the analysis, as defined by Eq. (3.11). The reason for selecting the relative part load points as a function of gas turbine load is because the GT dictates the overall plant load. By changing the GT load, the steam cycle, as well as the pre-combustion process, will follow.

Gas turbine part load operation commonly employs variable guide vanes (VGV). This is the case for the GE 9FB which has one row of VGVs where the flow angle entering the first stage of the compressor can be varied. The VGV operation allows reduction of the air flow and the turbine exhaust temperature can remain high at part load operation. The high exhaust temperature means the part load combined cycle efficiency can be maintained at a high level. However, at the lower part load range the cycle efficiency drops off quicker. The steam cycle part load operating concept involves sliding pressure operation with fully open steam valves down to approximately 50% steam turbine load (Kehlhofer et al., 1999). At lower loads the operating concept is based on fixed steam pressure operation by closing of the steam valves. This leads to throttling losses in the ST inlet valves. These factors combined may suggest that it does not make sense to operate a plant, such as the one presented in this chapter, at a much lower GT load than 60%. Also, NO_x and CO emissions could be an issue at low part load operation. Certainly, the plant still has to be able to operate at lower part load points, not the least during transients such as startups and shutdowns; however, transient analysis was not covered in this thesis.

The turbine inlet temperature reduction (due to hydrogen-rich fuel) was reduced (80% case) or removed (60% case) for the off-design simulations since the temperature was decreased anyway for part load operation. The air booster compressor pressure ratio and isentropic efficiency were calculated with compressor maps as described in Section 3.3.1.

Table 4.4: Key numbers and ratios for the IRCC model. Values were calculated in the process simulation, except for S/C and subsystem capture ratio which were assumed.

ATR	
Model type	Air-blown
S/C	1.5
O_2/C inlet	0.64
H_2/CO outlet	2.8
CH_4 slip (mol% out/mol% in)	2.4
HTS	
S/CO	2.2
CO conversion (%)	68
LTS	
S/CO	4.7
CO conversion (%)	86
Total CO conversion: HTS+LTS (%)	96
CO_2 capture	
Process	Hot potassium carbonate
Subsystem capture rate (%)	98
Subsystem outlet pressure (bar)	1.1
Reboiler duty (kJ/kg CO_2 cap.)	2250

For the CO_2 compression train, compressor maps were not utilized. The main reason for this was uncertainties in the design philosophy when employing a four-stage train. It was not clear how a part load solution for such a train would look like. Also, the specific reboiler duty (kJ/kg CO_2 cap.) for the capture subsystem was assumed constant from the design case.

In the design case, the inlet temperatures to the ATR and the water-gas shift reactors were fixed. For the off-design calculations, these constraints were removed (although for the water-gas shift reactors, the inlet temperatures could to some degree be controlled by altering the steam generation in the HXs prior to the HTS and LTS). Instead, for each part load case a check was performed to see if the inlet temperatures were within the operational window of each reactor. Based on the resulting inlet temperatures it was not necessary to use bypass valves for the various heat exchangers at the steady-state part load cases simulated (although likely needed during lower part load and startup and shutdown).

4.8 Results and discussion

4.8.1 Design case

Key numbers and ratios for the IRCC model is presented in Table 4.4. Results for the design case, in terms of power, efficiency, and capture rate, are presented in Table 4.5. A stream table for the design case is presented in Appendix A, Table A.1. The specific results for the GT and ST are presented in Tables 4.6 and 4.7.

Table 4.5: Results from the IRCC design case simulation.

Natural gas LHV input (MW)	924.0
Gross power output GT (MW)	253.5
Gross power output ST (MW)	199.1
Gross power output (MW)	452.6
Gross power output (% of LHV input)	49.0
Air compression (MW)	6.4
Air compression (% of LHV input)	0.7
CO_2 compression (MW)	16.7
CO_2 compression (% of LHV input)	1.8
CO_2 capture pumps (MW)	1.9
CO_2 capture pumps (% of LHV input)	0.2
Auxiliaries (MW)	8.9
Auxiliaries (% of LHV input)	1.0
Net power output (MW)	418.7
Net plant efficiency (% of LHV input)	45.3
Efficiency capture penalty (%-point loss to ref. case)	12.8
CO_2 emissions (g CO_2/net kWh el.)	70.1
CO_2 capture rate (%)	85.1

The LHV based net plant efficiency was 45.3% with a net power output of approximately 419 MW. The CO_2 capture rate was just above 85%. Included in Table 4.5 are the power consumption for the air booster compressor, the CO_2 compression, the pump work in the chemical absorption system, and the plant auxiliaries. The auxiliaries post in Table 4.5 includes, among other items, the boiler feedwater pumps and cooling water pumps. The net power output is here defined as the gross power output at the generator terminals minus the power needed for air compression, CO_2 compression, pump work, and auxiliaries, as displayed in Table 4.5. Step-up transformer losses were not included. The net plant efficiency is the net power output divided by the natural gas lower heating value input. The design case results were compared to the reference case's, as presented in Section 4.8.3, net power output of approximately 439 MW and efficiency of 58.1% leading to a capture efficiency penalty of approximately 12.8%-points.

Figure 4.4 shows a T-Q diagram of the HRSG. Notable is that the HP boiler, displayed as the horizontal line in the diagram, is small compared to an NGCC HRSG design. The reason for this is the large amount of steam generated in the syngas cooler. This means the economizer and the superheater in the HRSG are rather large but with a smaller boiler. Therefore, the HRSG has a different design than would be present in a typical NGCC plant, as discussed in Section 2.3.4. Because of the steam introduced from the syngas cooler and the following superheaters, the steam mass flow to the HP superheaters was almost *four times* higher than the steam mass flow generated in the HP boiler.

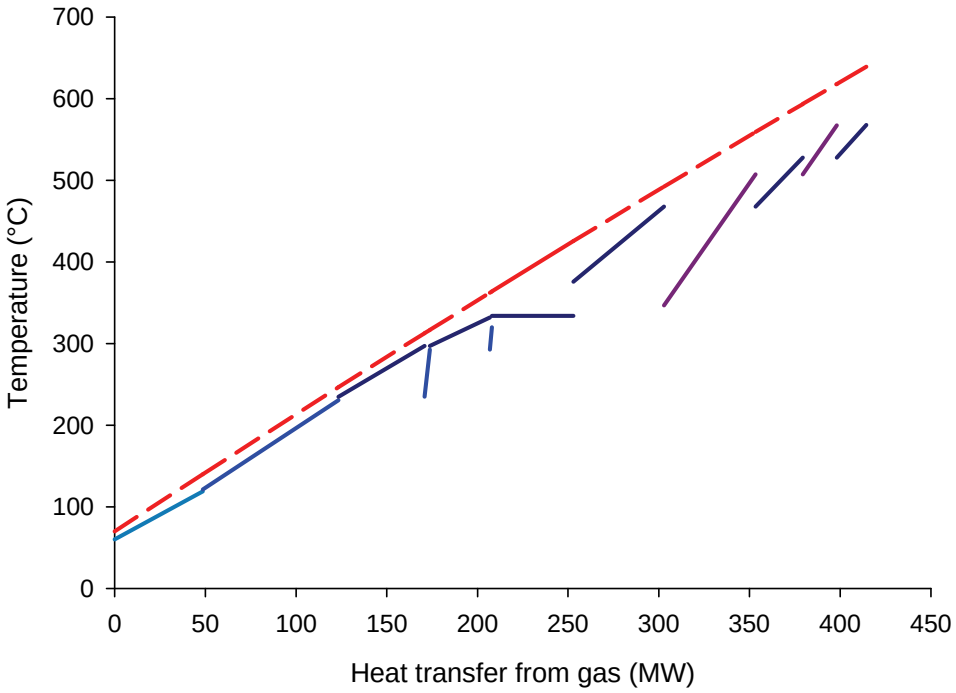

Figure 4.4: T-Q diagram for heat recovery steam generator in IRCC plant. Dashed lines refer to HRSG flue gas, solid lines to water/steam cycle.

Table 4.6: Gas turbine results from the IRCC design case simulation.

Fuel gas LHV input GT (at 200 °C) (MW)	709.6
Inlet air mass flow (kg/s)	642.1
Extracted air mass flow for ATR (kg/s)	92.0
Extracted air mass flow for ATR (% of inlet air mass flow)	14.3
Cooling air (compressor to turbine) (kg/s)	84.6
Cooling air (% of inlet air mass flow)	13.2
Compressor pressure ratio (-)	16.2
Turbine power (MW)	498.8
Compressor power (MW)	239.9
Mechanical efficiency (%)	99.3
Generator efficiency (%)	98.6
GT power output at generator terminals (MW)	253.5
GT efficiency at generator terminals (% of LHV input)	35.7

Table 4.7: Steam turbine results from the IRCC design case simulation.

Steam quality at outlet (-)	0.916
Turbine power (MW)	203.4
Mechanical efficiency (%)	99.5
Generator efficiency (%)	98.6
ST power output at generator terminals (MW)	199.6

4.8.2 Off-design cases

The off-design calculations resulted in net plant efficiencies of 44.0% and 42.3% for the 80% and 60% load cases respectively. The capture penalties for the part load cases were very similar to the design case, that is, between 12 and 13%-points. The CO_2 capture rate was 85.2% for both off-design cases, with CO_2 emissions of 72–74 g/net kWh electricity. The results are presented in Table 4.8. Stream tables for the off-design cases are presented in Appendix A, Tables A.2 and A.3.

The air extraction from the compressor discharge was decreased to 79 kg/s (approximately 14% of GT inlet air flow) for the 80% case and 65 kg/s (approximately 14% of GT inlet air flow) for the 60% case. Based on the compressor maps, the air booster compressor pressure ratio was 1.850 and isentropic efficiency 85.07% for the 80% case. For the 60% case, the pressure ratio was 1.717 with an isentropic efficiency of 84.47%. This should be compared to the design point values of 1.918 for pressure ratio and 84.77% for isentropic efficiency. In Fig. 4.5, pressure ratio and isentropic efficiency is plotted as a function of corrected mass flow $\frac{\dot{m}\sqrt{T_{01}}}{p_{01}}$ for different corrected speeds $\frac{N}{\sqrt{T_{01}}}$. The corrected mass flow and the corrected speed are relative to design value. The surge line is also visible in the figure. The chosen design point for the booster air compressor is indicated in the graph. For off-design operating conditions it is assumed that the compressor can be speed controlled. For the GT compressor, GT MASTER used maps built-in to the program.

4.8.3 Reference plant

As a reference plant, a state-of-the-art NGCC plant was simulated in GT PRO and GT MASTER. The reference plant did not include any CO_2 capture. Included in the plant was the same type gas turbine, a GE 9FB, as for the IRCC, but was instead of the IGCC combustor using a regular premix natural gas combustor and operating at the full 9FB TIT of 1427 °C. The steam cycle was a triple-pressure reheat cycle with HP pressure of 130 bar, IP pressure of 27.5 bar and LP pressure of 3.4 bar (all pressures at inlet of ST). A process flow sheet of the reference plant is displayed in Fig. 4.6.

For the design case of the reference plant, the net plant efficiency (excluding transformer losses) was 58.1% based on the lower heating value. Net plant power output was 439 MW (excluding transformer losses) and CO_2 emissions were 365 g CO_2/net kWh electricity. For the 80% off-design case the net plant efficiency was 56.7% with a net power output of 365 MW. The 60% case resulted in a net plant efficiency of 54.6% and a net power output of 290 MW.

Table 4.8: Summary of results from the IRCC off-design simulations. For comparison, the design case is included.

Relative GT load (%)	100.0	80.0	60.0
Natural gas LHV input (MW)	924.0	797.8	666.4
Gross power output GT (MW)	253.5	202.8	152.1
Gross power output ST (MW)	199.1	178.0	155.5
Gross power output (MW)	452.6	380.8	307.6
Gross power output (% of LHV input)	49.0	47.7	46.2
Air compression (MW)	6.4	5.2	3.8
Air compression (% of LHV input)	0.7	0.6	0.6
CO_2 compression (MW)	16.7	14.5	12.1
CO_2 compression (% of LHV input)	1.8	1.8	1.8
CO_2 capture pumps (MW)	1.9	1.6	1.3
CO_2 capture pumps (% of LHV input)	0.2	0.2	0.2
Auxiliaries (MW)	8.9	8.6	8.3
Auxiliaries (% of LHV input)	1.0	1.1	1.2
Net power output (MW)	418.7	351.0	282.1
Net plant efficiency (% of LHV input)	45.3	44.0	42.3
Efficiency capture penalty (%-point loss to ref. case)	12.8	12.7	12.3
CO_2 emissions (g CO_2/net kWh el.)	70.1	71.9	74.3
CO_2 capture rate (%)	85.1	85.2	85.2

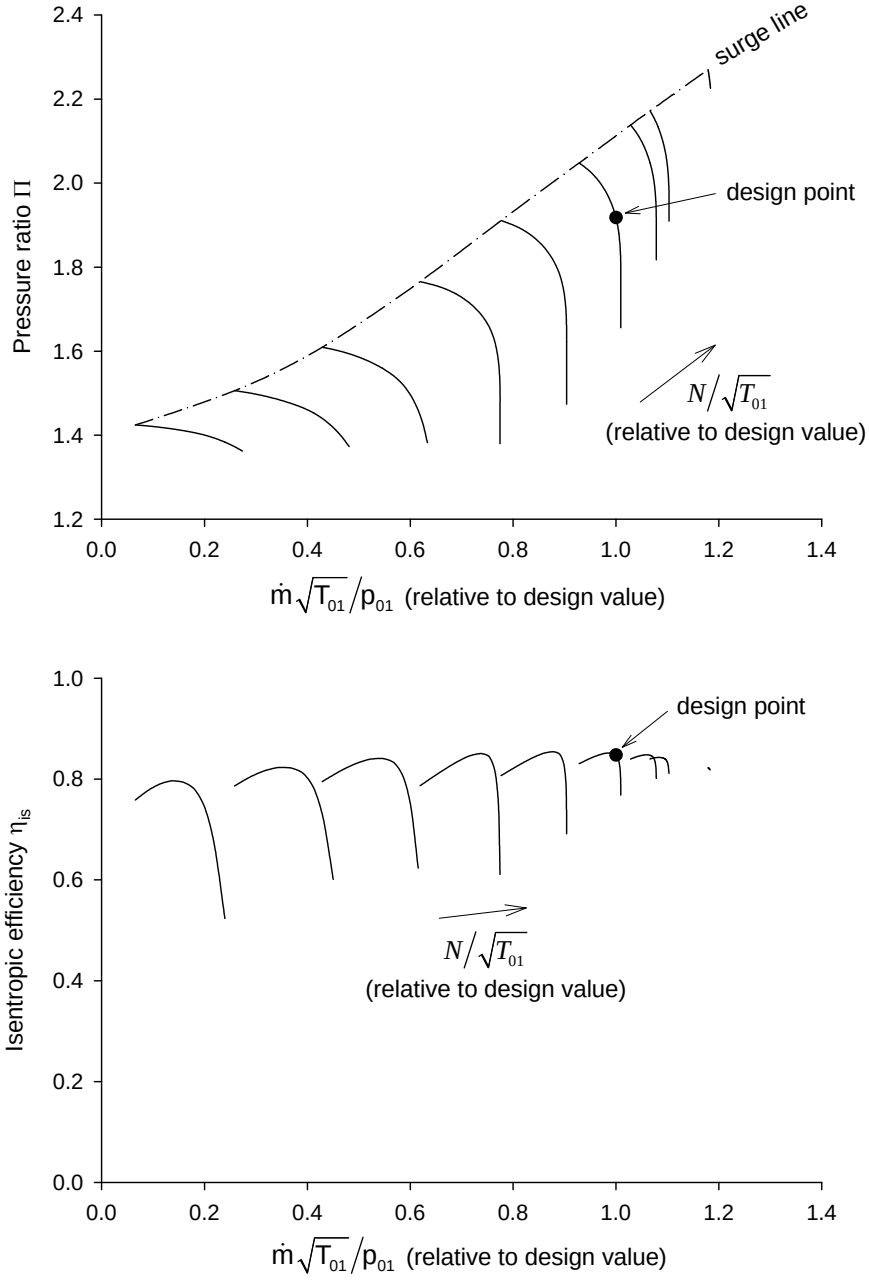

Figure 4.5: Compressor maps for the air booster compressor. The chosen design point is indicated.

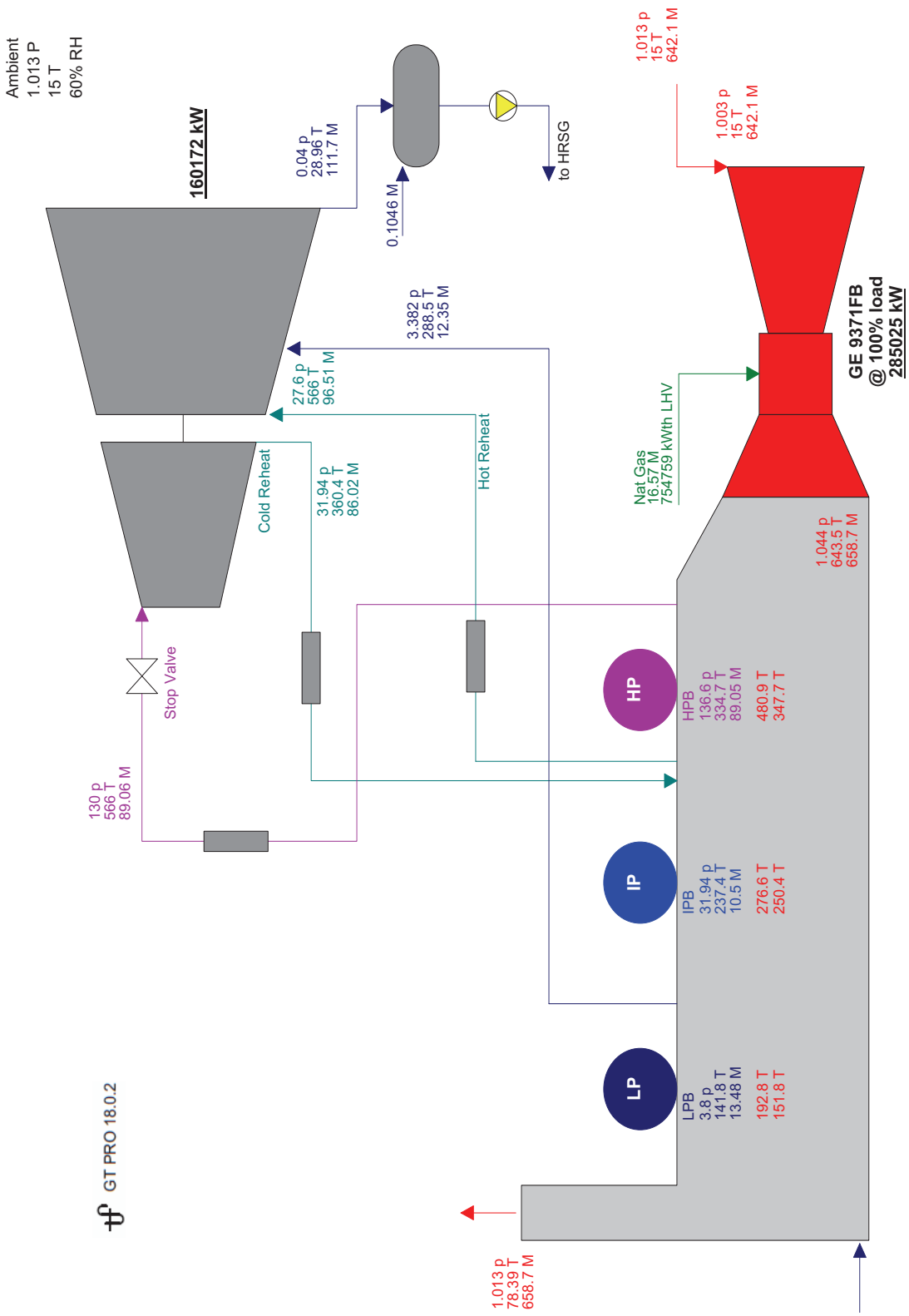

Figure 4.6: Process flow sheet of reference plant modeled in GT PRO. Annotations: pressure p (bar); mass flow M (kg/s); temperature T (°C).

4.8.4 System losses

In terms of fuel LHV input, losses for the various subsystems were calculated. For the reference NGCC plant the net plant efficiency was 58.1%. With an IRCC net plant efficiency of 45.3% this meant the CO_2 capture penalty was 12.8%-points. It was of interest to know where this loss originated from, for example, in order to determine where to focus process improvement efforts to decrease the capture penalty. Some of the losses were readily quantifiable in terms of loss in plant power output and then as follows from the power loss, a net plant efficiency drop. The readily quantifiable losses included, for example, air and CO_2 compression, losses due to CO_2 capture pumps, and the need for extra auxiliaries due to higher gross power output in the IRCC compared to the NGCC reference plant. Other losses were more laborious to quantify, like the fuel conversion losses in the reactors and the effect of preheating. The individual losses are described in the following sections and summarized in Table 4.9.

TIT reduction

TIT was reduced by 100 K for the IRCC GT compared to the full NGCC GE 9FB firing temperature. This has a negative effect on GT efficiency and it lowers the GT exhaust temperature which in turn decreases the steam generation and subsequently the ST power drops. By increasing the TIT for the IRCC to the full NGCC TIT, the effect on the reduction could be investigated. Results indicate that this led to a net plant efficiency drop of 1.8%-points, as shown in Table 4.9.

Air compression

The GT compressor discharge pressure was boosted up to the reforming pressure with an air booster compressor. This compressor would not be present in an NGCC plant and were therefore part of the capture penalty. In the simulations, the required compressor power for the design case was 6.4 MW. Thanks to the inlet air cooling for the booster, the required power could be kept at a fairly low level. 6.4 MW corresponded to an efficiency loss of 0.7%-points as is displayed in Table 4.9.

Preheating

Duct-firing in the HRSG was utilized to provide the heat required for the preheating streams. The effect of preheating was calculated by taking the difference of the natural gas heat content (with an NGCC combined cycle efficiency of 58.1%) and the steam that could have been generated if preheating was not done in the HRSG. With an NG mass flow in the duct burner of 1.1 kg/s and an LHV of 45517.56 kJ/kg, the loss in power due to duct firing was 29.1 MW if assuming this NG could have been used in a combined cycle with a 58.1% net plant efficiency. The additional steam that could have been generated in the HRSG, and subsequently used in an ST, led to a recover of 19.5 MW of the 29.1 MW. This meant the approximate loss in power due to preheating was 9.6 MW, which corresponded to a net plant efficiency drop of 1.0%-points.

Reforming steam

To calculate the effect of the reforming steam, the ST extraction point for the reforming steam was removed for the IRCC simulation. By comparing the results from the IRCC with and without the extraction, the effect on the ST power could be calculated. This effect was found to be 28.8 MW which corresponded to a 3.1%-point efficiency drop.

Reforming and water-gas shift

Losses due to fuel conversion from natural gas to syngas and then further on to a hydrogen-rich fuel were quantified. Figs. 4.7, 4.8, and 4.9 display schematics of the reforming and water-gas shift sections including the system boundary used for the loss analysis. Included in the figures are the reactors, heat exchangers, and the temperature after each step of the process. The control volumes for the analysis are indicated by the dashed lines in the figures.

The loss in power due to fuel conversion losses in the reactors, $\dot{W}_{loss}$, was defined as:

$$\dot{W}_{loss} = \eta_{ngcc}[(LHV \cdot \dot{m})_{in} - (LHV \cdot \dot{m})_{out}] - \dot{W}_{st,cv} \tag{4.15}$$

Where η_{ngcc} is the net electrical efficiency (excluding transformer losses) for the triple-pressure reheat NGCC plant, $(LHV \cdot \dot{m})_{in}$ is the input in kW from the feed gas to the reactor, $(LHV \cdot \dot{m})_{out}$ is the output in kW from the product gas, and $\dot{W}_{st,cv}$ is the ST power from the steam generated in the control volumes in Figs. 4.7, 4.8, and 4.9.

For the analysis, only steam that was generated from the heat of reaction, within each reactor, was considered. For the ATR, this meant that since the input temperature of the NG/steam mixture and the air was 500 °C, the heat generated from the reforming reactions was limited to the steam generated from the difference between the ATR outlet temperature of 950 °C and the first HX outlet temperature of 500 °C. Likewise for the HXs after the HTS and the LTS, only heat generated from the exothermic water-gas shift reaction was considered for HP steam superheating (after HTS) and IP steam economizing (after LTS).

The power loss in the ATR due to the change in LHV was approximately 73.2 MW. Out of the loss in power of 73.2 MW, 64.9 MW was recovered in the steam turbine due to the steam generated from the heat in the reactor. This 8.3 MW drop in power corresponded to a net plant efficiency drop of 0.9%-points. For the HTS, the loss in power due to change in the LHV was approximately 11.8 MW of which 8.7 MW was recovered in the ST. The 3.1 MW drop in power corresponded to a net plant efficiency drop of 0.34%-points. For the LTS, the loss in power due to change in the LHV was approximately 4.9 MW of which 2.6 MW was recovered in the ST. The 2.3 MW drop in power corresponded to a net plant efficiency drop of 0.25%-points. This meant the total fuel conversion loss in the reforming and water-gas shift sections was approximately 13.7 MW in plant power output which corresponded to a net plant efficiency drop of 1.5%-points.

Reboiler steam

To calculate the effect of the reboiler steam, the ST extraction point for the reboiler steam was removed for the IRCC simulation. By comparing the results from the IRCC with and without the extraction, the effect on the ST power could be calculated. This effect was found to be 22.4 MW which corresponded to a 2.4%-point efficiency drop.

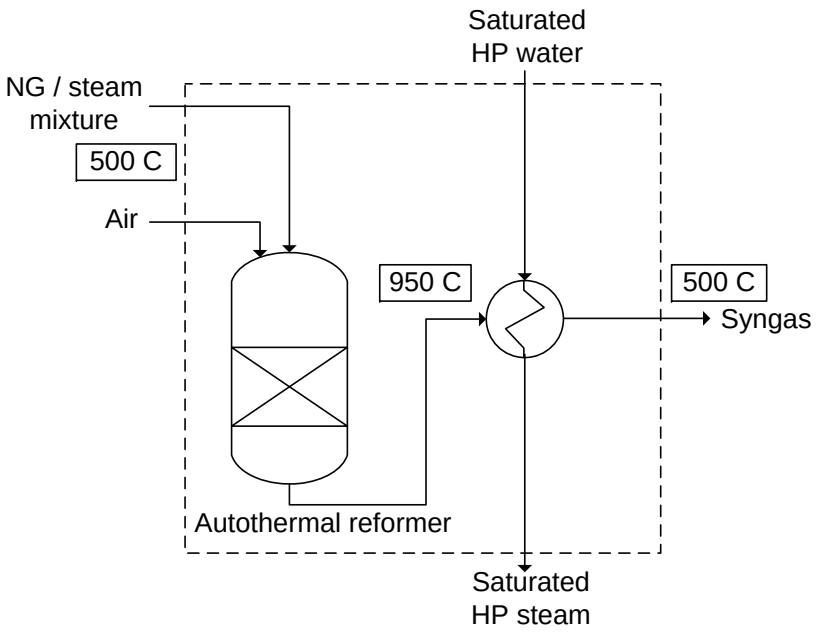

Figure 4.7: Schematic of reforming section including control volume for loss analysis.

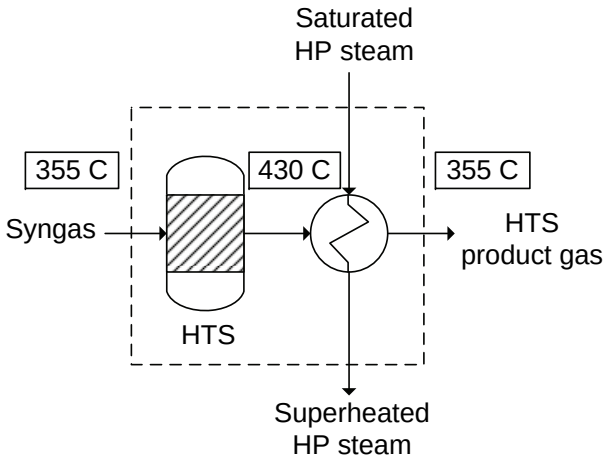

Figure 4.8: Schematic of high-temperature water-gas shift section.

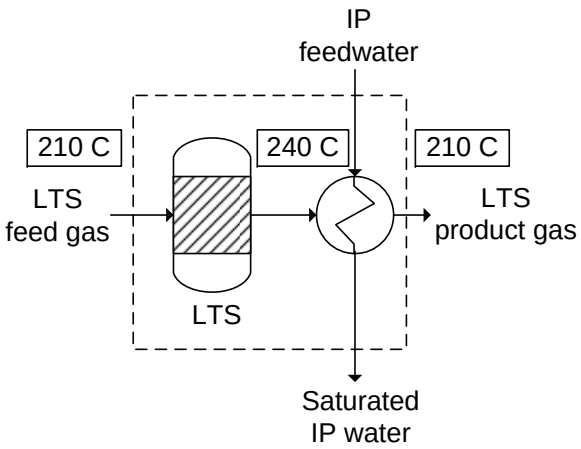

Figure 4.9: Schematic of low-temperature water-gas shift section.

CO_2 capture pumps

Pumping of lean mixture, reflux water, and cooling water in the CO_2 capture subsystem required approximately 1.9 MW of power. This corresponded to 0.2%-points in net plant efficiency drop.

CO_2 compression

Compression followed by pumping to the specified pressure of 150 bar required 16.8 MW of power. The four-stage compression train included cooling between each stage. The power consumption of the compression and pump train corresponded to an efficiency drop of 1.8%-points.

Extra auxiliaries

Due to the higher gross power output in the IRCC compared to the NGCC, the auxiliary load increased. The extra auxiliary load for the IRCC compared to the NGCC was 2.8 MW which corresponded to 0.3%-points in net plant efficiency drop.

Total quantified losses

Summing up the quantified losses described in the previous sections, resulted in a total net plant efficiency drop of 12.8%-points as is displayed in Table 4.9. This number should be compared to the calculated efficiency penalty of 12.8%-points, as presented in Section 4.8.1. It should be noted that the two numbers were arrived at with different calculations. The number presented in Section 4.8.1 was achieved by running two separate simulations: the reference NGCC plant simulation, and the design case IRCC simulation. The number resulting from a sum of the individual losses were achieved by making modifications to the design case IRCC model.

The losses are graphically presented in Fig. 4.10. Starting from the left of the figure, the first bar represents the reference NGCC net plant efficiency of 58.1%. Each following bar represent the net plant efficiency after each subsequent loss. Some of losses in Table 4.9 have been grouped for the graphical presentation in Fig. 4.10. The TIT loss consist of the 100 K TIT reduction loss. The power needed for the air booster compressor follows. In the reforming section, losses due to preheating of ATR feeds, fuel conversion losses in the reformer, and loss of power due to extraction of reforming steam are included. The fuel conversion losses in the HTS and LTS are grouped together. So are the losses due to extraction of reboiler steam and pump work in the CO_2 capture subsystem. Lastly, the losses due to extra auxiliaries are subtracted to arrive at an IRCC net plant efficiency of 45.3%.

Notable is that the reforming losses are almost twice as high as the CO_2 capture losses. Even more clear is this difference if considering that by selecting hot potassium carbonate as the chemical absorber in the capture subsystem, the reboiler duty was higher compared to a-MDEA (Göttlicher, 2004). From Fig. 4.10 it is evident that to decrease the capture penalty in an IRCC process, efforts should be concentrated towards improving:

1. The reforming process to decrease fuel conversion losses and needed steam mass flow.

Table 4.9: Subsystem efficiency losses in IRCC.

	MW	% of LHV input
Natural gas LHV input	924.0	100.0
Loss in power due to 100 K TIT reduction	16.5	1.8
Air compression	6.4	0.7
Loss in power due to preheating of process streams	9.6	1.0
Loss in ST power due to reforming steam	28.8	3.1
Fuel conversion losses in ATR	8.3	0.9
Fuel conversion losses in water-gas shift section	5.4	0.6
Loss in ST power due to reboiler steam	22.4	2.4
CO_2 capture pumps	1.9	0.2
CO_2 compression	16.8	1.8
Extra auxiliaries compared to NGCC	2.8	0.3
Sum of losses	118.9	12.8

2. The CO_2 capture process to decrease the reboiler duty.
3. The gas turbine technology to allow for a higher firing temperature.
4. The CO_2 compression process.

4.8.5 Effects of input parameters

To investigate the sensitivity of the net plant efficiency and CO_2 capture rate, a number of model input parameters were varied. A total of eleven parameters, as listed in Table 4.10, were selected for the variation runs. In order not to change the design of the plant and to achieve flowsheet convergence, there were limits on how much each parameter could be changed. For example, the ATR inlet temperature could not be raised above the base case value of 500 °C since the HRSG, where the preheating took place, would then have needed a redesign. Results from the analysis are shown in Figs. 4.11 and 4.12. Note the difference in x- and y-axes scaling in the two figures.

Base case

The base case for the analysis was based on inputs and results from Section 4.8.1. Values for these parameters are presented in Table 4.10.

TIT

A higher TIT meant more fuel was supplied to the gas turbine, and the GT efficiency and power output increased. Also, because of a higher GT exhaust temperature, when raising TIT, the steam production in the HRSG went up. Since the ratio between GT fuel flow and duct burner fuel flow increased (duct burner fuel flow held constant) the CO_2 capture rate also increased. As displayed in Fig. 4.11, a change in TIT of 150 K

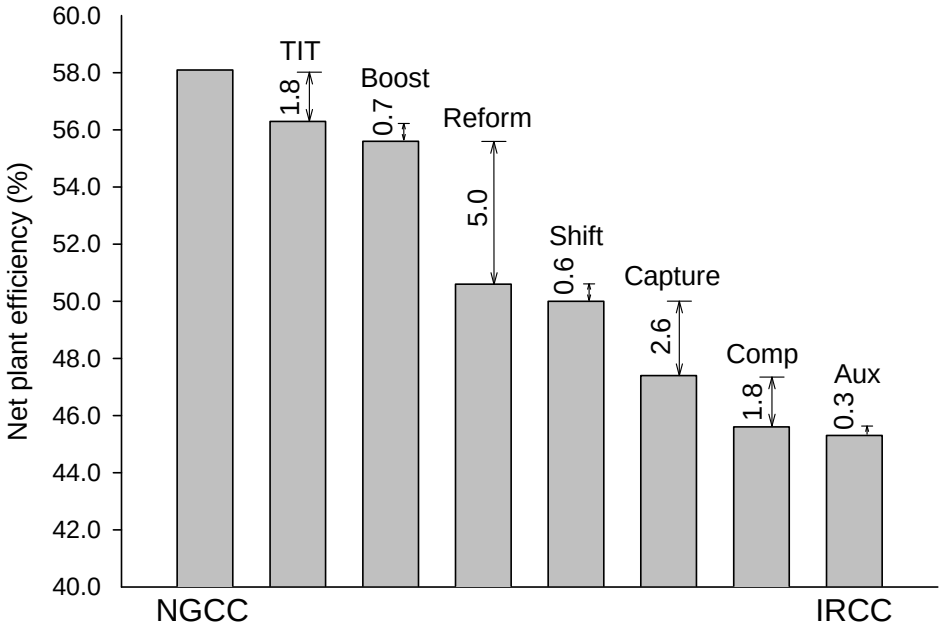

Figure 4.10: Efficiency system losses in IRCC. The left bar represents the net plant efficiency of the reference NGCC and the right bar the net plant efficiency of the IRCC. The bars in between represent the net plant efficiency after each system loss. The %-point drop for each system loss is indicated on the arrows. The losses are grouped in: loss due to 100 K TIT reduction (TIT); air booster compression power (Boost); loss from extraction of reforming steam, preheating of ATR feeds, and fuel conversion loss in the reformer (Reform); fuel conversion losses in the HTS and LTS (Shift); pump power and loss from extraction of reboiler steam for the CO_2 capture subsystem (Capture); CO_2 compression (Comp); extra auxiliaries compared to an NGCC (Aux).

Table 4.10: Selected model inputs for variation runs including range of variation and base case values.

Input parameter	**Range**	**Base case**
TIT (°C)	1277–1327	1327
Minimum stack T (°C)	60–120	70
Reboiler duty (kJ/kg CO_2 cap.)	1000–2500	2250
Condenser pressure (bar)	0.02–0.1	0.04
S/C (-)	1.0–1.75	1.5
ATR T_{inlet} (°C)	400–500	500
ATR T_{outlet} (°C)	850–1150	950
ATR p_{inlet} (bar)	27.5–32.5	30.0
HTS T_{inlet} (°C)	345–375	355
LTS T_{inlet} (°C)	202–232	212
CO_2 cap. rate for capture subsystem (%)	90–98	98

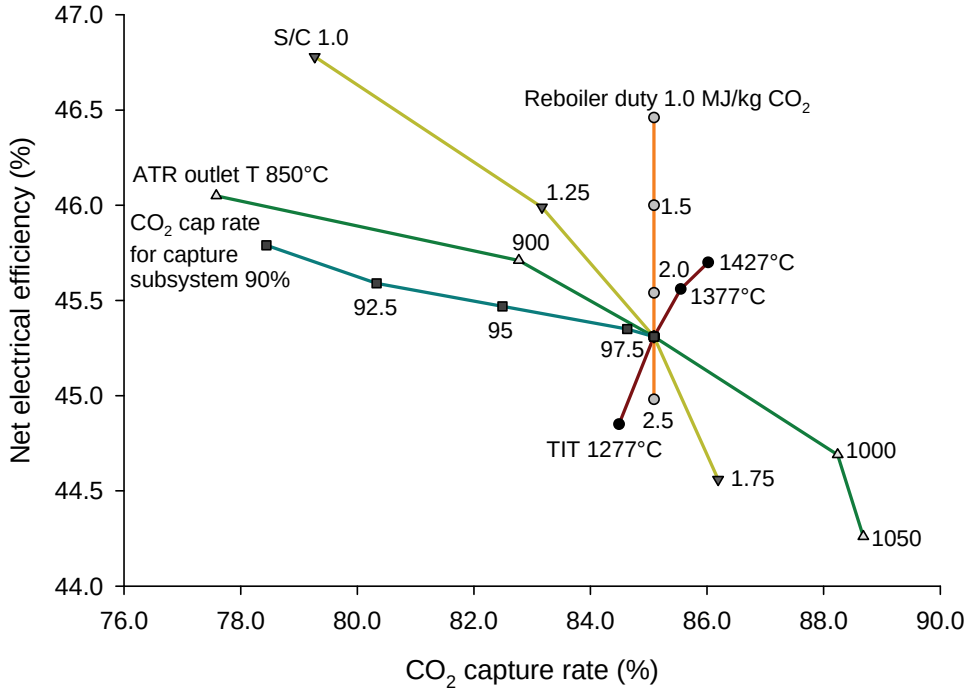

Figure 4.11: Effect of input parameters (1).

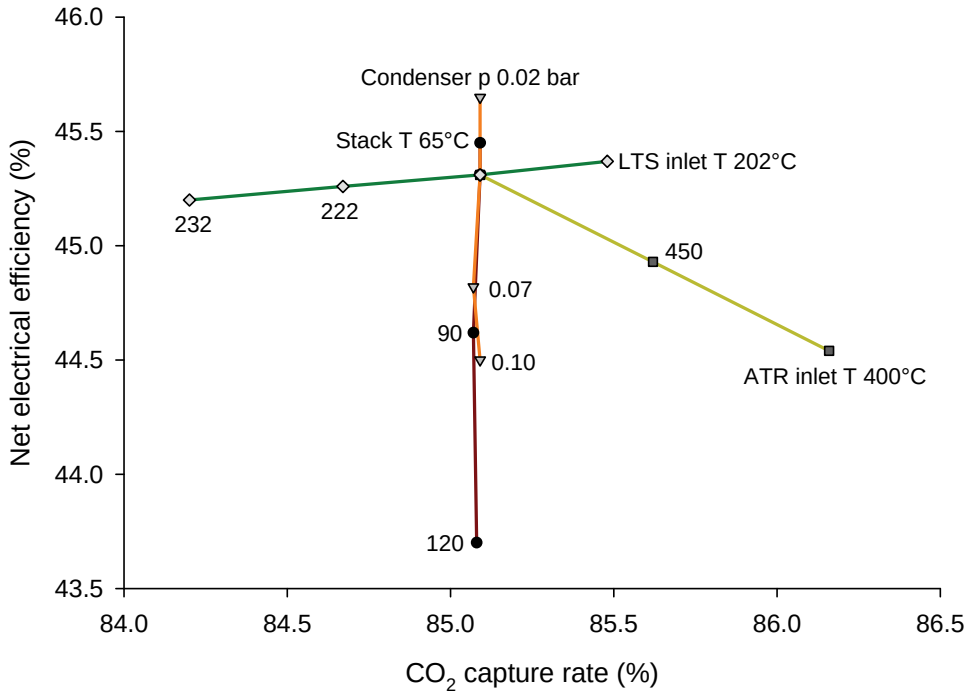

Figure 4.12: Effect of input parameters (2).

from 1277 °C to 1427 °C led to a 1.9% (0.85%-points) change in net plant efficiency and a 1.8% (1.5%-points) change in CO_2 capture rate in relation to the base case values.

Stack temperature

The stack temperature was varied by changing the minimum allowed stack temperature. Varying the stack temperature had, as expected, no impact on the CO_2 capture rate but some effect on the net plant efficiency as displayed in Fig. 4.12. Lowering the stack temperature meant more of the energy in the GT exhaust stream could be utilized for steam generation (since the pinch point was at the stack). A 60 K change in stack temperature led to 3.9% (1.75%-points) change in net plant efficiency.

Reboiler duty

The reboiler duty was changed without changing the capture rate for the capture subsystem. As follows, the overall CO_2 capture rate was unaffected. With a lower reboiler duty, less steam was extracted from the ST and as follows the net plant efficiency increased due to the increased ST power output. The results are displayed in Fig. 4.11. On a percentage basis, a 66.7% (1500 kJ/kg CO_2 cap.) change in reboiler duty resulted in a 3.3% (1.5%-points) change in net plant efficiency.

Condenser pressure

By changing the condenser pressure, the power output of the steam turbine changes. A decrease in pressure means an increase in power output and as follows, the net plant efficiency increased. CO_2 capture rate was unaffected. A 200% (0.08 bar) change in condenser pressure resulted in a 2.5% (1.1%-points) change in net plant efficiency, as displayed in Fig. 4.12.

S/C

Steam-to-carbon ratio is a critical parameter for an IRCC. By changing the S/C, the methane slip out of the ATR changes and so does the CO conversion in the HTS. In addition, the ST power output changes. As follows from this, both the net plant efficiency and the CO_2 capture rate are affected by the S/C. An increase in S/C resulted in a higher CO_2 capture rate and a lower net plant efficiency as is displayed in Fig. 4.11. A 50% (0.75) change in S/C led to a a 4.9% change in efficiency and an 8.1% change in capture rate.

ATR inlet temperature

In order not to redesign the HRSG, the preheat temperature for the ATR was only decreased from the base case value. No increase was possible since the flue gas temperature in the HRSG at the preheating section did not allow for this. A decrease of 100 K resulted in a 1.7% decrease in net plant efficiency and 1.3% increase in CO_2 capture rate. With a lower preheat temperature, more of the natural gas was combusted to reach the ATR exit temperature. This meant more air was needed, leading to a lower GT power output since more air was extracted from the GT compressor discharge. This led to a lower net plant

efficiency. Also, the compressor discharge pressure decreased when more air was extracted. In addition, the extra extracted air meant more fuel diluent nitrogen was introduced to the GT combustor. This nitrogen was preheated to 200 °C meaning more fuel was spent to raise the nitrogen temperature to the turbine inlet temperature (since the 200 °C preheat temperature was lower than the compressor discharge temperature). The lower compressor discharge pressure had the effect of lowering the inlet pressure to the ATR (with a constant pressure ratio of the air booster compressor). A lower reforming pressure meant the CH_4 slip decreased and as follows, the overall CO_2 capture rate increased. The data are presented in Fig. 4.12.

ATR outlet temperature

A decrease in ATR outlet temperature, while keeping the pressure constant, led to a higher CH_4 slip from the ATR. Removing heat from an endothermic reaction, like the methane-steam reforming reaction, leads to, according to Le Chatelier's principle, a shift in the equilibrium towards the reactants. As methane is one of the reactants, the methane slip increased at lower reforming temperatures. This meant the CO_2 capture rate decreased when lowering ATR outlet temperature. However, with a lower ATR outlet temperature, less air was extracted from the GT and less fuel was combusted in the ATR. This led to an increase in net plant efficiency. A total change in ATR outlet temperature of 200 K led to a 4.0% change in net plant efficiency and a 13.0% change in capture rate. The results are presented in Fig. 4.11.

ATR inlet pressure

In order to stay within the given design of the plant, the reforming pressure was only slightly changed. For the ATR it is advantageous to operate at the lowest possible pressure for increased net plant efficiency and CO_2 capture rate. A lower pressure is, according to Le Chatelier's principle, favorable for the methane-steam reforming reaction. Also, a lower reforming pressure means steam can be extracted at a lower pressure from the ST and the air booster compressor can be operated with a lower pressure ratio. These effects increase the net plant efficiency. However, to avoid a fuel compressor, there was a limit to how low the pressure could be decreased to maintain a sufficient pressure for the GT fuel nozzles. A 16.7% (5 bar) change in pressure led to a 0.5% change in net plant efficiency and a 0.4% change in capture rate.

HTS inlet temperature

The HTS inlet temperature is not a critical parameter. Since the water-gas shift reaction is exothermic, a lower temperature increases the CO conversion leading to a slightly increased CO_2 capture rate for the plant. A 30 K change in the inlet temperature lead to a 0.3% in capture rate and a negligible change in net plant efficiency.

LTS inlet temperature

The LTS inlet temperature is an important parameter for the capture rate of the plant. A lower inlet temperature leads to a higher overall CO conversion and as follows a higher CO_2 capture rate. The unconverted CO would be burned in the GT combustor and

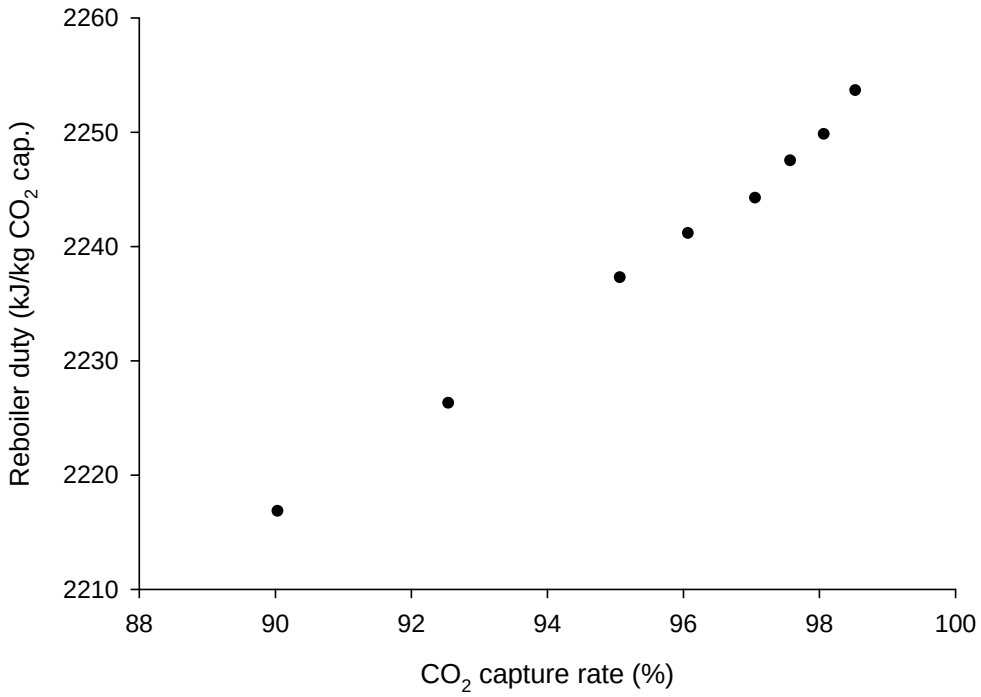

Figure 4.13: Reboiler duty as a function of capture rate for the CO_2 capture subsystem.

contribute to the CO_2 emissions from the plant. The effect on the net plant efficiency was very small. A 30 K change in inlet temperature led to a 1.5% change in capture rate and a 0.4% change in net plant efficiency. The data are presented in Fig. 4.12.

CO_2 capture rate for capture subsystem

An increased subsystem capture rate leads to a higher reboiler duty meaning more steam is extracted from the ST and the net plant efficiency drops. However, the effect on the overall CO_2 capture rate was more pronounced. Fig. 4.13 shows the reboiler duty as a function of CO_2 subsystem capture rate. For the overall plant performance, it was found to be most advantageous to run the subsystem at as high capture rate as possible. A 8.2% (8.0%-points) change in the subsystem capture rate led to a 1.1% (0.5%-points) change in net plant efficiency and a 7.8% (6.7%-points) change in CO_2 capture rate as displayed in Fig. 4.11.

Table 4.11: Comparison of pilot plant, industrial plant[a], and Aspen Plus ATR model.

	Pilot plant[b]	Industrial plant[b]	Model[c]	p and S/C adj model[c]
Feed ratios				
S/C	1.43	1.4	1.50	1.43
O_2/C	0.60	0.54	0.64	0.64
Product gas				
T (°C)	950	950	950	950
p (bar)	24.5	25	29.3	24.5
H_2/CO	2.97	2.84	2.81	2.76
CH_4 leakage (dry mole%)	1.00	1.1	0.30	0.23
CH_4 leakage (dry and N_2 free mole%)	∼1.0	∼1.1	0.53	0.41

[a]pilot and industrial plant data from Christensen and Primdahl (1994)
[b]oxygen-blown, [c]air-blown

4.9 Model validation

The model validation included comparisons of:

1. The reforming process.
2. The power island including both simple cycle and combined cycle operation.
3. The full IRCC plant.

4.9.1 Reforming process

Pilot plant test results (case A) and industrial plant data (case 5) presented by Christensen and Primdahl (1994) have similar inputs and outputs as the RGibbs ATR results in Aspen Plus, as displayed in Table 4.11. Also, for comparison purposes, the inlet pressure and the S/C were modified in the model to match the pilot and industrial plants. The adjusted model is displayed in the last column of Table 4.11.

An important difference between the pilot and industrial results and the model results is that the pilot and industrial plants are utilizing an oxygen-blown ATR but the model was using an air-blown ATR. For the model, this means more oxygen is needed to reach the desired outlet temperature since the inert nitrogen in the air needs to be heated up to the outlet temperature. Since the combustion is substoichiometric, a higher air flow leads to a higher temperature (more fuel is combusted). The higher O_2/C means more of the fuel will combust and subsequently more of the CH_4 will be combusted leading to a lower CH_4 leakage. Also, the emitted CO will increase leading to a lower H_2/CO. No comparable plant data for an air-blown ATR were found in the literature.

Comparing the pressure and S/C adjusted model to the pilot plant, a 6.7% difference in O_2/C and a 7.1% difference in H_2/CO are noted. The methane leakage in the model was recalculated by removing the N_2 content in the outlet of the ATR to get a more comparable basis for the mole%. Nevertheless, the leakage is clearly higher for the oxygen-

Table 4.12: Comparison of natural gas fired simple and combined cycle plants: GT PRO models versus 2009 Gas Turbine World Handbook (GTW).

Plant type	simple cycle	simple cycle	combined cycle[a]	combined cycle[a]
Source	GTW	GT PRO	GTW	GT PRO
Gas turbine	GE 9FB	GE 9FB	GE 9FB	GE 9FB
Net plant output (MW)	not reported	285.9	412.9	434.4
GT gross power (MW)	279.2	287.4	266.7	286.3
ST gross power (MW)	-	-	151.7	154.3
Electrical efficiency[b] (%)	37.9	38.1	58.0	57.5
Pressure ratio (-)	18.3	18.2	not reported	18.2
Air mass flow (kg/s)	655	642	not reported	642
Exhaust T (°C)	629	640	not reported	643

[a]triple-pressure reheat steam cycle, [b]gross for simple cycle; net for combined cycle

blown ATRs. Compared to the industrial plant, the adjusted model showed a 18.5% higher O_2/C and a 2.8% lower H_2/CO.

4.9.2 Power island

For validation of the power plant model, comparisons were made between 1) simple cycle natural gas fired GT and 2) combined cycle natural gas fired plant. The reference data were gathered from Gas Turbine World (2009) (GTW). Syngas fired GT reference performance was not found in literature. In general, comparisons were challenging because of unknown differences in input data. And to date there is no commercial 9FB hydrogen fired GT. Mostly, the GT PRO database is based on input from the original equipment manufacturers (OEM) or from available literature. GTW is based on data supplied by the OEMs.

ISO ambient conditions and default settings in GT PRO with a typical NG composition were assumed. Fuel pressure was chosen sufficiently high to avoid a fuel compressor. For the combined cycle, a triple-pressure steam cycle with reheat was selected. Step-up transformer losses were not included when calculating net plant efficiency. A condenser pressure of 0.0576 bar was selected to match the GTW combined cycle condenser pressure. Table 4.12 displays the simple and combined cycles comparison.

For the simple cycle, the GT gross output from the GT PRO model is within 3% of the GTW reference data. Pressure ratio and net electrical efficiency (0.5% difference) are very similar between model and reference data. Model air mass flow is approximately 2% different from reference data. Exhaust temperature was within 11 °C.

For the combined cycle model there were more unknown input data and therefore a larger uncertainty in comparison of output data. The description of input data were very limited for the reference cycle. Expectedly, the differences for the combined cycle were larger between the model and the reference compared to the simple cycle. Net plant power output was about 5% higher than GTW plant data. This difference mainly comes from the GT gross power output (7% higher for model) but also to some extent from ST

Table 4.13: Comparison of IRCC system level studies: (a) Andersen et al. (2000) Case 1; (b) Ertesvåg et al. (2005) AC 30 bar; (c) Corradetti and Desideri (2005) Ref. 950 °C; (d) IRCC presented in Chapter 4.

Study	(a)	(b)	(c)	(d)
GT	GE 9FA	GE 9FA	Siemens V94.3A	GE 9FB
HRSG	3PR[a]	3PR[a]	3PR[a]	2PR[b]
S/C (-)	2.0	1.64	1.46	1.5
Reboiler duty (kJ/kg CO_2)	not reported	not reported	2130	2250
Capture rate (%)	82.0	not reported	88.1	85.1
Net electrical efficiency (%)	45.9	48.4	46.9	45.3

[a]triple-pressure reheat, [b]dual-pressure reheat

gross power output difference (2% higher for model). The net electrical efficiency for the model was about 1% lower than the reference.

4.9.3 IRCC plant

On a full IRCC plant level, the model was validated against similar analyses available in the literature as displayed in Table 4.13. The studies used as reference were done by Andersen et al. (2000); Ertesvåg et al. (2005); Corradetti and Desideri (2005). In each of the reference studies, several cases were analyzed. For the model validation, the case in each study that most resembled the setup presented in this chapter was selected. The selected cases are indicated in the heading of Table 4.13.

For an IRCC, many configuration options exist and none of the referenced studies exactly matched the cycle analyzed in this chapter. However, the studies in Table 4.13 were the closest matches found in the literature. Some notable differences were:

- System pressure, and therefore reforming pressure, were different. (Ertesvåg et al. (2005); Corradetti and Desideri (2005) use a fuel compressor before the GT. Andersen et al. (2000) use an air booster compressor in their 30 bar air pressure case).
- S/C, capture rate, and reboiler duty were different (or not reported).
- Different steam cycles were used.
- Different gas turbines were used.
- None of the referenced studies take off-design into consideration.

Comparing the modeled cycle with the analysis by Andersen et al. (2000), the difference in net plant efficiency is 1.3% (0.6%-points) with a 3.8% difference in CO_2 capture rate. In the cited study it is not clear from where the heat required for the capture subsystem was taken and the reboiler duty was not specified.

Ertesvåg et al. (2005) focus on an exergy based analysis but energy based analysis was also conducted. Here, a big difference is noted when comparing the net plant efficiency to the analysis in this chapter. A 6.4% difference (3.1%-points) was noted when comparing the IRCC presented in this chapter to the referenced cycle. An assumption of providing the

heat necessary for the reboiler from the last heat exchanger before the capture subsystem (corresponds to HE4 in Fig. 4.1) may not be realistic, but this was not the focus of that study. However, this assumption could affect the results significantly (several %-points in net plant efficiency) since it was shown in Fig. 4.10 that for the cycle studied in this chapter, the loss in efficiency due to the capture subsystem (basically because of the reboiler duty) was 2.6%-points.

Comparing the analyzed system to the one studied by Corradetti and Desideri (2005) showed a difference in net plant efficiency of 3.4% (1.6%-points) and in capture rate also of 3.4%. The reboiler duties were here similar. The referenced study used a triple-pressure reheat steam cycle. A fuel compressor, instead of an air booster compressor, was utilized.

Overall, the results of the model presented in this chapter are similar to the results of the referenced studies. However, significant model output uncertainties (e.g., in the range of 3%-points in net plant efficiency) exist as is presented in Paper IV. The paper describes an uncertainty analysis of an IRCC setup.

Chapter 5

IRCC with single-pressure HRSG

The IRCC process with a single-pressure HRSG is described and analyzed in Papers III and IV. To allow for comparison to the model presented in Chapter 4, some modifications were done to the assumptions and inputs for the models analyzed in Papers III and IV. The model, with the modified assumptions and inputs, is presented in this chapter.

5.1 Process description

The process is described in Papers III and IV and will only briefly be described in this section. To better utilize the available heat in the process stream after the LTS, one design change was made to the process analyzed in Papers III and IV. Instead of economizing LP steam after the LTS, the LP steam was now evaporated (HE4 in Fig. 5.1). This decreased the need for ST extracted steam and the net plant efficiency increased. The modified process flow sheet is displayed in Fig. 5.1.

5.2 Process assumptions

Some of the assumptions and inputs of the model presented in Papers III and IV were modified to be able to compare to the thesis main model as presented in Chapter 4 (here called IRCC 2PR). The modified assumptions and inputs included:

- TIT was increased from 1297 °C to 1327 °C.
- Equipment pressure losses were modified to correspond to IRCC 2PR model. Because of this change, the air booster pressure ratio could be decreased.
- Reforming steam extraction pressure was decreased from 42 bar to 36 bar.
- Reboiler steam extraction pressure was decreased from 4 bar to 3 bar.

Assumptions for the IRCC with single-pressure HRSG (here called IRCC 1P) are listed in Table 5.1.

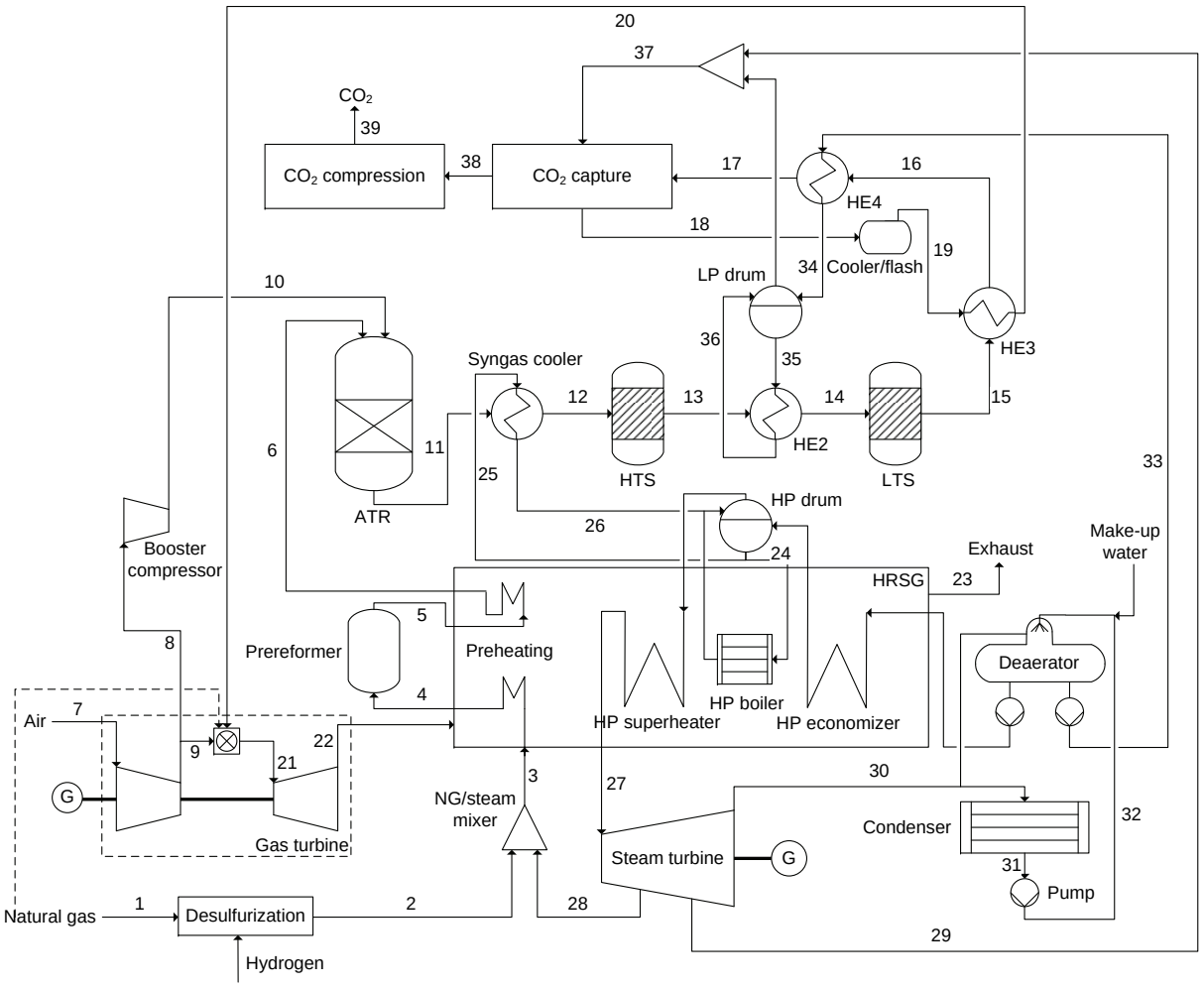

Figure 5.1: Process flow sheet for IRCC with single-pressure HRSG.

Table 5.1: Assumptions for the IRCC with single-pressure HRSG

Site	
Ambient T (°C)	15
Ambient pressure (bar)	1.013
Ambient relative humidity (%)	60
Gas turbine	
Model type	GE 9FB
TIT (°C)	1327
Turbine nozzle area increase (%)	6
Water/steam cycle	
Cycle type	single-pressure
HP pressure level (bar)	87.6
HP T (°C)	558
Condenser pressure (bar)	0.04
HRSG	
Minimum pinch point HP (K)	13
Approach subcooling HP (K)	3
Minimum stack T (°C)	70
Air booster	
Pressure ratio	1.836
Isentropic efficiency	0.85
Mechanical efficiency	0.995
Syngas processing	
Reforming technology	ATR
CO_2 capture	
Capture rate (%)	90
CO_2 compression	
Number of compression stages	4
Stage 1 isentropic efficiency	0.85
Stage 2 isentropic efficiency	0.8
Stage 3 isentropic efficiency	0.8
Stage 4 isentropic efficiency	0.75
Mechanical efficiency	0.995
Intercooling T (°C)	30
Compression outlet pressure (bar)	75
Pump efficiency	0.7
Pump outlet pressure (bar)	150

5.3 Design and off-design analyses

Design and off-design analyses of the process were performed in Paper III. To be able to compare to the thesis main model, the design case analysis was repeated for the process but with the modified assumptions as described in Section 5.2. Results from the design case analysis is presented in Section 5.5.

5.4 Uncertainty analysis

When analyzing process models, the results are typically presented as point estimates. By incorporating uncertainty in selected inputs of the process model, an answer to the following question is sought for: *how uncertain are the process model outputs?* Uncertainties of model input parameters were propagated through the process model using the deterministic equivalent modeling method developed at MIT (Tatang, 1995). In addition to quantifying uncertainties in model outputs, the method quantifies the effect of each parameter on the total uncertainty of model outputs. The IRCC process model was evaluated in terms of four performance metrics for the uncertainty analysis:

1. Net plant power output.
2. Net plant efficiency.
3. CO_2 capture rate.
4. CO_2 emitted per kWh of generated electricity.

The uncertainty analysis is presented in Paper IV, where further details of the study can be found.

5.5 Results

Notably, the net plant efficiency increased by 1.5%-points compared to the model presented in Paper III. The increase in efficiency was due to the increase in TIT, the decrease in pressure drops, the decrease in steam extraction pressures, and the design change to superheat LP steam after LTS. Results from the simulation are shown in Table 5.2. Stream data are presented in Appendix A, Table A.4.

5.6 Comparison to IRCC with dual-pressure reheat HRSG

How does the cycle presented in this chapter compare to the model analyzed in Chapter 4? Table 5.3 lists some of the features and outputs of the two models. The system with a single-pressure HRSG was less complex with a similar net plant efficiency. The difference of 0.6%-points in net plant efficiency, as displayed in Table 5.3, would be even less if inlet air cooling for the booster compressor was implemented for the single-pressure HRSG model. Also, the CO_2 capture rate was slightly higher for the IRCC 1P model. If, by

Table 5.2: Summary of results for the IRCC with single-pressure HRSG

Natural gas LHV input (MW)	838.5
Gross power output GT (MW)	256.8
Gross power output ST (MW)	154.8
Gross power output (MW)	411.7
Gross power output (% of LHV input)	49.1
Air compression (MW)	13.4
Air compression (% of LHV input)	1.6
CO_2 compression (MW)	15.3
CO_2 compression (% of LHV input)	1.8
CO_2 capture pumps (MW)	1.6
CO_2 capture pumps (% of LHV input)	0.2
Auxiliaries (MW)	6.2
Auxiliaries (% of LHV input)	0.7
Net power output (MW)	375.2
Net plant efficiency (% of LHV input)	44.7
Efficiency capture penalty (%-point loss to ref. case)	13.8
CO_2 emissions (g CO_2/net kWh el.)	66.9
CO_2 capture rate (%)	85.9

Table 5.3: Comparison between IRCC with single-pressure HRSG (IRCC 1P) and thesis main model (IRCC 2PR)

Simulation	IRCC 1P	IRCC 2PR
HRSG pressure levels	1	2 with reheat
Duct-firing	No	Yes
Reforming technology	ATR with prereformer	ATR
Air booster cooling	No	Yes
Superheating process steam	No	Yes
Capture rate in K_2CO_3 subsystem (%)	90	98
Net plant output (MW)	375.2	418.7
Net plant efficiency (%)	44.7	45.3
CO_2 emissions (g CO_2/net kWh el.)	66.9	70.1
CO_2 capture rate (%)	85.9	85.1
Steam quality at ST outlet (-)	0.863	0.916

decreasing the S/C, the capture rate would be lowered to the IRCC 2PR value of 85.1%, the net plant efficiency would increase slightly.

Power output was lower in the single-pressure HRSG model since no duct-firing was done, as is displayed in Table 5.3. Duct-firing can increase steam generation in the HRSG, and therby increase ST power output.

A prereformer could make the plant more flexible to potential future process changes, for example, changes in S/C or preheating temperatures. At present S/C and the relatively low preheating temperatures, a prereformer would not be needed, however, for the analysis performed the results with and without a prereformer would be very similar. The difference basically comes from the additional pressure drop. If economics were taken into consideration, the difference would be more pronounced.

A notable difference between the two processes was the capture rate in the hot potassium carbonate subsystem. For the IRCC 2PR process, the capture rate was very high (98%) enabling the use of NG for duct-firing in the HRSG. For the IRCC 1P process the capture rate was lower (90%). The capture rate could be increased and the S/C decreased for a constant plant capture rate. This could increase the net plant efficiency depending on the relation between the reboiler duty and the efficiency change due to an S/C change.

A disadvantage with the IRCC 1P was the lower steam quality at the ST outlet. A steam quality of 0.863 is borderline of being too low. A higher steam quality would be achieved if the HP pressure level would be lowered, however, this would lower the net plant efficiency. For the dual-pressure reheat system, the steam quality (0.916) was not an issue.

To summarize, the performance of the two systems are similar and a clear winner based on these analyses is not there. In the end, the selection decision would be strongly influenced by the economics. Economic analysis was not part of the thesis work.

Chapter 6

IRCC with relaxed practical constraints

To examine the potential of the IRCC process and investigate the impact of the numerous practical constraints employed in the process, the constraints were relaxed although still kept within realistic bounds. The other processes presented in the thesis have employed many constraints due to practical considerations. For this IRCC, with relaxed practical constraints, the following simplifications have been made:

1. Full gas turbine TIT was assumed (same TIT as for NG-fired GT). No TIT consideration was taken to the difference in flue gas composition when operating with a hydrogen-rich fuel.

2. Metal dusting in heat exchangers was not considered. This means that, for example, steam superheating or gas-to-gas heat exchanging could take place right after the ATR.

3. Low reboiler duty for CO_2 capture subsystem was selected. The reboiler duty was dropped from a value of 2 MJ/kg CO_2 captured to 1 MJ/kg CO_2 captured.

4. Low equipment, subsystem, and GT fuel nozzle pressure drops were assumed. The total pressure drop from inlet of ATR to outlet of GT burner fuel nozzles was decreased from approximately 9.7 bar to 5.2 bar. This means the reforming could take place at a lower pressure. Also, the needed air booster power would decrease and the reforming steam could be extracted at a lower pressure.

5. No consideration to off-design was taken. This means that a lower extracted steam pressure and a lower booster pressure ratio were needed.

6.1 Pinch analysis

Since the goal of the analysis was to investigate the potential of the process, rather than to come up with a specific HX network design, energy targets were sought via pinch analysis (Smith, 2005). Instead of heat exchangers in the flow sheet for the reforming process, temperature targets were added, as is displayed in Fig. 6.1. The supply temperatures T_s and the target temperatures T_t were used when setting the energy targets for the

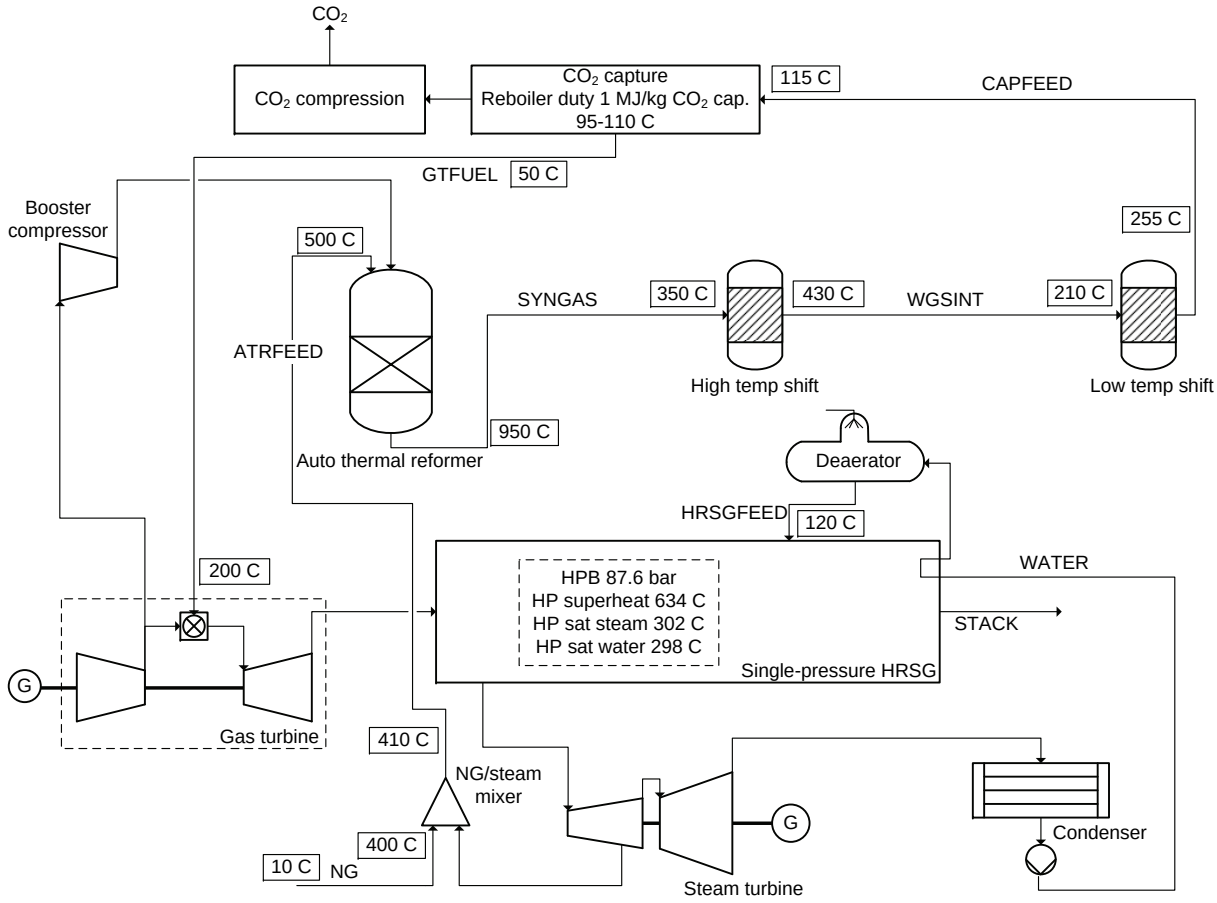

Figure 6.1: Process flow sheet for IRCC with relaxed practical constraints.

HX network. The temperatures would vary slightly from case to case but would stay in the vicinity of the temperatures in Fig. 6.1. In the Aspen Plus flow sheet, heaters and coolers were added to reach the temperature targets. In Tables 6.1 and 6.2 some of the streams, as defined in Fig. 6.1, are divided into several temperature ranges to get a more representative value of the heat capacity c_p. For each temperature range an average c_p has been calculated.

The idea with the analysis was to recover all possible heat between the process streams and to avoid any hot utility. For simplicity of the system and since a lot of steam will be generated in the process external to the HRSG, a single-pressure system was selected. An ST extraction for the reboiler heat input was not considered. Instead, heat for the reboiler was to be recovered from the process streams. An ATR, without a prereformer, was selected for the reforming process. A global minimum temperature difference was set at 10 K for the pinch analysis. For the CO_2 capture subsystem, the same split ratios, temperatures, and pressures as for the hot potassium carbonate process presented in Chapter 4 were assumed, with the exception of the reboiler duty. Assumptions for the model are listed in Table 6.3.

Table 6.1: Stream data for pinch analysis. Stream naming according to Fig. 6.1.

Stream	Type	T_s (°C)	T_t (°C)	$\dot{m}$ (kg/s)	c_p (kJ/kg·K)	Q (kW)
NG1	Cold	10	100	20.4	2.29	4204
NG2	Cold	100	200	20.4	2.50	5100
NG3	Cold	200	300	20.4	2.81	5732
NG4	Cold	300	400	20.4	3.125	6375
ATRFEED	Cold	411	500	40.6	2.835	10244
SYNGAS	Hot	950	350	141.0	1.775	150165
WGSINT	Hot	430	210	141.0	1.73	53665
CAPFEED1	Hot	255	175	141.0	1.745	19684
CAPFEED2	Hot	175	160	141.0	1.82	3849
CAPFEED3	Hot	160	150	141.0	1.99	2806
CAPFEED4	Hot	150	140	141.0	1.76	2482
CAPFEED5	Hot	140	115	141.0	1.44	5076
GTFUEL	Cold	50	200	88.0	2.005	26466

Table 6.2: Utility data for pinch analysis.

Stream	Type	T_s (°C)	T_t (°C)	$\dot{m}$ (kg/s)	q (kJ/kg)	Q (kW)
REBOIL	Cold	95	110	47	1000.0	47000
HP FW1	Cold	120	200	12	347.0	4164
HP FW2	Cold	200	250	12	231.3	2775
HP FW3	Cold	250	280	12	150.3	1804
HP FW4	Cold	280	298	12	98.0	1176
HP ST	Cold	298	302	78	1417.3	110553
HP SH1	Cold	302	350	12	205.0	2460
HP SH2	Cold	350	400	12	156.0	1872
HP SH3	Cold	400	634	12	591.0	7092

Table 6.3: Assumptions for the IRCC with relaxed practical constraints.

Site	
Ambient T (°C)	15
Ambient pressure (bar)	1.013
Ambient relative humidity (%)	60
Gas turbine	
Model type	GE 9FB
TIT (°C)	1427
Turbine nozzle area increase (%)	6
Water/steam cycle	
Cycle type	single-pressure
HP pressure level (bar)	87.6
HP T (°C)	634
Condenser pressure (bar)	0.04
HRSG	
Minimum pinch point HP (K)	13
Approach subcooling HP (K)	3
Minimum stack T (°C)	70
Air booster	
Outlet pressure (bar)	22
Isentropic efficiency	0.85
Mechanical efficiency	0.995
Syngas processing	
Reforming technology	ATR
CO_2 capture	
Capture rate (%)	98
CO_2 compression	
Number of compression stages	4
Stage 1 isentropic efficiency	0.85
Stage 2 isentropic efficiency	0.8
Stage 3 isentropic efficiency	0.8
Stage 4 isentropic efficiency	0.75
Mechanical efficiency	0.995
Intercooling T (°C)	30
Compression outlet pressure (bar)	75
Pump efficiency	0.7
Pump outlet pressure (bar)	150
HX network	
Minimum ΔT (K)	10

6.2 Incorporation of practical constraints

To investigate the impact of the various constraints, four of them were made stricter one-by-one by:

- Reducing TIT.
- Increasing the reboiler duty for the capture subsystem.
- Increasing the reformer pressure and thereby considering an increase in the equipment and fuel nozzle pressure drops.
- Increasing the extracted reformer steam pressure and the booster compressor outlet pressure and thereby considering off-design operation.

The metal dusting issue was difficult to evaluate without doing a full design of the system. Since only a conceptual design was performed, without a complete heat exchanger network layout, inclusion of this issue was not done.

For each of the four cases listed, the values in Tables 6.1 and 6.2 could vary slightly but would be in close proximity to those displayed.

6.3 Cooling of booster compressor air

In addition to reducing some of the practical constraints, a case where the inlet air for the booster compressor was cooled, was included. Cooling of the booster inlet air would lower the compression power. However, additional equipment in terms of heat exchangers and cooler would be needed if cooling the inlet air (and subsequently heating the outlet air). Also, depending on the process configuration, additional air stream preheating before ATR entrance or additional air mass flow to the ATR would be needed to keep the ATR outlet temperature at the same level. Depending on the configuration of the system and the criteria evaluated, cooling the inlet air for the booster compressor could therefore be advantageous or disadvantageous. In the case presented here, inlet cooling was advantageous, from a net plant efficiency standpoint, as is presented in Section 6.4.

6.4 Results and discussion

The relaxed constraints case showed a net plant efficiency of 48.8% as displayed in Table 6.4. With a high capture rate for the CO_2 capture subsystem (98%) and the relatively low reforming pressure, the S/C could be kept at a low level (0.85). A low S/C was positive for the net plant efficiency since less steam was extracted from the ST and because less steam means that less air was needed in the ATR to reach the required outlet temperature (a lower portion of the fuel was combusted). One disadvantage with a lower S/C was a higher methane slip and subsequently a lower CO_2 capture rate. However, by capturing 98% of the CO_2 that entered the capture subsystem, an overall capture rate of at least 85% was possible. Other disadvantages with a low S/C could be soot formation in the ATR burner and the need for a prereformer. These issues were not considered in the relaxed practical constraint simulations.

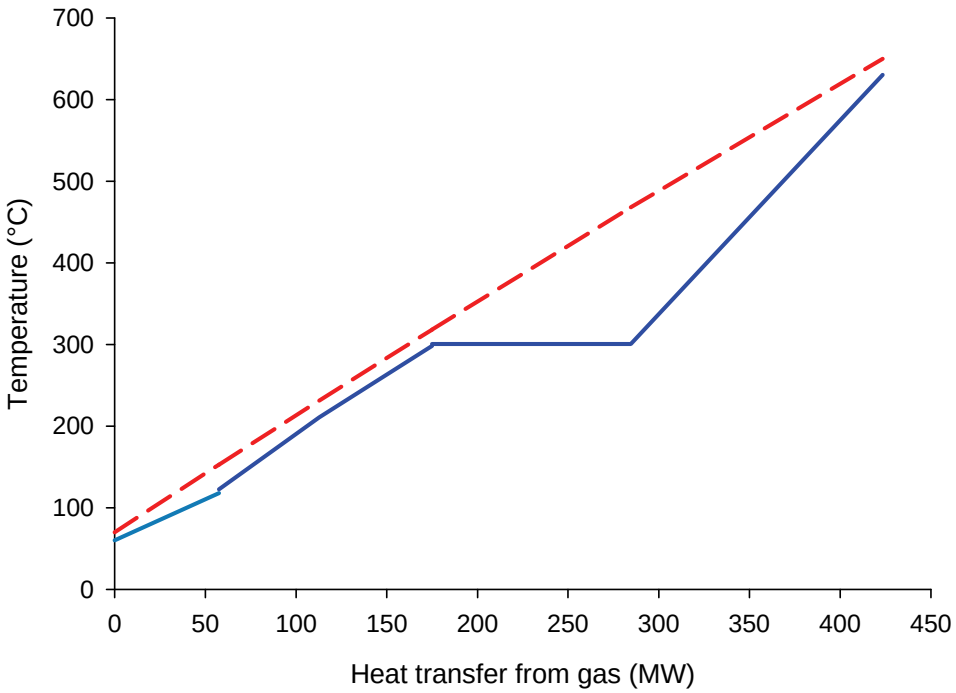

Figure 6.2: T-Q diagram for HRSG in relaxed practical constraints IRCC. Dashed lines refer to HRSG flue gas, solid lines to water/steam cycle.

Hot and cold composite curves are displayed in Fig. 6.3. The steam mass flow was set as to avoid any hot utility. Very little cooling water cold utility, 0.7 MW, was needed. Also, from Fig. 6.4, which displays the grand composite curve, one can clearly see that no hot utility and very limited cooling water were needed. The generated steam mass flow and reboiler heat can be seen as the nearly horizontal lines in Figs. 6.3 and 6.4. The global minimum temperature difference of 10 K was not close to being reached, as can be seen in both figures. The pinch point, the temperature at which the heat flow is zero, was located at the exit of the ATR at $T = 950$ °C.

The maximum amount of steam, without the need of any hot utility, was generated in the process. The economizing and superheating mass flows were selected to get a good utilization of the HRSG flue gas heat content. If too much water is preheated or if too much steam is superheated outside of the HRSG, the flue gas heat content could not be utilized in the best manner. 12 kg/s of economizing and superheating external of the HRSG proved to be a good level as is shown in the HRSG T-Q diagram in Fig. 6.2. The flue gas heat content was utilized the maximum amount, within the given constraints, with the flue gas exhaust at the lower temperature limit of 70 °C. For simplicity of the system, the external economizing and superheating mass flows were kept the same. Note that different results would be achieved if considering extracting steam from ST for the reboiler in the capture subsystem. By doing so, more HP steam could be generated in the process as seen in Fig. 6.3.

When reducing TIT by 100 K the GT efficiency decreased, leading to a lower overall net plant efficiency as is shown in Table 6.4. In addition, a low TIT led to a lower GT exhaust temperature which decreased the steam production in the HRSG. A total efficiency drop of 2.0%-points was noted compared to the relaxed constraints case.

By increasing the reboiler duty for the CO_2 capture subsystem from 1 MJ/kg CO_2

captured to 2 MJ/kg CO_2 captured, the net plant efficiency dropped approximately 3.1%-points. The increased reboiler duty meant more process heat was diverted to the reboiler; with a captured CO_2 mass flow of about 47 kg/s the heat required for the reboiler increased from 47 MW to 94 MW. Again, this meant less process steam could be generated, which led to a drop in net plant efficiency as displayed in Table 6.4. By extracting LP steam from ST, which was not considered in this analysis, the effect would be less pronounced and the net plant efficiency drop would be lower.

By increasing the total pressure drop in the system (from inlet of ATR to outlet of GT burner fuel nozzles) by 4.5 bar (5.2 bar to 9.7 bar), the net plant efficiency dropped 0.4%-points as displayed in Table 6.4. This was due to several reasons:

1. The reforming pressure increased, meaning a higher S/C was needed to reach the same CO_2 capture rate.

2. The needed air booster power increased.

3. The reforming steam needed to be extracted at a higher pressure from the ST which meant a loss in power for the ST.

When including off-design considerations, a similar behavior as for the increased pressure drop case resulted. Considering off-design means taking into account a lower pressure ratio at reduced load for the air booster compressor and extracting reforming steam at a higher pressure than would be necessary if only considering operation at the design point. A net plant efficiency drop of 0.5%-points resulted as is presented in Table 6.4.

Results from the booster air cooling case, including composite and grand composite curves, are presented in Table 6.5 and Figs. 6.5 and 6.6. A net plant efficiency of 49.1% was noted, which was 0.3%-points higher than for the relaxed constraints IRCC process presented in Table 6.4. With relaxed practical constraints, the net plant efficiency did increase with inclusion of air cooling. Comparing Figs. 6.4 and 6.6 one can see that more steam was generated in the relaxed constraints case compared to the case with inlet cooling for booster compressor. Some of the heat generated in the process heat exchangers was now used for heating the air after the booster compressor instead of for generating more steam. However, the gain from lowering the booster compressor power was greater than the loss resulting from a decrease in process steam generation. The booster compressor power was decreased from 6.3 MW for the relaxed constraints case to 2.6 MW for the air cooling case.

Table 6.4: Simulation inputs and results for relaxed practical constraint cases.

	Rel con	TIT red	Q_{re} incr	Δp incr	Off-design incl
TIT (°C)	1427	1327	1427	1427	1427
Reboiler duty (MJ/kg CO_2 cap.)	1.0	1.0	2.0	1.0	1.0
$T_{boost,in}$ (°C)	388	381	388	388	388
p_{atr} (bar)	22.0	22.0	22.0	26.5	25.9
S/C (mol H_2O/mol C)	0.85	0.85	0.85	0.87	0.87
$p_{refsteam}$ (bar)	22.0	22.0	22.0	26.5	31.5
$p_{boost,out}$ (bar)	22.0	22.0	22.0	26.5	25.9
CO_2 capture rate (%)	85.5	85.5	85.5	85.5	85.6
η (%)	48.8	46.8	45.7	48.4	48.3
$\Delta\eta$ (%-points)	-	2.0	3.1	0.4	0.5

Table 6.5: Simulation inputs and results for case with relaxed practical constraints *and* air booster inlet cooling.

	Air boost cool
TIT (°C)	1427
Reboiler duty (MJ/kg CO_2 cap.)	1.0
$T_{boost,in}$ (°C)	15
p_{atr} (bar)	22.0
S/C (mol H_2O/mol C)	0.90
$p_{refsteam}$ (bar)	22.0
$p_{boost,out}$ (bar)	22.0
CO_2 capture rate (%)	85.5
η (%)	49.1

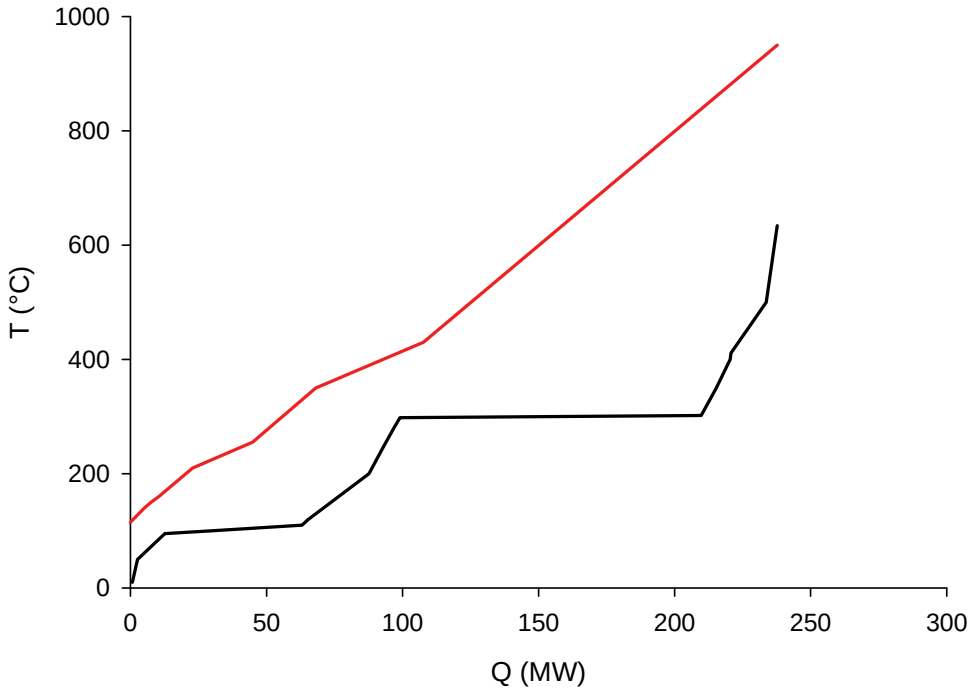

Figure 6.3: Hot (red, upper) and cold (black, lower) composite curves for the relaxed constraints case.

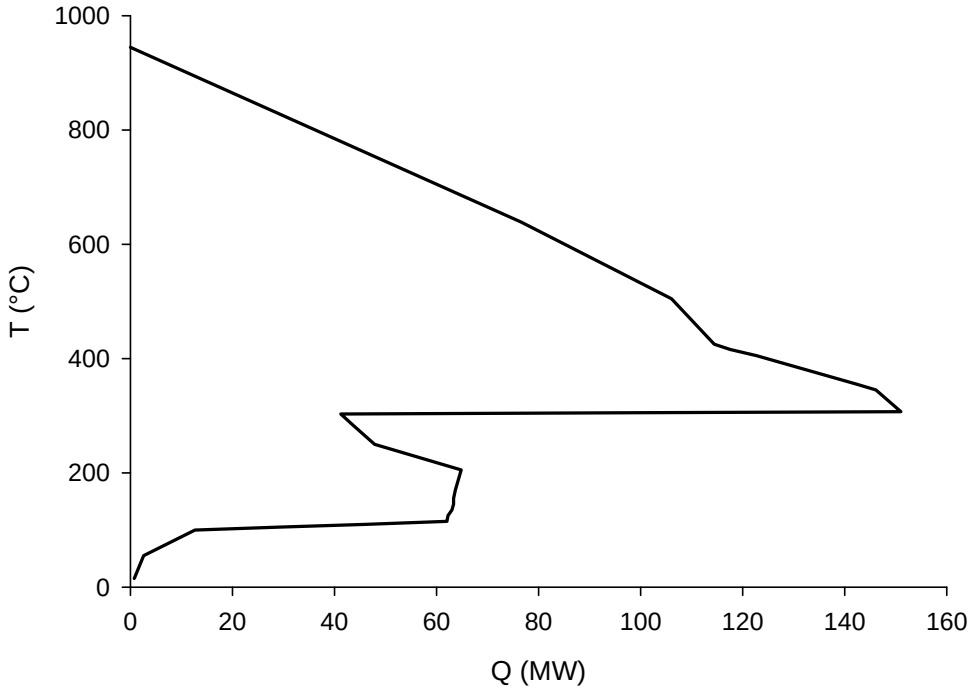

Figure 6.4: Grand composite curve for the relaxed constraints case.

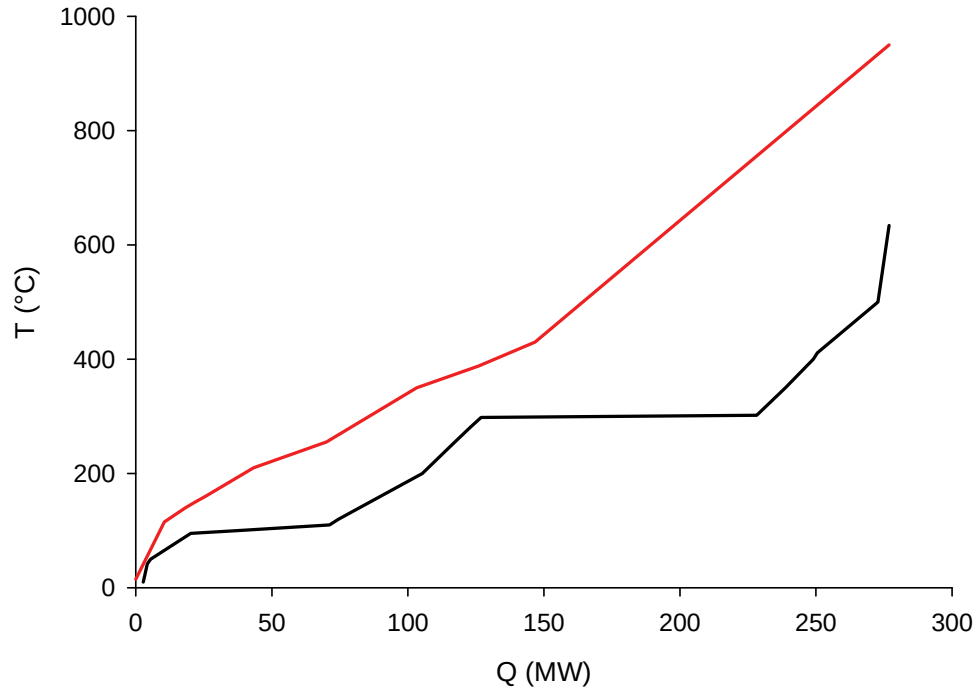

Figure 6.5: Hot (red, upper) and cold (black, lower) composite curves for the booster inlet air cooling case.

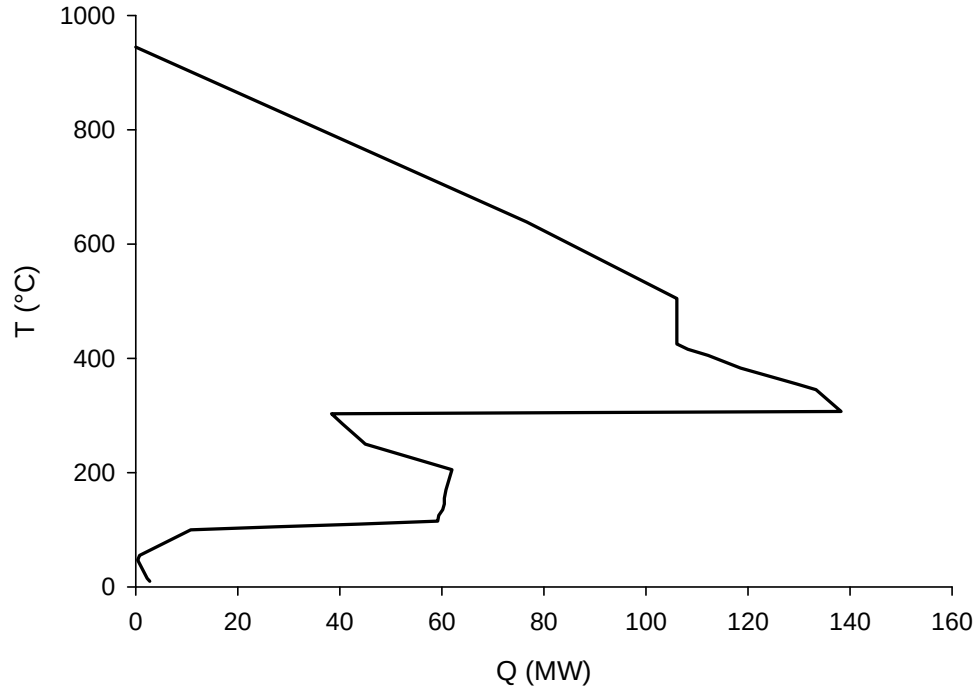

Figure 6.6: Grand composite curve for the booster inlet air cooling case.

Chapter 7

Conclusions and further work

7.1 Conclusions

As part of the design process, heat recovery steam generator (HRSG) design proved important. The design of an HRSG for an IRCC plant requires the ability to operate on both a hydrogen-rich fuel and on NG. Also, since a significant amount of steam is produced from the heat generated in the autoreforming process, the HRSG design differs from a design in an NGCC plant. For an IRCC with a lot of HP saturated steam generated in the process, a single-pressure steam cycle can actually perform in parity with a dual- or triple-pressure system (with or without reheat). Preheating of process streams further add to the complexity. The complexity of selecting an HRSG design increased when also considering that steam could be superheated, and LP and IP steam could be generated in the reforming process heat exchangers. For the concept studied it was also of importance to maintain a high net plant efficiency when operating on NG. Therefore the selection of HRSG design had to be a compromise between NGCC and IRCC operating modes. Duct burning proved positive for plant flexibility and the option to switch between a hydrogen-rich fuel and NG for the GT.

Functional analysis and FMECA are important steps in a system reliability analysis, as they can serve as a platform and basis for further analysis. Also, the results from the FMECA can be interesting for determining how the failures propagate through the system and their failure effects on the operation of the process. From the FMECA performed in this work, it is clear that the gas turbine is the most critical equipment in an IRCC plant. One of the reasons for this is the process integration between the power island and the pre-combustion process. For example, the gas turbine feeds air to the ATR and receives fuel from the pre-combustion process. This integration has an effect on the overall reliability of the system. In addition to integration issues, the gas turbine technology is less mature for hydrogen fuels than for natural gas. It should also be mentioned that even in an NG-fired combined cycle plant, the gas turbine is the most critical equipment. The need for part load analysis and consideration to dual fuel capability were important conclusions from the reliability analysis since many of the failures resulted in IRCC plant shutdown (if no backup fuel) or operation at reduced load.

By combining simulation tools for chemical engineering and power plant engineering analyses respectively, a representation of the overall system can be accomplished for an IRCC process. The IRCC process may involve heat integration between the power cycle and the reforming process, as was the case for the cycle studied, meaning an efficient way of

linking the softwares are important. The Aspen Simulation Workbook and Thermoflow's E-link proved capable of performing this task for an IRCC process.

For the IRCC setup studied in the uncertainty analysis, results showed that there was considerable uncertainty in the predicted net power output whereas net plant efficiency, CO_2 capture rate, and CO_2 emitted were less affected by input uncertainties. The median value for the net power output was 352.7 MW and the standard deviation 9.4 MW. The IRCC plant was predicted to have a median net plant efficiency of 43.4% with a standard deviation of 0.5%. Results also indicated that the probability of meeting the requirement of at least 85% CO_2 capture rate for the plant was approximately 95%. Parameters with the largest impact on uncertainties of power output and efficiency predictions proved to be gas turbine inlet temperature, and compressor and turbine efficiencies. For the CO_2 emissions, the equipment pressure drop and the steam-to-carbon ratio proved important. Therefore, the focus of future work should be to reduce uncertainties in these parameters in order to improve the confidence of the IRCC model. Improvement of confidence in the prediction of power output can be achieved by reducing the uncertainty in the estimate of turbine inlet temperature. Such results can help highlight the parameters where reduction of uncertainty via additional research can most effectively improve confidence in model predictions.

Analysis of the contribution to efficiency losses in the IRCC process showed that the reforming losses were almost twice as high as the CO_2 capture losses. Even more clear is this difference if considering that by selecting hot potassium carbonate as the chemical absorber in the capture subsystem, the reboiler duty was higher compared to a-MDEA. From the analysis, it was evident that to decrease the efficiency losses in an IRCC process, efforts should be concentrated towards improving (1) the reforming process to decrease fuel conversion losses and needed steam mass flow, (2) the CO_2 capture process to decrease the reboiler duty, (3) the gas turbine technology to allow for a higher firing temperature, and (4) the CO_2 compression process.

The off-design simulation results show the possibility to operate an IRCC plant at part load conditions down to approximately 60% gas turbine load with capture efficiency penalties at part load similar to full load operation. Also, it can be concluded that considering off-design conditions, such as part load steam turbine extraction pressures and air booster compressor pressure ratio, are important during the design stage of a plant.

When investigating the potential of the type of IRCC concepts studied in the thesis work, net plant efficiencies of 49% was achieved and based on these results it is conceivable that efficiencies up towards 50% could be realistic in a 5–10 years time horizon. Challenges to overcome to reach these high efficiencies include attenuating or eliminating process limitations due to metal dusting and reduced gas turbine TIT.

7.2 Further work

Simulations for an IRCC model with backup fuel (natural gas) would be interesting to examine. The HRSG and turbomachinery design would be locked when going from IRCC to NGCC operation mode. An important question to answer is: *could the plant operate on NG with the proposed design?* In the work presented in this thesis, dual fuel capability was only evaluated from a qualitative standpoint. The goal of further studying this topic

would be to quantify this capability, that is, to perform thermodynamic analyses on both fuel operation modes. To accomplish this, some items to consider are:

- Two separate models are needed within the simulation software environment. One for IRCC mode and one for NGCC mode. Because of dry sections, and thereby unused HXs, in the HRSG in the different operating modes, two models would need to be developed. The same simulation model could likely not handle this feature.
- ST design needs to be evaluated to allow for the large change in steam mass flow when switching operation modes. Less steam is generated in NGCC mode since the reforming process HXs would not generate any steam.

A detailed study on effect of turbomachinery equipment due to CO_2 capture would be important. This analysis should include heat transfer effects in turbine section of the GT and additional cooling air needs. The effect on steam turbine design when switching from primary fuel to backup fuel should also be investigated. In this thesis, the effect due to the increased steam content in the turbine section of the GT was taken into account by assuming a temperature reduction from the NGCC TIT.

Uncertainty analysis of off-design models would be of interest to investigate in order to evaluate how uncertain the part load model outputs are. Specifically, to compare the uncertainty in model outputs of off-design model to design model. *Are the results more uncertain when simulating an IRCC in off-design conditions, and if so, how much more uncertain?*

Further development of hot potassium carbonate model, in an IRCC setup, to decrease the reboiler duty is a suggestion for further investigation. Developments could include a split flow arrangement.

Dynamic simulation of IRCC process is a suggestion for a future study. This analysis could include startup, shutdown, load changes, and process disturbances of the IRCC plant. Potentially, this could be extended to operation with both primary and backup fuels including fuel switchover.

Investigation of future technologies and technology advancements, such as membrane reforming reactor, sorption enhanced reforming, membrane water-gas shift reactor, and sorption enchanced water-gas shift could be of interest. This includes options displayed in Fig. 2.18. Also, advanced gas turbines with elevated turbine inlet temperature and pressure ratio, designed for hydrogen applications, could be explored.

Bibliography

Aasberg-Petersen, K., Christensen, T. S., Dybkjær, I., Sehested, J., Østberg, M., Coertzen, R. M., Keyser, M. J., Steynberg, A. P., 2004. Chapter 4: Synthesis gas production for FT synthesis. In: Steynberg, A., Dry, M. (Eds.), Studies in Surface Science and Catalysis. Vol. 152. Elsevier, pp. 258–405.

Abashar, M. E. E., 2004. Coupling of steam and dry reforming of methane in catalytic fluidized bed membrane reactors. International Journal of Hydrogen Energy 29 (8), 799–808.

ACIA, 2005. Arctic Climate Impact Assessment. Cambridge University Press.

Alvarez, H., 1990. Energiteknik. Vol. 2. Studentlitteratur, Lund, Sweden.

Amann, J.-M., Kanniche, M., Bouallou, C., 2009. Reforming natural gas for CO_2 pre-combustion capture in combined cycle power plant. Clean Technologies and Environmental Policy 11 (1), 67–76.

Andersen, T., Kvamsdal, H. M., Bolland, O., 2000. Gas turbine combined cycle with CO_2 capture using auto-thermal reforming of natural gas. In: ASME Turbo Expo. Munich, Germany, ASME Paper No. 2000-GT-162.

Aspen Technology, 2003. Aspen Plus 12.1 User Guide. Aspen Technology, Inc., Cambridge, MA, USA.

Aspen Technology, 2008. Aspen Plus 2006.5. Aspen Technology, Inc.

Barton, G. W., Chan, W. K., Perkins, J. D., 1991. Interaction between process design and process control: The role of open-loop indicators. Journal of Process Control 1 (3), 161–170.

Bartoo, R. K., 1984. Removing acid gas by the Benfield process. Chemical Engineering Progress 80 (10), 35–39.

Bevilacqua, M., Braglia, M., Gabbrielli, R., 2000. Monte Carlo simulation approach for a modified FMECA in a power plant. Quality and Reliability Engineering International 16 (4), 313–324.

Blanco, A. M., Bandoni, J. A., 2003. Interaction between process design and process operability of chemical processes: An eigenvalue optimization approach. Computers & Chemical Engineering 27 (8-9), 1291–1301.

Bohm, M. C., Herzog, H. J., Parsons, J. E., Sekar, R. C., 2007. Capture-ready coal plants–Options, technologies and economics. International Journal of Greenhouse Gas Control 1 (1), 113–120.

Bonzani, F., Gobbo, P., 2007. Operating experience of high flexibility syngas burner for IGCC power plant. Vol. 2 of Proceedings of the ASME Turbo Expo. American Society of Mechanical Engineers, New York, pp. 65–71.

Brohan, P., Kennedy, J., Haris, I., Tett, S., Jones, P., 2006. Uncertainty estimates in regional and global observed temperature changes: a new dataset from 1850. Journal of Geophysical Research 111 (D12106).

Carlson, E. C., 1996. Don't gamble with physical properties for simulations. Chemical Engineering Progress 92 (10), 35–46.

Chapel, D. G., Mariz, C. L., 1999. Recovery of CO_2 from flue gases: commercial trends. In: The Canadian Society of Chemical Engineers annual meeting. Saskatoon, Saskatchewan, Canada.

Chiesa, P., Lozza, G., Mazzocchi, L., 2005. Using hydrogen as gas turbine fuel. Journal of Engineering for Gas Turbines and Power 127 (1), 73–80.

Christensen, T. S., Christensen, P. S., Dybkjær, I., Hansen, J. H. B., Primdahl, I. I., 1998. Developments in autothermal reforming. Studies in Surface Science and Catalysis 119, 883–888.

Christensen, T. S., Primdahl, I. I., 1994. Improve syngas production using autothermal reforming. Hydrocarbon Processing 73 (3).

CIT Industriell Energianalys, 1999. ProPi version 1.2d for Excel 97. CIT Industriell Energianalys AB.

Climate and Pollution Agency, 2007. Tillatelse til virksomhet etter forurensningsloven for Statoil Mongstad 10.05.2007. Oslo, Norway.

Corradetti, A., Desideri, U., 2005. Analysis of gas-steam combined cycles with natural gas reforming and CO_2 capture. Journal of Engineering for Gas Turbines and Power 127 (3), 545–552.

Di Gabriele, F., Bernstein, J. R., Al-Qhatani, M. M., Liu, Z., Jordan, M. P., Richardson, J. A., Stott, F. H., 2003. Study of the metal dusting behaviour of high-temperature alloys. Materials and Corrosion 54 (11), 854–859.

Dybkjær, I., 1995. Tubular reforming and autothermal reforming of natural gas – an overview of available processes. Fuel Processing Technology 42 (2-3), 85–107.

Eide, L. I., Bailey, D. W., 2005. Precombustion decarbonisation processes. Oil and Gas Science and Technology 60 (3), 475–484.

Ertesvåg, I. S., Kvamsdal, H. M., Bolland, O., 2005. Exergy analysis of a gas-turbine combined-cycle power plant with precombustion CO_2 capture. Energy 30 (1), 5–39.

Gas Turbine World, 2009. GTW Handbook. Pequot Publishing Inc., Fairfield, CT, USA.

Golan, A., Judge, G., Miller, D., 1996. Maximum entropy econometrics: Robust estimation with limited data. Wiley, New York, NY, USA.

Grabke, H. J., Krajak, R., Müller-Lorenz, E. M., 1993a. Metal dusting of high temperature alloys. Werkstoffe und Korrosion 44 (3), 89–97.

Grabke, H. J., Krajak, R., Nava Paz, J. C., 1993b. On the mechanism of catastrophic carburization: 'metal dusting'. Corrosion Science 35 (5–8 pt 2), 1141–1150.

Griffin, T., Sundkvist, S. G., Åsen, K., Bruun, T., 2005. Advanced zero emissions gas turbine power plant. Journal of Engineering for Gas Turbines and Power 127 (1), 81–85.

Göttlicher, G., 2004. The energetics of carbon dioxide capture in power plants. U.S. Department of Energy, National Energy Technology Laboratory.

Haag, J. C., Hildebrandt, A., Hönen, H., Assadi, M., Kneer, R., 2007. Turbomachinery simulation in design point and part-load operation for advanced CO_2 capture power plant cycles. Vol. 3 of Proceedings of the ASME Turbo Expo. American Society of Mechanical Engineers, New York, NY, USA, pp. 239–250.

Heck, R. M., 1999. Catalytic abatement of nitrogen oxides – stationary applications. Catalysis Today 53 (4), 519–523.

Hoffmann, S., Bartlett, M., Finkenrath, M., Evulet, A., Ursin, T. P., 2009. Performance and cost analysis of advanced gas turbine cycles with precombustion CO_2 capture. Journal of Engineering for Gas Turbines and Power 131 (2), 021701 (7 pp.).

IEC 60812, 2006. Analysis techniques for system reliability - Procedures for failure mode and effect analysis (FMEA). International Electrotechnical Commission, Geneva, Switzerland.

Incropera, F. P., DeWitt, D. P., 1990. Fundamentals of heat and mass transfer, 3rd Edition. John Wiley & Sons, Inc.

Intergovernmental Panel on Climate Change, 2007. Climate change 2007: The physical science basis.

International Energy Agency, 2008. World Energy Outlook 2008.

Ishida, M., Jin, H., 1994. A new advanced power-generation system using chemical-looping combustion. Energy 19 (4), 415–422.

Jericha, H., Gottlich, E., Sanz, W., Heitmeir, F., 2004. Design optimization of the Graz cycle prototype plant. Journal of Engineering for Gas Turbines and Power-Transactions of the ASME 126 (4), 733–740.

Johannessen, O. M., Bengtsson, L., Miles, M. W., Kuzmina, S. I., Semenov, V. A., Alekseev, G. V., Nagurnyi, A. P., Zakharov, V. F., Bobylev, L. P., Pettersson, L. H., Hasselmann, K., Cattle, H. P., 2004. Arctic climate change: observed and modelled temperature and sea-ice variability. Tellus 56A (4), 328–341.

Jordal, K., Bredesen, R., Kvamsdal, H. M., Bolland, O., 2004. Integration of H2-separating membrane technology in gas turbine processes for CO_2 capture. Energy 29 (9-10), 1269–1278.

Keeling, C., Bacastow, R., Bainbridge, A., Ekdahl, C., Guenther, P., Waterman, L., 1976. Atmospheric carbon dioxide variations at Mauna Loa Observatory, Hawaii. Tellus 28, 538–551.

Kehlhofer, R. H., Warner, J., Nielsen, H., Bachmann, R., 1999. Combined-cycle gas & steam turbine power plants, 2nd Edition. PennWell Publishing Company, Tulsa, OK, USA.

Knudsen, J. N., Vilhelmsen, P. J., Biede, O., Jensen, J. N., 2006. CASTOR 1 t/h CO_2 absorption pilot plant at the Elsam Kraft A/S Esbjerg power plant – First year operation experience. In: 8th International Conference on Greenhouse Gas Technologies (GHGT-8). Trondheim, Norway.

Kohl, A., Nielsen, R., 1997. Gas purification, 5th Edition. Gulf Publishing Company, Houston, TX, USA.

Kothandaraman, A., Nord, L., Bolland, O., Herzog, H. J., McRae, G. J., 2009. Comparison of solvents for post-combustion capture of CO_2 by chemical absorption. Energy Procedia 1 (1), 1373–1380.

Kurzke, J., 2004. Compressor and turbine maps for gas turbine performance computer programs: Component map collection 2. Dachau, Germany.

Le Thiez, P., Mosditchian, G., Torp, T., Feron, P., Ritsema, I., Zweigel, P., Lindeberg, E., 2004. CASTOR: from pie in the sky to commercial reality. Modern Power Systems 24 (7), 19–20.

Lee, S. H. D., Applegate, D. V., Ahmed, S., Calderone, S. G., Harvey, T. L., 2005. Hydrogen from natural gas: part I – autothermal reforming in an integrated fuel processor. International Journal of Hydrogen Energy 30 (8), 829–842.

Lozza, G., Chiesa, P., 2002a. Natural gas decarbonization to reduce CO_2 emission from combined cycles - Part I: partial oxidation. Journal of Engineering for Gas Turbines and Power 124 (1), 82–88.

Lozza, G., Chiesa, P., 2002b. Natural gas decarbonization to reduce CO_2 emission from combined cycles - Part II: steam-methane reforming. Journal of Engineering for Gas Turbines and Power 124 (1), 89–95.

Mathieu, P., Nihart, R., 1999. Zero-emission MATIANT cycle. Journal of Engineering for Gas Turbines and Power 121 (1), 116–20.

Moulijn, J. A., Makkee, M., Diepen, A. v., 2007. Chemical process technology. John Wiley & Sons Ltd, Chichester, West Sussex, England.

NERC, 2007. North American Electric Reliability Corporation: GADS report 2002–2006. `http://www.nerc.com`.

OREDA, 2002. Offshore Reliability Data Handbook, 4th Edition. DNV, Høvik, Norway.

Overpeck, J., Hughen, K., Hardy, D., Bradley, R., Case, R., Douglas, M., Finney, B., Gajewski, K., Jacoby, G., Jennings, A., Lamoureux, S., Lasca, A., MacDonald, G., Moore, J., Retelle, M., et al., 1997. Arctic environmental change of the last four centuries. Science 278 (5341), 1251.

Perrow, C., 1999. Normal accidents; living with high-risk technologies. Princeton University Press, Princeton, NJ, USA.

Petit, J. R., Jouzel, J., Raynaud, D., Barkov, N. I., Barnola, J. M., Basile, I., Bender, M., Chappellaz, J., Davis, M., Delaygue, G., Delmotte, M., Kotlyakov, V. M., Legrand, M., Lipenkov, V. Y., Lorius, C., Pépin, L., Ritz, C., Saltzman, E., Stievenard, M., 1999. Climate and atmospheric history of the past 420,000 years from the Vostok ice core, Antarctica. Nature 399 (6735), 429–436.

Phenix, B. D., Dinaro, J. L., Tatang, M. A., Tester, J. W., Howard, J. B., McRae, G. J., 1997. Incorporation of parametric uncertainty into complex kinetic mechanisms: Application to hydrogen oxidation in supercritical water. Combustion and Flame 112 (1-2), 132–146.

Rausand, M., Høyland, A., 2004. System reliability theory: Models, statistical methods, and applications, 2nd Edition. John Wiley & Sons Inc., Hoboken, NJ, USA.

Resnik, K. P., Yeh, J. T., Pennline, H. W., 2004. Aqua ammonia process for simultaneous removal of CO_2, SO_2 and NOx. International Journal of Environmental Technology and Management 4 (1-2), 89–104.

Richter, H. J., Knoche, K. F., 1983. Reversibility of combustion processes. In: Gaggioli, R. A. (Ed.), A.C.S. Symposium Series 235. Washington D.C., USA, pp. 71–85.

Robert, C. P., 1994. The Bayesian choice: a decision-theoretic motivation. Springer-Verlag, New York, NY, USA.

Shah, R. K., Sekulić, D. P., 2003. Fundamentals of heat exchanger design. John Wiley and Sons, Inc., Hoboken, NJ, USA.

Shilling, N. Z., Jones, R. M., 2003. The impact of fuel flexible gas turbine control systems on integrated gasification combined cycle performance. Vol. 1 of Proceedings of the ASME Turbo Expo. American Society of Mechanical Engineers, New York, NY, USA, pp. 259–265.

Skogestad, S., 2004. Control structure design for complete chemical plants. Computers and Chemical Engineering 28 (1-2), 219–234.

Smith, R., 2005. Chemical process design and integration. John Wiley & Sons Ltd, Chichester, West Sussex, England.

Sperle, T., Chen, D., Lødeng, R., Holmen, A., 2005. Pre-reforming of natural gas on a Ni catalyst: Criteria for carbon free operation. Applied Catalysis A: General 282 (1-2), 195–204.

Tatang, M. A., 1995. Direct incorporation of uncertainty in chemical and environmental engineering systems. Ph.D. thesis, Massachusetts Institute of Technology, Cambridge, MA, USA.

Tatang, M. A., Wenwei, P., Prinn, R. G., McRae, G. J., 1997. An efficient method for parametric uncertainty analysis of numerical geophysical models. Journal of Geophysical Research 102 (D18), 21925–21932.

Teng, S.-H., Ho, S.-Y., 1996. Failure mode and effects analysis: An integrated approach for product design and process control. The International Journal of Quality & Reliability Management 13 (5), 8–26.

Teoh, P. C., Case, K., 2004. Failure modes and effects analysis through knowledge modelling. Journal of Materials Processing Technology 153-154 (1-3), 253–260.

Thermoflow, 2008. GT PRO Version 18. Thermoflow Inc.

Thitakamol, B., Veawab, A., Aroonwilas, A., 2007. Environmental impacts of absorption-based CO_2 capture unit for post-combustion treatment of flue gas from coal-fired power plant. International Journal of Greenhouse Gas Control 1 (3), 318–342.

Thoning, K., Tans, P., Komhyr, W., 1989. Atmospheric carbon dioxide at Mauna Loa Observatory 2. Analysis of the NOAA GMCC data 1974–1985. J. Geophys. Research 94, 8549–8565.

Todd, D. M., Battista, Robert, A., 2000. Demonstrated applicability of hydrogen fuel for gas turbines. In: Gasification 4 the Future. Noordwijk, Netherlands.

United Nations Framework Convention on Climate Change, 2008. Greenhouse gas inventory data. `http://unfccc.int/ghg_data/items/3800.php`.

Vannby, R., Winter Madsen, S. E. L., 1992. Adiabatic preforming. Ammonia Plant Safety & Related Facilities 32, 122–128.

Veltman, K., Singh, B., Hertwich, E. G., 2010. Human and environmental impact assessment of postcombustion CO_2 capture focusing on emissions from amine-based scrubbing solvents to air. Environmental Science and Technology 44 (4), 1496–1502.

Verduijn, W. D., 1993. Experience with a prereformer. Ammonia Plant Safety & Related Facilities 33.

Wagner, W., Cooper, J. R., Dittmann, A., Kijima, J., Kretzschmar, H. J., Kruse, A., Mares, R., Oguchi, K., Sato, H., Stöcker, I., Šifner, O., Takaishi, Y., Tanishita, I., Trübenbach, J., Willkommen, T., 2000. The IAPWS industrial formulation 1997 for the thermodynamic properties of water and steam. Journal of Engineering for Gas Turbines and Power 122 (1), 150–180.

Wilson, M., Tontiwachwuthikul, P., Chakma, A., Idem, R., Veawab, A., Aroonwilas, A., Gelowitz, D., Barrie, J., Mariz, C., 2004. Test results from a CO_2 extraction pilot plant at Boundary Dam coal-fired power station. Energy 29 (9-10), 1259–1267.

Yegani, R., Hirozawa, H., Teramoto, M., Himei, H., Okada, O., Takigawa, T., Ohmura, N., Matsumiya, N., Matsuyama, H., 2007. Selective separation of CO_2 by using novel facilitated transport membrane at elevated temperatures and pressures. Journal of Membrane Science 291 (1-2), 157–164.

Zhang, N., Lior, N., 2008. Comparative study of two low CO_2 emission power generation system options with natural gas reforming. Journal of Engineering for Gas Turbines and Power 130 (5), 051701.

Appendix A

Stream data

Table A.1: Stream table for IRCC with dual-pressure reheat HRSG.

No.	T (°C)	p (bar)	$\dot{m}$ (kg/s)	MW (kg/kmol)	CH_4 (vol%)	C_2+ (vol%)	H_2 (vol%)	CO (vol%)	CO_2 (vol%)	H_2O (vol%)	O_2 (vol%)	N_2 (vol%)	Ar (vol%)
1	10.0	30.6	18.4	20.73	79.84	16.73	-	-	2.92	-	-	0.51	-
2	145.0	30.4	18.4	20.73	79.84	16.73	-	-	2.92	-	-	0.51	-
3	400.0	30.2	18.4	20.73	79.84	16.73	-	-	2.92	-	-	0.51	-
4	384.6	30.2	48.8	18.95	27.53	5.77	-	-	1.01	65.52	-	0.18	-
5	500.0	30.0	48.8	18.95	27.53	5.77	-	-	1.01	65.52	-	0.18	-
6	15.0	1.013	642.1	28.85	-	-	-	-	0.03	1.01	20.74	77.30	0.92
7	380.1	16.2	91.9	28.85	-	-	-	-	0.03	1.01	20.74	77.30	0.92
8	380.1	16.2	465.6	28.85	-	-	-	-	0.03	1.01	20.74	77.30	0.92
9	168.1	16.0	91.9	28.85	-	-	-	-	0.03	1.01	20.74	77.30	0.92
10	15.0	15.8	91.9	28.85	-	-	-	-	0.03	1.01	20.74	77.30	0.92
11	84.6	30.4	91.4	28.96	-	-	-	-	0.03	0.09	20.93	78.02	0.93
12	300.0	30.2	91.4	28.96	-	-	-	-	0.03	0.09	20.93	78.02	0.93
13	500.0	30.0	91.4	28.96	-	-	-	-	0.03	0.09	20.93	78.02	0.93
14	950.0	29.3	140.2	19.38	0.24	0.00	28.18	10.02	5.31	21.74	0.00	34.11	0.41
15	450.0	29.1	140.2	19.38	0.24	0.00	28.18	10.02	5.31	21.74	0.00	34.11	0.41
16	355.0	28.9	140.2	19.38	0.24	0.00	28.18	10.02	5.31	21.74	0.00	34.11	0.41
17	430.6	28.5	140.2	19.38	0.24	0.00	35.03	3.17	12.16	14.89	0.00	34.11	0.41
18	367.3	28.3	140.2	19.38	0.24	0.00	35.03	3.17	12.16	14.89	0.00	34.11	0.41
19	244.9	28.1	140.2	19.38	0.24	0.00	35.03	3.17	12.16	14.89	0.00	34.11	0.41
20	212.1	27.9	140.2	19.38	0.24	0.00	35.03	3.17	12.16	14.89	0.00	34.11	0.41
21	240.1	27.5	140.2	19.38	0.24	0.00	37.75	0.44	14.88	12.17	0.00	34.11	0.41
22	160.6	27.3	140.2	19.38	0.24	0.00	37.75	0.44	14.88	12.17	0.00	34.11	0.41
23	133.5	27.1	140.2	19.38	0.24	0.00	37.75	0.44	14.88	12.17	0.00	34.11	0.41
24	50.0	26.1	78.3	14.72	0.30	0.00	51.34	0.60	0.40	0.42	0.00	46.39	0.54
25	200.0	25.9	78.3	14.72	0.30	0.00	51.34	0.60	0.40	0.42	0.00	46.39	0.54
26	1327.2	15.4	543.9	27.09	0.00	0.00	0.00	0.00	0.35	14.70	9.63	74.42	0.89
27	594.7	1.036	628.4	27.32	0.00	0.00	0.00	0.00	0.33	12.94	11.05	74.79	0.90
28	70.0	1.013	630.3	27.28	0.00	0.00	0.00	0.00	0.81	13.77	10.07	74.45	0.89
29	119.0	2.0	128.4	18.02	-	-	-	-	-	100.00	-	-	-
30	121.4	31.5	16.9	18.02	-	-	-	-	-	100.00	-	-	-
31	236.0	31.5	16.9	18.02	-	-	-	-	-	100.00	-	-	-
32	236.0	31.5	16.9	18.02	-	-	-	-	-	100.00	-	-	-
33	238.6	31.5	16.9	18.02	-	-	-	-	-	100.00	-	-	-
34	332.1	135.6	112.4	18.02	-	-	-	-	-	100.00	-	-	-
35	336.2	135.6	112.4	18.02	-	-	-	-	-	100.00	-	-	-
36A	336.2	135.6	67.1	18.02	-	-	-	-	-	100.00	-	-	-
36B	336.2	135.6	45.3	18.02	-	-	-	-	-	100.00	-	-	-
37A	400.0	135.6	67.1	18.02	-	-	-	-	-	100.00	-	-	-
37B	400.0	135.6	45.3	18.02	-	-	-	-	-	100.00	-	-	-
38	566.0	130.0	152.9	18.02	-	-	-	-	-	100.00	-	-	-
39	376.3	36.0	30.4	18.02	-	-	-	-	-	100.00	-	-	-
40	353.0	30.9	119.8	18.02	-	-	-	-	-	100.00	-	-	-
41	566.0	27.5	136.8	18.02	-	-	-	-	-	100.00	-	-	-
42	275.0	2.0	41.5	18.02	-	-	-	-	-	100.00	-	-	-
43	29.0	0.04	97.9	18.02	-	-	-	-	-	100.00	-	-	-
44	29.0	0.4	98.0	18.02	-	-	-	-	-	100.00	-	-	-
45	29.6	4.4	98.0	18.02	-	-	-	-	-	100.00	-	-	-
46	50.0	1.1	48.4	41.58	0.11	0.00	0.00	0.02	90.62	9.20	0.00	0.00	0.05
47	53.8	150.0	46.5	43.87	0.13	0.00	0.00	0.02	99.40	0.40	0.00	0.00	0.05

Table A.2: Stream table for IRCC with dual-pressure reheat HRSG at 80% relative GT load.

No.	T (°C)	p (bar)	$\dot{m}$ (kg/s)	MW (kg/kmol)	CH_4 (vol%)	C_2+ (vol%)	H_2 (vol%)	CO (vol%)	CO_2 (vol%)	H_2O (vol%)	O_2 (vol%)	N_2 (vol%)	Ar (vol%)
1	10.0	30.6	15.8	20.73	79.84	16.73	-	-	2.92	-	-	0.51	-
2	139.0	30.5	15.8	20.73	79.84	16.73	-	-	2.92	-	-	0.51	-
3	408.5	30.3	15.8	20.73	79.84	16.73	-	-	2.92	-	-	0.51	-
4	389.7	30.3	42.0	18.95	27.53	5.77	-	-	1.01	65.51	-	0.18	-
5	508.4	30.2	42.0	18.95	27.53	5.77	-	-	1.01	65.51	-	0.18	-
6	15.0	1.013	551.1	28.85	-	-	-	-	0.03	1.01	20.74	77.30	0.92
7	372.7	13.9	78.9	28.85	-	-	-	-	0.03	1.01	20.74	77.30	0.92
8	372.7	13.9	399.6	28.85	-	-	-	-	0.03	1.01	20.74	77.30	0.92
9	159.7	13.8	78.9	28.85	-	-	-	-	0.03	1.01	20.74	77.30	0.92
10	15.0	13.6	78.9	28.85	-	-	-	-	0.03	1.01	20.74	77.30	0.92
11	80.3	25.2	78.4	28.95	-	-	-	-	0.03	0.10	20.93	78.01	0.93
12	297.0	25.0	78.4	28.95	-	-	-	-	0.03	0.10	20.93	78.01	0.93
13	506.5	24.8	78.4	28.95	-	-	-	-	0.03	0.10	20.93	78.01	0.93
14	950.0	24.3	120.4	19.34	0.17	0.00	28.38	10.10	5.28	21.64	0.00	34.02	0.41
15	437.6	24.1	120.4	19.34	0.17	0.00	28.38	10.10	5.28	21.64	0.00	34.02	0.41
16	354.3	23.9	120.4	19.34	0.17	0.00	28.38	10.10	5.28	21.64	0.00	34.02	0.41
17	430.9	23.6	120.4	19.34	0.17	0.00	35.26	3.22	12.16	14.77	0.00	34.02	0.41
18	371.0	23.4	120.4	19.34	0.17	0.00	35.26	3.22	12.16	14.77	0.00	34.02	0.41
19	242.9	23.2	120.4	19.34	0.17	0.00	35.26	3.22	12.16	14.77	0.00	34.02	0.41
20	208.3	23.0	120.4	19.34	0.17	0.00	35.26	3.22	12.16	14.77	0.00	34.02	0.41
21	238.3	22.7	120.4	19.34	0.17	0.00	38.04	0.44	14.94	11.99	0.00	34.02	0.41
22	151.4	22.5	120.4	19.34	0.17	0.00	38.04	0.44	14.94	11.99	0.00	34.02	0.41
23	128.6	22.3	120.4	19.34	0.17	0.00	38.04	0.44	14.94	11.99	0.00	34.02	0.41
24	50.0	21.5	67.2	14.65	0.21	0.00	51.60	0.59	0.41	0.51	0.00	46.15	0.54
25	203.0	21.3	67.2	14.65	0.21	0.00	51.60	0.59	0.41	0.51	0.00	46.15	0.54
26	1326.3	13.2	466.8	27.08	0.00	0.00	0.00	0.00	0.35	14.79	9.60	74.37	0.89
27	622.4	1.030	539.4	27.31	0.00	0.00	0.00	0.00	0.31	13.03	11.02	74.74	0.90
28	70.0	1.013	541.1	27.26	0.00	0.00	0.00	0.00	0.83	13.88	10.00	74.39	0.89
29	108.8	3.1	114.8	18.02	-	-	-	-	-	100.00	-	-	-
30	119.9	31.2	15.0	18.02	-	-	-	-	-	100.00	-	-	-
31	234.0	31.2	15.0	18.02	-	-	-	-	-	100.00	-	-	-
32	234.1	31.2	15.0	18.02	-	-	-	-	-	100.00	-	-	-
33	239.0	31.2	15.0	18.02	-	-	-	-	-	100.00	-	-	-
34	330.2	134.3	95.0	18.02	-	-	-	-	-	100.00	-	-	-
35	338.7	134.3	95.0	18.02	-	-	-	-	-	100.00	-	-	-
36A	338.7	134.3	58.0	18.02	-	-	-	-	-	100.00	-	-	-
36B	338.7	134.3	37.0	18.02	-	-	-	-	-	100.00	-	-	-
37A	395.6	134.3	58.0	18.02	-	-	-	-	-	100.00	-	-	-
37B	395.6	134.3	37.0	18.02	-	-	-	-	-	100.00	-	-	-
38	566.2	566.2	134.1	18.02	-	-	-	-	-	100.00	-	-	-
39	375.2	32.3	26.1	18.02	-	-	-	-	-	100.00	-	-	-
40	352.8	27.8	105.3	18.02	-	-	-	-	-	100.00	-	-	-
41	566.0	566.0	123.7	18.02	-	-	-	-	-	100.00	-	-	-
42	275.4	2.0	35.8	18.02	-	-	-	-	-	100.00	-	-	-
43	27.0	0.04	88.6	18.02	-	-	-	-	-	100.00	-	-	-
44	27.0	0.4	88.7	18.02	-	-	-	-	-	100.00	-	-	-
45	27.6	3.7	88.7	18.02	-	-	-	-	-	100.00	-	-	-
46	50.0	1.1	41.8	41.59	0.08	0.00	0.00	0.02	90.65	9.20	0.00	0.00	0.05
47	53.7	150.0	40.2	43.88	0.09	0.00	0.00	0.02	99.44	0.40	0.00	0.00	0.05

Table A.3: Stream table for IRCC with dual-pressure reheat HRSG at 60% relative GT load.

No.	T (°C)	p (bar)	$\dot{m}$ (kg/s)	MW (kg/kmol)	CH_4 (vol%)	C_2+ (vol%)	H_2 (vol%)	CO (vol%)	CO_2 (vol%)	H_2O (vol%)	O_2 (vol%)	N_2 (vol%)	Ar (vol%)
1	10.0	30.6	13.2	20.73	79.84	16.73	-	-	2.92	-	-	0.51	-
2	136.0	30.5	13.2	20.73	79.84	16.73	-	-	2.92	-	-	0.51	-
3	420.4	30.4	13.2	20.73	79.84	16.73	-	-	2.92	-	-	0.51	-
4	395.3	28.4	35.0	18.95	27.53	5.77	-	-	1.01	65.52	-	0.18	-
5	518.3	28.3	35.0	18.95	27.53	5.77	-	-	1.01	65.52	-	0.18	-
6	15.0	1.013	465.6	28.85	-	-	-	-	0.03	1.01	20.74	77.30	0.92
7	362.1	11.7	65.5	28.85	-	-	-	-	0.03	1.01	20.74	77.30	0.92
8	362.1	11.7	338.8	28.85	-	-	-	-	0.03	1.01	20.74	77.30	0.92
9	148.1	11.6	65.5	28.85	-	-	-	-	0.03	1.01	20.74	77.30	0.92
10	15.0	11.5	65.5	28.85	-	-	-	-	0.03	1.01	20.74	77.30	0.92
11	72.2	19.7	65.1	28.95	-	-	-	-	0.03	0.12	20.93	78.00	0.93
12	290.0	19.5	65.1	28.95	-	-	-	-	0.03	0.12	20.93	78.00	0.93
13	513.9	19.4	65.1	28.95	-	-	-	-	0.03	0.12	20.93	78.00	0.93
14	950.0	19.0	100.1	19.30	0.11	0.00	28.61	10.18	5.26	21.55	0.00	33.89	0.40
15	420.2	18.8	100.1	19.30	0.11	0.00	28.61	10.18	5.26	21.55	0.00	33.89	0.40
16	345.8	18.7	100.1	19.30	0.11	0.00	28.61	10.18	5.26	21.55	0.00	33.89	0.40
17	425.0	18.4	100.1	19.30	0.11	0.00	35.63	3.16	12.28	14.52	0.00	33.89	0.40
18	360.0	18.2	100.1	19.30	0.11	0.00	35.63	3.16	12.28	14.52	0.00	33.89	0.40
19	240.9	18.1	100.1	19.30	0.11	0.00	35.63	3.16	12.28	14.52	0.00	33.89	0.40
20	208.1	17.9	100.1	19.30	0.11	0.00	35.63	3.16	12.28	14.52	0.00	33.89	0.40
21	238.4	17.6	100.1	19.30	0.11	0.00	38.34	0.45	14.99	11.82	0.00	33.89	0.40
22	144.2	17.4	100.1	19.30	0.11	0.00	38.34	0.45	14.99	11.82	0.00	33.89	0.40
23	128.7	17.3	100.1	19.30	0.11	0.00	38.34	0.45	14.99	11.82	0.00	33.89	0.40
24	50.0	16.5	55.9	14.58	0.13	0.00	51.85	0.60	0.41	0.65	0.00	45.83	0.54
25	204.0	16.4	55.9	14.58	0.13	0.00	51.85	0.60	0.41	0.65	0.00	45.83	0.54
26	1310.4	11.2	394.7	27.09	0.00	0.00	0.00	0.00	0.33	14.70	9.74	74.35	0.89
27	649.1	1.026	456.1	27.32	0.00	0.00	0.00	0.00	0.29	12.96	11.14	74.72	0.90
28	70.0	1.013	457.5	27.27	0.00	0.00	0.00	0.00	0.81	13.82	10.11	74.37	0.89
29	100.7	3.1	99.9	18.02	-	-	-	-	-	100.00	-	-	-
30	120.0	30.9	11.5	18.02	-	-	-	-	-	100.00	-	-	-
31	234.5	30.9	11.5	18.02	-	-	-	-	-	100.00	-	-	-
32	234.2	30.9	11.5	18.02	-	-	-	-	-	100.00	-	-	-
33	238.7	30.9	11.5	18.02	-	-	-	-	-	100.00	-	-	-
34	327.2	133.2	82.0	18.02	-	-	-	-	-	100.00	-	-	-
35	334.7	133.2	82.0	18.02	-	-	-	-	-	100.00	-	-	-
36A	334.7	133.2	47.0	18.02	-	-	-	-	-	100.00	-	-	-
36B	334.7	133.2	35.0	18.02	-	-	-	-	-	100.00	-	-	-
37A	381.4	133.2	47.0	18.02	-	-	-	-	-	100.00	-	-	-
37B	381.4	133.2	35.0	18.02	-	-	-	-	-	100.00	-	-	-
38	566.4	566.4	116.6	18.02	-	-	-	-	-	100.00	-	-	-
39	373.4	28.4	21.8	18.02	-	-	-	-	-	100.00	-	-	-
40	351.0	24.4	92.1	18.02	-	-	-	-	-	100.00	-	-	-
41	566.1	566.1	108.3	18.02	-	-	-	-	-	100.00	-	-	-
42	276.5	2.0	29.9	18.02	-	-	-	-	-	100.00	-	-	-
43	24.8	0.03	78.0	18.02	-	-	-	-	-	100.00	-	-	-
44	24.8	0.4	78.1	18.02	-	-	-	-	-	100.00	-	-	-
45	25.5	3.5	78.1	18.02	-	-	-	-	-	100.00	-	-	-
46	50.0	1.1	35.0	41.60	0.05	0.00	0.00	0.02	90.68	9.20	0.00	0.00	0.05
47	53.6	150.0	33.6	43.88	0.06	0.00	0.00	0.02	99.47	0.40	0.00	0.00	0.05

Table A.4: Stream table for IRCC with single-pressure HRSG.

No.	T (°C)	p (bar)	$\dot{m}$ (kg/s)	MW (kg/kmol)	CH_4 (vol%)	C_2+ (vol%)	H_2 (vol%)	CO (vol%)	CO_2 (vol%)	H_2O (vol%)	O_2 (vol%)	N_2 (vol%)	Ar (vol%)
1	10.0	37.0	18.4	20.73	79.84	16.73	-	-	2.92	-	-	0.51	-
2	10.0	36.2	18.4	20.73	79.84	16.73	-	-	2.92	-	-	0.51	-
3	274.5	36.0	48.8	18.95	27.53	5.77	-	-	1.01	65.52	-	0.18	-
4	500.0	35.4	48.8	18.95	27.53	5.77	-	-	1.01	65.52	-	0.18	-
5	468.6	34.9	48.8	17.47	35.44	0.00	6.87	0.10	4.73	52.70	-	0.16	-
6	500.0	34.7	48.8	17.47	35.44	0.00	6.87	0.10	4.73	52.70	-	0.16	-
7	15.0	1.013	642.1	28.85	-	-	-	-	0.03	1.01	20.74	77.30	0.92
8	381.4	16.3	90.3	28.85	-	-	-	-	0.03	1.01	20.74	77.30	0.92
9	381.4	16.3	467.2	28.85	-	-	-	-	0.03	1.01	20.74	77.30	0.92
10	516.1	30.0	90.3	28.85	-	-	-	-	0.03	1.01	20.74	77.30	0.92
11	950.0	29.3	139.1	19.27	0.24	0.00	28.53	10.06	5.30	21.89	0.00	33.58	0.40
12	350.0	29.1	139.1	19.27	0.24	0.00	28.53	10.06	5.30	21.89	0.00	33.58	0.40
13	426.7	28.7	139.1	19.27	0.24	0.00	35.48	3.11	12.25	14.94	0.00	33.58	0.40
14	210.0	28.5	139.1	19.27	0.24	0.00	35.48	3.11	12.25	14.94	0.00	33.58	0.40
15	237.2	28.1	139.1	19.27	0.24	0.00	38.16	0.43	14.93	12.26	0.00	33.58	0.40
16	149.9	27.9	139.1	19.27	0.24	0.00	38.16	0.43	14.93	12.26	0.00	33.58	0.40
17	115.0	27.7	139.1	19.27	0.24	0.00	38.16	0.43	14.93	12.26	0.00	33.58	0.40
18	90.0	27.2	86.5	15.20	0.28	0.00	48.38	0.53	1.97	5.77	0.00	42.57	0.50
19	50.0	27.2	81.0	15.04	0.30	0.00	51.14	0.56	2.08	0.41	0.00	44.99	0.52
20	200.0	27.0	81.0	15.04	0.30	0.00	51.14	0.56	2.08	0.41	0.00	44.99	0.52
21	1327.4	15.5	548.2	27.16	-	-	-	-	0.81	14.72	9.58	74.00	0.89
22	595.4	1.036	632.8	27.37	-	-	-	-	0.71	12.98	10.99	74.42	0.89
23	77.6	1.013	632.8	27.37	-	-	-	-	0.71	12.98	10.99	74.42	0.89
24	298.4	87.6	41.8	18.02	-	-	-	-	-	100.00	-	-	-
25	298.4	87.6	106.2	18.02	-	-	-	-	-	100.00	-	-	-
26	303.5	87.6	106.2	18.02	-	-	-	-	-	100.00	-	-	-
27	557.8	83.0	148.0	18.02	-	-	-	-	-	100.00	-	-	-
28	436.2	36.0	30.4	18.02	-	-	-	-	-	100.00	-	-	-
29	154.8	3.0	0.0	18.02	-	-	-	-	-	100.00	-	-	-
30	29.0	0.04	113.5	18.02	-	-	-	-	-	100.00	-	-	-
31	29.0	0.4	113.6	18.02	-	-	-	-	-	100.00	-	-	-
32	29.1	1.3	113.6	18.02	-	-	-	-	-	100.00	-	-	-
33	107.0	2.0	10.0	18.02	-	-	-	-	-	100.00	-	-	-
34	122.2	2.0	10.0	18.02	-	-	-	-	-	100.00	-	-	-
35	107.0	2.0	23.9	18.02	-	-	-	-	-	100.00	-	-	-
36	122.0	2.0	23.9	18.02	-	-	-	-	-	100.00	-	-	-
37	125.1	2.0	37.9	18.02	-	-	-	-	-	100.00	-	-	-
38	50.0	1.100	44.6	41.14	0.11	0.00	0.00	0.02	88.92	10.90	0.00	0.00	0.05
39	53.8	150.0	42.5	43.87	0.13	0.00	0.00	0.02	99.40	0.40	0.00	0.00	0.05

Appendix B

Papers

Paper I

Nord, L.O., Anantharaman, R., Bolland, O., 2009. Design and off-design analyses of a pre-combustion CO_2 capture process in a natural gas combined cycle power plant. International Journal of Greenhouse Gas Control 3 (4), 385–392.

International Journal of Greenhouse Gas Control 3 (2009) 385–392

Contents lists available at ScienceDirect

International Journal of Greenhouse Gas Control

journal homepage: www.elsevier.com/locate/ijggc

Design and off-design analyses of a pre-combustion CO_2 capture process in a natural gas combined cycle power plant

Lars Olof Nord *, Rahul Anantharaman, Olav Bolland

Department of Energy and Process Engineering, Norwegian University of Science and Technology, NO-7491 Trondheim, Norway

ARTICLE INFO

Article history:
Received 2 May 2008
Received in revised form 10 February 2009
Accepted 10 February 2009
Available online 17 March 2009

Keywords:
Carbon capture and storage (CCS)
CO_2 capture
Pre-combustion capture
Off-design analysis
Process simulation

ABSTRACT

In this study, a cycle designed for capturing the greenhouse gas CO_2 in a natural gas combined cycle power plant has been analyzed. The process is a pre-combustion CO_2 capture cycle utilizing reforming of natural gas and removal of the carbon in the fuel prior to combustion in the gas turbine. The power cycle consists of a H_2-fired gas turbine and a triple pressure steam cycle. Nitrogen is used as fuel diluent and steam is injected into the flame for additional NO_x control. The heat recovery steam generator includes pre-heating for the various process streams. The pre-combustion cycle consists of an air-blown auto-thermal reformer, water–gas shift reactors, an amine absorption system to separate out the CO_2, as well as a CO_2 compression block. Included in the thermodynamic analysis are design calculations, as well as steady-state off-design calculations. Even though the aim is to operate a plant, as the one in this study, at full load there is also a need to be able to operate at part load, meaning off-design analysis is important. A reference case which excludes the pre-combustion cycle and only consists of the power cycle without CO_2 capture was analyzed at both design and off-design conditions for comparison. A high degree of process integration is present in the cycle studied. This can be advantageous from an efficiency standpoint but the complexity of the plant increases. The part load calculations is one way of investigating how flexible the plant is to off-design conditions. In the analysis performed, part load behavior is rather good with efficiency reductions from base load operation comparable to the reference combined cycle plant.

1. Introduction

Levels of atmospheric carbon dioxide, methane, and other greenhouse gases are on the rise and are contributing to the warming of the atmosphere due to the greenhouse effect. Natural causes can only explain part of this global warming. Fossil fueled power generation, transportation, industrial processes, and other man-made greenhouse gas emission sources add to the picture, mainly because of CO_2 emissions. Out of the energy related carbon dioxide emission sources, the power generation sector is the largest emitter (International Energy Agency, 2006). Thus, if one tries to control and limit the emission of greenhouse gases and thereby attenuating the rise in atmospheric temperature, CO_2 capture from fossil fuel power plants can be a viable path. Among the fossil fuels, the capture of the carbon from coal is attracting the main attention because of the high carbon dioxide emissions per kilowatt hour of electricity and the abundance of coal-fired plants in the world. However, for Norway, with large natural gas reserves and the planned and already built gas-fired power plants in the country, CO_2 capture from such plants will be important.

The methods for capture of CO_2 from fossil fuel power generation sources can be divided into three main categories:

(1) Post-combustion capture, where the CO_2 is captured at the tail end of the plant from the flue gases, i.e., after the combustion (Chapel and Mariz, 1999). Capture of CO_2 from the flue gases of a power plant may be the best option for capture retrofits of existing power plants. It is also a viable option for new plants. The currently preferred option is capture by absorption processes based on chemical solvents and have been implemented in a number of pilot projects world-wide for CO_2 capture purposes, for example, the Castor pilot project in Denmark (LeThiez et al., 2004; Knudsen et al., 2006), and the Boundary Dam pilot plant in Canada (Wilson et al., 2004).
(2) Pre-combustion capture, where the fossil fuel is used for producing a syngas and the carbon (as CO_2) is separated out before the combustion takes place. The fuel for the combustion mainly consists of hydrogen mixed with a diluent, such as, nitrogen or steam. An existing technology for power plant applications, the integrated gasification combined cycle (IGCC),

* *Corresponding author.*
E-mail address: lars.nord@ntnu.no (L.O. Nord).

1750-5836/$ – see front matter © 2009 Elsevier Ltd. All rights reserved.
doi:10.1016/j.ijggc.2009.02.001

could be attractive as part of a coal based pre-combustion CO_2 capture method (Bohm et al., 2007).

(3) Oxy-fuel combustion, where the oxidizer for the combustion is oxygen instead of air. The combustion products are mainly carbon dioxide and steam, and the CO_2 can be separated out by condensing the steam. Many proposals for cycle configurations have been suggested in the oxy-fuel category. Examples include the Graz cycle (Jericha et al., 2004), the Matiant cycle (Mathieu and Nihart, 1999), the advanced zero emissions power plant (Griffin et al., 2005), and chemical looping combustion (Richter and Knoche, 1983; Ishida and Jin, 1994).

This study focuses on the pre-combustion approach. More specifically, pre-combustion capture utilizing an air-blown auto-thermal reformer (ATR) in a natural gas fueled combined cycle (NGCC) plant. Similar process configurations have been studied by Andersen et al. (2000); Lozza and Chiesa (2002a, b); Corradetti and Desideri (2005); Ertesvag et al. (2005). Their results from heat and mass balance analyses show lower heating value (LHV) net plant efficiencies ranging from approximately 46% to 49%. Another possibility for this type of plant is to utilize it for co-production of hydrogen and electricity (Consonni and Vigano, 2005); however, the focus of this paper is on power production only. Kvamsdal et al. (2007) performs comparative heat and mass balance simulations for a number of CO_2 capture cycles including pre-combustion cases. The cited studies focus on design case analysis. Little is found in the literature in terms of off-design analysis of CO_2 capture cycles. Part load analyses of post-combustion systems are performed for coal cycles by Chalmers and Gibbins (2007) and for natural gas cycles by Möller et al. (2007). Haag et al. (2007) and Naqvi et al. (2007) analyze the part load behavior of some of the proposed oxy-fuel cycles. For NGCC pre-combustion plants no off-design publications have been found by the author.

The remainder of the paper is divided into the following sections: Section 2 describes the process where the details of the cycle are explained. Section 3 describes the methodology and lists the assumptions used in the study. The results are shown and analyzed in Section 4 and concluding remarks are given in Section 5.

2. Process description

The selected process for the work is a pre-combustion CO_2 capture cycle in a natural gas combined cycle power plant as shown in Fig. 1. The power cycle consists of a General Electric (GE) 9FA H_2-fired gas turbine (GT) and a triple pressure steam cycle. The heat recovery steam generator (HRSG) includes pre-heating for the various process streams. The pre-combustion cycle consists of a pre-reformer, an air-blown auto-thermal reformer, two water–gas shift reactors, a gas separation stage in form of amine absorption to separate out the CO_2, as well as a CO_2 compression block.

As mentioned, the fuel input to the process is natural gas (stream 1 in Fig. 1). After the natural gas has been regulated down to system pressure (stream 2), pre-heated to 400 °C (3), and desulfurized (4), it is mixed with steam (5) before another pre-heating section (500 °C) and introduced to the pre-reformer (6). The steam to carbon ratio (S/C) is set at 1.5. In the pre-reforming reactor the hydrocarbons higher than methane are converted to protect against coking in the primary reformer according to reactions (1) and (2).

$$C_xH_y + xH_2O_{(g)} \rightleftharpoons xCO + \left(x + \frac{y}{2}\right)H_2 \quad -\Delta H^0_{298} < 0\,\text{kJ/mol} \tag{1}$$

$$CO + 3H_2 \rightleftharpoons CH_4 + H_2O_{(g)} \quad -\Delta H^0_{298} = 206\,\text{kJ/mol} \tag{2}$$

Also, the exothermic water–gas shift reaction (3) converting the CO into CO_2 occurs to some degree in the pre-reforming reactor.

$$CO + H_2O_{(g)} \rightleftharpoons CO_2 + H_2 \quad -\Delta H^0_{298} = 41\,\text{kJ/mol} \tag{3}$$

Before entering the ATR the stream from the pre-reformer (7) is again pre-heated to 500 °C (8). Also, air extracted from the compressor discharge stream of the gas turbine (10) combined with an additional compressor air stream (13) is pre-heated and supplied to the ATR (15). The external compressor is introduced in order to better utilize the operation of the gas turbine. If too much air is removed prior to the combustion chamber in the gas turbine the effect on performance and temperature profile can be negative. With the additional compressor another degree of freedom is attained and the gas turbine can be utilized in a more efficient manner.

In the ATR the exothermic reaction (4) provide heat to the endothermic reaction (5).

$$CH_4 + \tfrac{1}{2}O_2 \rightarrow CO + 2H_2 \quad -\Delta H^0_{298} = 36\,\text{kJ/mol} \tag{4}$$

$$CH_4 + H_2O_{(g)} \rightleftharpoons CO + 3H_2 \quad -\Delta H^0_{298} = -206\,\text{kJ/mol} \tag{5}$$

As in the pre-reformer the water–gas shift reaction (3) converts some of the CO into CO_2. Further on, the syngas is cooled in the syngas cooler before entering the water–gas shift reactors where most of the remaining CO is converted into CO_2 according to reaction (3). The reasons behind dividing the water–gas shift reaction into a high temperature reactor and a low temperature one are due to conversion rate and catalysts. To get a higher degree of conversion of the CO to CO_2, two reactors are favorable compared to a one-reactor setup. Also, there is a need for a more active catalyst at the lower region of the temperature range (Moulijn et al., 2007). It can therefore make sense to use a standard catalyst at the higher temperature range and then have a separate reactor with a more active catalyst for the low end temperature. Heat exchanger 3 (HE3) and the syngas cooler are utilized for producing high-pressure saturated steam to be added to the high-pressure superheater in the HRSG. The reason for not superheating the steam in the heat exchanger is because of the risk of metal dusting (Grabke and Spiegel, 2003). Heat exchanger 4 (HE4) is used to pre-heat the fuel to the gas turbine to 200 °C (29). In this model the pre-combustion capture (Gas separation) is using the chemical absorbent activated MDEA (Zhang et al., 2003; van Loo et al., 2007) and is modeled as a 'black box'. Assumptions for the capture section include a CO_2 capture rate of 95% and the heat required for the stripper reboiler at 1.5 MJ/kg CO_2. Heat exchanger 5 (HE5) is producing some of the steam necessary for the reboiler in the amine absorption process. The CO_2 (54) is passed on to the compression section where the gas is compressed in the four compressor/intercooler stages and excess water is removed. To achieve the exit pressure of 110 bar a pump is utilized at the end of the compression train.

From the gas separation stage the fuel mix (27) is passed on to the gas turbine via a fuel compressor. In principle, the fuel consists of an H_2/N_2 mixture. The N_2 diluent is used to be able to operate with available IGCC-type combustors in the gas turbine. For further NO_x control, steam is injected into the flame. In addition to running the GT on a hydrogen based fuel, the idea is to be able to operate on natural gas if the pre-combustion process is shut-down and during plant start-up. This requires fuel flexibility for the combustor system (Tomczak et al., 2002; Shilling and Jones, 2003; Moliere, 2005). The gas turbine exhaust stream (40) passes through the HRSG for pre-heating of process streams and steam generation before emitted to the atmosphere through the stack (41).

The steam cycle is designed for pressure levels of approximately 83/10/3 bars for the high, intermediate, and low pressure (HP/IP/LP)

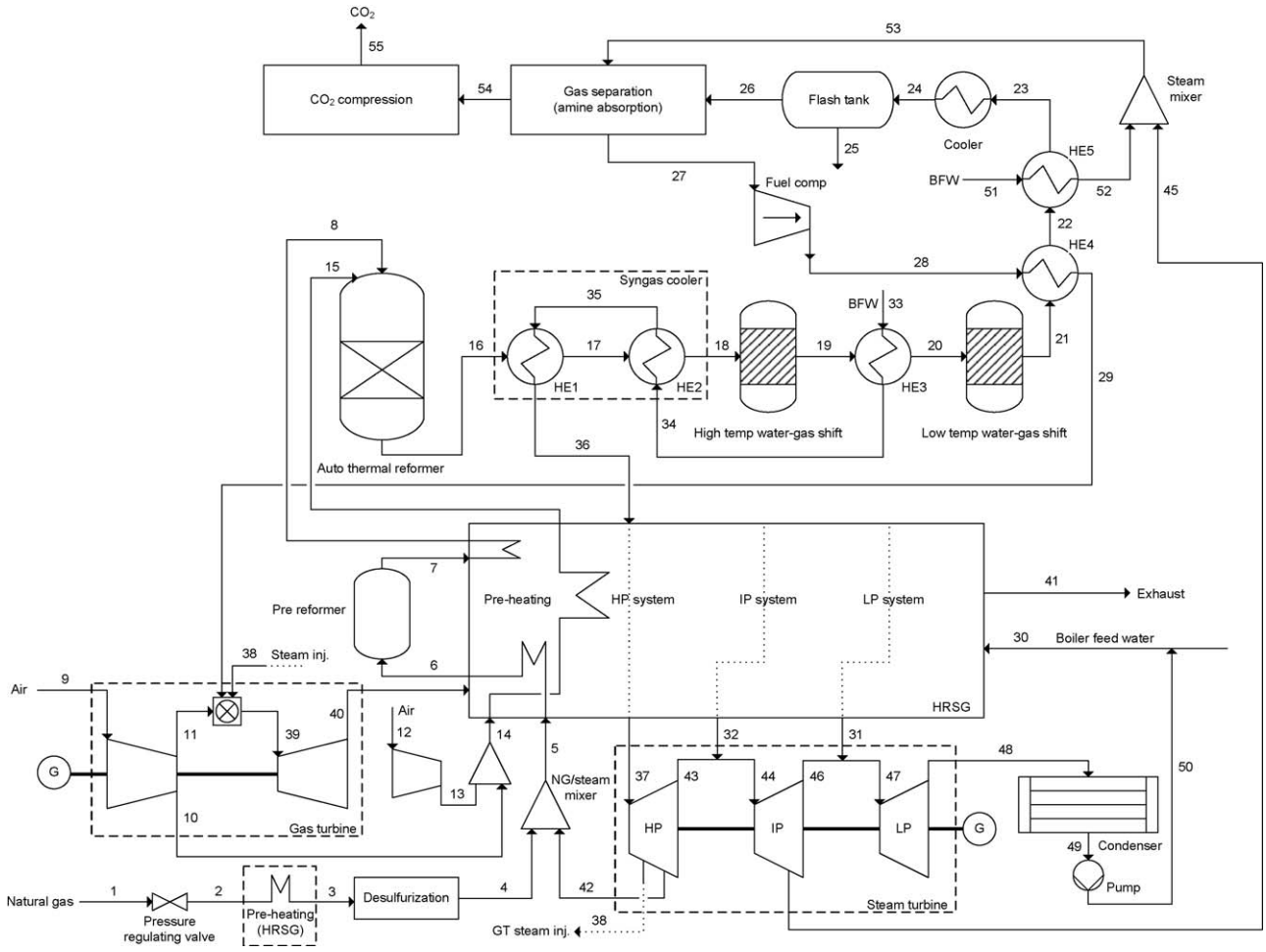

Fig. 1. Pre-combustion process flow sheet.

systems respectively. The pre-heating makes the HRSG design more complex and a lot of heat is removed from the gas stream at the hot part of the HRSG due to the high temperature requirements of some of the process streams. Note that the pre-heating is not entirely in the hot end of the HRSG but instead inter-mixed with the low, intermediate, and high-pressure sections. The steam turbine (ST) has extractions for the GT steam injection (38), the reforming process steam (42), and for the reboiler in the amine absorption system (45). After exiting the last low pressure turbine stage (48) the steam is condensed in the direct seawater cooled condenser (49). The condenser pressure is assumed at 0.04 bar.

There are certainly many configuration options for a plant like this. For example, one could operate the system at a higher pressure by boosting the air pressure from the gas turbine compressor discharge with an additional compressor. In this way a fuel compressor would not be necessary. The impact of this option was investigated by Andersen et al. (2000) where it was concluded that operating at a lower system pressure and having a fuel compressor improves the overall efficiency for the cycle in their study. This effect was due to the need for extra process stream pre-heating in the elevated pressure case since the air was cooled before the compression to minimize compressor work. Other configuration options include utilizing an oxygen-blown ATR with an air separation unit (ASU) for the oxygen supply. Or using a steam reformer instead of the ATR. Configurations with less integration between the power cycle and syngas process could also be attractive. For the power cycle one could employ a more recent gas turbine model as for example the GE 9FB type with a higher turbine inlet temperature (TIT) and cycle efficiency. The steam cycle could include a reheat cycle leading to a higher efficiency but also more complexity. For the capture section one could use other absorbants, such as, hot potassium carbonate.

A reference case which excludes the pre-combustion cycle and only consist of the power cycle without CO_2 capture was analyzed at both design and off-design conditions for comparison. The reference case consists of the same type GE 9FA gas turbine but is instead of the IGCC combustor using a regular pre-mix natural gas combustor without steam injection. The steam cycle is again triple pressure without reheat.

3. Methodology

This section provides details into the process models simulated in the study. Assumptions for the design case analysis are described in Section 3.1. Included in the thermodynamic analysis are steady-state off-design calculations, that is, analysis when the plant is operating at part load. In a scenario where CO_2 capture plants become common-place, part load operation will be an important part of the operation scheme. For a plant such as the one modeled in this work the goal is certainly to run it at base load operation for the majority of the time but as part of an overall grid strategy part load operation will come into play. Assumptions for the part load cases are described in Section 3.2.

The pre-combustion cycle, including the pre-heating section, was modeled with Aspen HYSYS. The property package was modeled with the Kabadi–Danner equation of state. The Kabadi–Danner is a modification of the Soave–Redlich–Kwong equation of state to take into account hydrocarbon solubility in the water

phase. The power cycle was modeled with GT PRO for the design case and GT MASTER for the off-design cases. For the steam properties in GT PRO/GT MASTER the IAPSW-IF97 formulation was used (Wagner et al., 2000).

3.1. Design model assumptions

The selected gas turbine is a GE 9FA from the model library of GT PRO version 17. Steam is injected into the flame for NO_x control at a rate of 20% of the fuel mass flow. The GT turbine inlet temperature has been reduced because of the high steam content in the turbine. The hydrogen fuel together with the injected steam lead to an H_2O content entering the turbine of about 18.2 vol%. This leads to a higher heat transfer rate to the blades compared to a natural gas-fired turbine. As a result, the metal temperature of the turbine blades is higher for the same turbine inlet temperature as in a conventional gas turbine. To obtain similar life of the turbine parts, the turbine inlet temperature reduction is necessary. Chiesa et al. (2005) report TIT decreases of 10–34 K for hydrogen combustion with nitrogen or steam diluent (VGV operation cases). As a model assumption, a TIT reduction of 30 K has been assumed for this work. The inlet filter pressure drop is set to 10 mbar and the total exhaust losses (GT exhaust and HRSG) to 25 mbar. The maximum allowable GT power output is increased from 260 to 286 MW (IGCC setup). Air from the compressor discharge is re-directed to the reforming section at a rate of 75 kg/s. This is approximately 12% of the GT inlet air flow. Additional air required for the reforming is supplied by an external (to the GT) compressor with a polytropic efficiency of 85%. A polytropic efficiency of 85% is also assumed for the fuel compressor for the hydrogen-rich fuel.

The high-pressure steam is set to 83 bar at 568 °C before the stop valve to the steam turbine. The intermediate-pressure level is 10.3 bar and the LP drum pressure is 2.8 bar. The pinch point temperature difference is assumed to be 10 K for all three pressure levels. The subcooling approach temperature difference at the exit of the economizers is assumed at 5 K.

The natural gas composition (stream 1) is listed in Table 2 with the exception of the H_2S content which is set to be 5 ppmvd. The sulfur is removed in the desulfurizer unit, which is modeled as a separator. The air composition (9) is also listed in Table 2. The ambient pressure is assumed to be 1.013 bar with a temperature of 15 °C and a relative humidity of 60%.

The pressure drops in the pre-reformer and ATR are set at 5% of the inlet pressure. The tube side pressure drop in the heat exchangers modeled in HYSYS is set to be 0.5 bar (approximately 3% of inlet pressure) with the exception of HE3–HE5 which each has an assumed pressure drop of 0.85 bar due to two shell passes compared to one shell pass for the other heat exchangers. The shift reactors are modeled with a 0.5 bar pressure drop. The pre-reformer and the water–gas shift reactors are modeled as equilibrium reactors. A Gibbs reactor model is used for the ATR.

A splitter is used for the amine absorption section model. The reboiler duty is set to 1.5 MJ/kg CO_2 and the total pump work is assumed to be 0.16 MJ/kg CO_2. The reboiler temperature is set to 120 °C. A 95% capture rate is assumed for the absorption system.

Polytropic efficiencies for the CO_2 compression train are assumed at 85%, 80%, 80%, and 75% for the four compressor stages respectively (listed in flow direction). The pump that pressurizes the CO_2 stream to the end pressure of 110 bar is assumed to have an adiabatic efficiency of 75%.

3.2. Off-design model assumptions

The selected part load points are 60% and 80% of the design case gas turbine load. The reason for selecting the relative part load points as a function of gas turbine load is because the GT dictates the overall plant load. By changing the GT load, the steam cycle, as well as the pre-combustion process, will follow. Gas turbine part load operation commonly employs variable inlet guide vanes (VIGV). This is the case for the GE 9FA which has one row of variable guide vanes where the flow angle entering the first stage of the compressor can be varied. The VIGV operation allows reduction of the air flow and the turbine exhaust temperature can remain high at part load operation. The high exhaust temperature means the part load combined cycle efficiency can be maintained at a high level. However, at the lower part load range the cycle efficiency drops off quicker. The steam cycle part load operating concept involves sliding pressure operation with fully open steam valves down to approximately 50% steam turbine load (Kehlhofer et al., 1999). At lower loads the operating concept is based on fixed steam pressure operation by closing of the steam valves. This leads to throttling losses in the ST inlet valves. These factors combined may suggest that it does not make sense to operate a plant, such as the one in the study, at a much lower GT load than 60%. Certainly, the plant still has to be able to operate at lower part load points, not the least during transients such as start-ups and shut-downs; however, transient analysis is not covered in this study.

All the hardware in the off-design cases are identical to the design case. This also means that the extractions of the steam turbine are set. Since the part load operation is with sliding pressure operation of the steam cycle the steam pressures at the extraction points will decrease. In the case of the steam for the reboiler in the amine absorption system the design case was actually "over-designed" to allow for a sufficient steam pressure (and hence a sufficiently high condensation temperature) for the part load cases.

The turbine inlet temperature reduction was removed for the off-design simulations since the temperature was decreased anyway for part load operation at the 80% and 60% relative load levels. The air extraction from the compressor discharge was decreased to 60 kg/s (approximately 11% of GT inlet air flow) for the 80% case and 45 kg/s (approximately 10% of GT inlet air flow) for the 60% case. The fuel compressor exit pressure is assumed constant from the design case.

In the design case the inlet temperatures to the desulfurization unit, the reforming reactors, and the water–gas shift reactors were fixed. For the off-design calculations these constraints were removed. Instead, for each part load case a check was performed to see if the inlet temperatures were within the operational window of each reactor. Based on the resulting inlet temperatures it was not necessary to use by-pass valves for the various heat exchangers at the steady-state part load cases simulated (although likely needed during lower part load and start-up and shut-down).

For the analysis of the various heat exchangers a correction of the heat transfer coefficient was done based on the gas massflow. The correction is based on course literature from Bolland (2006) as displayed in Eq. (6).

$$\frac{U}{U_{\text{design}}} = \left(\frac{\dot{m}_{\text{gas}}}{\dot{m}_{\text{gas,design}}}\right)^{m} \tag{6}$$

U is here the heat transfer coefficient, $\dot{m}_{\text{gas}}$ the gas massflow, and m a constant. For a staggered tubes configuration with assumed tube pitches of 2.5 (Incropera and DeWitt, 1990):

$$\left.\begin{aligned}\frac{S_T}{D} &= 2.5\\ \frac{S_L}{D} &= 2.5\end{aligned}\right\} \Rightarrow m \simeq 0.57$$

S_T is the transverse pitch, that is, the distance 90° off from the flow direction between the centers of two adjacent tubes. S_L is the longitudinal pitch, that is, the distance in flow direction between

Table 1
Summary of results for design case (100%), off-design cases (80% and 60%), and reference cases (100% ref., 80% ref., and 60% ref.).

	100%	100% ref.	80%	80% ref.	60%	60% ref.
Natural gas LHV input [MW]	865.2	689.1	729.8	599.0	588.2	501.0
Gross power output GT [MW]	277.0	253.5	221.6	204.0	166.2	153.8
Gross power output ST [MW]	137.6	137.2	122.5	127.6	103.8	113.7
Gross power output [MW]	414.6	390.7	344.1	331.6	270.0	267.5
Gross power output [% of LHV input]	47.9	56.7	47.1	55.4	45.9	53.4
Air compression [MW]	8.2	–	7.9	–	6.9	–
Air compression [% of LHV input]	0.9	–	1.1	–	1.2	–
Fuel compression [MW]	13.6	–	14.7	–	17.0	–
Fuel compression [% of LHV input]	1.6	–	2.0	–	2.9	–
CO_2 compression [MW]	17.7	–	15.0	–	12.2	–
CO_2 compression [% of LHV input]	2.0	–	2.1	–	2.1	–
Gas separation pumps [MW]	7.6	–	6.4	–	5.2	–
Gas separation pumps [% of LHV input]	0.9	–	0.9	–	0.9	–
BFW pumps in pre-comb process [MW]	1.0	–	0.8	–	0.5	–
BFW pumps in pre-comb process [% of LHV input]	0.1	–	0.1	–	0.1	–
Auxiliaries [MW]	4.5	5.4	4.4	5.3	4.3	5.2
Auxiliaries [% of LHV input]	0.5	1.4	0.6	1.6	0.7	1.9
Net power output [MW]	362.2	385.3	294.9	326.3	223.8	262.3
Net plant efficiency [% of LHV input]	41.9	55.9	40.4	54.5	38.0	52.4
Efficiency capture penalty [%-point loss to ref. case]	14.0	–	14.1	–	14.3	–
CO_2 emissions [g CO_2/net kWh el.]	33.2	380.1	30.7	390.1	29.3	405.9
CO_2 capture rate [%]	93.4	0	94.1	0	94.7	0

the centers of two adjacent tubes. D is the tube diameter in the heat exchanger. In HYSYS there is the option to lock in the UA specification for a heat exchanger. Since the area A is constant one could re-write Eq. (6) as:

$$UA = U_{\text{design}} A \left(\frac{\dot{m}_{\text{gas}}}{\dot{m}_{\text{gas,design}}} \right)^{0.57} \tag{7}$$

A similar expression, the exception being the m-factor which was set at 0.6, was used by Haag et al. (2007).

4. Results

The main results are summarized in Table 1. Included in the table is the power consumption for the air compressor (external to GT), the fuel compressor, the CO_2 compression, the pump work in the amine absorption system (gas separation pumps), as well as the additional boiler feed water pumps in the pre-combustion system, and the remaining plant auxiliaries. The auxiliaries post in Table 1 includes, among other items, the regular boiler feed water pumps and the cooling water pumps.

The design case LHV based cycle efficiency is 41.9% with a net power output of approximately 362 MW. The net power output is here defined as the gross power output at the generator terminals minus the power needed for air compression, fuel compression, CO_2 compression, pump work, and auxiliaries, as displayed in Table 1. The cycle efficiency is the net power output divided by the natural gas lower heating value input. The design case results should be compared to the reference case net power output of

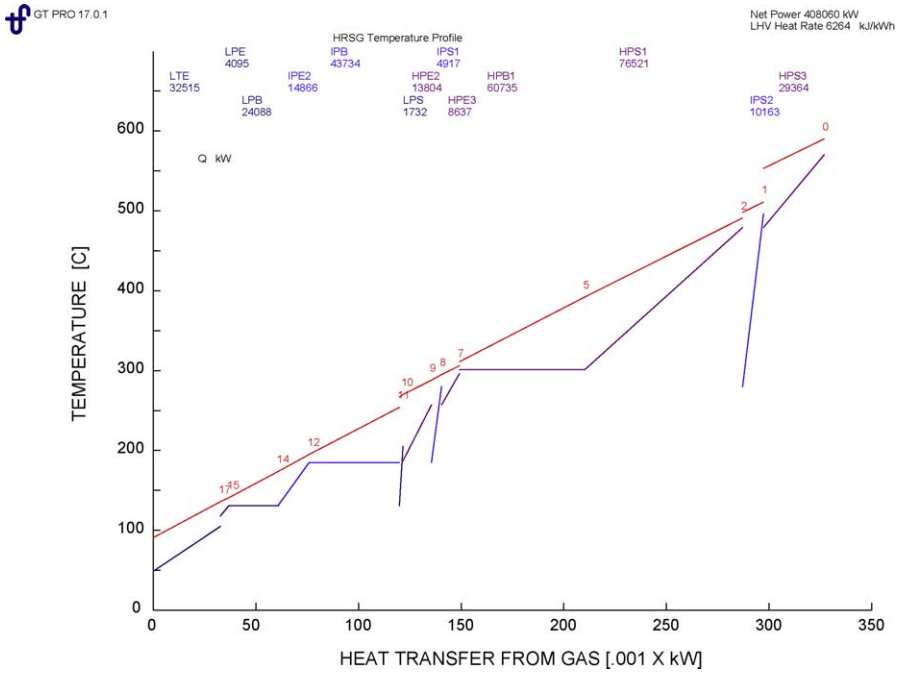

Fig. 2. GT PRO T-Q diagram for heat recovery steam generator.

Table 2
Stream results for the design case.

No.	T (°C)	p (bar)	$\dot{m}$ (kg/s)	MW (kg/kmol)	CH_4 (vol%)	C_2+ (vol%)	H_2 (vol%)	CO (vol%)	CO_2 (vol%)	H_2O (vol%)	O_2 (vol%)	N_2 (vol%)	Ar (vol%)
1	16.0	31.00	19.0	20.73	79.84	16.72	–	–	2.92	–	–	0.51	–
3	400.0	17.68	19.0	20.73	79.84	16.72	–	–	2.92	–	–	0.51	–
5	371.3	17.68	49.5	18.97	28.01	5.86	–	–	1.03	64.91	–	0.18	–
6	500.0	17.18	49.5	18.97	28.01	5.86	–	–	1.03	64.91	–	0.18	–
7	451.4	16.32	49.5	17.30	35.20	0.00	8.77	0.12	5.21	50.53	–	0.16	–
8	500.0	15.82	49.5	17.30	35.20	0.00	8.77	0.12	5.21	50.53	–	0.16	–
9	15.0	1.01	629.3	28.86	–	–	–	–	0.03	1.01	20.74	77.29	0.93
10	394.0	16.35	75.0	28.85	–	–	–	–	0.03	1.02	20.73	77.29	0.92
11	394.0	16.35	483.9	28.86	–	–	–	–	0.03	1.01	20.74	77.29	0.93
13	436.1	16.35	18.5	28.85	–	–	–	–	0.03	1.02	20.73	77.29	0.92
15	500.0	15.85	93.5	28.85	–	–	–	–	0.03	1.02	20.73	77.29	0.92
16	950.0	15.03	143.0	19.24	0.08	0.00	28.87	10.38	5.16	21.36	0.00	33.74	0.40
18	350.0	14.03	143.0	19.24	0.08	0.00	28.87	10.38	5.16	21.36	0.00	33.74	0.40
19	433.7	13.53	143.0	19.24	0.08	0.00	35.94	3.31	12.23	14.29	0.00	33.74	0.40
20	205.8	12.68	143.0	19.24	0.08	0.00	35.94	3.31	12.23	14.29	0.00	33.74	0.40
21	241.4	12.18	143.0	19.24	0.08	0.00	38.79	0.46	15.08	11.44	0.00	33.74	0.40
26	25.0	9.98	128.1	19.39	0.09	0.00	43.65	0.52	16.96	0.35	0.00	37.97	0.45
29	200.0	20.00	79.9	14.55	0.11	0.00	52.32	0.63	0.64	0.19	0.00	45.56	0.54
31	203.3	2.47	11.1	18.02	–	–	–	–	–	100.00	–	–	–
32	494.8	10.30	21.9	18.02	–	–	–	–	–	100.00	–	–	–
36	301.4	87.62	86.7	18.02	–	–	–	–	–	100.00	–	–	–
37	568.0	83.00	129.4	18.02	–	–	–	–	–	100.00	–	–	–
38	377.0	22.00	16.0	18.02	–	–	–	–	–	100.00	–	–	–
39	1295.0	15.70	579.8	26.73	–	–	–	–	0.37	18.21	9.28	71.28	0.86
40	591.0	1.04	650.1	26.94	–	–	–	–	0.34	16.48	10.43	71.89	0.87
41	90.6	1.01	650.1	26.94	–	–	–	–	0.34	16.48	10.43	71.89	0.87
42	346.0	17.68	30.5	18.02	–	–	–	–	–	100.00	–	–	–
45	227.0	4.00	24.0	18.02	–	–	–	–	–	100.00	–	–	–
53	209.6	4.00	30.5	18.02	–	–	–	–	–	100.00	–	–	–
55	40.9	110.00	47.4	43.89	0.00	0.00	0.12	0.00	99.58	0.25	0.00	0.05	0.00

approximately 385 MW and efficiency of 55.9% leading to a capture efficiency penalty of approximately 14%-points. The calculated design case cycle efficiency is low and the capture efficiency penalty high compared to the literature (Andersen et al., 2000; Lozza and Chiesa, 2002a, b; Corradetti and Desideri, 2005; Ertesvag et al., 2005). This can be explained to a large degree by the practical considerations included in this work. For one, steam is injected into the gas turbine for NO_x control which lowers the overall efficiency. Also, the turbine inlet temperature is decreased by 30 K which further will bring the efficiency down. In addition, for the design case, considerations were taken of the part load scenarios. For example, a steam turbine extraction had to be taken at a higher than necessary pressure during design case analysis to have sufficient pressure also at the off-design cases. This also has a negative effect on the design case plant efficiency.

The HRSG has a different design than would be present in a typical NGCC plant. A large portion of the heat in the GT exhaust gases are utilized in the pre-heating and in the HP superheaters, as displayed in Fig. 2. Because of the saturated steam introduced from the syngas cooler the massflow to the high-pressure superheaters are more than three times as high as the massflow in the HP boiler. The vertical gas temperature jumps in the T-Q diagram represent the pre-heating sections in the HRSG.

The off-design calculations resulted in net plant efficiencies of 40.4% and 38.0% for the 80% and 60% load cases respectively. The

Table 3
Stream results for the 80% load case.

No.	T (°C)	p (bar)	$\dot{m}$ (kg/s)	MW (kg/kmol)	CH_4 (vol%)	C_2+ (vol%)	H_2 (vol%)	CO (vol%)	CO_2 (vol%)	H_2O (vol%)	O_2 (vol%)	N_2 (vol%)	Ar (vol%)
1	16.0	31.00	16.0	20.73	79.84	16.72	–	–	2.92	–	–	0.51	–
3	397.5	17.68	16.0	20.73	79.84	16.72	–	–	2.92	–	–	0.51	–
6	494.9	15.56	41.8	18.97	28.01	5.86	–	–	1.03	64.91	–	0.18	–
8	494.2	14.28	41.8	17.30	35.21	0.00	8.76	0.11	5.22	50.53	–	0.16	–
9	15.0	1.01	535.6	28.86	–	–	–	–	0.03	1.01	20.74	77.29	0.93
10	377.0	13.91	60.0	28.85	–	–	–	–	0.03	1.02	20.73	77.29	0.92
15	489.3	13.41	79.5	28.85	–	–	–	–	0.03	1.02	20.73	77.29	0.92
18	334.9	11.70	121.3	19.27	0.06	0.00	28.74	10.34	5.18	21.38	0.00	33.90	0.40
20	195.4	10.35	121.3	19.27	0.06	0.00	36.03	3.06	12.46	14.10	0.00	33.90	0.40
21	229.2	9.85	121.3	19.27	0.06	0.00	38.71	0.37	15.15	11.41	0.00	33.90	0.40
29	200.4	20.00	67.8	14.57	0.08	0.00	52.24	0.50	0.65	0.20	0.00	45.78	0.55
31	207.5	2.21	8.0	18.02	–	–	–	–	–	100.00	–	–	–
32	486.2	9.26	18.9	18.02	–	–	–	–	–	100.00	–	–	–
36	297.5	82.88	74.1	18.02	–	–	–	–	–	100.00	–	–	–
37	568.0	73.69	114.4	18.02	–	–	–	–	–	100.00	–	–	–
39	1270.0	13.35	497.0	26.75	–	–	–	–	0.33	17.98	9.45	71.38	0.86
40	602.0	1.03	556.8	26.96	–	–	–	–	0.30	16.28	10.58	71.98	0.87
45	228.0	3.68	19.9	18.02	–	–	–	–	–	100.00	–	–	–
53	208.3	3.68	25.8	18.02	–	–	–	–	–	100.00	–	–	–
55	40.9	110.00	40.3	43.89	0.00	0.00	0.12	0.00	99.58	0.25	0.00	0.05	0.00

Table 4
Stream results for the 60% load case.

No.	T (°C)	p (bar)	$\dot{m}$ (kg/s)	MW (kg/kmol)	CH_4 (vol%)	C_2+ (vol%)	H_2 (vol%)	CO (vol%)	CO_2 (vol%)	H_2O (vol%)	O_2 (vol%)	N_2 (vol%)	Ar (vol%)
1	16.0	31.00	12.9	20.73	79.84	16.72	–	–	2.92	–	–	0.51	–
3	400.5	13.22	12.9	20.73	79.84	16.72	–	–	2.92	–	–	0.51	–
6	501.6	12.72	33.7	18.97	28.02	5.86	–	–	1.03	64.90	–	0.18	–
8	497.9	11.58	33.7	17.24	34.89	0.00	9.50	0.12	5.38	49.95	–	0.16	–
9	15.0	1.01	465.3	28.86	–	–	–	–	0.03	1.01	20.74	77.29	0.93
10	355.0	11.84	45.0	28.85	–	–	–	–	0.03	1.02	20.73	77.29	0.92
15	489.6	11.34	63.8	28.85	–	–	–	–	0.03	1.02	20.73	77.29	0.92
18	314.5	9.76	97.4	19.24	0.04	0.00	28.89	10.39	5.16	21.32	0.00	33.79	0.40
20	182.4	8.41	97.4	19.24	0.04	0.00	36.49	2.79	12.76	13.72	0.00	33.79	0.40
21	214.2	7.91	97.4	19.24	0.04	0.00	39.00	0.29	15.27	11.22	0.00	33.79	0.40
29	205.1	20.00	54.3	14.49	0.06	0.00	52.56	0.39	0.65	0.21	0.00	45.58	0.55
31	204.0	1.92	6.4	18.02	–	–	–	–	–	100.00	–	–	–
32	489.6	7.90	15.6	18.02	–	–	–	–	–	100.00	–	–	–
36	286.0	69.98	60.2	18.02	–	–	–	–	–	100.00	–	–	–
37	568.1	62.25	95.5	18.02	–	–	–	–	–	100.00	–	–	–
39	1200.0	11.36	433.5	26.89	–	–	–	–	0.28	16.82	10.25	71.79	0.86
40	590.0	1.03	485.5	27.09	–	–	–	–	0.26	15.23	11.30	72.35	0.87
45	233.0	3.27	14.8	18.02	–	–	–	–	–	100.00	–	–	–
53	207.0	3.27	20.8	18.02	–	–	–	–	–	100.00	–	–	–
55	40.9	110.00	32.7	43.89	0.00	0.00	0.12	0.00	99.58	0.25	0.00	0.05	0.00

capture penalties for the part load cases are very similar to the design case, that is, around 14%-points.

The CO_2 capture rate varies between 93% and 95% for the different cases, with CO_2 emissions of 29–33 g/net kWh electricity. The CO_2 capture rate is defined as the fraction of formed CO_2 that is captured.

Stream data for the design case is displayed in Table 2, for the 80% load case in Table 3, and for the 60% load case in Table 4.

5. Conclusions

The pre-combustion NGCC cycle is a system well worth studying. Advantages include the reduced size of the capture system and the increased CO_2 partial pressure compared to post-combustion capture. A post-combustion capture system would have to deal with separating out CO_2 from flue gases with very large flow rates at a low pressure. Disadvantages compared to post-combustion capture include conversion losses in the natural gas reforming process. Another advantage for a post-combustion capture system is that natural gas-fired gas turbines are more mature product than hydrogen fired ones. Pre-mix combustion with low NO_x emissions is one of the advantages of a standard GT fired with natural gas. In the case of the hydrogen diffusion combustion system, diluents such as steam and nitrogen are necessary. In this study, nitrogen was used as diluent and steam was injected directly into the flame in the combustor.

A high degree of process integration is present in the cycle studied. This can be advantageous from an efficiency stand-point but the complexity of the plant increases. This is exemplified in the HRSG where several of the process streams are pre-heated and high-pressure steam are introduced from the syngas cooler to the HP superheaters. The heat from the syngas is used for the economizing and boiling of the high-pressure water. This heat integration increases the cycle efficiency but the price is paid in the resulting increased plant complexity.

Part load calculations are one way of investigating how flexible the plant is to off-design conditions. In the analysis performed in the study, part load behavior is rather good with efficiency reductions from baseload operation comparable to the reference combined cycle plant. Based on the analysis performed in the paper, it is possible to operate a complex plant like this one at part loads down to 60% GT load and possibly lower. Not included in the part load study are compressor mapping for off-design calculations for the air compressor, fuel compressor, and CO_2 compression train. Energy requirement changes per kg of CO_2 for the reboiler in the amine absorption system at off-design points are not considered either. Including these details in the model could show a different part load behavior.

Acknowledgments

This work was supported by the Norwegian Research Council and StatoilHydro. The authors are thankful for the work done by the reviewer and editor.

References

Andersen, T., Kvamsdal, Hanne, M., Bolland, O., 2000. Gas turbine combined cycle with CO_2 capture using auto-thermal reforming of natural gas. In: ASME Turbo Expo. Munich, Germany.

Bohm, M.C., Herzog, H.J., Parsons, J.E., Sekar, R.C., 2007. Capture-ready coal plants—options, technologies and economics. International Journal of Greenhouse Gas Control 1 (1), 113–120.

Bolland, O., 2006. Thermal power generation, part of the literature in the course "Thermal power cycles and co-generation,"-Norwegian University of Science and Technology, p. 126.

Chalmers, H., Gibbins, J., 2007. Initial evaluation of the impact of post-combustion capture of carbon dioxide on supercritical pulverised coal power plant part load performance. Fuel 86 (14), 2109–2123.

Chapel, D.G., Mariz, C.L., 1999. Recovery of CO_2 from flue gases: commercial trends. In: Canadian Society of Chemical Engineers Annual Meeting, Saskatoon, Saskatchewan, Canada, October 4–6.

Chiesa, P., Lozza, G., Mazzocchi, L., 2005. Using hydrogen as gas turbine fuel. Journal of Engineering for Gas Turbines and Power 127 (1), 73–80.

Consonni, S., Viganò, F., 2005. Decarbonized hydrogen and electricity from natural gas. International Journal of Hydrogen Energy 30 (7), 701–718.

Corradetti, A., Desideri, U., 2005. Analysis of gas-steam combined cycles with natural gas reforming and CO_2 capture. Journal of Engineering for Gas Turbines and Power 127 (3), 545–552.

Ertesvåg, I.S., Kvamsdal, H.M., Bolland, O., 2005. Exergy analysis of a gas-turbine combined-cycle power plant with precombustion CO_2 capture. Energy 30 (1), 5–39.

Grabke, H.J., Spiegel, M., 2003. Occurrence of metal dusting—referring to failure cases. Materials and Corrosion 54 (10), 799–804.

Griffin, T., Sundkvist, S.G., Åsen, K., Bruun, T., 2005. Advanced zero emissions gas turbine power plant. Journal of Engineering for Gas Turbines and Power 127 (1), 81–85.

Haag, J.C., Hildebrandt, A., Hönen, H., Assadi, M., Kneer, R., 2007. Turbomachinery simulation in design point and part-load operation for advanced CO_2 capture power plant cycles. Proceedings of the ASME Turbo Expo, vol. 3. American Society of Mechanical Engineers, New York, NY, United States, pp. 239–250.

Incropera, F.P., DeWitt, D.P., 1990. Fundamentals of heat and mass transfer, 3rd ed. John Wiley & Sons, Inc., p. 422.

International, Energy Agency, 2006. World Energy Outlook.

Ishida, M., Jin, H., 1994. A new advanced power-generation system using chemical-looping combustion. Energy 19 (4), 415–422.

Jericha, H., Göttlich, E., Sanz, W., Heitmeir, F., 2004. Design optimization of the Graz cycle prototype plant. Journal of Engineering for Gas Turbines and Power 126 (4), 733–740.

Kehlhofer, R.H., Warner, J., Nielsen, H., Bachmann, R., 1999. Combined-Cycle Gas & Steam Turbine Power Plants, 2nd ed. PennWell Publishing Company.

Knudsen, J.N., Vilhelmsen, P.J., Biede, O., Jensen, J.N., 2006. Castor 1 t/h CO_2 absorption pilot plant at the Elsam Kraft A/S Esbjerg power plant—first year operation experience. 8th International Conference on Greenhouse Gas Control Technologies. Trondheim, Norway, June 19–22.

Kvamsdal, H.M., Jordal, K., Bolland, O., 2007. A quantitative comparison of gas turbine cycles with CO_2 capture. Energy 32 (1), 10–24.

LeThiez, P., Mosditchian, G., Torp, T., Feron, P., Ritsema, I., Zweigel, P., Lindeberg, E., 2004. CASTOR: from pie in the sky to commercial reality. Modern Power Systems 24 (7), 19–20.

Lozza, G., Chiesa, P., 2002a. Natural gas decarbonization to reduce CO_2 emission from combined cycles—part I: partial oxidation. Journal of Engineering for Gas Turbines and Power 124 (1), 82–88.

Lozza, G., Chiesa, P., 2002b. Natural gas decarbonization to reduce CO_2 emission from combined cycles—part II: steam-methane reforming. Journal of Engineering for Gas Turbines and Power 124 (1), 89–95.

Mathieu, P., Nihart, R., 1999. Zero-emission MATIANT cycle. Journal of Engineering for Gas Turbines and Power 121 (1), 116–120.

Moliere, M., 2005. Expanding fuel flexibility of gas turbines. In: Proc. Inst. Mech. Eng. part A: J. Power Energy (UK). Mech. Eng. Publications, vol. 219, Brussels, Belgium, pp. 109–119.

Möller, B.F., Genrup, M., Assadi, M., 2007. On the off-design of a natural gas-fired combined cycle with CO_2 capture. Energy 32 (4), 353–359.

Moulijn, J.A., Makkee, M., Diepen, A.v., 2007. Chemical Process Technology. John Wiley & Sons Ltd., pp. 158–159.

Naqvi, R., Wolf, J., Bolland, O., 2007. Part-load analysis of a chemical looping combustion (CLC) combined cycle with CO_2 capture. Energy 32 (4), 360–370.

Richter, H.J., Knoche, K.F., 1983. Reversibility of combustion processes. In: Gaggioli, R.A. (Ed.), A.C.S. Symposium Series 235. Washington, DC, USA, 71–85.

Shilling, N.Z., Jones, R.M., 2003. The impact of fuel flexible gas turbine control systems on integrated gasification combined cycle performance. In: Proceedings of the ASME Turbo Expo. American Society of Mechanical Engineers, vol. 1, New York, NY, United States, pp. 259–265.

Tomczak, H.-J., Benelli, G., Carrai, L., Cecchini, D., 2002. Investigation of a gas turbine combustion system fired with mixtures of natural gas and hydrogen. IFRF Combustion Journal.

van Loo, S., van Elk, E.P., Versteeg, G.F., 2007. The removal of carbon dioxide with activated solutions of methyl-diethanol-amine. Journal of Petroleum Science and Engineering 55 (1–2), 135–145.

Wagner, W., Cooper, J.R., Dittmann, A., Kijima, J., Kretzschmar, H.J., Kruse, A., Mares, R., Oguchi, K., Sato, H., Stöcker, I., Šifner, O., Takaishi, Y., Tanishita, I., Trübenbach, J., Willkommen, T., 2000. The IAPWS industrial formulation 1997 for the thermodynamic properties of water and steam. Journal of Engineering for Gas Turbines and Power 122 (1), 150–180.

Wilson, M., Tontiwachwuthikul, P., Chakma, A., Idem, R., Veawab, A., Aroonwilas, A., Gelowitz, D., Barrie, J., Mariz, C., 2004. Test results from a CO_2 extraction pilot plant at Boundary Dam coal-fired power station. Energy 29 (9–10), 1259–1267.

Zhang, X., Wang, J., Zhang, C.-f., Yang, Y.-h., Xu, J.-j., 2003. Absorption rate into a MDEA aqueous solution blended with piperazine under a high CO_2 partial pressure. Industrial and Engineering Chemistry Research 42 (1), 118–122.

Paper II

Nord, L.O., Anantharaman, R., Rausand, M., Bolland, O., 2009. A qualitative reliability and operability analysis of an integrated reforming combined cycle plant with CO_2 capture. International Journal of Greenhouse Gas Control 3 (4), 411–421.

International Journal of Greenhouse Gas Control 3 (2009) 411–421

Contents lists available at ScienceDirect

International Journal of Greenhouse Gas Control

journal homepage: www.elsevier.com/locate/ijggc

A qualitative reliability and operability analysis of an integrated reforming combined cycle plant with CO_2 capture

Lars Olof Nord [a,*], Rahul Anantharaman [a], Marvin Rausand [b], Olav Bolland [a]

[a] Department of Energy and Process Engineering, Norwegian University of Science and Technology, NO-7491 Trondheim, Norway
[b] Department of Production and Quality Engineering, Norwegian University of Science and Technology, NO-7491 Trondheim, Norway

ARTICLE INFO

Article history:
Received 11 November 2008
Received in revised form 5 February 2009
Accepted 7 February 2009
Available online 17 March 2009

Keywords:
CO_2 capture
Pre-combustion
Reliability
FMECA
Operability
Control degrees of freedom

ABSTRACT

Most of the current CO_2 capture technologies are associated with large energy penalties that reduce their economic viability. Efficiency has therefore become the most important issue when designing and selecting power plants with CO_2 capture. Other aspects, like reliability and operability, have been given less importance, if any at all, in the literature.

This article deals with qualitative reliability and operability analyses of an integrated reforming combined cycle concept. The plant reforms natural gas into a syngas, the carbon is separated out as CO_2 after a water-gas shift section, and the hydrogen-rich fuel is used for a gas turbine. The qualitative reliability analysis in the article consists of a functional analysis followed by a failure mode, effects, and criticality analysis (FMECA). The operability analysis introduces the comparative complexity indicator (CCI) concept.

Functional analysis and FMECA are important steps in a system reliability analysis, as they can serve as a platform and basis for further analysis. Also, the results from the FMECA can be interesting for determining how the failures propagate through the system and their effects on the operation of the process. The CCI is a helpful tool in choosing the level of integration and to investigate whether or not to include a certain process feature. Incorporating the analytical approach presented in the article during the design stage of a plant can be advantageous for the overall plant performance.

1. Introduction

Capturing the CO_2 from fossil fueled power plants can be part of an overall mitigation strategy to reduce the rise in atmospheric temperature. There are several approaches for capturing CO_2 from power generation. One is pre-combustion capture, where the fossil fuel is decarbonized to produce a syngas. The carbon, as CO_2, is separated out before the combustion takes place. For coal, one could implement pre-combustion CO_2 capture in the integrated gasification combined cycle (IGCC). IGCC plants exist, but none of them employs CO_2 capture. There are, however, a number of IGCC plants with CO_2 capture in the planning phase (Scottish Centre for Carbon Storage, 2009). For natural gas pre-combustion capture, the integrated reforming combined cycle (IRCC) that reforms natural gas into a hydrogen-rich fuel (Andersen et al., 2000), could be attractive. This technology has yet to be implemented in practice. The gas turbines in an IGCC or IRCC plant would fire a hydrogen-rich fuel.

The IGCC cycle has been studied extensively in terms of thermodynamical analyses to arrive at a cycle efficiency, and also economical analyses (e.g., Bohm et al., 2007; Descamps et al., 2008). To a lesser extent, aspects such as reliability, availability, and maintainability (RAM) have been studied for the IGCC cycle (Higman et al., 2006). Limited literature is available on reliability analyses of pre-combustion natural gas cycles. However, as large-scale implementation of CO_2 capture from power plants draws nearer, there will likely be more focus on areas such as RAM and operability.

A main issue related to pre-combustion techniques is that the plant becomes more complex with the significant integration between the power cycle and the gasification (for the IGCC case) or reforming (for the IRCC case) process. In addition, some of the technology is less mature than for a pulverized coal plant or for a natural gas combined cycle (NGCC) plant. The gas turbine (GT) technology is, for example, much more mature for natural gas firing than for firing a hydrogen-rich fuel. Chiesa et al. (2005) address issues related to using hydrogen as fuel for GTs. Also, a GT designed for an IGCC or IRCC plant typically needs to be more fuel flexible, which requires special attention to the burner design (Bonzani and Gobbo, 2007) and the control system (Shilling and Jones, 2003). The less-mature technology and the integration

* Corresponding author.
E-mail address: lars.nord@ntnu.no (L.O. Nord).

1750-5836/$ – see front matter © 2009 Elsevier B.V. All rights reserved.
doi:10.1016/j.ijggc.2009.02.004

present in IGCC plants are some of the reasons for the initially low availability of such plants (Higman et al., 2006; Beér, 2007). However, the availability of IGCC plants have steadily been improving since first introduced to the market.

In the RAM field, more literature is found if one looks for analyses of power plants in general and do not limit oneself to CO_2 capture plants. Examples of RAM analyses in the literature include Eti et al. (2007) and ? Aström et al. (2007). Another related area is reliability analysis of chemical systems. A thorough literature review related to chemical system reliability is given by Dhillon and Rayapati (1988). An international standard for production assurance and reliability management has recently been published (ISO 20815, 2008). In this standard, the term "production assurance" is used with the same meaning as operability in this article.

Failure modes, effects, and criticality analysis (FMECA) is a widely used qualitative method for reliability analysis (e.g., see Rausand and Høyland, 2004; IEC 60812, 2006). Teng and Ho (1996) discuss the use of FMECA for product design and process control. Teoh and Case (2004) describe, among other topics, the connection between system functional diagrams and FMECA. FMECA can be used to identify critical areas during the design stage of the system. When the criticality of failures is not investigated, the FMECA is sometimes called failure mode and effect analysis (FMEA).

The complexity and efficiency of a process plant normally increase with the degree of integration. While the increase in efficiency is a desired result, the increased complexity can give rise to operability and risk issues (e.g., see Perrow, 1999). The degree of integration in a process plant should therefore be determined based on a trade-off between efficiency and complexity. Operability is dependent on plant design and efforts have been made to incorporate process operability and control at an early stage of the design process (Barton et al., 1991; Blanco and Bandoni, 2003). The procedures presented in literature are computationally intensive and provide a level of rigor not required for the purposes of this work. A new index called the comparative complexity indicator (CCI) presented here is a parameter for comparing complexity of processes that provides a simple guide to the engineer on the extent of integration. As the name suggests, this indicator is useful only when comparing two processes and the absolute value of the indicator for a single process has no significance by itself.

The main objectives of this article are: (i) to illustrate and discuss the use of qualitative reliability and operability analyses in the field of CO_2 capture as a first step in developing a methodology for the design of a power plant with pre-combustion CO_2 capture, and (ii) to introduce a new concept, the comparative complexity indicator, as a tool for choosing the level of process integration and to gauge the complexity of a CO_2 capture plant.

The remainder of the article is divided into the following sections: Section 2 describes the process with functional descriptions of the building blocks. Section 3 describes the details of the methodologies used in the article. The results are shown and analyzed in Section 4, and concluding remarks are given in Section 5.

2. Functional description of process

A functional diagram of the cycle studied is shown in Fig. 1. The purpose of the plant is to generate fossil fueled power with low CO_2 emissions. The process has a defined system boundary as shown in Fig. 1. Inputs to the system include natural gas, ambient air, make-up water, and cooling water. Outputs across the system

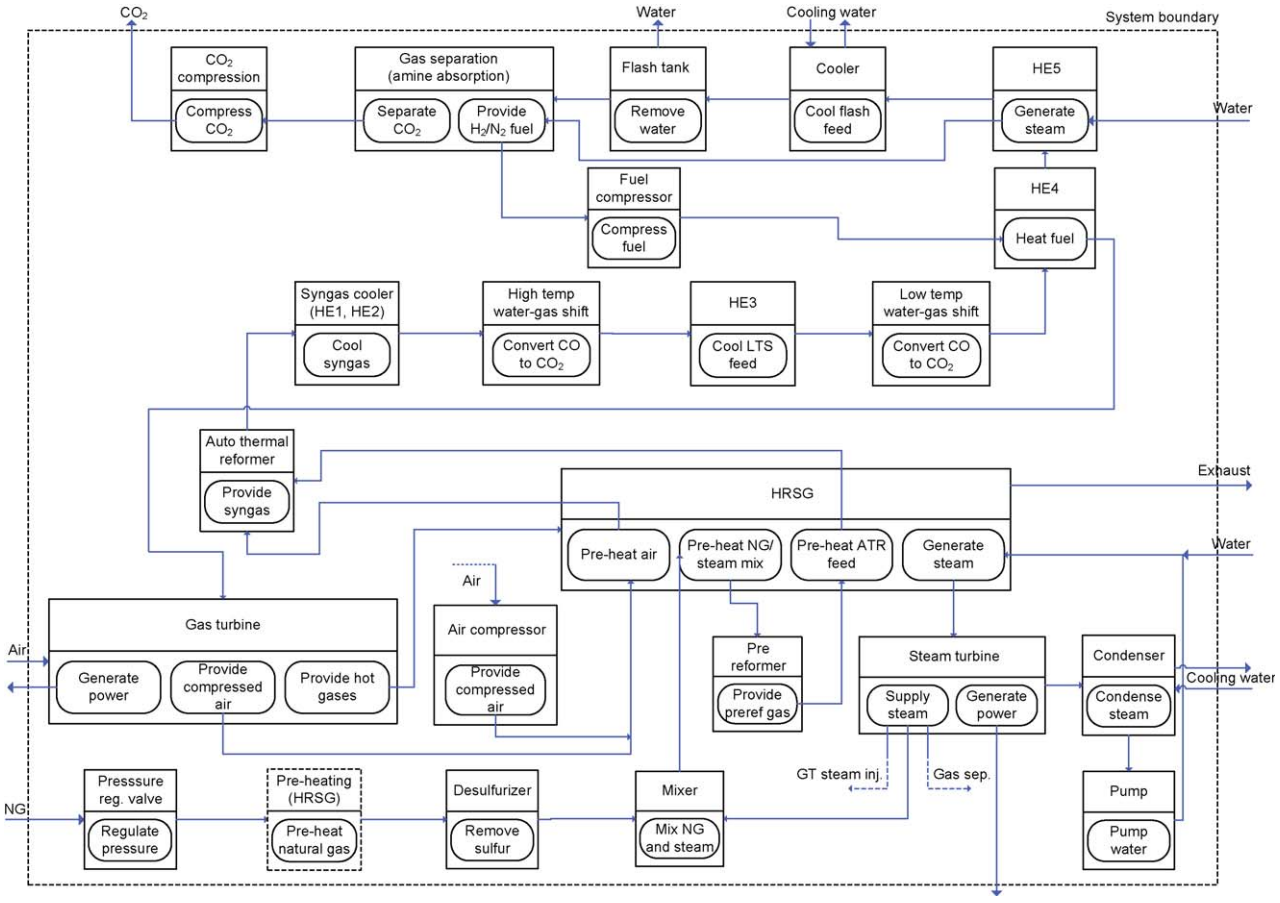

Fig. 1. Functional block diagram of an integrated reforming combined cycle plant.

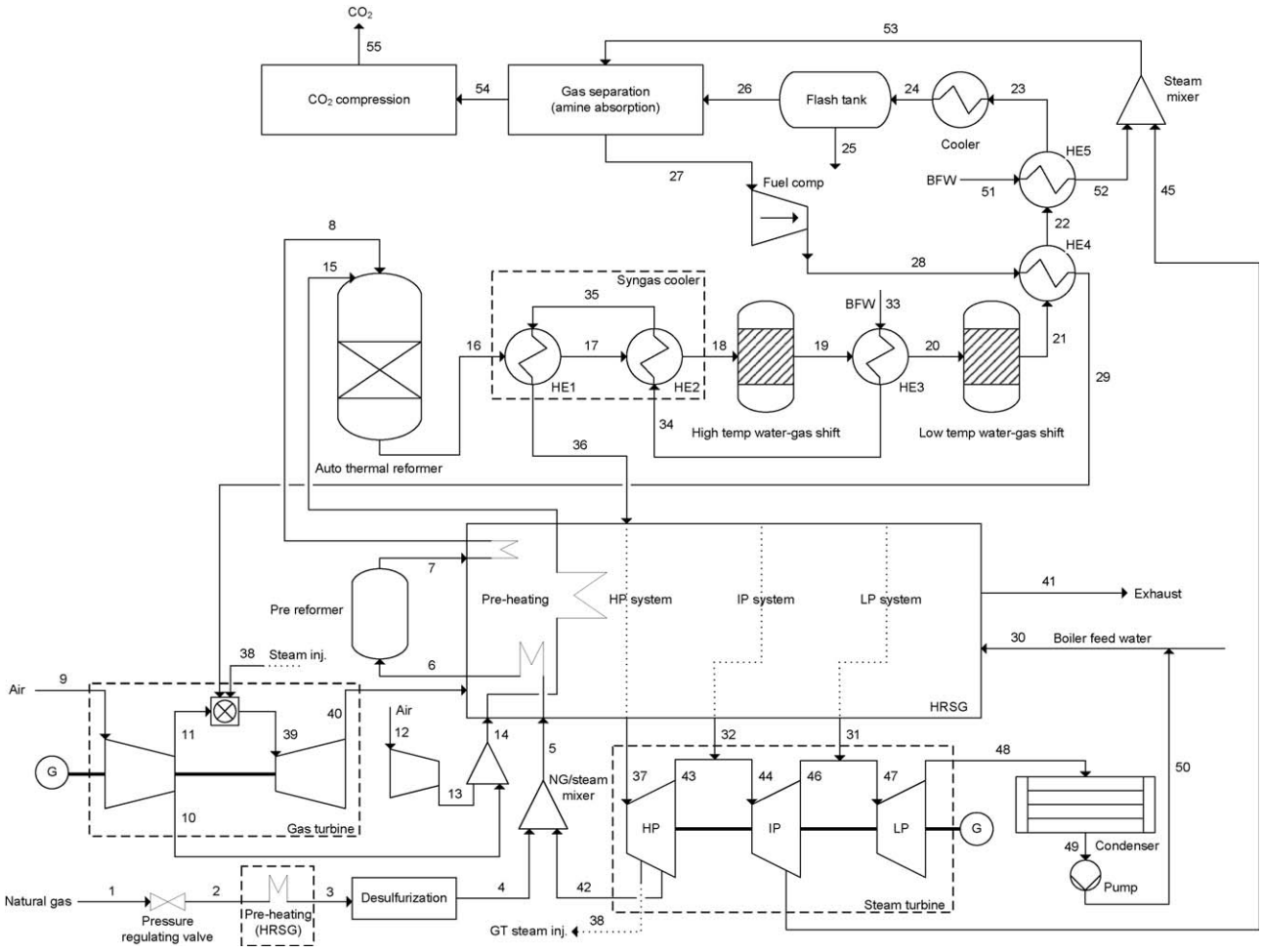

Fig. 2. IRCC process flow sheet.

boundary include compressed CO_2, water that has been separated out, cooling water, exhaust from the heat recovery steam generator (HRSG) that originated in the gas turbine exhaust, as well as power generated in the generator connected to the power train. In Fig. 1 the generator is incorporated into the gas turbine and steam turbine blocks.

In addition to the functional diagram in Fig. 1, a process flow sheet of the system is shown in Fig. 2. This representation of the system gives further insight and will prove helpful in the operability analysis.

2.1. Description of system inputs and outputs

The system inputs and outputs crossing the system boundary in Fig. 1 are described below.

Table 1
Natural gas composition in model.

Component name	Chemical formula	Unit	Value
Methane	CH_4	vol%	79.84
Ethane	C_2H_6	vol%	9.69
Propane	C_3H_8	vol%	4.45
i-Butane	C_4H_{10}	vol%	0.73
n-Butane	C_4H_{10}	vol%	1.23
i-Pentane	C_5H_{12}	vol%	0.21
n-Pentane	C_5H_{12}	vol%	0.20
Hexane	C_6H_{14}	vol%	0.21
Carbon dioxide	CO_2	vol%	2.92
Nitrogen	N_2	vol%	0.51
Hydrogen sulfide	H_2S	ppmvd	5

2.1.1. Natural gas

The supplied natural gas has an assumed pressure of 3.1 MPa and a temperature of 16 °C with a mass flow of 19 kg/s. The stream composition is given in Table 1.

2.1.2. Ambient air

The ambient air is assumed at 0.1013 MPa and 15 °C with 60% relative humidity and a total mass flow (air to gas turbine and to air compressor) of 648 kg/s. The air composition is given in Table 2.

2.1.3. Exhaust

The exhaust originating from the gas turbine exhaust, passing through the HRSG, and exiting through the stack has a temperature of about 90 °C and a pressure of 0.1013 MPa with a mass flow of 650 kg/s.

2.1.4. Water

Make-up water has an inlet temperature of 49 °C and a pressure of 0.19 MPa.

Table 2
Ambient air composition in model.

Component name	Chemical formula	Unit	Value
Oxygen	O_2	vol%	20.74
Nitrogen	N_2	vol%	77.30
Argon	Ar	vol%	0.92
Carbon dioxide	CO_2	vol%	0.03
Water	H_2O	vol%	1.01

2.1.5. Cooling water

The incoming cooling water for the condenser and cooler has an assumed temperature of 15 °C with a temperature increase in the heat exchangers of 10 K. Direct cooling by sea water is assumed.

2.1.6. CO_2

The compressed CO_2 stream has above 99 vol% CO_2 and a pressure of 11.0 MPa with a temperature of about 41 °C. The mass flow is 47 kg/s.

2.1.7. Power

The net power output from the plant is approximately 362 MW.

2.2. Functionality and description of equipment

The functional blocks in Fig. 1 are described below.

2.2.1. Pressure regulating valve

Function: To reduce the natural gas pressure from a delivery pressure of 3.1 MPa to approximately 1.9 MPa.

The pressure is set in order to match the compressed air pressure at the entrance of the auto thermal reformer (ATR).

2.2.2. Desulfurizer

Function: To reduce the H_2S content in the natural gas to 2 ppmvd.

Sulfur removal is necessary to protect the catalysts in the reforming and water-gas shift reactors. Because of the low sulfur content in the selected natural gas composition, 5 ppmvd H_2S, a ZnO desulfurizer is selected. The sulfur is removed by flowing of the natural gas through a bed of ZnO granules according to the reaction

$$H_2S + ZnO \rightarrow H_2O + ZnS \quad (1)$$

2.2.3. Mixer

Function: To mix the desulfurized natural gas with steam extracted from the steam turbine.

The steam to carbon ratio is set to 1.5 on a molar basis.

2.2.4. Gas turbine

Function: To generate power; to provide compressed air to the ATR; to provide hot flue gases to the HRSG.

The power cycle consists of a General Electric (GE) 9FA H_2-fired gas turbine (GT). The fuel fed to the GT combustor in principle consists of a mixture of H_2 and N_2. Because of the air-blown ATR, the water-gas shift reactors and the CO_2 capture processes, the fuel consists of approximately 50 vol% hydrogen. This enables use of available IGCC-type diffusion combustors (Todd et al., 2000; Shilling and Jones, 2003). The nitrogen acts as a fuel diluent. For further NO_x control, steam is injected into the flame. From the gas separation stage the fuel mix is passed on to the gas turbine via a fuel compressor. The GT turbine inlet temperature has been reduced because of the high steam content in the turbine. The hydrogen fuel together with the injected steam lead to an H_2O content entering the turbine of about 18.2 vol%. This leads to a higher heat transfer rate to the blades compared to a natural gas fired turbine. As a result, the metal temperature of the turbine blades is higher for the same turbine inlet temperature as in a conventional gas turbine. To obtain similar life of the turbine parts, the turbine inlet temperature reduction is necessary. Chiesa et al. (2005) report TIT decreases of 10–34 K for hydrogen combustion with nitrogen or steam diluent (VGV operation cases). As a model assumption, a TIT reduction of 30 K has been assumed for this work. In addition to running the GT on a hydrogen-rich fuel, the idea is to be able to operate on natural gas as a back-up fuel if the pre-combustion process is shut-down. This requires fuel flexibility for the combustor system (Shilling and Jones, 2003; Bonzani and Gobbo, 2007). In addition, start-up of the GT would be with natural gas fuel. It is also possible to run with a mixture of natural gas and the hydrogen-rich fuel. The gas turbine exhaust stream passes through the HRSG for pre-heating of the process streams and steam generation before emitted to the atmosphere through the stack.

2.2.5. Air compressor

Function: To provide compressed air to the ATR.

The external compressor is introduced in order to better utilize the operation of the gas turbine. If too much air is removed prior to the combustion chamber in the gas turbine, the effect on the performance and temperature profile can be negative.

2.2.6. Heat recovery steam generator

Function: To pre-heat the compressed air, the natural gas/steam mixture, and the pre-reformed ATR feed; to generate steam.

A triple pressure steam cycle was selected. The HRSG includes pre-heating for the various process streams. The pre-heated streams include the NG/steam feed to the pre-reformer, the ATR feed stream coming from the pre-reformer, and air extracted from the compressor discharge stream of the gas turbine combined with an additional compressor air stream before supplied to the ATR. The steam cycle is designed for pressure levels of approximately 8.3/1.0/0.3 MPa for the high, intermediate, and low pressure (HP/IP/LP) systems respectively. The pre-heating makes the HRSG design more complex and a lot of heat is removed from the gas stream at the hot part of the HRSG due to the high temperature requirements of some of the process streams. Note that the pre-heating is not entirely in the hot end of the HRSG but instead intermixed with the low, intermediate, and high-pressure sections. Equipment such as pumps for the different pressure levels, drums, valves, and so on, are not shown in the functional diagram.

2.2.7. Steam turbine

Function: To supply steam for the reforming process, the gas turbine, and the gas separation sub-system; to generate power.

The steam turbine (ST) has extractions for the GT steam injection, the reforming process steam, and for the reboiler in the amine absorption system.

2.2.8. Condenser

Function: To condense the steam.

After exiting the last low pressure turbine stage the steam is condensed in the condenser.

2.2.9. Pump

Function: To pump the water up to feed water pressure.

2.2.10. Pre-reformer

Function: To convert the higher hydrocarbons into hydrogen and carbon monoxide.

Adiabatic pre-reforming of hydrocarbons is described by Vannby and Winter Madsen (1992). In the pre-reforming reactor the hydrocarbons higher than methane are converted to protect against coking in the primary reformer according to the reactions

$$C_xH_y + xH_2O_{(g)} \rightarrow xCO + \left(x + \frac{y}{2}\right)H_2 \quad -\Delta H^0_{298} < 0\,\text{kJ/mol} \quad (2)$$

$$CO + 3H_2 \rightleftharpoons CH_4 + H_2O_{(g)} \quad -\Delta H^0_{298} = 206\,\text{kJ/mol} \quad (3)$$

Also, the exothermic water-gas shift reaction (4) converting the CO into CO_2 takes place in the pre-reforming reactor.

$$CO + H_2O_{(g)} \rightleftharpoons CO_2 + H_2 \quad -\Delta H^0_{298} = 41\,\text{kJ/mol} \quad (4)$$

2.2.11. Auto thermal reformer

Function: To reform the stream from the pre-reformer into syngas.

Auto thermal reforming is described by Christensen and Primdahl (1994), Dybkjær (1995), Christensen et al. (1998). In the ATR the exothermic reaction (5) provide heat to the endothermic reaction (6).

$$CH_4 + \tfrac{1}{2}O_2 \rightarrow CO + 2H_2 \quad -\Delta H^0_{298} = 36\,\text{kJ/mol} \tag{5}$$

$$CH_4 + H_2O_{(g)} \rightleftharpoons CO + 3H_2 \quad -\Delta H^0_{298} = -206\,\text{kJ/mol} \tag{6}$$

As in the pre-reformer, the water-gas shift reaction (4) converts some of the CO into CO_2.

2.2.12. Syngas cooler

Function: To cool the syngas supplied by the ATR.

The syngas is cooled in the syngas cooler before entering the water-gas shift reactors. As a secondary function the hot stream supplied by the ATR is generating high-pressure steam in the syngas cooler. This steam is then supplied to the HP superheaters in the HRSG. The reason for using the syngas cooler as an evaporator rather than as a superheater is due to the risk of metal dusting. Metal dusting is further discussed in Section 3.1.2.

2.2.13. Water-gas shift reactors

Function: To convert CO to CO_2.

The rest of the CO is converted to CO_2 according to reaction (4). The reasons behind dividing the water-gas shift reaction into a high temperature reactor and a low temperature one (HTS and LTS) are due to conversion rate and catalysts. To get a higher degree of conversion of the CO to CO_2, two reactors are favorable compared to a one-reactor setup. Also, there is a need for a more active catalyst at the lower region of the temperature range (Moulijn et al., 2007). It can therefore make sense to use a standard catalyst at the higher temperature range and then have a separate reactor with a more active catalyst for the low end temperature.

2.2.14. Heat exchanger 3

Function: To cool the stream from the HTS going to the LTS.

HE3 is also, together with the syngas cooler, producing high-pressure saturated steam to be added to the high-pressure superheater in the HRSG.

2.2.15. Heat exchanger 4

Function: To pre-heat the hydrogen-rich fuel for the gas turbine.

2.2.16. Heat exchanger 5

Function: To cool down the gas for the gas separation process.

Heat exchanger 5 (HE5) is also producing some of the steam necessary for the reboiler in the amine absorption process.

2.2.17. Cooler and flash tank

Function: To cool down the stream from HE5 and remove the water before the gas separation stage.

2.2.18. Gas separation (amine absorption)

Function: To separate out CO_2; to provide H_2-rich fuel.

In this model the gas separation stage is using the chemical absorbent activated MDEA (van Loo et al., 2007).

2.2.19. CO_2 compression

Function: To compress CO_2 up to delivery pressure.

The CO_2 is passed on to the compression section where the gas is compressed in the four compressor/intercooler stages and excess water is removed. To achieve the exit pressure of 11.0 MPa a pump is used at the end of the compression train.

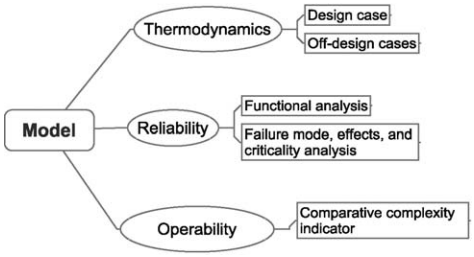

Fig. 3. Analytical approach to process model study.

3. Methodology

The plant model in Figs. 1 and 2 was analyzed from several angles, as illustrated in Fig. 3, in order to determine reliability and operability aspects of the plant design. As basis for the reliability analysis the process was first thermodynamically analyzed. This is important to be able to define the functional requirements and reveal the part load behavior of the plant. Some of the failure modes may affect the ability of the plant to operate at full load and the reliability of the plant will depend on the part loads. Even though the aim is to operate the plant at full load, it is also necessary to be able to operate the plant at part load. The thermodynamic analysis is not documented in this article, but indicates that part load operation down to 60% relative gas turbine load is possible. The relative load is here defined as the actual load of the GT divided by the full GT load at actual ambient conditions.

The reliability analysis was carried out as a functional analysis followed by an FMECA. The operability analysis is based on the new CCI concept. In the following sections, the reliability and operability analyses are described.

3.1. Reliability analysis

The first step of the reliability analysis was a detailed functional analysis that was carried out to reveal and define all the required functions of the plant elements. For each function, the associated performance criteria were determined. A thorough understanding of all required functions and their associated performance criteria is a prerequisite for the FMECA.

The FMECA involves analyzing all the potential failure modes of the system elements (components and subsystems) and identify the causes and effects of these failure modes. The FMECA is also used to determine how failures may propagate through the system, and to reveal the failure effects on the operation of the plant. Another purpose of the FMECA was to identify the most critical components/integration points for further and more detailed analyses at later stages of the project.

3.1.1. Functional analysis

The functional analysis was carried out at the equipment level of the system, as shown in Fig. 4. The different subsystems and their equipments are listed in Table 3 together with the functional requirements (e.g., see Murthy et al., 2008). On system (plant) level the functional requirements are: plant power output $\geq$300 MW (ISO); CO_2 capture rate $\geq$90%. The CO_2 capture rate is defined as the fraction of the formed CO_2 that is captured. The functional analysis that is documented in this article only includes the essential functions, meaning that auxiliary functions, protective functions, and so forth, are not covered.

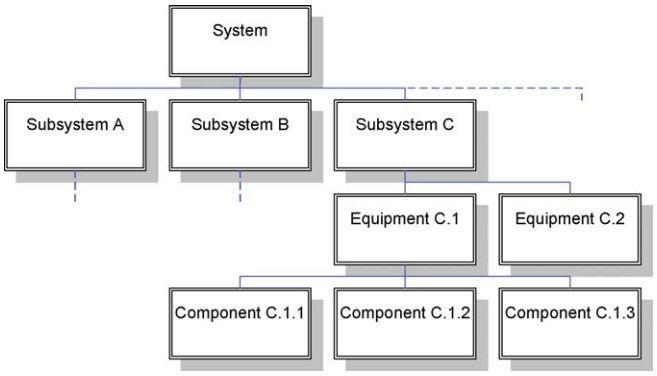

Fig. 4. Functional levels of a system.

3.1.2. FMECA

The FMECA approach that was selected for this project is illustrated in Fig. 5. In this approach, a risk, or criticality, number is assigned to each and every failure mode as a risk priority number (RPN). The RPN of a failure mode is calculated based on an evaluation of the factors: detection, failure rate, and severity, of a failure mode. Each of these three factors are typically assigned numbers ranging from 1 to 10. There are several approaches for assigning these numbers, one is described by Bevilacqua et al. (2000) where a Monte Carlo simulation approach is used for testing the weights assigned to the RPNs. In this article, the normal 1–10 scale was modified to the more limited 1–3 scale. The reason for this modification was to more readily being able to identify the numbers the RPN are based upon.

The detection scale was defined as: 1 = highly detectable, almost certain detection; 2 = moderately detectable; and 3 = non-detectable.

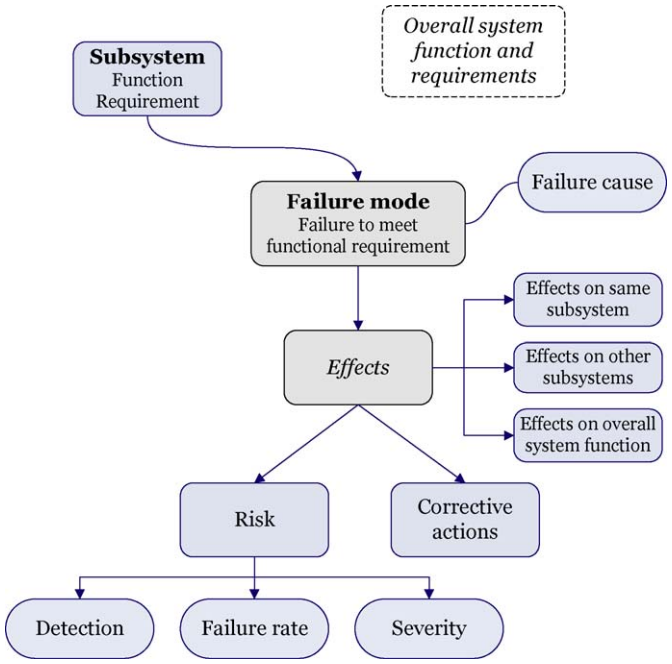

Fig. 5. Graphical representation of the FMECA approach.

The failure rate scale was defined as: 1 = failure unlikely; 2 = occasional failure; and 3 = frequent failure.

The severity scale was defined as: 1 = no, or very small effect; 2 = plant operating at part load or bypassing CO_2 capture; and 3 = plant shutdown.

As a basis of the analysis, it is assumed that the plant is operating at full load when a failure occurs. Furthermore, potential human errors are not considered in the analysis.

Table 3
Functional requirements of the system. Subscript numbering in accordance with Fig. 2 stream numbering.

Subsystem	Equipment	Function	Functional requirement
NG processing	Pressure regulating valve	Decrease line pressure down to system pressure	1.8 MPa $\leq p_2 \leq$ 2.0 MPa
NG processing	Desulfurizer	Remove sulfur	Exhaust $H_2S \leq 2$ ppmv
Power cycle	Gas turbine	Generate power	$P_{rel,GT} \geq 90\%$
Power cycle	Gas turbine	Provide air	$m_{10} \geq 67.5$ kg/s, $T_{10} \geq 350\,^{\circ}C$
Power cycle	Gas turbine	Provide hot gases	$T_{40} \geq 560\,^{\circ}C$
Power cycle	Steam turbine	Generate power	$P_{ST} \geq 125$ MW
Power cycle	Steam turbine	Supply steam to pre-reformer	$S/C = 1.5 \pm 0.1$
Power cycle	Steam turbine	Supply steam to reboiler in amine system	$p_{45} \geq 0.32$ MPa. Heat flow provided ≥ 70 MJ/s
Power cycle	Generator	Generate power	Power output ≥ 300 MW (ISO)
Pre-heating	NG pre-heater	Pre-heat NG	$350\,^{\circ}C \leq T_3 \leq 425\,^{\circ}C$
Pre-heating	NG/steam pre-heater	Pre-heat NG/steam mix	$T_6 \geq 480\,^{\circ}C$
Pre-heating	Air pre-heater	Pre-heat air	$T_{15} \geq 450\,^{\circ}C$
Pre-heating	ATR feed pre-heater	Pre-heat ATR feed gas	$T_8 \geq 450\,^{\circ}C$
HRSG	LP	Generate LP steam	$m_{31} \geq 10$ kg/s
HRSG	IP	Generate IP steam	$m_{32} \geq 20$ kg/s
HRSG	HP	Generate HP steam	$m_{37} \geq 40$ kg/s
Reforming	Pre-reformer	Convert higher hydrocarbons. Provide preref gas	$T_6 - T_7 \geq 40$ K, $T_7 \geq 430\,^{\circ}C$
Reforming	ATR	Convert methane. Provide syngas	$900\,^{\circ}C \leq T_{16} \leq 1000\,^{\circ}C$
W-G shift	HTS	Convert CO to CO_2	$\Delta T \geq 75$ K
W-G shift	LTS	Convert CO to CO_2	$\Delta T \geq 30$ K
HX network	Syngas cooler (HE1, HE2)	Cool ATR product	$300\,^{\circ}C \leq T_{18} \leq 450\,^{\circ}C$
HX network	HE3	Cool LTS feed	$180\,^{\circ}C \leq T_{20} \leq 250\,^{\circ}C$
HX network	HE4	Heat fuel	$T_{29} \geq 180\,^{\circ}C$
HX network	HE5	Generate steam	$x_{52} = 1.0$
HX network	Cooler	Cool flash feed	$T_{24} \leq 30\,^{\circ}C$
HX network	Condenser	Condense steam	$p_{49} \leq 0.0044$ MPa
HX network	Condenser	Condense steam	$p_{50} \geq 0.18$ MPa
Pre-comb capture	Gas separation	Separate out CO_2	Remove $\geq 95\%$ CO_2
Compression	Air compressor	Compress air for ATR	$p_{13} = p_{10} \cdot m_{13} \rightarrow T_{16} = 950\,^{\circ}C$
Compression	CO_2 compression	Compress CO_2	$p_{55} \geq 10.0$ MPa
Compression	Fuel compressor	Compress fuel	$p_{28} \geq 1.8$ MPa

A failure mode is defined as a failure to meet a functional requirement of a specific equipment. Once a failure mode has been specified, the causes and effects of the failure need to be identified. Regarding failure effects, the effects on the same equipment where the failure occurred were first analyzed. Secondly, the effects on other equipment in the system were investigated, and finally, the overall system effects were identified. One example of failure causes and their effects is coking, or metal dusting, in the reactors and heat exchangers (Grabke and Wolf, 1986; Grabke et al., 1993). Coking in pre-reformers is investigated by Sperle et al. (2005). Several failure causes, including metal dusting in a heat exchanger for synthesis gas, are investigated by Grabke and Spiegel (2003). Catalyst degradation due to coking in reactors is analyzed by Rostrup-Nielsen (1997).

Some of the failure causes for the gas turbine were listed as a protective load shed (PLS) cause or a trip cause. A protective load shed is described as an automatic deload of the GT due to an abnormal situation such as an elevated temperature. A trip occurs when a more critical event takes place. The reason for listing a failure cause as a PLS or trip cause is because the reasons for the PLS or trip can be many.

The most common protective load shed causes are found to be:

- Thermo-acoustic instabilities
- Abnormal exhaust temperature
- Controls and instrument problems
- HRSG trip

The most common trip causes are found to be:

- Thermo-acoustic instabilities
- Flame monitor
- Abnormal exhaust temperature
- Controls and instrument problems
- Bearings (temperature, vibration)
- Manual trip

The detection rating was, for the most part, derived based on knowledge in instrumentation and controls. For example, an abnormal temperature or pressure change is easy to detect, whereas a change in a gas composition can be more difficult to sense. With the 1–3 scale, the numbers were fairly easy to assign. To determine the failure rate numbers, several data sources were consulted (OREDA, 2002; NERC, 2007). The severity ranking was established based on studying the effects of the various failure modes. The RPNs were computed by multiplying the detection, failure rate, and severity numbers, and must therefore range from 1 to 9.

3.2. Operability analysis

Main contributors to operability problems are (i) component and subsystem failures and (ii) system complexity and coupling between subsystems. The first aspect was discussed in the previous section.

The complexity of a plant and its control system is directly related to the number of manipulated variables. A *manipulated variable* is the variable that is changed, in a control strategy, to achieve a certain process condition. It is desirable that the complexity of a control system is as low as possible (Skogestad, 2004). The main aim is thus to have a system with a small number of manipulated variables for better operability.

As a qualitative measure of the complexity of a process we introduce the new *comparative complexity indicator*, as the number of variables that can be manipulated in a process while accounting for integration between different process areas.

The CCI is based on a well-established concept in control system design—the control degrees of freedom (CDOF), defined to be the number of manipulated variables that can be used in control loops. The CDOF of a process is therefore the number of process variables: temperatures, pressures, compositions, flow rates, or component flow rates, that can be set by the control system once the non-adjustable design variables, such as vessel dimensions, have been fixed.

It is important to distinguish between the CDOF and the design degrees of freedom, even tough the CDOF is the same as the design degree of freedom for some classes of processes (Luyben, 1996). If there are C components, then there are $(C + 2)$ *design* degrees of freedom. This implies that the designer has choice over feed stream composition, pressure, and temperature. This is true during the design of a process. In an actual control scenario, the only manipulation possible is to change the stream flow. Whatever may be the nature of the control loop (flow, level, pressure, temperature, or composition), ultimately the manipulated variable is the flow rate of a process stream.

3.2.1. Procedure for calculating control degrees of freedom

To determine the CDOF of a process is the most important step in evaluating the CCI. The procedure used in this article is adapted from Murthy Konda et al. (2006) and further expanded in Vasudevan et al. (2008). As mentioned above, the manipulated variables will always be process stream flows. The motivating question behind calculating CDOF is whether it is possible to manipulate all the process streams and, if not, what are the restrictions? This leads to:

- CDOF of a unit $\leq$ total number of streams associated with that unit, or
- CDOF of a unit + restraining number = total number of streams associated with that unit.

The *restraining number* is the number of streams that cannot be manipulated. Murthy Konda et al. (2006) and Vasudevan et al. (2008) list the restraining number of commonly used units in process plants. To find the CDOF for a process, the following formula is used:

$$\text{CDOF} = N_S - N_R \tag{7}$$

where N_S is the total number of streams in the process and N_R is the sum of restraining numbers for all units in the process.

A simple utility heater or cooler has a CDOF of 2 (Murthy Konda et al., 2006). A heat exchanger implies a more complex and tightly integrated process. In this analysis, a heat exchanger should therefore have a higher CDOF than the value of 2 proposed by Murthy Konda et al. (2006). In practice, many heat exchangers have by-pass streams that usually are not shown on process flow diagrams. The number of streams for a process/process heat exchanger would then be 6, rather than 4, leading to a CDOF of 4 (compared to 2). In this article, this is included in the procedure to calculate the CDOF of heat exchangers.

Fig. 6 shows a simple Westerberg process with ten process streams (including the energy stream). The restraining numbers for each of the units in the process are shown in Table 4.

The CDOF of the Westerberg process is $10 - 4 = 6$.

3.2.2. Evaluating the comparative complexity indicator

The CDOF does not sufficiently represent how tightly a plant is integrated and particularly, integration between different process areas. The CCI adds a level of realism to the CDOF procedure by considering the way the different process areas of a plant are integrated.

The procedure for evaluating the CCI is shown by the flow diagram in Fig. 7. The first step involves decomposing the plant

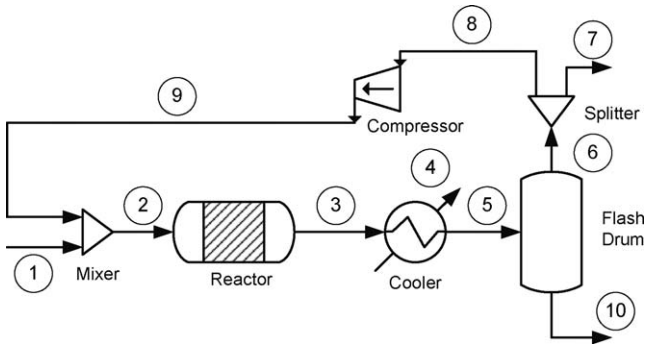

Fig. 6. Westerberg process

into *functional* process areas. For example, in the IRCC plant the reforming section is one process area and the CO_2 compression section another. The CDOF of each process area is then calculated as described in the previous section. If the flow between two process areas is a manipulated variable then an extra degree of freedom is added. This check is repeated for each stream between the different process areas in the plant. The CCI is then calculated as the sum of the CDOFs of the process areas and the "extra degrees of freedom". This means the CCI is an addition of the total number of CDOFs and the, between process areas, connecting streams that are manipulated variables.

The calculation of the CCI for different IRCC configurations, as well as, for an NGCC plant with and without post-combustion capture are presented in the next section.

4. Results and discussion

The documentation of the analysis and of the results of the FMECA is comprehensive. Therefore, only a part of the results is shown in this article. Table 5 includes the failure modes with an RPN greater than 6. As seen from the table, many of the high risk results are linked to the gas turbine. This is not unexpected. In a regular NGCC plant the gas turbine and its auxiliaries are also responsible for the largest part of the forced outages (NERC, 2007).

For an IRCC, there may be additional GT failures stemming from issues related to the supply of the hydrogen-rich fuel and because of the lower level of experience with hydrogen-fired GTs compared to NG-fired GTs.

One may criticize the risk priority rankings and argue that some of them should be changed. Certainly, if another person performed the FMECA, different results would arise, but the key results, such as what equipment is most critical in the plant, should be similar if performed by someone else.

For the operability analysis, the IRCC process can be decomposed into the following five process areas:

(1) Reforming area
(2) CO_2 capture area
(3) CO_2 compression area

Table 4
Restraining numbers for units in the Westerberg process.

Unit	Restraining no.
Mixer	1
Reactor	0
Cooler	1
Flash drum	0
Splitter	1
Compressor	1
Total	4

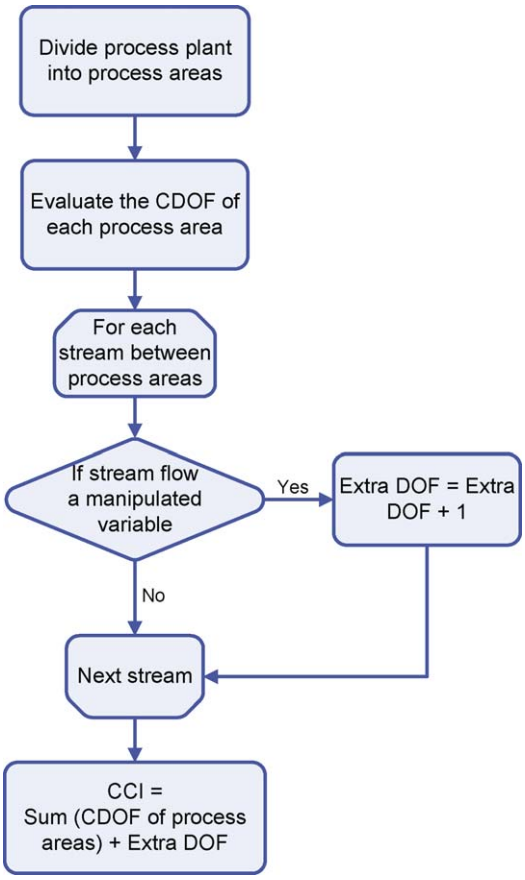

Fig. 7. Calculating the comparative complexity indicator (CCI) of a process.

(4) Gas turbine fuel preparation area
(5) Combined cycle power plant area

The CDOF of the five areas are calculated and shown in Table 6.

The total "extra degrees of freedom" in the system equals 3. Thus the comparative complexity indicator for the IRCC plant shown in Fig. 2 is 115. The overall efficiency of the process is 41.9%.

Process modifications will affect both efficiency and the CCI of the overall process. The subsequent paragraphs briefly analyse two process modifications with regard to the efficiency and CCI of the process and identify if the modification is favorable or not.

4.1. Process modification 1

Streams 33 and 51 are extracted from the deaerator (not shown in Fig. 2) at 105 °C (pre-heated in low-temperature economizer before entering the deaerator). The low temperature heat in stream 23 could be used to pre-heat the boiler feed water from 30 to 105 °C for HP and LP steam generation in the reforming process (rather than pre-heating in low-temperature economizer). The efficiency increase by including this modification is negligible, whereas the CCI of this modified process is 118. This implies this process modification is not favorable as the complexity of the process increases without any corresponding improvement to efficiency, the decision variable.

Thus for processes with the same efficiencies, the heuristic is to select the one with least CCI.

4.2. Process modification 2

If the LP steam generator HE5 in Fig. 2 were ignored, the cooling water requirement would increase and the stream extraction from

Table 5
Failure modes with a risk priority number greater than six. Subscript numbering in accordance with Fig. 2 stream numbering.

Subsystem	Equipment	Function	Functional requirement	Failure mode	Failure cause	Effects on same equipment	Effects on other equipment	Effects on overall system function	Detection (1–3)	Failure rate (1–3)	Severity (1–3)	Risk ($D \times F \times S$)
Power cycle	Gas turbine	Generate power	$P_{rel,GT} \geq 90\%$	$60\% \leq P_{rel,GT} < 90\%$	Fuel supply	Part load operation	Reduced steam production in HRSG. Reduced power output from steam turbine	Reduced plant load	2	2	2	8
Power cycle	Gas turbine	Provide hot gases	$T_{40} \geq 560\ ^\circ C$	$T_{40} < 560\ ^\circ C$	Fuel supply	Part load operation	Reduced steam production in HRSG. Reduced power output from steam turbine	Reduced plant load	2	2	2	8
Reforming	Pre-reformer	Convert higher hydrocarbons. Provide preref gas	$T_6 - T_7 \geq 40$ K, $T_7 \geq 430\ ^\circ C$	$T_6 - T_7 < 40$ K, $T_7 < 430\ ^\circ C$	Catalyst issue	Lower conversion rate	Higher hydrocarbons to ATR (coking)	Reduced plant load. Decreased CO_2 capture rate	2	2	2	8
Reforming	ATR	Convert methane. Provide syngas	$900\ ^\circ C \leq T_{16} \leq 1000\ ^\circ C$	T_{16} outside range	Catalyst issue	Lower conversion rate	Hydrocarbons to HTS	Reduced plant load. Decreased CO_2 capture rate	2	2	2	8
Reforming	ATR	Convert methane. Provide syngas	$900\ ^\circ C \leq T_{16} \leq 1000\ ^\circ C$	T_{16} outside range	Burner issue	Possibly lower temperature. Flame shape distortion → mechanical damage to reactor walls	Hydrocarbons to HTS. Lower temp to HE1	Reduced plant load. Decreased CO_2 capture rate	2	2	2	8
W-G shift	HTS	Convert CO to CO_2	$\Delta T \geq 75$ K	$\Delta T < 75$ K	Catalyst issue	Lower conversion rate	Higher CO content to LTS	Reduced plant load. Decreased CO_2 capture rate	2	2	2	8
W-G shift	LTS	Convert CO to CO_2	$\Delta T \geq 30$ K	$\Delta T < 30$ K	Catalyst issue	Lower conversion rate	CO content to gas separation stage	Reduced plant load. Decreased CO_2 capture rate	2	2	2	8
NG processing	Pressure regulating valve	Decrease supply pressure down to system pressure	1.8 MPa $\leq p_2 \leq$ 2.0 MPa	$p_2 > 2.0$ MPa	Valve malfunction	–	Shutdown of all subsystems	Plant shutdown	1	2	3	6
Power cycle	Gas turbine	Generate power	$P_{rel,GT} \geq 90\%$	$P_{rel,GT} < 60\%$	Trip cause	GT trip	Shutdown of all subsystems	Plant shutdown	1	2	3	6
Power cycle	Gas turbine	Generate power	$P_{rel,GT} \geq 90\%$	$P_{rel,GT} < 60\%$	Protective load shed cause	GT shutdown	Shutdown of all subsystems	Plant shutdown	1	2	3	6
Power cycle	Gas turbine	Generate power	$P_{rel,GT} \geq 90\%$	$P_{rel,GT} < 60\%$	Combustion problems	GT shutdown	Shutdown of all subsystems	Plant shutdown	1	2	3	6
Power cycle	Gas turbine	Generate power	$P_{rel,GT} \geq 90\%$	$P_{rel,GT} < 60\%$	NO_x emissions	GT shutdown	Shutdown of all subsystems	Plant shutdown	1	2	3	6
Power cycle	Gas turbine	Generate power	$P_{rel,GT} \geq 90\%$	$P_{rel,GT} < 60\%$	Other gas turbine problems	GT shutdown	Shutdown of all subsystems	Plant shutdown	2	1	3	6
Power cycle	Gas turbine	Provide air	$m_{10} \geq 67.5$ kg/s, $T_{10} \geq 350\ ^\circ C$	$m_{10} < 67.5$ kg/s, $T_{10} < 350\ ^\circ C$	Trip cause	GT trip	Shutdown of all subsystems	Plant shutdown	1	2	3	6
Power cycle	Gas turbine	Provide air	$m_{10} \geq 67.5$ kg/s, $T_{10} \geq 350\ ^\circ C$	$m_{10} < 67.5$ kg/s, $T_{10} < 350\ ^\circ C$	Protective load shed cause	GT shutdown	Shutdown of all subsystems	Plant shutdown	1	2	3	6
Power cycle	Gas turbine	Provide air	$m_{10} \geq 67.5$ kg/s, $T_{10} \geq 350\ ^\circ C$	$m_{10} < 67.5$ kg/s, $T_{10} < 350\ ^\circ C$	Combustion problems	GT shutdown	Shutdown of all subsystems	Plant shutdown	1	2	3	6
Power cycle	Gas turbine	Provide air	$m_{10} \geq 67.5$ kg/s, $T_{10} \geq 350\ ^\circ C$	$m_{10} < 67.5$ kg/s, $T_{10} < 350\ ^\circ C$	NO_x emissions	GT shutdown	Shutdown of all subsystems	Plant shutdown	1	2	3	6
Power cycle	Gas turbine	Provide air	$m_{10} \geq 67.5$ kg/s, $T_{10} \geq 350\ ^\circ C$	$m_{10} < 67.5$ kg/s, $T_{10} < 350\ ^\circ C$	Other gas turbine problems	GT shutdown	Shutdown of all subsystems	Plant shutdown	2	1	3	6
Power cycle	Gas turbine	Provide hot gases	$T_{40} \geq 560\ ^\circ C$	$T_{40} < 560\ ^\circ C$	Trip cause	GT trip	Shutdown of all subsystems	Plant shutdown	1	2	3	6
Power cycle	Gas turbine	Provide hot gases	$T_{40} \geq 560\ ^\circ C$	$T_{40} < 560\ ^\circ C$	Protective load shed cause	GT shutdown	Shutdown of all subsystems	Plant shutdown	1	2	3	6
Power cycle	Gas turbine	Provide hot gases	$T_{40} \geq 560\ ^\circ C$	$T_{40} < 560\ ^\circ C$	Combustion problems	GT shutdown	Shutdown of all subsystems	Plant shutdown	1	2	3	6
Power cycle	Gas turbine	Provide hot gases	$T_{40} \geq 560\ ^\circ C$	$T_{40} < 560\ ^\circ C$	NO_x emissions	GT shutdown	Shutdown of all subsystems	Plant shutdown	1	2	3	6
Power cycle	Gas turbine	Provide hot gases	$T_{40} \geq 560\ ^\circ C$	$T_{40} < 560\ ^\circ C$	Other gas turbine problems	GT shutdown	Shutdown of all subsystems	Plant shutdown	2	1	3	6

Table 6
CDOF evaluation for process areas in IRCC plant.

Area	Total streams	Restraining no.	CDOF
Reforming area	36	7	29
CO_2 capture area	24	9	15
CO_2 compression area	24	10	14
GT fuel preparation area	5	2	3
CCPP area	79	28	51
Total			112

the steam turbine to the CO_2 removal section would increase. This reduces the overall efficiency to 41.5%. The CCI for this modified process is 111. The efficiency drop of 0.4%-point is significant in the context of this process. Thus, even though the complexity of this option is less than the original design, the efficiency drop causes this process modification to be disregarded.

In processes where efficiency improvements are essential, increasing complexity is acceptable within limits. For example, a process modification causing the efficiency to increase by 0.5%-points while increasing the CCI by 15 can be deemed less favorable compared to a modification that causes an efficiency increase by 0.4%-point with a CCI increase of 7.

For reference, the CCI for a natural gas combined cycle power plant without CO_2 capture is 48. Process areas such as reforming, CO_2 capture, and CO_2 compression are not included in an NGCC plant without CO_2 capture. The CCI for a natural gas combined cycle power plant with post-combustion CO_2 capture is 82.

5. Conclusions

Functional analysis and FMECA are important steps in a system reliability analysis, as they can serve as a platform and basis for further analysis. Also, the results from the FMECA can be interesting in themselves. From the FMECA performed in this work, it is clear that the gas turbine is the most critical equipment in an IRCC plant. One of the reasons for this is the significant integration present. The gas turbine feeds air to the ATR, receives fuel from the pre-combustion process, and the steam turbine supplies steam to the GT combustor. This integration has an effect on the overall reliability of the system and shows up in the FMECA, not the least in the "Effects on other equipment" column in Table 5. In addition to the integration issues, the gas turbine technology is less mature for hydrogen fuels than for natural gas fuels. It should also be mentioned that even in a natural gas fired combined cycle plant the gas turbine is the most critical equipment. With all this said, the strong dominance of gas turbine failures in a list with the highest risk priority numbers such as in Table 5 is not unexpected. Operability analysis is another important tool during the design stage. The CCI is a helpful tool in choosing the level of integration and when investigating whether or not to include a certain process feature. Incorporating the analytical approach presented in the article and displayed in Fig. 3, during the design stage of a plant, can be advantageous for the overall plant performance.

Acknowledgements

This work was supported by the Norwegian Research Council and StatoilHydro. The authors are grateful for valuable comments received from the reviewers and editor.

References

Andersen, T., Kvamsdal, H.M., Bolland, O., 2000. Gas turbine combined cycle with CO_2 capture using auto-thermal reforming of natural gas. In: ASME Turbo Expo 2000, Munich, Germany.

Åström, K., Fontell, E., Virtanen, S., 2007. Reliability analysis and initial requirements for FC systems and stacks. Journal of Power Sources 171 (1), 46–54.

Barton, G.W., Chan, W.K., Perkins, J.D., 1991. Interaction between process design and process control: the role of open-loop indicators. Journal of Process Control 1 (3), 161–170.

Beér, J.M., 2007. High efficiency electric power generation: the environmental role. Progress in Energy and Combustion Science 33 (2), 107–134.

Bevilacqua, M., Braglia, M., Gabbrielli, R., 2000. Monte Carlo simulation approach for a modified FMECA in a power plant. Quality and Reliability Engineering International 16 (4), 313–324.

Blanco, A.M., Bandoni, J.A., 2003. Interaction between process design and process operability of chemical processes: an eigenvalue optimization approach. Computers & Chemical Engineering 27 (8–9), 1291–1301.

Bohm, M.C., Herzog, H.J., Parsons, J.E., Sekar, R.C., 2007. Capture-ready coal plants—options, technologies and economics. International Journal of Greenhouse Gas Control 1 (1), 113–120.

Bonzani, F., Gobbo, P., 2007. Operating experience of high flexibility syngas burner for IGCC power plant. Proceedings of the ASME Turbo Expo, vol. 2. American Society of Mechanical Engineers, New York, NY, 65–71.

Chiesa, P., Lozza, G., Mazzocchi, L., 2005. Using hydrogen as gas turbine fuel. Journal of Engineering for Gas Turbines and Power 127 (1), 73–80.

Christensen, T.S., Christensen, P.S., Dybkjær, I., Hansen, J.H.B., Primdahl, I.I., 1998. Developments in autothermal reforming. Studies in Surface Science and Catalysis 119, 883–888.

Christensen, T.S., Primdahl, I.I., 1994. Improve syngas production using autothermal reforming. Hydrocarbon Processing 73 (3).

Descamps, C., Bouallou, C., Kanniche, M., 2008. Efficiency of an Integrated Gasification Combined Cycle (IGCC) power plant including CO_2 removal. Energy 33 (6), 874–881.

Dhillon, B.S., Rayapati, S.N., 1988. Chemical-system reliability: a review. IEEE Transactions on Reliability 37 (2), 199–208.

Dybkjær, I., 1995. Tubular reforming and autothermal reforming of natural gas—an overview of available processes. Fuel Processing Technology 42 (2–3), 85–107.

Eti, M.C., Ogaji, S.O.T., Probert, S.D., 2007. Integrating reliability, availability, maintainability and supportability with risk analysis for improved operation of the Afam thermal power-station. Applied Energy 84 (2), 202–221.

Grabke, H.J., Krajak, R., Müller-Lorenz, E.M., 1993. Metal dusting of high temperature alloys. Werkstoffe und Korrosion 44 (3), 89–97.

Grabke, H.J., Spiegel, M., 2003. Occurrence of metal dusting—referring to failure cases. Materials and Corrosion 54 (10), 799–804.

Grabke, H.J., Wolf, I., 1986. Carburization and oxidation. Materials Science and Engineering 87, 23–33.

Higman, C., DellaVilla, S., Steele, B., 2006. The Reliability of Integrated Gasification Combined Cycle (IGCC) Power Generation Units. In: Achema, Frankfurt, Germany.

IEC 60812, 2006. Analysis Techniques for System Reliability—Procedures for Failure Mode and Effect Analysis (FMEA). International Electrotechnical Commission, Geneva.

ISO 20815, 2008. Petroleum, Petrochemical and Natural Gas Industries—Production Assurance and Reliability Management. International Organization for Standardization, Geneva.

Luyben, W.L., 1996. Design and control degrees of freedom. Industrial and Engineering Chemistry Research 35 (7), 2204–2214.

Moulijn, J.A., Makkee, M., Diepen, A.v., 2007. Chemical Process Technology. Wiley, Hoboken, NJ.

Murthy, D.N.P., Rausand, M., Østerås, T., 2008. Product Reliability; Specification and Performanace. Springer, London.

Murthy Konda, N.V.S.N., Rangaiah, G.P., Krishnaswamy, P.R., 2006. A simple and effective procedure for control degrees of freedom. Chemical Engineering Science 61 (4), 1184–1194.

NERC, 2007. North American Electric Reliability Corporation: GADS Report 2002–2006. http://www.nerc.com.

OREDA, 2002. Offshore Reliability Data Handbook, 4th edition. DNV, Høvik, Norway.

Perrow, C., 1999. Normal Accidents; Living with High-Risk Technologies. Princeton University Press, Princeton, NJ.

Rausand, M., Høyland, A., 2004. System Reliability Theory: Models, Statistical Methods, and Applications, 2nd edition. Wiley, Hoboken, NJ.

Rostrup-Nielsen, J.R., 1997. Industrial relevance of coking. Catalysis Today 37 (3), 225–232.

Scottish Centre for Carbon Storage, 2009. School of Geosciences, University of Edinburgh, Scotland. http://www.geos.ed.ac.uk/ccsmap.

Shilling, N.Z., Jones, R.M., 2003. The impact of fuel flexible gas turbine control systems on integrated gasification combined cycle performance. Proceedings of the ASME Turbo Expo, vol. 1. American Society of Mechanical Engineers, New York, NY, 259–265.

Skogestad, S., 2004. Control structure design for complete chemical plants. Computers and Chemical Engineering 28 (1–2), 219–234.

Sperle, T., Chen, D., Lodeng, R., Holmen, A., 2005. Pre-reforming of natural gas on a Ni catalyst: criteria for carbon free operation. Applied Catalysis A: General 282 (1–2), 195–204.

Teng, S.-H., Ho, S.-Y., 1996. Failure mode and effects analysis: an integrated approach for product design and process control. The International Journal of Quality & Reliability Management 13 (5), 8–26.

Teoh, P.C., Case, K., 2004. Failure modes and effects analysis through knowledge modelling. Journal of Materials Processing Technology 153–154 (1–3), 253–260.

Todd, D.M., Battista, R.A., 2000. Demonstrated applicability of hydrogen fuel for gas turbines. In: Gasification 4 the Future, Noordwijk, Netherlands.
van Loo, S., van Elk, E.P., Versteeg, G.F., 2007. The removal of carbon dioxide with activated solutions of methyl-diethanol-amine. Journal of Petroleum Science and Engineering 55 (1–2), 135–145.
Vannby, R., Winter Madsen, S.E.L., 1992. Adiabatic performing. Ammonia Plant Safety (and Related Facilities) 32, 122–128.
Vasudevan, S., Murthy Konda, N.V.S.N., Rangaiah, G.P., 2008. Control degrees of freedom using the restraining number: further evaluation. Asia-Pacific Journal of Chemical Engineering 3 (6), 638–647.

Paper III

Nord, L.O., Kothandaraman, A., Herzog, H., McRae, G., Bolland, O., 2009. A modeling software linking approach for the analysis of an integrated reforming combined cycle with hot potassium carbonate CO_2 capture. Energy Procedia 1 (1), 741–748.

Available online at www.sciencedirect.com

ScienceDirect

Energy Procedia 1 (2009) 741–748

Energy Procedia

www.elsevier.com/locate/procedia

GHGT-9

A modeling software linking approach for the analysis of an integrated reforming combined cycle with hot potassium carbonate CO_2 capture

Lars Olof Nord[a,*], Anusha Kothandaraman[b], Howard Herzog[c], Greg McRae[b], Olav Bolland[a]

[a]*Department of Energy and Process Engineering, the Norwegian University of Science and Technology, NO-7491 Trondheim, Norway*
[b]*Department of Chemical Engineering, Massachusetts Institute of Technology, Cambridge, MA 02139, USA*
[c]*Laboratory for Energy and the Environment, Massachusetts Institute of Technology, Cambridge, MA 02139, USA*

Abstract

The focus of this study is the analysis of an integrated reforming combined cycle (IRCC) with natural gas as fuel input. This IRCC consisted of a hydrogen-fired gas turbine (GT) with a single-pressure steam bottoming cycle for power production. The reforming process section consisted of a pre-reformer and an air-blown auto thermal reformer (ATR) followed by water-gas shift reactors. The air to the ATR was discharged from the GT compressor and boosted up to system pressure by an air booster compressor. For the CO_2 capture sub-system, a chemical absorption setup was modeled. The design case model was modeled in GT PRO by Thermoflow, and in Aspen Plus. The Aspen Plus simulations consisted of two separate models, one that included the reforming process and the water-gas shift reactors. In this model were also numerous heat exchangers including the whole pre-heating section. Air and CO_2 compression was also incorporated into the model. As a separate flow sheet the chemical absorption process was modeled as a hot potassium carbonate process. The models were linked by Microsoft Excel. For the CO_2 capture system the model was not directly linked to Excel but instead a simple separator model was included in the reforming flow sheet with inputs such as split ratios, temperatures, and pressures from the absorption model. Outputs from the potassium model also included pump work and reboiler duty. A main focal point of the study was off-design simulations. For these steady-state off-design simulations GT MASTER by Thermoflow in conjunction with Aspen Plus were used. Also, inputs such as heat exchanger areas, compressor design point, etc., were linked in from the Aspen Plus reforming *design* model. Results indicate a net plant efficiency of 43.2% with approximately a 2%-point drop for an 80% part load case. Another off-design simulation, at 60% load, was simulated with a net plant efficiency around 39%. The CO_2 capture rate for all cases was about 86%, except for the reference case which had no CO_2 capture.

Keywords: Carbon capture and storage (CCS); CO_2 capture; Pre combustion capture; Integrated reforming combined cycle (IRCC); hot potassium carbonate; modeling; process simulation

1. Introduction

Pre-combustion CO_2 capture is one possible route to fossil fueled power generation with low CO_2 emissions. There exist many possible configurations for a pre-combustion plant, not the least in relation to the fuel feed. Eide and Bailey [1] describe and discuss different pre-combustion decarbonization processes. One such process is the integrated reforming combined cycle (IRCC). An IRCC is fueled by natural gas which is reformed to a synthetic gas, mainly consisting of H_2 and CO. The reformed gas is water-gas-shifted, the CO_2 can be separated out, and the resulting hydrogen-rich fuel used in a gas turbine (GT). For the CO_2 separation many options exist. One alternative is to use a chemical absorption system utilizing a hot potassium carbonate solution. The potassium carbonate solvent is an aqueous alkaline solvent particularly suited for processes with high total pressure and high CO_2 concentration. The process performs on the principle of a pressure swing absorption-desorption cycle

* Corresponding author. Tel.: +47 735 93728; fax: +47 735 98390.
E-mail address: lars.nord@ntnu.no.

doi:10.1016/j.egypro.2009.01.098

with absorption taking place at high pressures. CO_2 capture by the use of potassium carbonate is, for example, described by Kohl and Nielsen [2].

The topic of this study is analysis of an IRCC process, with a special focus on off-design simulations. Similar pre-combustion process configurations have been studied by Andersen et al. [3] and Ertesvåg et al. [4]. Consonni and Viganò [5] also analyzes a pre-combustion setup but with co-generation of power and hydrogen. Hoffmann et al. [6] investigates a pre-combustion cycle using partial oxidation reforming. The cited studies focus on design case analysis. There is limited amount of literature in terms of off-design analysis of CO_2 capture cycles. Part load analyses of natural gas post-combustion systems are performed by Möller et al. [7]. Haag et al. [8] and Naqvi et al. [9] analyze the part load behavior of some of the proposed oxy-fuel cycles.

The remainder of the paper is divided into the following sections: Section 2 describes the process. Section 3 describes the details of the methodologies used in the paper. The results are shown and analyzed in Section 4, and concluding remarks are given in Section 5.

2. Process description

The process reforms natural gas to a syngas as shown in Figure 1. The syngas is water-gas shifted converting CO to CO_2 and the CO_2 separated out before the hydrogen-rich fuel is used for the gas turbine. As the auto-thermal reformer (ATR) is air-blown there will be a significant portion of nitrogen in the gas. This nitrogen is used as fuel diluent for NO_x abatement in the GT combustor. The air needed for the ATR is bled from the GT compressor discharge plenum and boosted up to system pressure with a booster compressor. There are a number of heat exchangers in the system. The pre-heating of the reforming streams is handled in various zones in the heat recovery steam generator (HRSG). The syngas cooler, located after the ATR, acts as an evaporator for the high-pressure (HP) steam cycle. The other heat exchangers for the process streams either generate low-pressure (LP) steam for the reboiler in the capture sub-system or pre-heat the fuel for the GT. The selected gas turbine is a GE 9FB set up for an integrated gasification combined cycle (IGCC). The requirements for an IRCC GT and an IGCC GT are very similar. The bottoming steam cycle, including the HRSG and a steam turbine (ST), is a one-pressure system at approximately 85 bar. The CO_2 capture sub-system consists of a hot potassium carbonate process. The CO_2 is compressed to 150 bar in the CO_2 compression and pump train.

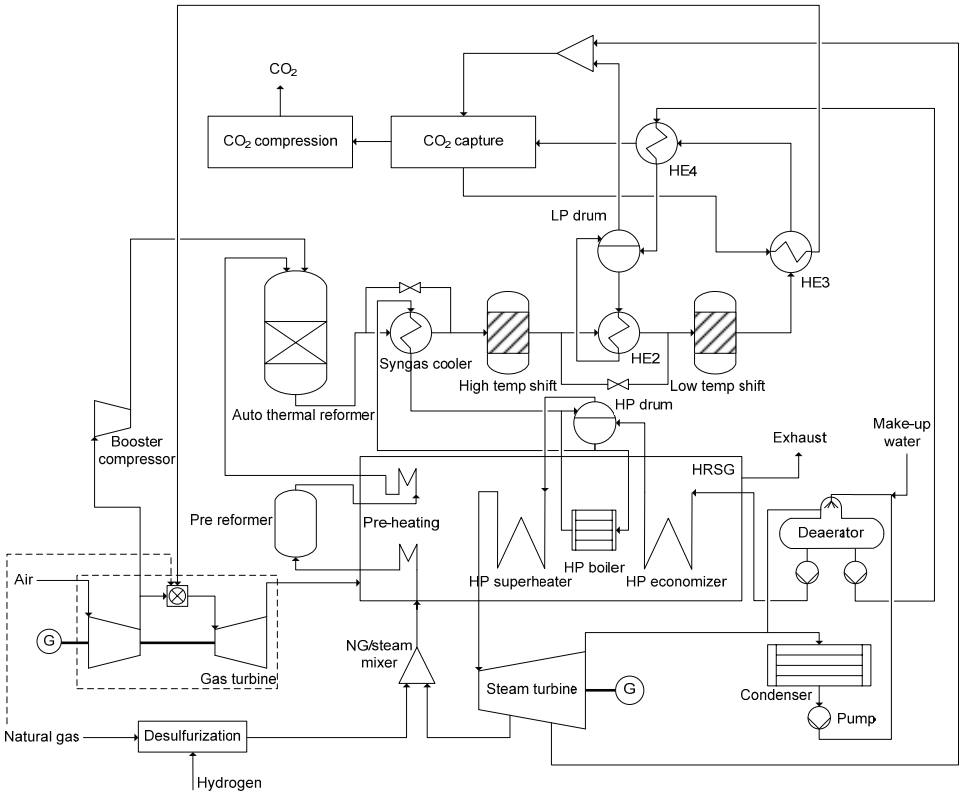

Figure 1. Process flow sheet of integrated reforming combined cycle

3. Methodology

The design case model was modeled in GT PRO by Thermoflow, and in Aspen Plus. The Aspen Plus simulations consisted of two separate models, one that included the reforming process and the water-gas shift reactors. In this model, numerous heat exchangers were included, among those the whole pre-heating section. Air and CO_2 compression was also incorporated into the model. The chemical absorption process was modeled as a hot potassium carbonate model in a separate flow sheet. The models were linked by Microsoft Excel utilizing Aspen Simulation Workbook and the Thermoflow E-LINK. For the CO_2 capture system the model was not directly linked to Excel, instead a simple separator model was included in the reforming flow sheet with inputs such as split ratios, temperatures, and pressures from the absorption model. Outputs from the capture model also included pump work and reboiler duty.

In a scenario where CO_2 capture plants become common-place, part load operation will be an important part of the operation scheme. For a plant such as the one modeled in this work the goal is certainly to run it at base load operation for the majority of the time but as part of an overall grid strategy part load operation will come into play. For these steady-state off-design simulations, GT MASTER by Thermoflow in conjunction with Aspen Plus were used. Also, inputs such as heat exchanger areas, compressor design point, etc., were linked in from the Aspen Plus reforming *design* model. The overall simulation overview with the linking is displayed in Figure 2.

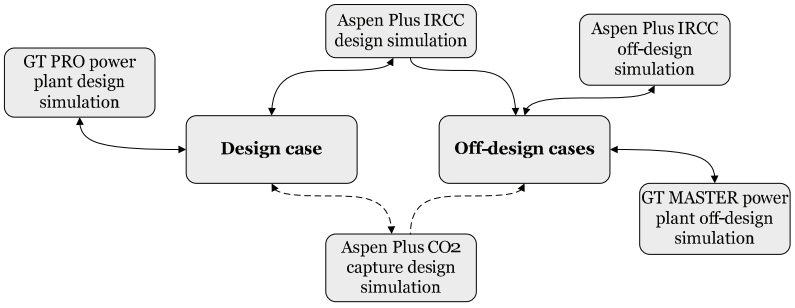

Figure 2. Overall simulation overview with software linking

3.1. Design case assumptions

The process was designed with a requirement of at least 85% CO_2 capture rate. The capture rate is here defined as the fraction of formed CO_2 that is captured. To achieve an overall capture rate of 85% the chemical absorption system was modeled for a 90% capture rate. It can be argued that the 90% capture rate is too low and that a higher design capture rate for the absorption sub-system would have been preferable and instead operate the system at a lower steam-to-carbon ratio (S/C) to achieve the overall capture rate of 85%. A lower S/C would lead to a higher methane slip from the ATR and a lower CO conversion in the water-gas-shift reactors but the lower amount of steam used would increase the net plant efficiency. The selected S/C for the simulations is 1.5. During the simulation work it was noted that the low-pressure and intermediate-pressure sections in the HRSG became quite small because of the significant pre-heating requirements (which could have been compensated with duct firing in the HRSG). Because of this and to simplify the process it was decided to have a one-pressure level in the HRSG. The pressure level was set at approximately 85 bar for the design case. Other assumptions include a condenser pressure of 0.04 bar, a 3% pressure drop (of inlet pressure) in the heat exchangers and reactors, and ISO ambient conditions.

3.2. Off-design analysis

One of the main focal points for the process analysis was related to off-design conditions. Two part load points were analyzed; 80% and 60% of the design case gas turbine load respectively. The off-design analyses were steady-state based. It should also be mentioned that off-design considerations can affect the design of the process. For example, in this process, steam extracted for the reboiler in the absorption system had to be extracted at a higher pressure than necessary to achieve a sufficient pressure level also at part load. In addition, off-design considerations for the booster compressor may lead to a selection of a less than optimum design point to achieve the required pressure ratio at reduced mass flow rates. In the following sub-sections the theory and methodology used for the part load scenarios will be presented.

3.2.1. Heat exchanger analysis

In the off-design scenarios the overall heat transfer coefficient U in the heat exchangers will vary. With inclusion of surface fouling and fin effects (extended surface) U can be expressed as:

$$\frac{1}{UA} = \frac{1}{(\eta_o hA)_c} + \frac{R''_{f,c}}{(\eta_o A)_c} + R_w + \frac{R''_{f,h}}{(\eta_o A)_h} + \frac{1}{(\eta_o hA)_h} \tag{1}$$

In the off-design analysis presented in this paper an as-new plant is assumed with no aging or fouling. The fouling factors $R''_{f,c}$ and $R''_{f,h}$ are therefore set to 0. The wall conduction term R_w is also neglected. η_o is the overall surface efficiency of a finned surface and A is the heat transfer area. Subscripts c and h refer to the cold and hot side of the heat exchanger, respectively. In the pre-heating heat exchangers in the HRSG the cold side has a high steam content. In the syngas cooler, as well as in HE2 and HE4 (refer to Figure 1) the cold side has water and steam only. Compared to the hot side, which contains gas with a lower level of steam, the cold side heat transfer coefficient is assumed much larger, that is $h_c \gg h_h$. Equation (1) can then be simplified to:

$$\frac{1}{UA} = \frac{1}{(\eta_o hA)_h} \tag{2}$$

The area A and fin efficiency η_o are constant when comparing design to off-design conditions. Using the Nusselt number and an empirical correlation including the Reynolds and Prandtl numbers (Incropera and DeWitt [10]):

$$Nu_D \equiv \frac{hD}{k} = C\, Re_D^m\, Pr^n \tag{3}$$

The constants C, m, and n, are assumed independent of the nature of the fluid. The Prandtl number Pr and thermal conductivity k are assumed constant from design to off-design conditions. The diameter D is constant. For the simulations, it is of interest relating the off-design UA to the design $(UA)_d$. Equation (2) can then be written as:

$$\frac{UA}{(UA)_d} = \frac{Re_D^m}{Re_{D,d}^m} \tag{4}$$

By using $Re_D = \frac{\dot{m}D}{A\mu}$, where the dynamic viscosity μ is assumed constant, a simple expression for correction of the UA-value when going from design to off-design simulations can then be derived:

$$\frac{UA}{(UA)_d} = \left(\frac{\dot{m}_h}{\dot{m}_{h,d}}\right)^m \tag{5}$$

The m-constant is dependent on the geometry of the shell and tube heat exchanger. $\dot{m}$ is the fluid mass flow. Subscript d refers to design conditions.

3.2.2. Pressure drop analysis

Assuming fully developed turbulent flow, meaning the pressure gradient dp/dx is a constant, the pressure drop from axial position x_1 to x_2 can be expressed as:

$$\Delta p = -\int_{p_1}^{p_2} dp = f\frac{\rho u_m^2}{2D}\int_{x_1}^{x_2} dx = f\frac{\rho u_m^2}{2D}(x_2 - x_1) \tag{6}$$

where u_m is the mean fluid velocity and ρ the density of the fluid. The Darcy friction factor f is defined as:

$$f \equiv \frac{-(dp/dx)D}{\rho u_m^2/2} \tag{7}$$

By using $\dot{m} = \rho u_m A$, and comparing to design conditions the following expression can be derived for off-design considerations:

$$\frac{\Delta p}{\Delta p_d} = \left(\frac{\dot{m}}{\dot{m}_d} \right)^2 \frac{\rho_d}{\rho} \tag{8}$$

3.2.3. Compressor map

For the air booster compressor in Figure 1, a compressor map has been used for calculating the outlet pressure and isentropic efficiency in off-design operating points. The map has been adopted from the original, presented in a map collection by Kurzke [11], to fit the process in the analysis. The following non-dimensional ratios have been used:

The pressure ratio $\Pi = \frac{p_{02}}{p_{01}}$, the corrected mass flow $\dot{m}_{corr} = \frac{\dot{m}\sqrt{T_{01}}}{p_{01}}$, and the corrected rotational speed $N_{corr} = \frac{N}{\sqrt{T_{01}}}$. p_{01} is the stagnation pressure at compressor inlet and p_{02} at compressor discharge. T_{01} is the stagnation temperature at compressor inlet.

In Figure 3, $\dot{m}_{corr}$ is plotted versus Π and the isentropic efficiency η_{is} for different N_{corr}. The corrected mass flow and the corrected speed are relative to design value. The surge line is also visible in the figure. The chosen design point for the booster air compressor is indicated in the graph. For off-design operating conditions it is assumed that the compressor can be speed controlled. For the GT compressor, GT MASTER used maps built-in to the program.

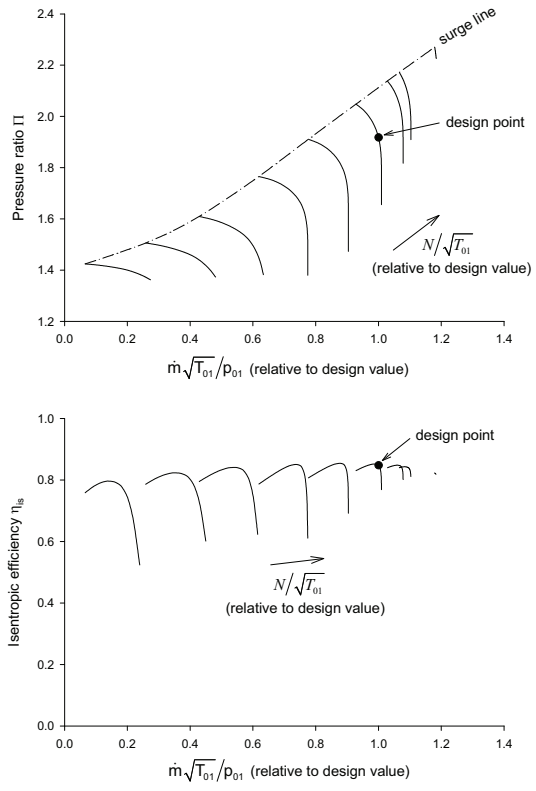

Figure 3. Compressor map for air booster compressor

When choosing the design and off-design operating points it is important to consider the surge margin to ensure stable compressor operation and avoid surge conditions. The surge margin is here defined as:

$$SM = \frac{\dot{m}_{corr,rel} - \dot{m}_{corr,rel,surge}}{\dot{m}_{corr,rel}} \tag{9}$$

Here $\dot{m}_{corr,rel}$ is the corrected mass flow relative to the design corrected mass flow. $\dot{m}_{corr,rel,surge}$ is the corrected mass flow at surge conditions on the operating line (constant speed line) relative to the design corrected mass flow.

4. Results and discussion

The main results for the design and off-design cases are presented in Table 1. The net plant efficiency is 43.2% for the design case with about two percentage-points drop to each subsequent part load case. The net plant efficiency is defined as:

$$\eta_{net,plant} = \frac{(W_t - W_c)\eta_m\eta_{gen} + W_s\eta_m\eta_{gen} - (W_{comp} + W_p)/(\eta_m\eta_{drive}) - W_{aux}}{\dot{m}_{NG} LHV_{NG}} \quad (10)$$

Here W_t is the GT turbine power, W_c the GT compressor power, W_s the ST power, W_{comp} the total power consumption by the air and CO_2 compression. W_p is the pump power for feed water pumps, pumps in the absorption sub-system, etc. W_{aux} is the auxiliary power requirement. η_m is the mechanical efficiency and η_{gen} is the generator efficiency. η_{drive} is the efficiency of the drives for the different compressors and pumps. $\dot{m}_{NG}$ is the natural gas mass flow entering the system and LHV_{NG} the lower heating value of the natural gas. Note that all the power terms are defined as their absolute values meaning all power terms are considered positive and the sign is handled in the equation itself.

The capture rate is just above 86% for all cases, except for the reference case which has no CO_2 capture. The reference case is based on a natural gas combined cycle plant with a GE 9FB gas turbine and a triple-pressure steam cycle.

Table 1. Result summary for design case (100%), off-design cases (80% and 60%) and reference case (100% ref.)

Gas turbine relative load [%]	100	100 (ref.)	80	60
Natural gas LHV input [MW]	805.4	754.1	690.9	573.9
Gross power output GT [MW]	245.6	285.1	196.5	147.4
Gross power output ST [MW]	139.3	144.6	119.4	102.1
Gross power output [MW]	384.8	429.6	316.0	249.4
Gross power output [% of LHV input]	47.8	57.0	45.7	43.5
Air compression [MW]	14.0	-	10.7	7.9
Air compression [% of LHV input]	1.7	-	1.6	1.4
CO_2 compression [MW]	15.5	-	12.9	10.8
CO_2 compression [% of LHV input]	1.9	-	1.9	1.9
CO_2 capture pumps [MW]	1.5	-	1.1	0.9
CO_2 capture pumps [% of LHV input]	0.2	-	0.2	0.2
BFW pumps in pre-comb process [MW]	0.0	-	0.0	0.0
BFW pumps in pre-comb process [% of LHV input]	0.0	-	0.0	0.0
Auxiliaries [MW]	5.8	5.2	5.5	5.3
Auxiliaries [% of LHV input]	0.7	0.7	0.8	0.9
Net power output [MW]	**348.1**	**424.4**	**285.6**	**224.5**
Net plant efficiency [% of LHV input]	**43.2**	**56.3**	**41.3**	**39.1**
Efficiency capture penalty [%-point loss to ref. case]	13.1	-	-	-
CO_2 emissions [g CO_2 / net kWh el.]	68.3	377.6	71.8	73.7
CO_2 capture rate [%]	**86.1**	**0**	**86.0**	**86.4**

The turbine inlet temperature for the gas turbine set is a critical parameter for the overall plant performance. For the base case of this analysis, a conservative temperature of 1297°C has been selected. The reason for this assumption is two-fold. For one, the IGCC setup of GE's 9FB GT includes replacing the hot gas path of the FB with FA parts. The 9FA design turbine inlet temperature is 1327°C. Secondly, because of the hydrogen fuel which leads to an increase in steam content in the turbine compared to when firing natural gas, the heat transfer rate to the turbine blades increase, leading to a higher blade metal temperature. Because of this, another 30°C decrease in firing rate has been implemented in the model leading to the 1297°C turbine inlet temperature. If the GT could be fired at the full 9FB firing rate of 1427°C the net plant efficiency would increase from 43.2% to 44.7%. Chiesa et al. [12], and Todd and Battista [13] addresses issues related to firing hydrogen in gas turbines.

The CO_2 capture reboiler duty is another parameter affecting the plant efficiency. With the setup as shown in Figure 1, a part of the steam for the reboiler in the capture sub-system is extracted from the ST. If the reboiler duty would decrease from the current 1980 kJ/kg CO_2 captured down to approximately 1250 kJ/kg CO_2 captured, no steam extraction from the ST to the capture sub-system would be necessary and the ST output would increase. This would increase the net plant efficiency from the base case efficiency of 43.2% to 43.9%.

Figure 4 shows a T-Q diagram of the HRSG. Notable is that the boiler (HPB1 in Figure 4) is small compared to a more standard HRSG design. The reason for this is the large amount of steam generated in the syngas cooler. This means the economizer and the superheater in the HRSG are rather large but with a smaller boiler. The vertical jumps of the gas temperature in the figure are due to the pre-heating of the process streams. It should be noted that the majority of the pre-heating is upstream of the superheater meaning a significant portion of the available heat of the gas stream is removed before any steam is generated. The unconventional design is because of the integration with the reforming process. One can argue that a triple-pressure steam cycle would have a higher efficiency compared to the single-pressure system applied here. However, because of all the pre-heat streams and the syngas cooler acting as an evaporator, the low-pressure and intermediate-pressure sub-systems would have been very small adding very limited value at an increased complexity. Duct firing could have changed this picture, however for this work it was decided not to utilize supplementary firing.

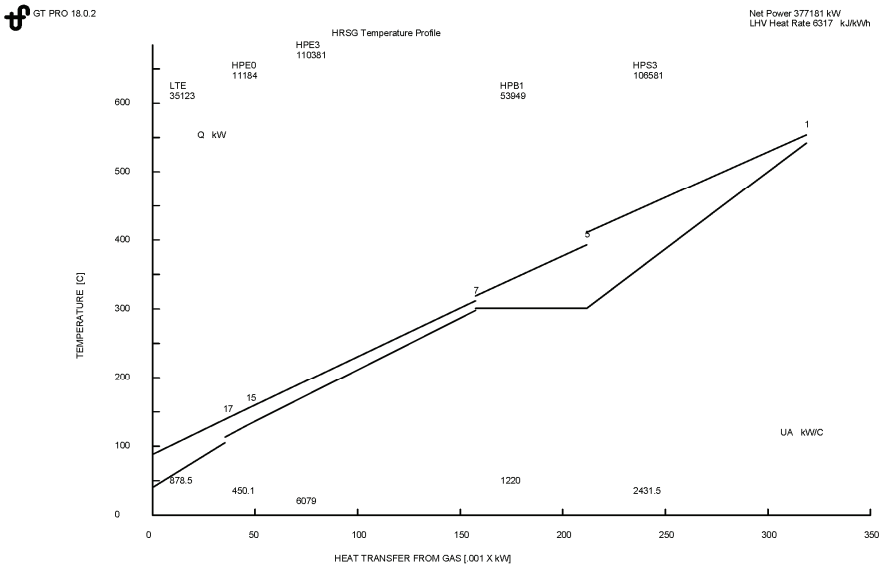

Figure 4. GT PRO T-Q diagram for single-pressure heat recovery steam generator

5. Conclusions

By combining simulation tools for chemical engineering and power plant engineering analyses respectively, a helpful representation of the overall system can be accomplished for an IRCC process. The IRCC process may involve a significant integration between the power cycle and the reforming process as is the case for the cycle studied. It can therefore be advantageous to combine the tools as is shown in this paper.

The results indicate a rather low net plant efficiency compared to the reference case. This is for one, strongly influenced by the conservative selection of turbine inlet temperature. An increase of the temperature would significantly reduce the capture penalty. Secondly, the reboiler duty could be lowered, again leading to a higher plant efficiency. Other items to consider is

supplementary firing in the HRSG to allow for a more standard design of the steam generator and the use of low-temperature process heat instead of low-pressure steam for the reboiler in the chemical absorption system. Also, a higher design CO_2 capture rate for the absorption system could be advantageous. However, it should be mentioned that the IRCC process is complex and many options and configuration possibilities are present. In the end, a line had to be drawn how far to extend the analysis work.

The off-design simulation results show the possibility to run a plant like this at part load conditions down to approximately 60% gas turbine load. Reducing the load further down may not be practical for several reasons. For example, the CO emissions from the GT would increase and potentially also NO_x. Further, the efficiency drop would at some point be too large to justify. The air booster compressor pressure ratio would continue to decrease (if using a one-compressor train and not multiple compressors) meaning the overall system pressure would keep decreasing until the level is too low for realistic plant operation. The possibility would then be to switch to natural gas fuel for the gas turbine. Indeed, the plant is designed for having natural gas as back-up fuel for the GT. In fact, to start up a plant like the one in the study, natural gas is required. At a load around 30% or above the switch-over to the hydrogen-rich fuel would take place during a start-up.

6. Acknowledgments

We would like to thank the Norwegian Research Council and StatoilHydro for providing the funding for the project.

7. References

1. Eide, L.I. and D.W. Bailey, *Precombustion decarbonisation processes.* Oil and Gas Science and Technology, 2005. **60**(3): p. 475-484.
2. Kohl, A. and R. Nielsen, *Gas purification*. 5th ed. 1997, Houston, Texas, USA: Gulf Publishing Company.
3. Andersen, T., H.M. Kvamsdal, and O. Bolland. *Gas turbine combined cycle with CO_2 capture using auto-thermal reforming of natural gas*. in *ASME Turbo Expo*. 2000. Munich, Germany.
4. Ertesvåg, I.S., H.M. Kvamsdal, and O. Bolland, *Exergy analysis of a gas-turbine combined-cycle power plant with precombustion CO_2 capture.* Energy, 2005. **30**(1): p. 5-39.
5. Consonni, S. and F. Vigano, *Decarbonized hydrogen and electricity from natural gas.* International Journal of Hydrogen Energy, 2005. **30**(7): p. 701-718.
6. Hoffmann, S., et al., *Performance and cost analysis of advanced gas turbine cycles with pre-combustion CO_2 capture*, in *ASME Turbo Expo*. 2008: Berlin, Germany.
7. Möller, B.F., M. Genrup, and M. Assadi, *On the off-design of a natural gas-fired combined cycle with CO_2 capture.* Energy, 2007. **32**(4): p. 353-359.
8. Haag, J.C., et al. *Turbomachinery simulation in design point and part-load operation for advanced CO_2 capture power plant cycles*. 2007. Montreal, Que., Canada: American Society of Mechanical Engineers, New York, NY, USA.
9. Naqvi, R., J. Wolf, and O. Bolland, *Part-load analysis of a chemical looping combustion (CLC) combined cycle with CO_2 capture.* Energy, 2007. **32**(4): p. 360-370.
10. Incropera, F.P. and D.P. DeWitt, *Fundamentals of heat and mass transfer*. 3rd ed. 1990: John Wiley & Sons, Inc.
11. Kurzke, J., *Compressor and turbine maps for gas turbine performance computer programs - Component map collection 2*. 2004: Germany.
12. Chiesa, P., G. Lozza, and L. Mazzocchi, *Using hydrogen as gas turbine fuel.* Journal of Engineering for Gas Turbines and Power, 2005. **127**(1): p. 73-80.
13. Todd, D.M. and R.A. Battista, *Demonstrated applicability of hydrogen fuel for gas turbines*, in *Gasification 4 the Future*. 2000: Noordwijk, Netherlands.

Paper IV

Nord, L.O., Gong. B., Bolland, O., McRae, G.J., in press. Incorporation of uncertainty analysis in modeling of integrated reforming combined cycle. Energy Conversion and Management.

Is not included due to copyright